Chemoselective Phospho–Anion Binding Studies

Paul Atkinson

A thesis submitted for the degree of Doctor of Philosophy

Department of Chemistry
University of Durham

2005

Abstract

An investigation has been carried out, studying the interaction of various bioactive anions, particularly phosphorylated species, with well–defined chiral lanthanide complexes. In each ternary anion adduct, proton NMR analysis revealed a distinctive pattern for the most high frequency shifted resonances. Furthermore, the mean chemical shift of these four resonances can be used to identify the anion adducts present in solution and indicate the binding mode exhibited towards the lanthanide(III) centre. Similar differentiation of anion binding modes is also available from luminescence spectroscopy, via observation of the splitting pattern for the $^7F_1 \leftarrow {}^5D_0$ transition in europium complexes.

Thulium and ytterbium complexes display the greatest affinity towards anions. With *O*–phosphorylated amino acids and peptides, amino acid or *N*–terminal chelation is a competitive binding mode. In contrast, the corresponding europium complexes display a significant preference towards the phosphate binding mode and such complexes may be considered to function as selective receptors for phosphorylated peptides or proteins. For all the lanthanides, complexes involving an *N*–methylated ligand show an increase in competition from the chelating binding modes. This effect is most significant for the smaller lanthanide(III) ions.

Parallel investigations into the suitability of 1–azaxanthone derivatives as long wavelength sensitisers for europium(III) and terbium(III) emission were performed. The introduction of electron donating groups into the 1–azaxanthone compound led to an increase in the absorption wavelength maximum. However, perturbation of the excited states was accompanied by competitive fluorescence emission and in certain cases quenching of the excited states via intramolecular hydrogen bonding. Formation of the *N*–oxide derivative of 1–azaxanthone also led to a significant red shift in the absorption maximum. The related 1–aza–10–thioxanthone compound displayed the greatest potential as a lanthanide(III) sensitiser, and its incorporation into a phosphate selective europium receptor was investigated with the aim of achieving optical detection of low concentration of anions.

Declaration

The work described herein was carried out in the Department of Chemistry, University of Durham between October 2002 and September 2005. All of the work is my own; no part has previously been submitted for a degree at this or any other university.

Statement of Copyright

Acknowledgements

I would like to thank Prof. David Parker, for his help, support and the wealth of knowledge that I have gained over the last three years.

I would also like to thank Dr. Alan Kenwright, Catherine Hefferman and Ian McKeag for their assistance with NMR spectroscopy. Furthermore, I would like to thank Ian McKeag for his patience in setting up the 'Watergate' peptide NMR experiments. Many thanks also to Dr. Mike Jones and Lara Turner for their advice and assistance with mass spectrometry measurements.

I would like to thank Gilles Muller at the San Jose State University, U.S.A. for performing the CPL measurements.

I am also very grateful to Karen Findlay for taking the time to measure the numerous triplet energies requested.

I would also like to thank the current and past members of the Wolfson laboratory (CG 27) for their friendly advice and friendship.

A special thanks to my mam and dad for supporting me throughout my time here and for providing me with the opportunity to achieve so much.

Finally, I am especially thankful to Sarah who has provided me with immense encouragement and support throughout my time here at Durham.

Abbreviations

AIBN	*N,N'*–azoisobutyronitrile
AMP	adenosine–5'–monophosphate
cAMP	adenosine–3',5'–monophosphate
Arg	arginine
Asp	aspartate
CPL	Circularly Polarised Luminescence
Cyclen	1,4,7,10–tetraazacyclododecane
DCC	dicyclohexylcarbodiimide
DiBOC	*tert*–butyldicarbonate anhydride
DMAP	*N,N*–dimethylaminopyridine
DMF	*N,N*–dimethylformamide
EDC	1–ethyl–3–(3–dimethylaminopropyl)carbodiimide hydrochloride
EPA	solvent mixture for low temperature optical studies; diethyl ether, isopentane and ethanol 5:5:2
G–6–P	glucose–6–phosphate
Glu	glutamate
HBTU	2–(1H–benzotriazole–1–yl)–1,1,3,3–tetramethyluronium hexafluorophosphate
HSQC	Heteronuclear Single Quantum Correlation
IC	internal conversion
Ile	isoleucine
ISC	inter system crossing
Lys	lysine
MALDI	Matrix Assisted Laser Desorption Ionisation
MCPBA	*m*–chloroperbenzoic acid
MeCN	acetonitrile
MOPS	3–(*N*–morpholino)propanesulfonic acid
MRI	Magnetic Resonance Imaging
MRS	Magnetic Resonance Spectroscopy
NBS	*N*–bromosuccinimide
NOESY	Nuclear Overhauser Effect SpectroscopY
PPA	polyphosphoric acid
SAP	square antiprism

Ser	serine
SPK	Serine Protein Kinase
TOCSY	TOtal Correlation SpectroscopY
TPK	Tyrosine Protein Kinase
TSAP	twisted square antiprism
Thr	threonine
Tyr	tyrosine

Table of Contents

CHAPTER 1

Introduction

1.1 Introduction

The selective recognition of chemical compounds and ions is an important aspect in Nature and the development of receptors capable of probing complex intracellular activities of specific compounds is essential to assist in our understanding of many biological processes. Given the prevalence and importance of anionic species in the biological world, it is surprising that the development of anion coordination chemistry in aqueous solution is still relatively unexplored, contrary to that of cations. On the other hand, it is well understood that careful design of the host structure is required to achieve anion selectivity. This is due to a number of complications inherent in the structure of anions relative to cations. Notably, there are numerous variations in the geometries exhibited by anions, from simple spherical species to the trigonal and tetrahedral polyatomic oxyanions. Furthermore, variations in the charge of an oxyanion, and hence its electrostatic interactions, are observed in the pH range 4–8. Finally, consideration of the solvation of anions is particularly important in determining the binding affinity of a receptor for a particular anion. For example, given the high free energy of hydration observed for many common anions, a large electrostatic contribution to receptor binding is essential to compete with the solvent environment.

Anion	Ionic radius / pm	ΔG^0_{hyd} / kJmol^{-1}
F^-	133	−465
Cl^-	181	−340
I^-	220	−275
CN^-	191	−295
HCO_3^-	156	−335
CO_3^{2-}	178	−1315
SO_4^{2-}	230	−1080
$H_2PO_4^-$	200	−465
PO_4^{3-}	238	−2765

Table 1.1 : Thermochemical radii and experimental hydration energies for some selected anions, illustrating the high hydration energies observed for the oxyanions.[1]

1.1.1 Elements of Receptor Design

Therefore, in devising synthetic receptors capable of sensing anionic species in solution, it is necessary to carefully consider the charge, geometry and solvent environment of the anion in order to design a system which binds selectively, and

with high affinity, to the target entity. Early work in the area of anion binding focused on protonated tricyclic azacrown compounds, such as **1.1**, which bind anions through a combination of electrostatic and hydrogen bonding interactions. The expanded cavity, formed through electrostatic repulsion of the positively charged nitrogen atoms, allows encapsulation of the spherical chloride ion with high affinity in aqueous media.[2] Thus, such compounds effectively operate as size–selective receptors, with selectivity controlled by the cavity size.

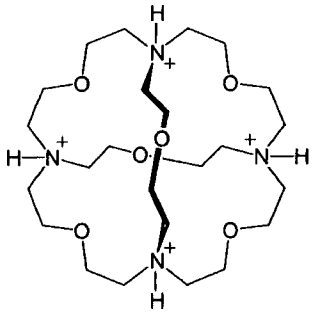

1.1

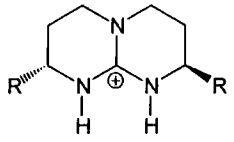

1.2

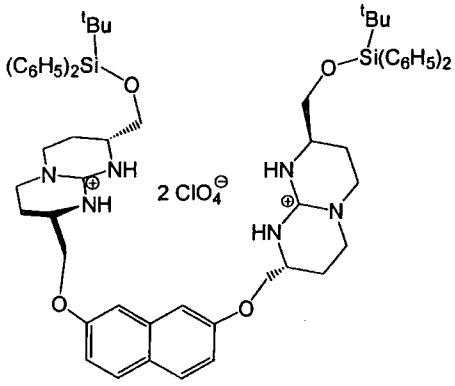

1.3

One major disadvantage of this type of receptor is the limited operational pH range required to maintain the electrostatic binding contribution. Avoiding pH dependence is easily achieved through the use of the more basic guanidinium moiety. Receptors incorporating the guanidinium ion utilise the planar positively charged structure, found extensively in natural anionic binding sites, which is capable of forming two parallel hydrogen bonds. However, the lower charge density and high solvation of the guanidinium moiety, in comparison to ammonium groups, results in much smaller binding constants when moving from non–polar solvents into water, indicative of a large electrostatic contribution to binding.[3] Therefore, lowering of solvation of the guanidinium moiety is the key to the improvement of the anion binding characteristics displayed. This has been achieved through incorporation of the guanidinium unit into a hydrophobic bicyclic framework (**1.2**), which also enables the inclusion of further functionalities to improve the specificity of binding.[4] However, receptors containing these bicyclic guanidinium units still suffer from competitive solvation in protic media. More promising results were obtained through the cooperative binding of two bicyclic guanidinium units, as in receptor **1.3**. This

receptor was found to bind most strongly to malonic acid in methanol (log K = 4.2). The affinity towards dicarboxylic acids with longer or shorter spacer groups between the carboxylic acid units was notably smaller (log K 2.4–3.4), suggesting that the cooperative binding between the guanidinium units is most effective for a suitably sized guest.[5]

Avoiding the use of positively charged receptors is a favourable approach, primarily due to the lack of interference from the anionic counterions present when working with these receptors. Through utilising the directional nature of hydrogen bonds, it is possible to create rigid, electroneutral receptors employing multiple hydrogen bonding interactions which complement the geometry of the target anion. For example, compound **1.4**, consisting of a urea in combination with an amide residue to produce three directional hydrogen bonds, exhibits a high selectivity and affinity for fluoride anions in chloroform.[6] This may be contrasted with the related compound, **1.5**, possessing two amide residues, and hence only two hydrogen bonds, which showed no significant halide binding.

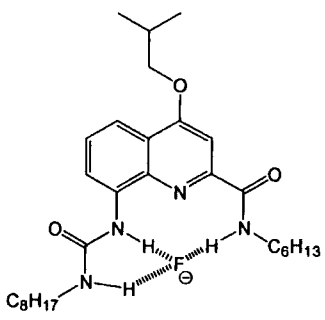

1.4

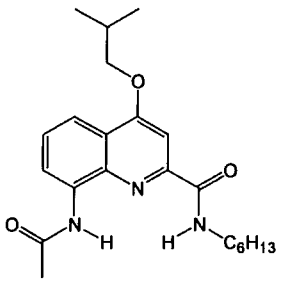

1.5

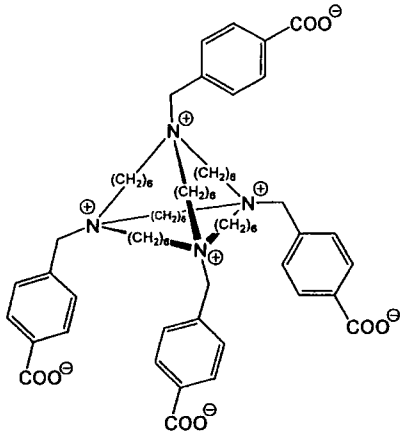

1.6

In general, however, the interaction between receptor and anion is quite weak. Consequently, synthetic receptors relying purely on hydrogen bonding only operate successfully in the absence of competitive hydrogen bond acceptors, restricting their use to non polar solvents. In contrast, natural receptors based upon hydrogen bonding networks display outstandingly high affinity and selectivity towards target anions. This is exemplified by the elegant arrangement of twelve hydrogen bonds holding a bound hydrogen phosphate anion into the binding cavity of phosphate binding

protein.[7] The difference in binding constants observed for phosphate over other tetrahedral oxyanions, such as sulphate, is approximately five orders of magnitude and discrimination is apparently achieved via a simple mechanism. The presence of an aspartate residue, positioned to accept a hydrogen bond from the hydroxyl group of hydrogen phosphate, causes electrostatic repulsion of the fully ionised sulphate anion.

The zwitterionic nature of natural ion receptors, which may incorporate the localisation of positively charged cavities, combined with well organised hydrogen bonding networks, seems to be the key in achieving good anion selectivity. Following Nature's approach to generate anion binding sites, the zwitterionic compound **1.6** has been investigated.[8] The neutral receptor, **1.6**, forms an expanded cavity, allowing formation of 1:1 complexes with the spherical halide anions in aqueous solution. Competitive titrations of the halides with this receptor, monitored by ^{35}Cl NMR, provide evidence for the formation of complexes in which the halide is present inside the molecular cavity. The selectivity displayed by receptor **1.6** is evidently based on size selectivity, with the observed association constants decreasing in the order $I^- >> Br^- > CN^- >> Cl^-$.

1.1.2 Signal Transduction Methods

Of equal importance in the design of a chemical receptor is the incorporation of a signalling unit which can provide information on the events occurring at the molecular level, in this case, the binding of anions to the receptor. The signalling unit must therefore communicate effectively with the receptor, such that any macroscopic response is modulated upon anion binding. This response may be in the form of many physical property changes that can easily be measured. Numerous examples can be envisaged, for instance, a redox potential shift in cyclic voltammetry (CV). To achieve an electrochemical response, a redox active compound, such as a tetrathiafulvalene[9] or ferrocene,[10] can be introduced in close proximity to the receptor binding site. The oxidation potential of the redox active compound is directly influenced by the proximate bound anion, thus signalling binding to the receptor. Another electrochemical method is based upon the application of a neutral lipophilic anion receptor. Typically, Lewis acidic[11] or hydrogen bonding compounds

are incorporated into a polymer membrane to produce an ion–selective electrode or potentiometric sensor. Binding of the target anion is monitored by changes in the measured potential across the membrane, which is proportional to anion concentration. However, such electrochemical methods display fairly slow response times and the working lifetime of polymer membranes is often short. Optical methods, on the other hand, present numerous advantages in favour of their use in responsive synthetic receptors. Most notably, the sensitivity of optical techniques is extraordinary, with detection limits as low as a single molecule.[12] This high sensitivity, combined with good spatial resolution (submicron),[13] fast response times and the ability to perturb the excited state properties of optically active compounds through changes in their environment, justifies the domination of optical sensory systems. Anion binding is generally followed by an intensity change or wavelength shift in UV/visible absorption or emission spectroscopy,[14] although monitoring variations in emission lifetime[15] or polarisation are also possible. Carefully balancing the information obtainable, together with the inherent sensitivity, resolution and instrumentation required in these signalling techniques will ultimately determine their suitability for a given analytical purpose. For example, although a great deal of structural information can be gleaned from NMR shift data, ultimately the lack of sensitivity combined with the need for large, expensive equipment limits the practicality of this method for monitoring anion binding.

Although the majority of anionic receptors are based on fluorescent organic molecules,[16] the increasing interest in emissive metal based receptors is understandable given the distinctive advantages they hold over organic fluorophores.[17] Notably, metal complexes possess a variety of accessible excited states due to metal centred (d–d or f–f), ligand centred and charge transfer transitions. This abundance of excited states available in metal complexes further increases the opportunity for perturbation of emission characteristics. Complexes involving heavier metals (i.e. 3rd row transition metals and lanthanides) also have the advantage of long–lived luminescence. In the former case this is due to efficient mixing between triplet and singlet states, which is a function of the large degree of spin–orbit coupling present. With the lanthanides, this may be ascribed to the forbidden nature of the f–f transitions,[18] giving low transition probabilities and long

natural excited state lifetimes. During the analysis of biological samples, the advantage of a long–lifetime luminescent probe becomes apparent. Simply allowing a short delay (say 1μs) between excitation and measurement of the emission spectrum ensures any background fluorescence or Rayleigh scattering, originating from the sample, does not interfere with any measurements. Such interference may obscure the emission from a conventional fluorescent organic sensor, but has decayed to zero for these longer lived probes. This feature enhances the intrinsic signal/noise ratio of the method.

Another attractive feature of metal based systems is the possibility of introducing a paramagnetic centre into the receptor. Interaction of the unpaired electrons with the nuclei of a target molecule lying in close proximity to the paramagnetic centre will result in enhancement of the nuclei's T_1 and T_2 relaxation rates, along with the possibility of a change in it's resonant frequency. The presence of such an interaction can be envisaged to assist in the analysis of Magnetic Resonance Spectroscopy (MRS) data and also decrease the acquisition times required to obtain this information. MRS is a complementary technique to the imaging technology MRI, which uses proton resonances in tissues to form anatomical images. MRS on the other hand, uses this information to provide the concentrations of important metabolites, such as choline, creatine and lactate, which may aid the diagnosis of central nervous system disorders.[19] The targeted binding of such metabolites with a paramagnetic receptor could potentially serve two purposes. Firstly, increases in the relaxivity of the metabolite's nuclei would allow a shorter acquisition time and hence faster repetition rates, effectively increasing the signal to noise ratio for a given acquisition period. Secondly, interaction of the metabolite with the paramagnetic centre could give rise to a shift in the observed resonance for that metabolite, resulting in increased sensitivity by eliminating interference from overlapping signals.

1.1.3 Overview of Phosphate Chemistry

The oxo–acid chemistry of phosphorus is extremely diverse and the importance of these compounds and their salts in industry and biological processes is often underestimated. The simplest acid is (ortho)phosphoric acid, which is commonly

encountered in the form of its Na, K, Ca and NH_4 salts, as components in detergents, fertilisers, toothpaste and baking powder. Calcium phosphates are crucial in the formation of strong, healthy teeth and bones, whilst the more soluble Na and K phosphates are widely used as buffering systems, see **Scheme 1.1**.

$$H_2O + H_3PO_4 \xrightleftharpoons{pK_1 = 2.16} H_3O^+ + H_2PO_4^-$$

$$H_2O + H_2PO_4^- \xrightleftharpoons{pK_2 = 7.21} H_3O^+ + HPO_4^{2-}$$

$$H_2O + HPO_4^{2-} \xrightleftharpoons{pK_3 = 12.32} H_3O^+ + PO_4^{3-}$$

Scheme 1.1 : Dissociation constants for phosphoric acid in aqueous solution (298K, I=0).[20]

Successive replacement of the protons of the triprotic acid with alkyl or aryl groups yields the mono–, di– or tri–phosphate esters respectively. The resistance of phosphoesters to hydrolysis under physiological conditions (in the absence of phosphatase enzymes) underpins their function as the linkage between the deoxyribose units of DNA. In fact, many phosphorylated species are in widespread abundance within cells, with diverse functions ranging from essential signalling molecules, such as cyclic adenosine–3′,5′–monophosphate (cAMP) and inositol–1,4,5–triphosphate, to energy transport with adenosine–5′–triphosphate (ATP). The phosphorylation of proteins is an important post–translational modification. Phosphorylation occurs via the action of ATP–dependent phosphotransferases (protein kinases), which transfer the terminal phosphoryl group from ATP to the hydroxyl group of serine, threonine or tyrosine residues on the protein.[21] Two distinct classes of protein kinases exist, firstly those which specifically phosphorylate serine/threonine residues (SPKs) and secondly, tyrosine specific protein kinases (TPKs). A third, very small, class which exhibits no specificity is also known to exist, termed dual–specific protein kinases. In general, within a protein the number of possible phosphorylation sites (P–sites) could well consist of every possible serine, threonine and tyrosine residue within a protein. However, protein kinases rely on specific consensus elements around the P–site to impart strong binding affinity, hence controlling the phosphorylation to specific sequences.[21] The reversible phosphorylation of proteins via these mechanisms, combined with the action of specific phosphatases, is central in controlling many cellular processes including

differentiation, proliferation and cell development.[22] Furthermore, the switching of protein kinase activity is itself often controlled by the reversible phosphorylation of the activation loop, which can lead to changes in the protein kinase activity by two to four orders of magnitude.[21] Perturbations from the signalling pathways controlled by TPKs in particular is thought to be involved in the development of neoplasms, since TPKs are often over–expressed in cancerous tissue compared to healthy tissue.[23]

1.1.4 Current Methodology for Phosphate Analysis

^{31}P NMR spectroscopy is particularly suited to the analysis of phosphate species, as each phosphorus oxyanion is distinguished by a unique chemical shift, allowing the concentration of many different phosphorylated species at millimolar levels to be monitored both *in vitro* and in cells. However, the lack of sensitivity and spatial resolution requires techniques based on optical methods to detect micromolar concentrations in analytical samples.

The most common method for the analysis of phosphates in water samples is a colorimetric method, based on a modified version of the molybdenum blue procedure.[24] This method uses a mixture of molybdate, ascorbic acid and antimony to produce an intense blue–purple complex (**Scheme 1.2**). Further optimisations of this procedure have led to more rapid formation of the intense blue colour[25] and have also allowed the use of sophisticated flow systems for analysis.[26]

$$PO_4^{2-} + 12MoO_4^{2-} \rightarrow PMo_{12}O_{40}^{3-} + 12O^{2-}$$

$$PMo_{12}O_{40}^{3-} \xrightarrow{Sb} PSb_2Mo_{10}O_{40}^{3-}$$

Scheme 1.2 : Equations representing the formation of the reduced phosphoantimonyl–molybdenum blue complex, which can be monitored at 882 nm.

For reasons discussed earlier, anion receptors for phosphate should provide a combination of electrostatic and directional hydrogen bonding interactions, which complement the tetrahedral geometry. For example, in chloroform a calix[6]arene modified with primary amides on the lower rim (**1.7**) forms a stable gel in the presence of phosphate, indicating a strong network of multiple hydrogen bonds involving the amide N–H bonds.[27] Another example of the use of hydrogen bonding in non–protic media, is illustrated by a bis–thiourea compound (**1.8**), which can form four well–oriented hydrogen bonds to three of the phosphate oxygen atoms.[28]

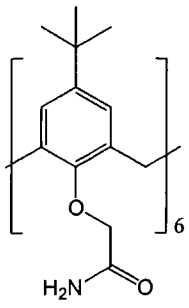

1.7

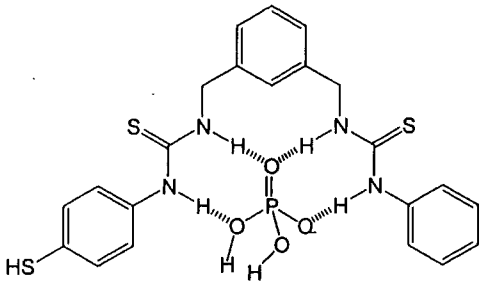

1.8

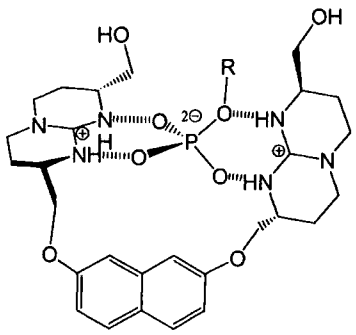

1.9

Achieving phosphate anion binding in protic media, through a combination of electrostatic and well–directed hydrogen bonding interactions, is illustrated by the conformationally flexible bis–bicycloguanidinium compound, **1.9**. In the presence of the tetrahedral phosphate anion, the chiral structure, combined with rigid planar spacing unit permits folding of the structure, enabling the two bicycloguanidinium units to form two perpendicular binding sites.[29] This cooperative binding mode produced respectable association constants with inorganic phosphate in aqueous solution (log K = 3.0), although comparison with values in methanol (log K = 4.3) is consistent with a predominantly electrostatic binding interaction.

As previously mentioned, in order to function practically as probes for the phosphate anion, such receptors must communicate the binding of phosphate to the observer. For neutral phosphate anion receptors, their incorporation into ion–selective electrodes is a common choice. Binding of phosphate anions can then be followed by monitoring changes in the potential of the electrode, relative to a reference cell.[27,28] However, in addition to problems discussed earlier, ion–selective electrodes often exhibit high selectivity for lipohilic anions, as predicted on the basis of relative hydration energies.[27] An interesting observation, with regards to anion selectivity, was made by Umezawa *et al.*[30] when using ion–selective electrodes incorporating a bis–thiourea receptor. Although this compound shows preferential selectivity towards phosphate in DMSO solution, when incorporated into polymeric membranes, the anion selectivity followed the trend of hydration energies. However, a contrasting result was obtained when implementing this bis–thiourea in an ion–channel sensor.[28] The sensor consists of a self–assembled monolayer (SAM) of the phosphate receptors, immobilised on a highly oriented pyrolytic graphite electrode.

The binding of phosphate in the receptor was followed by monitoring the redox reaction of the $[Fe(CN)_6]^{4-/3-}$ at the electrode, using CV. Formation of the phosphate–receptor complex, causes electrostatic repulsion of the iron species, thus inhibiting the redox reaction occurring at the electrode. This design shows good selectivity for phosphate over other anions (AcO^-, NO_3^- and SO_4^{2-}), although the electrode also displayed a significant response in the presence of chloride anions. The contrasting behaviour under the two sensory regimes may be attributed to the fact that the phosphate anion requires significant hydration even when bound to the receptor, which is not possible when the receptor is embedded in the polymer membrane.

Other electrode systems for phosphate detection rely on the selectivity of enzyme reactions. One such example is based on the phosphate dependent pyruvate oxidase enzyme reaction, which produces hydrogen peroxide.[31] Detection of the hydrogen peroxide produced from this enzymatic reaction, which is proportional to the concentration of phosphate in solution, is achieved through the chemiluminescence of luminol. Other systems based on phosphorylase enzyme reactions,[32] which are dependant upon inorganic phosphate, allow quantification of the phosphate concentration in solution. Another example illustrates the inherent specificity of enzymes in the application of electrode systems. In this system the detection of glucose–6–phosphate by utilising gluocose–6–phosphate hydrogenase can be performed using a phosphate buffered solution.[33] However, despite the advantages of high selectivity in enzyme based systems, they are often very complex, require freshly prepared solutions and the stability of the immobilised enzymes used can vary significantly.

The identification of phosphorylated proteins is usually performed using advanced mass–spectrometry techniques, such as MALDI–ToF.[34] The inherent sensitivity of mass spectrometry techniques ensures that they are valuable tools in the identification of proteins. However, identification of phosphorylated proteins is a challenge due to their small population within a huge number of non–phosphorylated peptides, and enrichment or purification of the phosphorylated species is usually required. Tandem mass spectrometry can also be used to identify the β–elimination

of phosphoric acid from the amino acids or via formation of the sulfite addition product prior to acquiring the mass spectrum.[35]

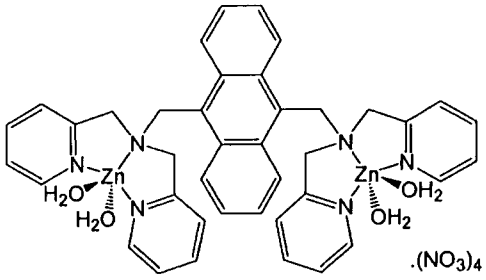

[$Zn_2$1.10]$^{4+}$

Recently, the fluorescent sensing of phosphate mono–esters in aqueous solution was reported using receptors based on a bi–metallic zinc complex, [Zn_2**1.10**]$^{4+}$.[36] The fluorescence observed from the anthracene moiety increases significantly upon binding phosphorylated species, with association constants of the order of 10^4–10^5 M^{-1} at pH 7.2. In contrast, the corresponding complex with only one zinc binding site shows no significant changes in fluorescence intensity upon addition of phosphorylated anions, indicating the strong binding results from cooperative binding at the two zinc centres. Furthermore, the bi–metallic receptor was shown to bind mono–phosphorylated peptides with an affinity which increased on raising the overall negative charge on the peptide, as expected for a primarily electrostatic interaction mechanism.[37] However, despite the good selectivity and high binding affinities towards phosphorylated species, the bi–metallic complex, [Zn_2**1.10**]$^{4+}$, is not a well–defined receptor. This is due to the presence of an equilibrium between the mono–zinc species, [Zn**1.10**]$^{2+}$ and free zinc(II) ions, such that the presence of five equivalents of zinc(II) ions is required to achieve maximum fluorescence intensity from the anthracene moiety. Thus the presence of phosphorylated anions simply increases the stability of the bis–zinc complex, so that saturation of the fluorescence intensity is achieved with just over two equivalents of zinc(II) ions.

Phosphate binding to lanthanide(III) ion complexes in aqueous solution has been demonstrated in only a small number of cases. In each example, the lanthanide(III) ion is encapsulated by a ligand with seven donors or less, allowing the coordination of the phosphate anion via displacement of one or more labile water molecules. Finding suitable lanthanide complexes for this purpose is often difficult as a result of

the lowering in complex stability. In an extreme case, the lanthanide(III) complex **1.11**, suffered from complete decomposition upon addition of phosphate, liberating the free ligand, driven by the formation of insoluble lanthanide(III) phosphate.[38]

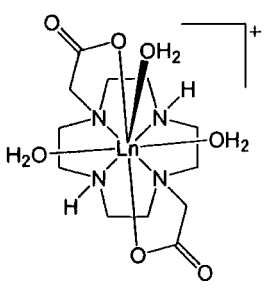

1.11

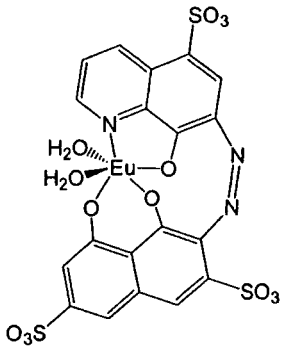

1.12

Other examples, where the decomposition of lanthanide(III) complexes occurs upon coordination of strongly binding phosphate or pyrophosphate anions, have been exploited to produce colorimetric receptors.[39,40] In the case of complex **1.12**, the presence of more than one equivalent of phosphate anion in solution is necessary to produce a change in the absorption profile, although no speciation studies were performed to confirm the final complex stoichiometry. The differential absorption profiles exhibited in the absence and presence of phosphate are markedly different, producing a colour change from pink to blue. The change in absorbance observed is associated with the displacement of only the naphthalene–1,8–diol coordinating component from the coordination sphere. However, no studies were performed to confirm the preferential displacement of this group over the quinolin–8–ol component. Furthermore, the similarity between absorption profiles of the complex in the presence of phosphate and of the free ligand may suggest complete dissociation of the ligand occurs in the presence of excess phosphate, although this was not investigated. Although this method allows the visible detection of phosphate species in solution, the lack of reversibility restricts its use as a real sensory system.

From looking at the current reports on the detection of phosphate species in aqueous solution, it is clear that although there is a recent interest in the lanthanide induced cleavage of phosphates,[41] there is very little information on the selective binding of phosphorylated anions within stable lanthanide(III) based systems. The rest of this

chapter will therefore outline the properties of the lanthanide(III) ions and their complexes, highlighting their practical uses and providing an insight into why such complexes were chosen for the investigation of phosphate binding.

1.2 Paramagnetic NMR of lanthanide(III) Complexes

Throughout the 1970s paramagnetic lanthanide(III) complexes were extensively used and studied as NMR shift reagents, based on initial observations by Hinckley that Eu(III) chelates induced isotropic shifts in the proton resonances of cholesterol.[42] Recent advances in NMR technology, such as higher fields and multidimensional techniques, have lessened the use of traditional lanthanide(III) shift reagents, although there is still considerable interest in the ability to resolve enantiomers through the use of chiral shift reagents.[43,44] The similarity in ionic radii between the lanthanide(III) ions (0.98–1.16 Å)[45] and calcium(II) (1.12 Å),[45] combined with the greater charge density of the lanthanide(III) ions, makes the f–block ions useful probes for the calcium binding sites in various proteins.[46] This provides a valuable tool to probe the structures within the vicinity of the otherwise spectroscopically inert calcium(II) ions. With careful choices of the lanthanide(III) ion, it is therefore possible to use the paramagnetically shifted resonances produced in order to assist in the structure determination of calcium binding proteins.[47]

1.2.1 Theory of Lanthanide Induced Shifts

The electronic configuration of the lanthanide(III) ions gives rise to a maximum of seven unpaired f–electrons. This occurs at the centre of the series for gadolinium(III). Each successive lanthanide(III) ion to the left or right possesses one less unpaired electron and therefore is also paramagnetic, with the exception of La^{3+} (f^0) and Lu^{3+} (f^{14}). Any NMR active nucleus within the vicinity of a paramagnetic lanthanide(III) ion experiences the fluctuating local magnetic field induced by the presence of the unpaired electrons in the lanthanide(III) ion, leading to broadening of its resonant signal, due to enhancement of both longitudinal and transverse relaxation rates (T_1 and T_2 respectively). Also, for all the paramagnetic lanthanide(III) ions, except gadolinium, which possess anisotropic magnetic moments, due to the asymmetric spatial distribution of electrons, a shift of the resonant frequency of the nucleus may occur.

There are three contributing mechanisms that determine the overall paramagnetic lanthanide induced shift (LIS). This can be written as the sum of three terms, **Equation 1**, where Δ_d, Δ_c and Δ_{pc} are the diamagnetic, contact and pseudo–contact shifts respectively.

$$\Delta = \Delta_d + \Delta_c + \Delta_{pc} \qquad (1)$$

The diamagnetic shift is a result of inductive effects and conformational changes in the ligand as it is bound to the lanthanide(III) ion. This shift can be neglected in most cases, due to its small contribution, except for the nuclei directly coordinated to the lanthanide(III) ion.[48] Determination of such shifts can be obtained following interpolation of the shifts obtained from the corresponding diamagnetic complexes incorporating lanthanum(III) or lutetium(III).

1.2.2 Contact Shift

Contact shifts occur due to the presence of unpaired electron density at the bound nucleus, which arises due to the delocalisation of spin density from the lanthanide(III) ion via polarisation of σ–character molecular orbitals.[49] The contact shift of any nucleus directly bound to the lanthanide(III) ion is usually huge, but decreases rapidly as the number of bonds between each nucleus and the lanthanide(III) ion increases.[50] The presence of large contact shift contributions to the observed chemical shift of a nucleus provides a good indication that the nucleus is directly bound to the lanthanide(III) ion. However, the resonances of such nuclei are usually severely broadened, and when exchange of the ligating atoms is slow on the NMR timescale the signal is not observable.[48]

The magnitude of the induced shift (in ppm) is calculated using **Equation 2**, where $\langle S_z \rangle$ is the reduced value of the average spin polarisation, β is the Bohr magneton, k is the Boltzmann constant, T is the absolute temperature, γ is the gyromagnetic ratio of the chosen nucleus and $A/\hbar$ is the hyperfine coupling constant.

$$\Delta_c = \langle S_z \rangle F = \langle S_z \rangle \frac{\beta}{3kT\gamma} \frac{A}{\hbar} 10^6 \qquad (2)$$

Despite the large spin–orbit contributions normally attributed to lanthanide(III) ions, in the calculation of contact shifts, calculations using $\langle J_z \rangle$ are not necessary, as only the spin can be delocalised onto the donor ligand.[51] Values of $\langle S_z \rangle$ have been calculated[52,53] at a temperature of 300K and are tabulated in **Table 1.2**. Only a minor variation of these calculated values is observed for the lanthanide(III) ions, with the exception of samarium(III), where the presence of low lying *J*–manifolds requires recalculation of $\langle S_z \rangle$ at each required temperature. Calculated values for europium(III) are subject to further uncertainty, arising from the fact that g_J is not well–defined for the ground state (J=0) and thus comparisons between experimental data and calculated values have been made in order to obtain a value for g_J and hence $\langle S_z \rangle$.[53]

Lanthanide ion	Electronic configuration	$\langle S_z \rangle$	C_D
Ce^{3+}	$4f^1$	−0.974	−6.3
Pr^{3+}	$4f^2$	−2.956	−11.0
Nd^{3+}	$4f^3$	−4.452	−4.2
Pm^{3+}	$4f^4$	−3.944	2.0
Sm^{3+}	$4f^5$	0.224	−0.7
Eu^{3+}	$4f^6$	7.569	4.0
Gd^{3+}	$4f^7$	31.500	0
Tb^{3+}	$4f^8$	31.853	−86
Dy^{3+}	$4f^9$	28.565	−100
Ho^{3+}	$4f^{10}$	22.642	−39
Er^{3+}	$4f^{11}$	15.382	33
Tm^{3+}	$4f^{12}$	8.210	53
Yb^{3+}	$4f^{13}$	2.589	22

Table 1.2 : Calculated values of $\langle S_z \rangle$[53] for the paramagnetic lanthanide(III) free ions at 300K and C_D,[54] scaled to −100 for dysprosium(III), taking into account excited states.

1.2.3 Pseudo–contact Shift

The pseudo–contact (dipolar) shift is a through–space interaction of the magnetic dipoles of the unpaired electrons on the lanthanide(III) ion with the nuclear magnetic moment of any proximate nuclei, and is dependent upon the magnitude of the interacting magnetic fields, their relative orientation and the distance between them. Assuming that the ligand field splittings for the lowest *J*–state are negligible

compared to kT,[55] the pseudocontact shift (in ppm) is given by **Equation 3**, where C_D is Bleaney's constant (see **Table 1.2**), $\langle r^2 \rangle A_2^0$ and $\langle r^2 \rangle A_2^2$ are second–order crystal field coefficients and the position of the chosen nucleus is given by the spherical coordinates r, θ, and φ, with the lanthanide(III) ion at the origin (see **Figure 1.1**).

$$\Delta_{pc} = C_D G = \frac{C_D \mu_B^2}{60k^2T^2}\left[\frac{\langle r^2 \rangle A_2^0 (3\cos^2\theta - 1)}{r^3} + \frac{\langle r^2 \rangle A_2^2 \sin^2\theta \cos 2\varphi}{r^3}\right] \qquad (3)$$

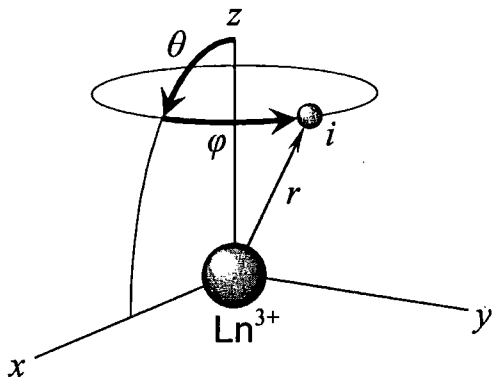

Figure 1.1 : Illustration of the spatial relationship between a nucleus *i* and a lanthanide(III) ion, positioned at the origin, as represented by the spherical coordinates θ, φ and r.

Following the combination of all the non–geometric terms, the equation can be simplified to give **Equation 4**.

$$\Delta_{pc} = D_1 \frac{3\cos^2\theta - 1}{r^3} + D_2 \frac{\sin^2\theta \cos 2\varphi}{r^3} \qquad (4)$$

For systems in which axial symmetry exists the second term becomes zero (or near zero) and **Equation 5** can be used.[56] In most cases, it is sufficient to calculate values using only the first term, even if there is no axial symmetry.

$$\Delta_{pc} = D_1 \frac{3\cos^2\theta - 1}{r^3} \qquad (5)$$

1.2.4 Separation of the Shift Contributions

In order to obtain useful information about the positions of the nuclei within the vicinity of the lanthanide(III) ion, it is necessary to isolate the pseudo–contact shift

contributions, which usually dominate, as these alone contain the geometrical data required.

Following the determination and subtraction of the diamagnetic shift contribution the LIS can be expressed as the paramagnetic shift (Δ′), given by **Equation 6**.

$$\Delta' = \Delta_c + \Delta_{pc} = \langle S_z \rangle F + C_D G \qquad (6)$$

This equation expresses the paramagnetic shift as the sum of two products, each containing a term which is characteristic of the lanthanide(III) ion, although independent upon the ligand ($\langle S_z \rangle$ and C_D), and a term for which the reverse is true (F and G). If it is assumed that the complexes of the ligand under study are isostructural, further separation of contact and pseudo contact shifts can be achieved through rearrangement of **Equation 6** to give the following equations:[57]

$$\frac{\Delta'}{\langle S_z \rangle} = F + \frac{C_D G}{\langle S_z \rangle} \qquad (7)$$

$$\frac{\Delta'}{C_D} = \frac{\langle S_z \rangle F}{C_D} + G \qquad (8)$$

This allows the determination of F and G when the paramagnetic shift (Δ′) is known for a given ligand nucleus in more than one lanthanide(III) complex, and the literature values for $\langle S_z \rangle$ and C_D are used (see **Table 1.2**). If the series of lanthanide(III) complexes of the ligand are truly isostructural, plots obtained from **Equations 7** and **8** are linear. However, changes in ionic radii across the lanthanide(III) ions often results in changes in the orientation of nuclei around the metal, inducing small changes in G, leading to breaks in the plots obtained. Such changes are amplified in **Equation 7** due to large differences between C_D values for the larger and smaller lanthanides, although since F is unaffected, **Equation 8** remains linear.[58]

1.2.5 Choice of Lanthanide(III) Ion for NMR Studies

Each of the lanthanide(III) ions behave differently under NMR conditions, as a result of their differing electronic configurations, imposing magnetic moments and

electronic relaxation times which vary across the series (**Table 1.3**). The calculated value of zero for the effective electronic magnetic moment of europium(III), results from the presence of a ground state with zero total angular momentum (J=0). However, observed values of the effective electronic magnetic moment of europium(III) are in the range 3.40–3.51 BM,[59] and are accounted for by the presence of close lying excited states which contribute to the overall electronic magnetic momentum for this ion. A similar temperature dependence occurs with samarium(III), and observed values are slightly higher than those calculated.

Lanthanide ion	Electronic configuration	μ_{eff}	τ_e (10^{-13}s)
Ce^{3+}	$4f^1$	2.54	1.1
Pr^{3+}	$4f^2$	3.58	0.62
Nd^{3+}	$4f^3$	3.62	1.4
Pm^{3+}	$4f^4$	2.68	–
Sm^{3+}	$4f^5$	0.85	0.53
Eu^{3+}	$4f^6$	0.00	0.10
Gd^{3+}	$4f^7$	7.94	10^4–10^5
Tb^{3+}	$4f^8$	9.72	2.4
Dy^{3+}	$4f^9$	10.65	3.4
Ho^{3+}	$4f^{10}$	10.61	2.2
Er^{3+}	$4f^{11}$	9.58	2.8
Tm^{3+}	$4f^{12}$	7.56	4.5
Yb^{3+}	$4f^{13}$	4.54	1.6

Table 1.3 : Calculated theoretical values of the effective electronic magnetic moments (μ_{eff}) in Bohr magnetons and the observed electronic relaxation times (τ_e) for lanthanide(III) aqua complexes at 298K, 2.7 MHz.[60]

In the application of lanthanide(III) complexes as shift reagents, it is necessary to strike a balance between the shifting ability of each lanthanide(III) ion with the associated line broadening. Since long electronic relaxation times contribute towards severe line–broadening, they are detrimental to the analysis of shifted resonances and should therefore be avoided. For example, gadolinium(III) possesses the longest electronic relaxation time in the lanthanide series, and broadening is often so severe that no spectrum can be observed.[61] It is therefore used primarily as a relaxation agent in MRI. In the analysis of protein structures by paramagnetic NMR, the distances between resonant nuclei and the lanthanide(III) ion often vary considerably. Thus, one single lanthanide(III) ion is insufficient to induce

paramagnetically shifted resonances for the entire range of nuclei. This incapability arises since lanthanide(III) ions with large magnetic anisotropies cause severe line broadening of nearby nuclei. In contrast, lanthanide(III) ions with low magnetic anisotropies produce insignificant shifts of the more distant nuclei.[62] Recently, a combination of cerium(III), ytterbium(III) and dysprosium(III) was shown to cooperatively assist in the structural refinement of a protein, with each lanthanide(III) most effective for nuclei a certain distance from the lanthanide(III) centre. The distance restraints for successful application of each lanthanide(III) ion were chosen based on a combination of the ability to detect a cross peak in HSQC experiments (ie. line broadening < 100Hz) and the maximum distance at which the paramagnetic shift was still measurable (ie. shift > 0.02 ppm).[63] This provides a measure of the effective resolution (shift relative to line broadening) obtainable using a lanthanide(III) ion as a shift reagent for nuclei a given distance from the lanthanide(III) centre, and subsequently, the most appropriate lanthanide(III) ion to use. The sign of the induced shifts observed varies across the series,[64] with Pr^{3+}, Nd^{3+}, Sm^{3+}, Tb^{3+}, Dy^{3+} and Ho^{3+} producing shifts to lower frequency, whereas Eu^{3+}, Er^{3+}, Tm^{3+} and Yb^{3+} produce higher frequency shifts.

1.3 Photophysical Properties of Lanthanide(III) Complexes

1.3.1 Effects of Electronic Structure

The tripositive lanthanide ions possess electronic configurations of the form $[Xe]f^n$, where $0 \leq n \leq 14$, and the energy levels associated with these electronic configurations are adequately accounted for using the Russell–Saunders coupling scheme. Interelectronic repulsion creates a series of spectroscopic terms $^{(2S+1)}\Gamma$, where Γ is a letter representation of the quantum number L (Γ=S, P, D, F etc., when L=0, 1, 2, 3 etc.). The exact number of states obtained depends upon the lanthanide ion, with their relative energies accounted for by Hund's rules. These rules state that the lowest energy terms are of highest spin multiplicity (2S+1) and in situations where multiplicities are equal, the term with the highest degeneracy (quantum number L) is of lowest energy. Further splitting of these electronic energy levels into J states occurs through the interaction of the electron magnetic dipole and the orbital angular

momentum (spin–orbit coupling). The relative energy of the resulting J states is again accounted for by Hund's rules; where the largest J–value produces the lowest energy state, unless the electronic sub–shell is less than half full, in which case the opposite is true. The relative energy levels and separations observed for the europium(III) ion are illustrated in **Figure 1.2**.

The lanthanide(III) ions possess filled outer shell 5s and 5p orbitals, such that the valence 4f orbitals are effectively shielded from their coordination environment. Consequently, the splitting of the J–states in the lanthanide ions due to ligand field effects is not as dramatic as in the case of the transition metals, with ligand field splitting energies typically two orders of magnitude lower than those observed for the transition metals (~10^2 cm^{-1} cf. ~10^4 cm^{-1}). This small interaction between the ligand field and 4f electrons allows only limited mixing of electronic and vibrational wavefunctions, resulting in weak electronic dipole transitions, which are formally Laporte forbidden.[65] Overall, this situation gives rise to very low extinction coefficients in absorption, long excited state lifetimes and sharp emission bands.

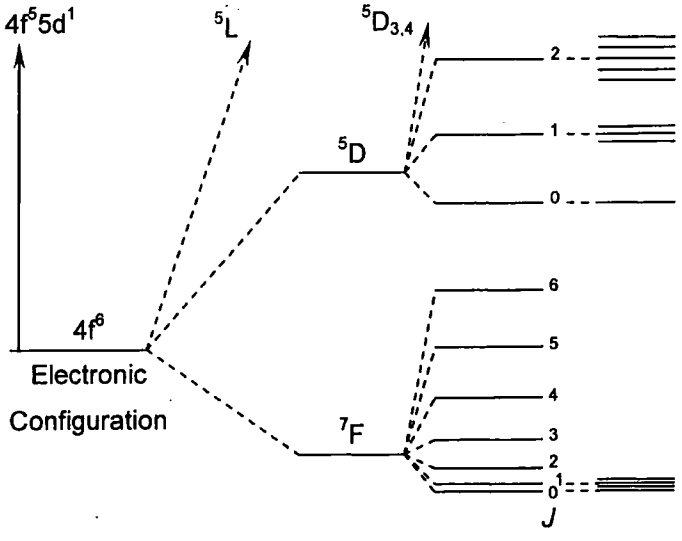

Figure 1.2 : Energy level diagram for Eu^{3+} ion illustrating the term symbols generated from interelectronic repulsion, spin–orbit coupling and ligand field effects and their relative energies predicted by Hund's rule.

1.3.2 Sensitised Emission

A major drawback resulting from the very low extinction coefficient of lanthanide(III) ions is that concentrated solutions or laser excitation are required for detailed luminescent studies. However, with careful consideration of the relative

energies involved, it is possible to make use of a suitable chromophore to populate the lanthanide(III) excited state via an energy transfer process as illustrated in **Figure 1.3**.[66] Thus, following excitation of the chromophore to the first singlet excited state, subsequent intersystem crossing yields the first triplet excited state of the chromophore. Energy transfer can then occur from the chromophore triplet state to the lanthanide(III) excited state, followed by characteristic lanthanide(III) based luminescence. Provided the energy transfer process is efficient, the use of a chromophore with a high extinction coefficient can effectively increase the rate of population of the lanthanide excited state, in comparison to direct excitation,[67] therefore overcoming the requirement for high intensity light sources.

A number of considerations are required in order to find a suitable donor for a particular lanthanide(III) ion. Most importantly, the energy of the triplet excited state, from which energy transfer occurs,[68] must be comparable in energy to the lanthanide(III) excited state, but sufficiently higher in energy to avoid competitive thermal repopulation of the chromophore triplet state.[69]

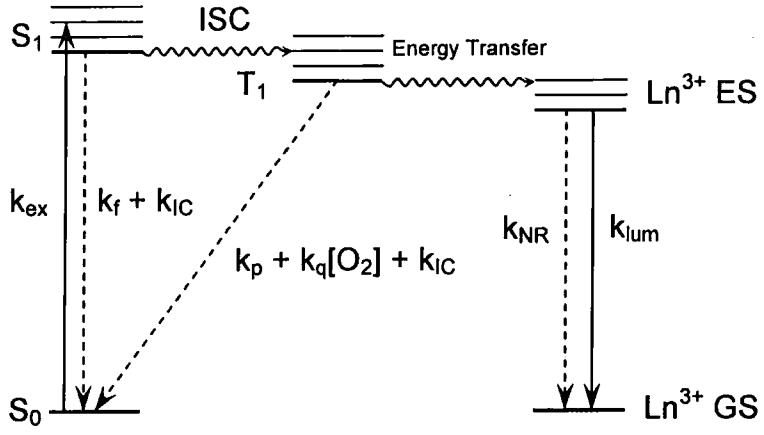

Figure 1.3 : Energy pathway for sensitised emission (solid arrows), showing the competitive deactivation processes occurring from the excited states (dashed arrows).

Secondly, the overall pathway for energy transfer via the singlet and triplet excited states of the chromophore should be as efficient as possible, and therefore minimise any of the competing processes shown in **Figure 1.3**. The efficiency of any process involving radiative decay from an excited state is defined as the quantum yield of

emission (φ_{EM}), and is simply the rate of radiative decay (k_{lum}) from the populated excited state relative to all non–radiative processes (k_{NR}).

$$\varphi_{EM} = \frac{k_{lum}}{k_{lum} + \sum k_{NR}} \qquad (9)$$

Given that the sum of all the rate constants of processes deactivating the excited state is simply the inverse of the lifetime of that state (τ_{obs}^{-1}), **Equation 9** can be written as:

$$\varphi_{EM} = k_{lum}\tau_{obs} \qquad (10)$$

However, in the situation involving sensitised emission, as illustrated in **Figure 1.3**, the emissive excited state is not obtained simply via excitation following absorption of a photon. The population of the lanthanide(III) excited state depends upon the efficiency in which the chromophore's triplet excited state is reached (φ_T) along with the efficiency of energy transfer into the lanthanide(III) excited state (η_{ET}), and the overall quantum yield is represented by **Equation 11**.[69]

$$\varphi_O = \varphi_T \eta_{ET} k_{lum}\tau_{obs} \qquad (11)$$

Thus, in order to obtain efficient sensitised emission processes, with regards to the design of the chromophore, it is necessary that the triplet energy is suitably matched and large quantum yields of triplet formation are desirable, to reduce competitive chromophore fluorescence. The quenching of lanthanide(III) emission and efficiency of energy transfer to the lanthanide(III) excited state is controlled by the ligand environment around the lanthanide(III) ion and the incorporation of the chromophore into the ligand structure, respectively (see **Section 1.3.3**).

An additional problem is encountered when applying sensitised emission within europium(III) complexes, due to the relatively low reduction potential exhibited in comparison with the other lanthanide(III) ions. This opens up the possibility for photoinduced electron transfer or ligand–to–metal charge transfer processes to occur, quenching the chromophore's singlet excited state,[70] transiently generating the europium(II) complex. Raising the oxidation potential of the chromophore via protonation,[71] or the introduction of strongly electron–withdrawing groups,[72] can

reduce the driving force for photoinduced electron transfer from the chromophore, and hence increase the overall efficiency of luminescence.

1.3.3 Quenching of Lanthanide(III) Emission

Once the lanthanide(III) excited state is populated, relaxation will occur in order to return to the ground state. Radiative deactivation occurs through the process of luminescence. However, the environment around the lanthanide(III) ion can greatly affect the competitiveness of non–radiative processes, and hence the overall quantum yield of luminescence. Nearby high frequency oscillators (notably O–H and N–H bond stretches) increase the rate of non–radiative deactivation, through mixing of the vibrational energy levels of the oscillator with the excited states of the lanthanide(III) ion.[73] The extent of this deactivation is dependent upon the oscillator frequency, and allows increased yields of luminescence to be obtained simply by deuteration of the solvent, since X–D bonds have a lower stretching frequency compared to X–H.[74] The largest effects are observed in protic media, such as water or methanol. A similar decrease in quenching due to high frequency oscillators is observed as the energy gap between the excited and ground state of the lanthanide(III) ion increases.[75] Clearly, a large energy gap between the lanthanide(III) excited and ground states increases the number of oscillator harmonics required to couple with the lanthanide(III) excited state. Given that the vibrational transition intensity is proportional to the square of the overlap integral between the initial and final vibrational states, as the number of harmonics increases, the efficiency of quenching decreases.[76] Thus, lanthanide(III) ions with small energy gaps are more readily quenched. A similar conclusion can be found when considering oscillators with lower frequencies. This leads to a useful method for determining the hydration number of the lanthanide(III) ion, through measurement of the relative rate of radiative decay in both H_2O and D_2O.[77]

$$k_{H_2O} = k_{nat} + k_{nr} + \sum k_{XH} + \sum k_{C=O} \qquad (12)$$

$$k_{D_2O} = k_{nat} + k_{nr} + \sum k_{C=O} \qquad (13)$$

The rates of deactivation from the lanthanide(III) excited state in H_2O and D_2O are represented by **Equations 12** and **13**, respectively, based on the assumption that all exchangeable X–H oscillators do not contribute in D_2O, where k_{nat} and k_{nr} are the

natural and non–radiative rate constants and $\sum k_{XH}$ and $\sum k_{C=O}$ are the total rates of quenching by proximate X–H and C=O oscillators. The difference in the values of rate constants measured in H_2O and D_2O are therefore representative of the rate of quenching caused by proximate X–H oscillators (**Equation 14**).

$$\Delta k = k_{H_2O} - k_{D_2O} = \sum k_{XH} \qquad (14)$$

Thus, following careful analysis of a series of complexes it is possible to anticipate the contributions towards Δk from non–coordinated second sphere O–H oscillators ($-0.25\ ms^{-1}$ and $-0.06\ ms^{-1}$ for Eu and Tb respectively) and all other X–H oscillators in the complex, yielding Δk_{cor}. Subsequent inclusion of a proportionality constant, A (1.2 ms and 5 ms for Eu and Tb), which accounts for the rate of quenching for each bound water molecule allows the hydration state, q, of the complex to be estimated (**Equation 15**).

$$q = A(\Delta k_{corr}) \qquad (15)$$

For complexes in which the number of metal bound water molecules is greater than zero, the displacement of directly bound water molecules by anions can be monitored using the same principle (also see **Section 1.4.2**).

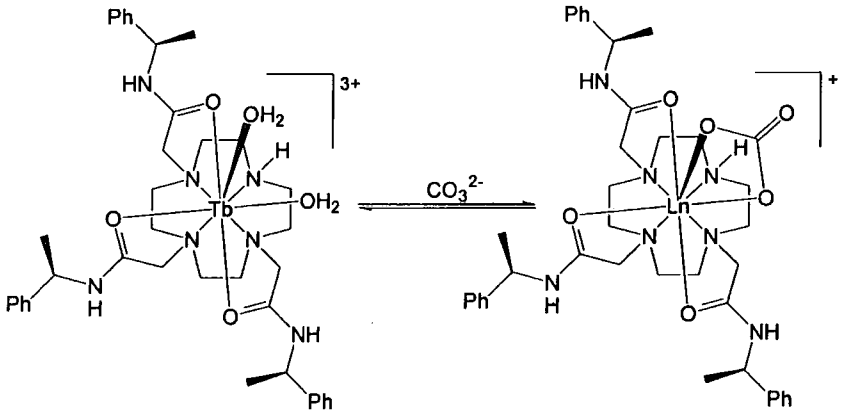

$k_{H_2O} = 0.82\ ms^{-1}$, $k_{D_2O} = 0.39\ ms^{-1}$
$\Delta k_{corr} = 0.39\ ms^{-1}$, $q = 2.0$

$k_{H_2O} = 0.53\ ms^{-1}$, $k_{D_2O} = 0.45\ ms^{-1}$
$\Delta k_{corr} = 0.02\ ms^{-1}$, $q = 0.1$

Scheme 1.2 : Binding of a carbonate anion to [Tb**DO3Ph**]$^{3+}$, illustrating the chelated binding mode predicted from changes in the rate of radiative decay to give the hydration state estimation.

For example, lanthanide(III) complexes of the macrocyclic ligand **DO3Ph** possess two labile water molecules in the coordination sphere. Monitoring the increase in the

rate of radiative decay upon addition of several anions to [Tb**DO3Ph**]$^{3+}$ can be used to determine whether or not anion binding has occurred, and if there are any coordinated water molecules remaining in the ternary anion complex.[78] When a hydration state is found to be approximately zero, e.g. for complexes bound to carbonate, lactate and acetate, such evidence suggests a chelated binding mode is adopted, in which both water molecules are displaced from the coordination sphere (**Scheme 1.2**). Subsequent X–ray structural analyses have led to the confirmation of these results.[79]

1.3.4 Choice of Lanthanide(III) Ion for Luminescent Studies

The suitability of the individual lanthanide(III) ions for a particular luminescent study is determined by the nature of the environment in which the study will be undertaken. Thus the lanthanide(III) ions with the largest energy gaps between the excited and ground states (Gd > Tb > Eu) are suitable for use in most environments, as they are less susceptible to quenching from nearby high frequency oscillators. However, the difficulty of selective excitation and the very high energy UV emission from gadolinium(III) leads to little practical use, such that europium(III) and terbium(III) are the most commonly favoured out of all the lanthanides.

Europium(III) is unique amongst the lanthanide(III) ions in that the $^5D_0$ emissive state is non–degenerate, so that the transitions observed are only dependent upon the splitting of the ^7F_J ground states. The $^7F_0$ state is also non–degenerate and thus only one very weak transition, $^7F_0 \leftarrow {}^5D_0$, is observed for each unique europium(III) excited state species.[80] The $^7F_1$ state can split into a maximum of three components in the presence of a ligand field, and although the oscillator strength of the magnetic dipole allowed transitions to this level are relatively independent of the coordination environment, the splitting pattern can provide useful information about the symmetry and ligand field strength around the europium(III) ion.[81] The electric dipole nature of the $^7F_2 \leftarrow {}^5D_0$ transition, results in an oscillator strength which is highly dependent upon the mixing of ligand states to induce the normally parity forbidden transitions.[82] This *hypersensitivity* allows the transition to be used as a probe for the environment around the europium(III) centre.

Despite exhibiting short luminescent lifetimes and low quantum yields, there has

been an increased interest in the near–IR emissive lanthanides, particularly neodymium(III) and ytterbium(III). The main impetus behind such work lies in the fairly transparent nature of biological tissue to the wavelengths involved in the excitation and emission of such complexes. Although under normal conditions the neodymium(III) ion displays very weak solution state luminescence, due to quenching resulting from a very small energy gap, relatively intense luminescence has been demonstrated through careful choice of ligand and solvent in order to minimise the occurrence of vibrational quenching due to nearby C–H, O–H and N–H bonds.[83] Ytterbium(III) is rare amongst the lanthanides in that only one emission band is observed, centred at 970 nm, due to the $^2F_{5/2} \rightarrow {}^2F_{7/2}$ transition. This transition is of higher energy than the lowest energy emission from neodymium(III), and thus is a more practically useful near–IR emissive lanthanide. Another attractive feature of ytterbium(III) is the sensitivity of the observed emission to the circular polarisation of the exciting radiation.[84]

1.4 Properties of Lanthanide(III) Complexes

The coordination chemistry of the lanthanide(III) ions is characterised by a large and variable coordination number, along with a distinct preference for hard bases as donors, such as oxygen and nitrogen atoms. As a result of this, mono–dentate ligands have difficulty displacing the coordinated water molecules in aqueous solution. However, lanthanide(III) complexes based on the macrocyclic ligands derived from the **DOTA** framework, form extremely thermodynamically and kinetically stable complexes.[85,86]

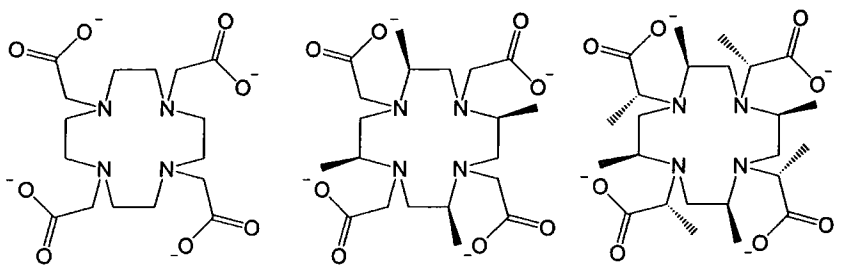

DOTA **M4DOTA** **M4DOTAM**

The macrocyclic ring adopts a very stable [3333] quadrangular conformation, in which all the methylene hydrogen atoms are staggered and the four nitrogen atoms

point towards the metal centre. Combined with the four ionisable acetate groups, the ligand forms a sterically demanding and rigid cavity for the lanthanide(III) ion.[87] The four nitrogen donors and four oxygen donors in these complexes form two planes, one above and one below the lanthanide(III) centre, and are axially symmetric exhibiting C_4–symmetry in the solid state.[88] Corresponding analysis of paramagnetically induced ^{1}H NMR shifts of [Ln**DOTA**]$^-$ complexes infer that the same structure exists in solution as in the solid state.[85] The lanthanide(III) complexes of the octadentate **DOTA** ligand are usually 9–coordinate due to a capping water molecule.[89] However, postulations into the existence of an 8–coordinate structure have recently been confirmed by X–ray analysis for the smaller lanthanide(III) ions.[90]

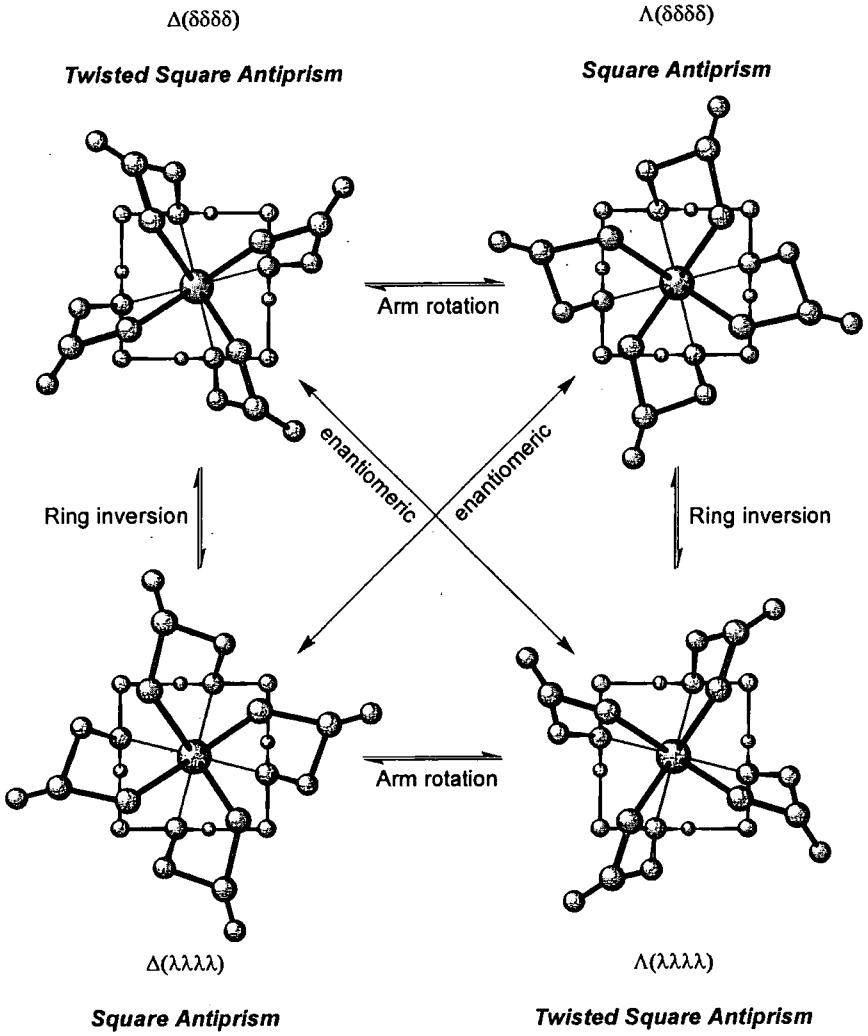

Figure 1.4 : Illustration of the two enantiomeric pairs of diastereoisomers of Ln(**DOTA**)$^-$ observed in solution and their interconversion via ring inversion and arm rotation.

In solution lanthanide(III) complexes of **DOTA** can exist in up to four stereoisomeric forms.[91] These four stereoisomers arise from the two different torsion angles in the complex. The first is associated with the two possible configurations of the macrocyclic ring, with the NCCN torsion angle of each ethylene diamine chelate being either cooperatively positive or negative ($\delta\delta\delta\delta$ and $\lambda\lambda\lambda\lambda$ respectively).[92] The second occurs due to the two possible orientations of the pendant acetate groups, with the NCCO torsion angle being either positive or negative (Δ or Λ respectively). Thus, in solution the lanthanide(III) complexes of **DOTA** derivatives exist as a mixture of two enantiomeric pairs of diastereoisomers (See **Figure 1.4**). Interconversion between these geometries is achieved either via ring inversion or arm rotation.[93] When the ring and pendant arms are of opposite configuration ($\Delta(\lambda\lambda\lambda\lambda)$ and $\Lambda(\delta\delta\delta\delta)$) a square antiprismatic structure results. Complementary configurations of both pendant arm and ring ($\Lambda(\lambda\lambda\lambda\lambda)$ and $\Delta(\delta\delta\delta\delta)$), results in a twisted square antiprismatic geometry and is found to be the more favourable isomeric structure for the larger lanthanides.[93,94]

Inhibition of the observed interconversion between geometries in solution is desired in order to facilitate the use of such lanthanide(III) complexes for analytical purposes, since each diastereoisomer displays different physical properties. Alterations to the ligand structure can be used to further increase the rigidity of the solution structure, therefore preventing interconversion between different geometries. For example introduction of methyl groups into the macrocyclic ring, as in **M4DOTA**, produces a complex retaining C_4–symmetry where ring inversion is impeded. Further modification of **M4DOTA**, via introduction of a methyl group onto each acetate arm, as in **M4DOTAM**, produces a totally rigid structure. The rigidity of **M4DOTAM** is such that in addition to restricting ring inversion, arm rotation is also impeded, and only one isomer is observed in solution.[95]

1.4.1 Effect of Axial Donor in Axially Symmetric Lanthanide(III) complexes

Investigations involving the corresponding amide derivatives of **DOTA**, such as the chiral **DOTAMPh** ligand, revealed that a chiral centre δ to the ring nitrogen not only impairs arm rotation, introducing considerable conformational rigidity, but also leads to the favouring of one major isomer in solution.[96] Consequently, the structural

analysis of ^{1}H NMR spectra of such complexes is simplified, due to the lack of interference from resonances of conformational isomers. The simple interpretation of these spectra has allowed the assessment of changes in the electronic and magnetic properties of the lanthanide(III) centre upon variation of the axial ligand.[97] In acetonitrile solution, the axial donor ligand of europium and ytterbium **DOTAMPh** complexes is the nitrogen bound acetonitrile molecule, which is easily displaced by various competitive ligands.

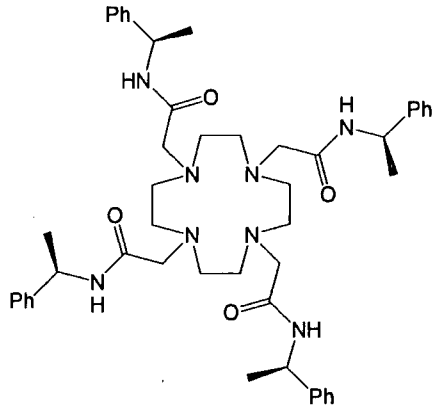

***(RRRR)*–DOTAMPh**

Variation of the axial donor ligand produced differences in the ^{1}H NMR spectral widths as a consequence of the proportionally shifted resonances, suggesting retention of the square antiprismatic structure.[98]

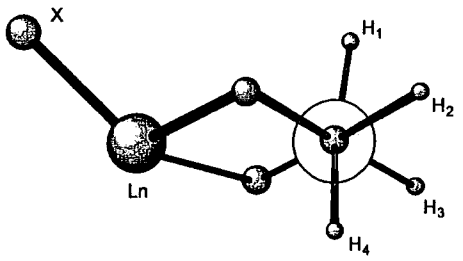

Figure 1.5 : Relative orientations of the diastereotopic cyclen ring protons in one ethylene diamine chelate in the macrocyclic ligand when complexed to the lanthanide(III) centre, viewed along the ethylene C–C bond. X corresponds to the position of the axial donor ligand.

The axial H_4 proton (see **Figure 1.5**) is shifted most and is particularly sensitive to variation of the axial ligand. These shifts, when plotted against the splitting in the $\Delta J = 1$ luminescence emission band of the corresponding europium(III) complex, produced a linear correlation. The splitting of this magnetic–dipole allowed transition for europium(III) complexes, provides a measure of the second order crystal field

parameter, which, in turn, is related to the magnetic anisotropy of the lanthanide(III) ion, through Bleaney's theory (**Equation 3**).[99,100] Hence, the axial ligand has a direct influence upon the magnetic anisotropy of the central lanthanide(III) ion.

Theory also predicts that the intensity of a hypersensitive transition should be proportional to the square of the ligand polarisability.[101] Therefore, increases in the relative intensities of the hypersensitive $\Delta J = 2$ to $\Delta J = 1$ emission bands for europium(III), as a function of added donor ligand, provided a good correlation with the axial donor polarisability. Thus, the more polarisable the axial donor ligand, the greater the overall ^{1}H NMR spectral width, the larger the $\Delta J = 2$ to the $\Delta J = 1$ intensity ratio, and the greater the affinity of the donor for the lanthanide(III) centre.[98]

1.4.2 Interaction of Lanthanide(III) Complexes with Bioactive Anions

In aqueous solutions, the displacement of the single bound water molecule from lanthanide(III) complexes of octadentate ligands is very difficult, and only excess fluoride ions have been shown to do this.[94] However, the bound water molecules in coordinatively unsaturated lanthanide(III) complexes are relatively easily displaced. The displacement of these water molecules can be followed by observing the accompanying increase in luminescence intensity, which is associated with the reduced quenching due to the bound O–H oscillators.[102,103] For example, one of the two bound water molecules of lanthanide(III) complexes of heptadentate ligands, such as **DO3Ph**, are relatively easily displaced by fluoride anions.[104] The europium complex of the octadentate Lehn cryptand has recently been shown to be coordinatively unsaturated, with 2.5 water molecules estimated in the coordination sphere. Displacement of two of these water molecules by fluoride anions was observed, due to the increase in intensity and the change in emission spectral form.[103] There is an additional benefit when using neutral ligands, in that the resulting lanthanide(III) complexes are cationic, producing strong Coulombic interactions, and hence have a greater affinity for anionic species.[103,105] Similarly, the complexes of the smaller, more charge dense lanthanide(III) ions also exhibit an increased affinity for anions. Binding of selected bioactive anions has been monitored for complexes of

DO3Ph with europium(III),[79,105,106] gadolinium(III),[79,104] terbium(III)[106] and ytterbium(III).[79,107]

^{1}H NMR spectra of [Eu**DO3Ph**]$^{3+}$ and [Yb**DO3Ph**]$^{3+}$ in aqueous solution, reveal a single major species at room temperature, although the lack of rigidity compared to complexes of **DOTAMPh** is evidenced by the presence of one major and three minor stereoisomers at −20°C.[106] The lower axial symmetry observed for these complexes leads to a significant number of resonances in the proton NMR spectra, when compared to the corresponding **DOTAMPh** complexes. The four inequivalent axial protons (H_4, see **Figure 1.5**) are easily distinguished in most cases and possess the highest frequency resonances and larger line widths, as a result of the large geminal coupling to H_3 and the large trans–diaxial coupling to H_1.

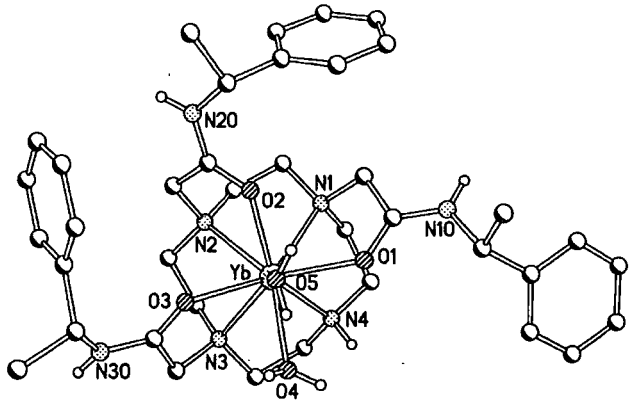

(RRR)– [Yb**DO3Ph**$(H_2O)_2$]$^{3+}$

The addition of less than one equivalent of various anions (see **Table 1.4**) to [Yb**DO3Ph**]$^{3+}$ gave rise to a new set of resonances, corresponding to the anion bound adduct. Further additions of anion led to an increase in the intensity of the new set of resonances, and ultimately complete disappearance of the resonances for the di–aqua complex, suggesting that the anion is in slow exchange with the di–aqua complex on the NMR timescale.[107] The chemical shifts of the four inequivalent axial protons, were found to be particularly sensitive to the anion coordinating to the lanthanide(III) centre. In particular, the average of the four axial proton shifts was found to correlate well with the polarisability of the axial ligand (**Table 1.4**),[105] as expected when compared to **DOTAMPh** complexes.[98] The unusually low average axial proton shift for hydrogen carbonate was originally attributed to a change in

geometry to a twisted square antiprism.[104] However, this was later shown to be due to the high polarisability of the bound carbonate oxygens. The presence of anions also perturbs the luminescence quantum yields to higher values, since the anions displace one or two quenching water molecules. Measurement of the hydration state of the lanthanide(III) centre allows differentiation between non–chelating and chelating anions, in suggesting possible anion binding modes (**Section 1.3.3**).

Anion	Axial donor	δH_{ax} (average)/ ppm	q^{Yb}
None (H_2O)	OH_2	75	2.00
Acetate	$C–O^{\delta-}$	68	0.13
Oxalate	$C–O^-$	37	0.10
Lactate	ROH	71	0.29
Hydrogen phosphate	OH_2	100	0.82
Hydrogen carbonate	$C–O^-$	27	0.34
Fluoride	OH_2	99	0.85
Serinate (pH 10)	RNH_2	43	0.33
Glycinate (pH 10)	$R'NH_2$	43	0.36

Table 1.4 : Variation of anion and the respective changes in axial donor, average shift of the four axial proton resonances and calculated hydration state, q, for [Yb**DO3Ph**]$^{3+}$.

More recent work has focused on the interaction of all twenty amino acids with [Yb**DO3Ph**]$^{3+}$.[107] As previously determined for serine and glycine,[105] the amino acids were found to form chelated adducts with the amino–group as the axial donor. However, following recent ^{1}H NMR studies, the adduct formed with 15 of the amino acids was found to exist as two species in solution, with ratios dependent upon the amino acid (see **Table 1.5**).

Amino acid	$\Lambda(\delta\delta\delta\delta):\Lambda(\lambda\lambda\lambda\lambda)$	Amino acid	$\Lambda(\delta\delta\delta\delta):\Lambda(\lambda\lambda\lambda\lambda)$
Gly	2:1	Glu	6:1
Ala	3:1	Asn	9:1
Val	5:1	Gln	5:1
Leu	4:1	Lys	2:1
Ile	3:1	Arg	2:1
Ser	>19:1	Phe	4:1
Thr	>19:1	Tyr	7:1
Cys	6:1	Pro	10:1
Met	2:1	His	>19:1
Asp	>19:1	Trp	>19:1

Table 1.5 : Relative ratios of diastereoisomers observed in solution for S–amino acid adducts of [Yb**DO3Ph**]$^{3+}$.

The shifts of both species were consistent with square antiprismatic geometries, namely *RRR*–Δ(*λλλλ*) and *RRR*–Λ(*δδδδ*) (which are diastereomeric), and were confirmed from the crystal structures obtained. The *RRR*–Λ(*δδδδ*) isomer has an open geometry in which the phenyl rings are equatorially arranged, whereas in the *RRR*–Δ(*λλλλ*) isomer the phenyl groups are oriented axially, creating a hydrophobic cavity for inclusion of the amino acid side chain (**Figure 1.6**). For the five remaining amino acids (Ser, Thr, Asp, His, Trp), each ternary complex exists as only one species, namely the *RRR*–Λ(*δδδδ*) isomer.

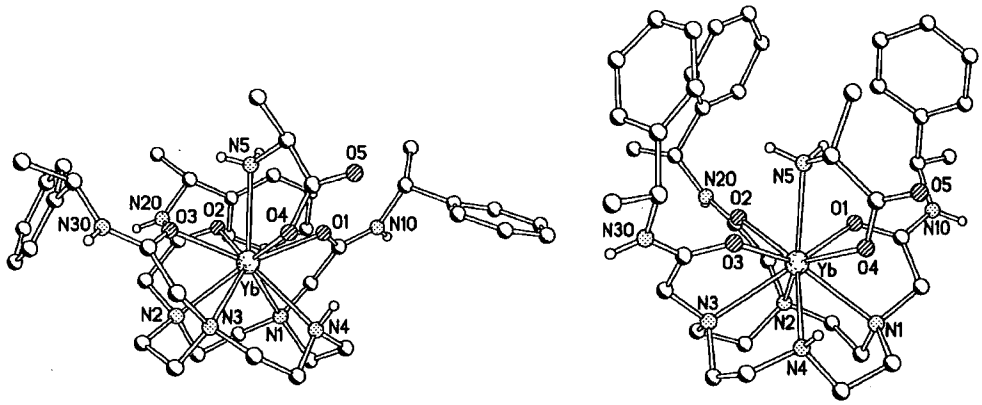

Figure 1.6 : Crystal structures of [Yb**DO3Ph**]$^{3+}$ in the presence of *S*–alanine (left) and *R*–alanine (right), illustrating the equatorial arrangement of phenyl groups in the corresponding *RRR*–Δ(*λλλλ*) isomer and the axial arrangement of phenyl groups, forming a hydrophobic cavity, in the *RRR*–Λ(*δδδδ*) isomer.[107]

Correlations were observed between the ratio of each isomer in solution and the nature of the amino acid side chain, suggesting that side chains which are sterically bulky or for which there is the potential for hydrogen bonding with the solvent, will prefer to adopt the more 'open' *RRR*–Λ(*δδδδ*) geometry. For example, moving from Gly through Ala to Val, the side chain increases from hydrogen to methyl to isopropyl and correspondingly, the increase in steric requirements disfavours the axially orientated phenyl groups. Similarly, as the hydrogen bonding group becomes more distant from the binding amino chelate, hydrogen bonding may still occur even with the phenyl groups axial, and a lesser preference is seen for the more 'open' geometry (compare Glu and Asn).

1.5 Summary

Research focusing on the selective binding of anions in solution is a relatively new field when compared to the wealth of information known about cation binding. In particular, the problems associated with the large free energies of hydration of the common oxyanions, such as hydrogen phosphate, have also hindered the development of suitable receptors which can operate in aqueous conditions. As a result of this, although many examples of novel anion receptors have recently appeared in the literature, with designs ranging from simple organic fluorophores to well–defined metal complexes, only a few of these exhibit strong binding to phosphorylated anions in aqueous solution. Moreover, the presence of lanthanide based receptors for phosphorylated anions is particularly rare and in most cases the binding of phosphate is essentially irreversible.[38–40] Thus, the work presented in the following chapters investigates the suitability of well–defined lanthanide complexes in order to achieve the reversible chemoselective sensing of phosphorylated anions.

1.6 References

1 Y. Marcus, *J. Chem. Soc., Faraday Trans.*, 1991, **87**, 2995.

2 E. Graf and J.–M. Lehn, *J. Am. Chem. Soc.*, 1976, **98**, 6403.

3 B. Dietrich, T. M. Fyles, J.–M. Lehn, L. G. Pease and D. L. Fyles, *J. Chem. Soc., Chem. Commun.*, 1978, 934.

4 F. P. Schmidtchen, *Tet. Lett.*, 1990, **31**, 2269.

5 P. Schießl and F. P. Schmidtchen, *Tet. Lett.*, 1993, **34**, 2449.

6 M. Albrecht, T. M. de Groot, M. Bahr and E. Weinhold, *Synlett*, 2005, 2095.

7 H. Luecke and F. A. Quiocho, *Nature*, 1990, **347**, 402.

8 K. Worm and F. P. Schmidtchen, *Angew. Chem. Int. Ed. Engl.*, 1995, **34**, 65.

9 H. Lu, W. Xu, D. Zhang and D. Zhu, *Chem. Commun.*, 2005, 4777.

10 P. V. Bernhardt and N. L. Creevey, *Dalton Trans.*, 2004, 914.

11 S. Sasaki, S. Ozawa, D. Citterio, K. Yamada and K. Suzuki, *Talanta*, 2004, **63**, 131; W. Wróblewski, K. Wojciechowski, A. Dybko, Z. Brzózka, R. J. M. Egberink, B. H. M. Snellink–Ruël and D. N. Reinhoult, *Sens. Actuators B*, 2000, **68**, 313.

12 P. M. Goodwin, W. P. Ambrose and R. A. Keller, *Acc. Chem. Res.*, 1996, **29**, 607.

13 W. Tan, Z.–Y. Shi, S. Smith, D. Birnbaum and R. Kopelman, *Science*, 1992, **258**, 778.

14 C. Yin, F. Gao, F. Huo and P. Yang, *Chem. Commun.*, 2004, 934.

15 C. Li and W.–T. Wong, *Tet. Lett.*, 2004, **45**, 6055.

16 For recent examples see: T. Gunnlaugsson, H. Dato P. Ali, M. Glynn, P. E. Kruger, G. M. Hussey, F. M. Pfeffer, C. M. G. dos Santos and J. Tierney, *J. Fluorescence,* 2005, **15**, 287; R. Martínez–Máñez and F. Sancenón, *Chem. Rev.*, 2003, **103**, 4419.

17 P. D. Beer and J. Cadman, *New J. Chem.*, 1999, **23**, 347; Y. Amao, Y. Ishikawa and I. Okura, *Anal. Chim. Acta*, 2001, **445**, 172; T. Mizuno, M. Takeushi, I. Hamachi, K. Nakashima and S. Shinkai, *J. Chem. Soc., Perkin Trans. 2*, 1998, 2281.

18 M. F. Reid and F. S. Richardson, *J. Phys. Chem.*, 1984, **88**, 3579.

19 S. K. Gujar, S. Maheshwari, I. Björkman–Burtscher and P. C. Sundgren, *J. Neuro–Ophthalmol*, 2005, **25**, 217.

20 D. D. Perrin, *Ionisation Constants of Inorganic Acids and Bases in Aqueous Solution*, Second Edition, Pergamon, Oxford, 1982.

21 J. A. Adams, *Chem. Rev.*, 2001, **101**, 2271.

22 X.–L. Zhan, M. J. Wishart and K.–L. Guan, *Chem. Rev.*, 2001, **101**, 2477.

23 M. D. Haskell, J. K. Slack, J. T. Parsons and S. J. Parsons, *Chem. Rev.*, 2001, **101**, 2425.

24 J. Murphy and J. P. Riley, *Anal. Chim. Acta*, 1962, **27**, 31.

25 L. Drummond and W. Maher, *Anal. Chim. Acta*, 1995, 302, 69.

26 K. Grudpan, P. Ampan, Y. Udnan, S. Jayasvati, S. Lapanantnoppakhun, J. Jakmunee, G.D. Christian and J. Ruzicka, *Talanta*, 2002, **58**, 1319.

27 V. K. Gupta, R. Ludwig and S. Agarwal, *Anal. Chim. Acta*, 2005, **538**, 213.

28 H. Aoki, K. Hasegawa, K. Tohda and Y. Umezawa, *Biosensors & Bioelectronics*, 2003, **18**, 261.

29 P. Schiessl and F. P. Schmidtchen, *J. Org. Chem.*, 1994, **59**, 509.

30 K. P. Xiao, P. Bühlmann and Y. Umezawa, *Anal. Chem.*, 1999, **71**, 1183.

31 H. Nakamura, K. Ikebukuro, S. M^{c}Niven, I. Karube, H. Yamamoto, K. Hayashi, M. Suzuki and I. Kubo, *Biosensors & Bioelectronics*, 1997, **12**, 959.

32 H. Nakamura, M. Hasegawa, Y. Nomura, Y. Arikawa, R. Matsukawa, K. Ikebukuro and I. Karube, *J. Biotechnol.*, 1999, **75**, 127.

33 C. Hung Tzang, R. Yuan and M. Yang, *Biosens. Bioelectron.*, 2001, **16**, 211.

34 M. Mann, R. C. Hendrickson and A. Pandey, *Annu. Rev. Biochem.*, 2001, **70**, 437.

35 W. Li, R. A. Boykins, P. S. Backlund, G. Wang and H–C. Chen, *Anal. Chem.*, 2002, **74**, 5701.

36 A. Ojida, Y. Mito–oka, M.–aki Inoue and I. Hamachi, *J. Am. Chem. Soc.*, 2002, **124**, 6256.

37 A. Ojida, Y. Mito–oka, K. Sada and I. Hamachi, *J. Am. Chem. Soc.*, 2004, **126**, 2454.

38 K. Kimpe, W. D'Olieslager, C. Görller–Walrand, A. Figueirinha, Z. Kovács and C. F. G. C. Geraldes, *J. Alloys Compds.*, 2001, **323**, 828.

39 S.–H. Li, C.–W. Yu, W.–T. Yuan and J.–G. Xu, *Anal. Sci.*, 2004, **20**, 1375.

40 S.–H. Li, W.–T. Yuan, C.–Q. Zhu and J.–G. Xu, *Anal. Biochem.*, 2004, **331**, 235.

41 T. Gunnlaugsson, R. J. H. Davies, P. E. Kruger, P. Jensen, T. M^{c}Cabe, S. Mulready, J. E. O'Brien, C. S. Stevenson and A.–M. Fanning, *Tet. Lett.*, 2005, **46**, 3761; E. Longhinotti, J. B. Domingos, P. L. F. da Silva, B. Szpoganicz and F. Nome, *J. Phys. Org. Chem.*, 2005, **18**, 167; T. Gunnlaugsson, R. J. H. Davies, M. Nieuwenhuyzen, J. E. O'Brien, C. S. Stevenson and S. Mulready, *Polyhedron*, 2003, **22**, 711; C. A. Chang, B. H. Wu and B. Y. Kuan, *Inorg. Chem.*, 2005, **44**, 6646.

42 C. C. Hinckley, *J. Am. Chem. Soc.*, 1969, **91**, 5160.

43 R. S. Dickins, C. Love and H. Puschmann, *Chem. Commun.*, 2001, 2308.

44 J. M. Coxon, J. R. A. Cambridge and S. G. C. Nam, *Org. Lett.*, 2001, **3**, 4225.

45 R. D. Shannon, *Acta Cryst.*, 1976, **A 32**, 751.

46 T. C. Williams, D. C. Corson and B. D. Sykes, *J. Am. Chem. Soc.*, 1984, **106**, 5698.

47 M. Allegrozzi, I. Bertini, M. B. L. Janik, Y.–M. Lee, G. Liu and C. Luchinat, *J. Am. Chem. Soc.*, 2000, **122**, 4154.

48 J. A. Peters, J. Huskens and D. J. Raber, *Prog. Nucl. Magn. Reson. Spectrsc.*, 1996, **28**, 283.

49 J. Lisowski, J. L. Sessler and T. D. Mody, *Inorg. Chem.*, 1995, **34**, 4336.

50 J. A. Peters, M. S. Nieuwenhuizen and D. J. Raber, *J. Magn. Reson.*, 1985, **65**, 417.

51 I. Bertini and C. Luchinat, *Coord. Chem. Rev.*, 1996, **150**, 29.

52 R. M. Golding and M. P. Halton, *Aust. J. Chem.*, 1972, **25**, 2577.

53 A. A. Pinkerton, M. Rossier and S. Spiliadis, *J. Magn. Reson.*, 1985, **64**, 420.

54 B. Bleaney, C. M. Dobson, B. A. Levine, R. B. Martin, R. J. P. Williams and A. V. Xavier, *J. Chem. Soc. Chem. Commun.*, 1972, 791.

55 B. Bleaney, *J. Magn. Reson.*, 1972, **8**, 91.

56 J. M. Briggs, G. P. Moss, E. W. Randall and K. D. Sales, *J. Chem. Soc., Chem. Commun.*, 1972, 1180.

57 J. Reuben and G. A. Elgavish, *J. Magn. Reson.*, 1980, **39**, 421.

58 M. Singh, J. J. Reynolds and A. D. Sherry, *J. Am. Chem. Soc.*, 1983, **105**, 4172.

59 H. Gysling and M. Tsutsui, *Adv. Organomet. Chem.*, 1970, **9**, 361.

60 B. M. Alsaadi, F. J. C. Rossotti and R. J. P. Williams, *J. Chem. Soc., Dalton Trans.*, 1980, 2147; I. Bertini, P. Turano and A. J. Vila, *Chem. Rev.*, 1993, **93**, 2833.

61 S. Aime, A. Barge, M. Botta, A. S. de Sousa and D. Parker, *Angew. Chem. Int. Ed.*, 1998, **37**, 2673.

62 C. F. G. C. Geraldes and C. Luchinat, *Metal Ions in Biological Systems*, **Volume 40**, 2003, Chapter 14.

63 M. Allegrozzi, I. Bertini, M. B. L. Janik, Y.–M. Lee, G. Liu and C. Luchinat, *J. Am. Chem. Soc.*, 2000, **122**, 4154.

64 W. DeW. Horrocks and J. P. Sipe, *J. Am. Chem Soc.*, 1971, **93**, 6800.

65 J. H. Van Vleck, *J. Phys. Chem.*, 1937, **41**, 67.

66 S. I. Weissman, *J. Chem. Phys.*, 1942, **10**, 214.

67 F. J. Steemers, W. Verboom, D. N. Reinhoudt, E. B. van der Tol and J. W. Verhoeven, *J. Am. Chem. Soc.*, 1995, **117**, 9408.

68 G. A. Crosby, R. E. Whan and R. M. Alire, *J. Chem. Phys.*, 1961, **34**, 743.

69 D. Parker and J. A. G. Williams, *J. Chem. Soc. Perkin Trans. 2*, 1996, 1581.

70 N. Sabbatini, M. T. Indelli, M. T. Gandolfi and V. Balzani, *J. Phys. Chem.*, 1982, **86**, 3585.

71 I. M. Clarkson, A. Beeby, J. I. Bruce, L. J. Govenlock, M. P. Lowe, C. E. Mathieu, D. Parker and K. Senanayake, *New J. Chem.*, 2000, 377.

72 R. S. Dickins, J. A. K. Howard, C. L. Maupin, J. M. Moloney, D. Parker, J. P. Riehl, G. Siligardi and J. A. G. Williams, *Chem. Eur. J.*, 1999, **5**, 1095.

73 J. L. Kropp and M. W. Windsor, *J. Chem. Phys.*, 1965, **42**, 1599.

74 J. L. Kropp and M. W. Windsor, *J. Chem. Phys.*, 1963, **39**, 2769.

75 W. Siebrand, J. *Chem. Phys.*, 1967, **46**, 440.

76 G. Stein and E. Würzberg, *J. Chem. Phys.*, 1975, **62**, 208.

77 A. Beeby, I. M. Clarkson, R. S. Dickins, S. Faulkner, D. Parker, L. Royle, A. S. de Sousa, J. A. G. Williams and M. Woods, *J. Chem. Soc., Perkin Trans. 2*, 1999, 493.

78 J. I. Bruce, R. S. Dickins, L. J. Govenlock, T. Gunnlaugsson, S. Lopinski, M. P. Lowe, D. Parker, R. D. Peacock, J. J. B. Perry, S. Aime and M. Botta, *J. Am. Chem. Soc.*, 2000, **122**, 9674.

79 R. S. Dickins, S. Aime, A. S. Batsanov, A. Beeby, M. Botta, J. I. Bruce, J. A. K. Howard, C. S. Love, D. Parker, R. D. Peacock and H. Puschmann, *J. Am. Chem. Soc.*, 2002, **124**, 12697.

80 M. Latva, H. Takalo, V.–M. Mukkalaand J. Kankare, *Inorg. Chim. Acta*, 1998, **267**, 63.

81 D. R. Foster and F. S. Richardson, *Inorg. Chem.*, 1983, **22**, 3996.

82 A. F. Kirby, D. Foster and F. S. Richardson, *Chem. Phys. Lett.*, 1983, **95**, 507.

83 Y. Hasegawa, K. Murakoshi, Y. Wada, S. Yanagida, J.–H. Kim, N. Nakashima and T. Yamanaka, *Chem. Phys. Lett.*, 1996, **248**, 8.

84 F. S. Richardson, *Inorg. Chem.*, 1980, 2806.

85 J. F. Desreux, *J. Am. Chem. Soc.*, 1980, **19**, 1319.

86 M. F. Loncin, J. F. Desreux and E. Merciny, *Inorg. Chem.*, **25**, 2646.

87 J. F. Desreux and M. F. Loncin, *Inorg. Chem.*, 1986, **25**, 69.

88 M.–R. Spirlet, J. Rebizant, J. F. Desreux and M.–F. Loncin, *Inorg. Chem.*, 1984, **23**, 359.

89 J. A. Peters, J. Huskens and D. J. Raber, *Prog. Nucl. Magn. Reson. Spectrsc.*, 1996, **28**, 283.

90 F. Benetollo, G. Bombieri, L. Calabi, S. Aime and M. Botta, *Inorg. Chem.*, 2003, **42**, 148.

91 D. Parker, R. S. Dickins, H. Puschmann, C. Crossland and J. A. K. Howard, *Chem. Rev.*, 2002, **102**, 1977.

92 E. J. Corey and J. C. Bailar, *J. Am. Chem. Soc.*, 1959, **81**, 2620.

93 S. Aime, M. Botta and G. Ermondi, *Inorg. Chem.*, 1992, **31**, 4291

94 S. Aime, M. Botta M. Fasano, M. P. M. Marques, C. F. G. C. Geraldes, D. Pubanz and A. E. Merbach, *Inorg. Chem.*, 1997, **36**, 2059. X

95 R. S. Ranganathan, N. Raju, H. Fan, X. Zhang, M. F. Tweedle, J. F. Desreux and V. Jacques, *Inorg. Chem.*, 2002, **41**, 6856.

96 R. S. Dickins, J. A. K. Howard, C. W. Lehmann, J. Moloney, D. Parker and R. D. Peacock, *Angew. Chem. Int. Ed. Engl.*, 1997, **36**, 521.

97 L. Di Bari, G. Pintacuda, P. Salvadori, R. S. Dickins and D. Parker, *J. Am. Chem. Soc.*, 2000, **122**, 9257.

98 R. S. Dickins, D. Parker, J. I. Bruce and D. J. Tozer, *Dalton Trans.*, 2003, 1264.

99 B. Bleaney, *J. Magn. Reson.*, 1972, **8**, 91.

100 V. S. Mironov, Y. G. Galyametdinov, A. Ceulemans, C. Gorlier–Walrand and K. Binnemans, *J. Chem. Phys.*, 2002, **116**, 4673.

101 D. F. Henrie, R. L. Fellows and G. R. Choppin, *Coord. Chem. Rev.*, 1976, **18**, 199.

102 J. Coates, E. Gay and P. G. Sammes, *Dyes and Pigments*, 1997, **34**, 195.

103 J. P. Cross, A. Dadabhoy and P. G. Sammes, *J. Lumin.*, 2004, **110**, 113.

104 R. S. Dickins, T. Gunnlaugsson, D. Parker and R. D. Peacock, *Chem. Commun.*, 1998, 1643.

105 J. I. Bruce, R. S. Dickins, L. J. Govenlock, T. Gunnlaugsson, S. Lopinski, M. P. Lowe, D. Parker, R. D. Peacock, J. J. B. Perry, S. Aime and M. Botta, *J. Am. Chem. Soc.*, 2000, **122**, 9674.

106 S. Aime, A. Barge, J. I. Bruce, M. Botta, J. A. K. Howard, R. Kataky, M. P. Lowe, J. M. Moloney, D. Parker and A. S. de Sousa, *Chem. Commun.*, 1999, 1047.

107 R. S. Dickins, A. S. Batsanov, J. A. K. Howard, D. Parker, H. Puschmann and S. Salamano, *Dalton Trans.*, 2004, 70.

108 R. S. Dickins, C. S. Love and H. Puschmann, *Chem. Commun.*, 2001, 2308.

CHAPTER 2

Phospho–Anion Binding Studies

2.1 Phospho–Anion Binding Studies

2.1.1 Introduction

In the search for synthetic receptors capable of chemoselective binding to *O*–phosphorylated anions, a number of considerations must be taken into account. Firstly, it is necessary to ensure that the receptor displays a high binding affinity towards the *O*–phosphorylated species in order to provide good selectivity over competing anionic or electron rich interferents. Secondly, the large free energy of hydration of the *O*–phosphorylated anions requires a receptor with a largely electrostatic binding contribution, possibly complemented by hydrogen bonding to assist in enhancing the selectivity for the tetrahedral anion geometry. Finally, it is desirable to devise a synthetic receptor that is capable of signalling the interaction of the target *O*–phosphorylated species to the observer. This may be achieved through monitoring a measurable change in the sign or magnitude of a certain physical property of the receptor, for example, changes in the intensity of UV/visible absorption or luminescence emission. Indeed, many of the anionic receptors reported recently in the literature display such responses.[3–4] However, it is highly desirable to obtain a receptor which can signal binding of the *O*–phosphorylated anion via a distinctive change in the observed spectral form, and such receptors are discussed in the rest of this chapter.

2.1.2 Receptors Based on Lanthanide(III) Complexes

The synthetic receptors selected to explore the binding of *O*–phosphorylated anions are based on the well–defined chiral lanthanide(III) complexes $[Ln\mathbf{7}]^{3+}$ and $[Ln\mathbf{8}]^{3+}$. These complexes were initially chosen in order to fulfil the necessary requirements imposed in the design of synthetic receptors for use in aqueous media, most notably the largely electrostatic interactions observed in lanthanide bonding. The complexes $[Ln\mathbf{7}]^{3+}$ and $[Ln\mathbf{8}]^{3+}$ consist of a macrocyclic ligand which occupies seven coordination sites around the central lanthanide(III) ion, with the two remaining sites occupied by labile water molecules.[5] These labile water molecules are easily displaced by a variety of anions[6] (**Scheme 2.1**) and amino acids[7] and the complex $[Eu\mathbf{7}]^{3+}$ exhibits a high binding affinity towards hydrogen phosphate (HPO_4^{2-}) in aqueous media (log K = 4.15, 298 K, pH = 7.4, I = 0.1 NaCl).[6] Furthermore, the

chirality of the pendant arms in the complexes $[Ln7]^{3+}$ and $[Ln8]^{3+}$ impairs arm rotation and introduces considerable structural rigidity within the complex, such that one major isomer is favoured in solution. This is a favourable situation when attempting to monitor anion binding since the presence of multiple isomers in solution undoubtedly complicates the assignment of any ternary adducts.

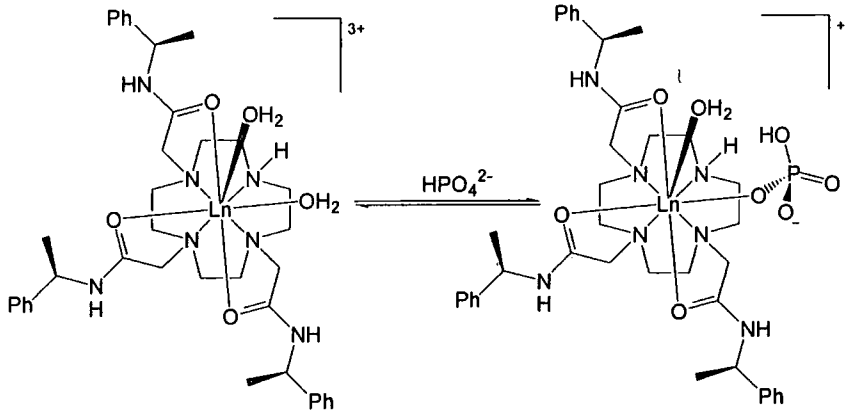

Scheme 2.1 : Reversible binding of hydrogen phosphate to the lanthanide(III) centre of $[LnDO3Ph(H_2O)_2]^{3+}$, following displacement of a labile water molecule from the coordination sphere.

Another advantage in using a macrocyclic ligand in combination with a lanthanide(III) ion is the ease with which the overall complex charge and hence binding affinity can be controlled. Simple permutations to the ligand determining the charge on the ligand also define the overall charge on the resulting complex, and thereby modulate the electrostatic affinity towards anions. Similarly, by variation of the lanthanide(III) ion in the complex, the anion affinity can be controlled. The relative charge density of the lanthanide(III) ions increases along the series, associated with the decrease in ionic radius across the series. Furthermore, numerous ligand based modifications can be envisaged, either through changes to the pendant arms or variation of substituents on the ring secondary amine group. The ease with which such modifications can be made to the ligand structure provides a versatile means of expanding this basic structure. Such versatility is important in the adaptation of such complexes for practical applications where drastic changes to the geometry around the lanthanide(III) ion may affect the selectivity exhibited.

2.1.3 Synthesis of Ligands and Complexes

The chiral chloroamide compound required as a precursor to the chiral pendant arms

of the macrocyclic ligand were synthesised via acylation of the chiral amine with chloroacetyl chloride in diethyl ether at 0°C (**Scheme 2.2**).

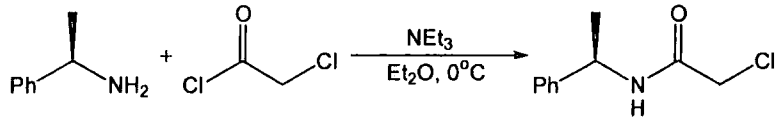

Scheme 2.2 : Outlining the reaction conditions used to obtain the *R*–chloroamide (**1**) required as pendant arms for the macrocyclic ligand.

Selective and controlled *N*–alkylation of cyclen is difficult due to the similar reactivity of the nitrogen atoms within the macrocycle, leading to mixtures of multiply alkylated macrocycles. This is evidenced by the previously reported synthesis of the desired ligand **7**. Direct alkylation of cyclen with the chiral chloroamide **1**, requires purification to separate the mixture of alkylated products.[6] The rather poor yields obtained via this method prompted the investigation of an alternative route, using protecting group chemistry in order to eliminate the possibility of multiple products (**Scheme 2.3**).

There are many strategies towards mono–substituted cyclen macrocycles, usually involving the selective coordination of three of the four nitrogen atoms in the macrocycle. Formation of a tri–protected boron protected cyclen occurs readily via the trans amination of tris–(dimethylamino)borane, leaving the fourth ring nitrogen available for alkylation.[8] A similar result is achieved via the formation of the molybdenum or chromium tricarbonyl complexes of cyclen,[9,10] although these compounds are air sensitive and hence careful handling is required. The reaction of cyclen with certain acylating agents, such as *tert*–butyldicarbonate anhydride[11] or chloral hydrate,[12] has been observed to form predominantly tri–substituted macrocycle under carefully controlled conditions. However, the deprotection of the resulting tri–protected cyclen is often performed under fairly harsh conditions,[12] which led to the choice of the trifluoroacetyl group[13] as a protecting group in this synthesis.

Recently Yang *et al.* reported a high yielding route towards the tris–trifluoroacetyl protected cyclen **3**,[13] in which no evidence for the formation of tetra substituted products was apparently observed. This procedure was replicated by reacting one equivalent of cyclen with four equivalents of ethyl trifluoroacetate in the presence of

triethylamine, producing the desired compound **3** in 92% yield following purification. Since removal of the trifluoroacetate protecting groups occurs under mildly basic conditions, it was necessary to insert a base stable group onto the remaining macrocyclic nitrogen atom, which would ultimately produce the desired mono–protected cyclen compound. Subsequent reaction of compound **3** with an excess of *tert*–butyldicarbonate anhydride produced the carbamate **4** in 77% yield.

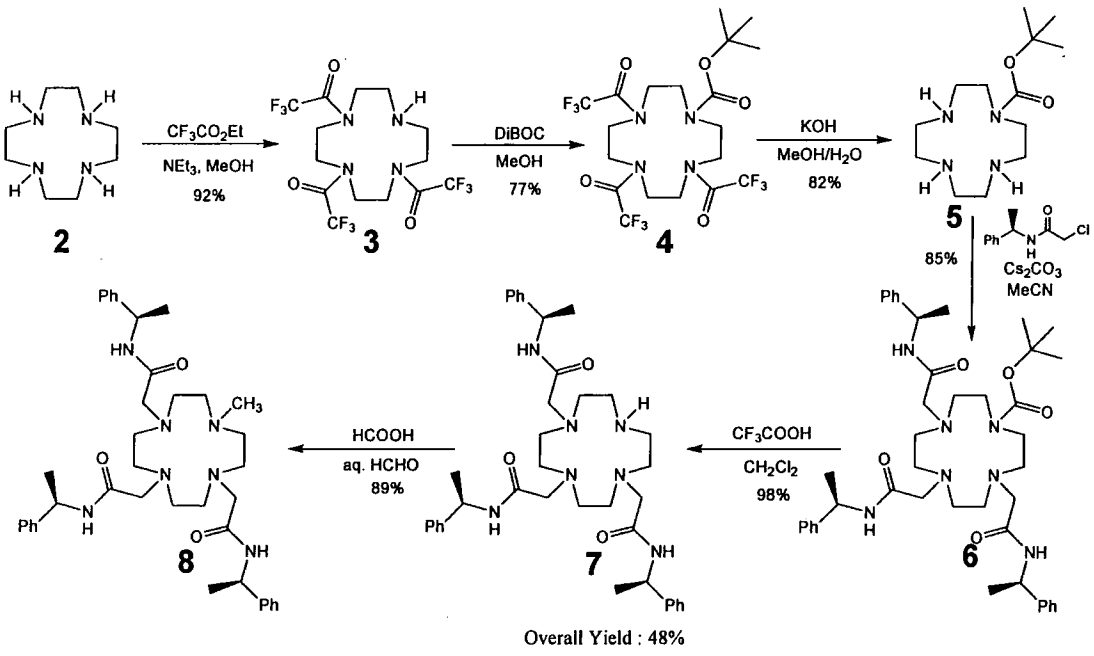

Scheme 2.3 : Outlining the synthetic route towards ligand **7** (**DO3Ph**), via the implementation of protecting groups and the subsequent reaction to provide the *N*–methylated analogue **8**.

The desired mono–protected compound **5** was obtained in 82% yield, following removal of the trifluoroacetyl groups using aqueous–methanolic potassium hydroxide.[13] This mono–protected cyclen, **5**, was successfully alkylated with a slight excess of the *R*–chloroamide **1** under forcing conditions, since no over–alkylation is possible in this case, to give the ligand precursor **6** in 85% yield following purification. Subsequent removal of the BOC protecting group using 95% trifluoroacetic acid in dichloromethane at room temperature yielded the desired tri–substituted macrocyclic ligand **7** in 98% yield. This route, despite being more long–winded than direct alkylation, provides the pure tri–substituted ligand **7** in an overall yield of 48% from cyclen. The *N*–methylated analogue, ligand **8**, was isolated following reductive amination of compound **7** using the Eschweiler–Clarke procedure.

The corresponding lanthanide(III) complexes of ligands **7** and **8** were prepared in anhydrous acetonitrile, via reaction with the appropriate lanthanide(III) trifluoromethanesulfonate salt in anhydrous MeCN at 80°C, followed by precipitation from diethyl ether.

2.2 NMR Studies of Phospho–Anion Binding

Proton NMR spectroscopy was used initially to monitor the binding of a series of phosphorylated anions to the lanthanide complexes of ligands **7** and **8**, since this analytical technique allows a great deal of structural information to be obtained. Furthermore, the presence of a paramagnetic lanthanide(III) ion in the receptor is particularly advantageous, since the induced dipolar shifts can be used to assist in the structural analysis of the anion bound adducts in solution. The presence of paramagnetically shifted resonances has proved to be an important element in the assignment of anion binding orientations in solution for the complexes $[Ln7(H_2O)_2]^{3+}$. For example, where there is the possibility of forming a chelated binding mode with an asymmetric anion, such as an amino acid, two isomeric complexes may form, distinguished by the nature of the axial donor atom (**Figure 2.1**).

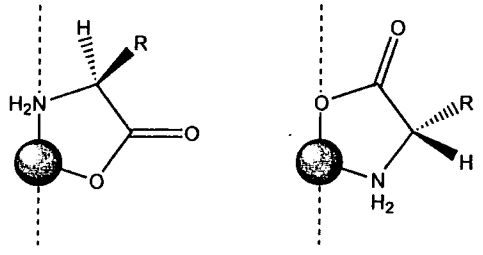

Figure 2.1 : Representation of the two possible binding modes of an amino acid chelate adduct with $[Ln7(H_2O)_2]^{3+}$, highlighting the variation in the angle between the principal magnetic axis in the complex (dashed line) and the α–proton and side chain, R, upon reversal of the chelating binding mode.

It is clear from **Figure 2.1** that the relative orientation of the amino acid α–proton and side chain group to the principal magnetic axis in the lanthanide complex, varies significantly upon reversal of the chelate orientation. The paramagnetically induced chemical shift can be assumed to be proportional to the angle from the principal magnetic axis in the complex to the nuclei in question (see **Section 1.2.3, Equation 5**), along with the constants associated with the lanthanide(III) ion and crystal field.

Therefore, if the lanthanide(III) ion and ligand are constant, it is expected that the shift of the α–proton and side chain group will be greatest when closest to the principal magnetic axis, ie. when the amino group occupies the axial donor position. Based on the observation of a resonance in the high frequency shifted region of the proton NMR spectra of amino acid ternary adducts, in addition to the four most shifted axial macrocyclic ring protons, this analysis led to the conclusion that the amino group was the axial donor group. Subsequent X–ray crystallographic studies confirmed this result,[3] illustrating the value of having a paramagnetic probe in the receptor.

2.2.1 O–Phosphate Binding Selectivity of Thulium and Ytterbium Complexes

The initial anion binding studies were performed using ^{1}H NMR spectroscopy with the model complexes $[Tm7(H_2O)_2]^{3+}$ and $[Yb7(H_2O)_2]^{3+}$, present as their trifluoromethanesulfonate salts. These lanthanide(III) ions were chosen primarily due to the fact that they are the smallest, and hence most charge dense of all the paramagnetic lanthanide(III) ions, leading to the greatest affinity towards anions. The presence of two water molecules coordinated to the ytterbium centre has been confirmed in the solid state, from X–ray crystallographic studies,[3] and in solution, through the measurement of relative radiative rate constants in H_2O and D_2O (see **Section 1.3.3**).[14]

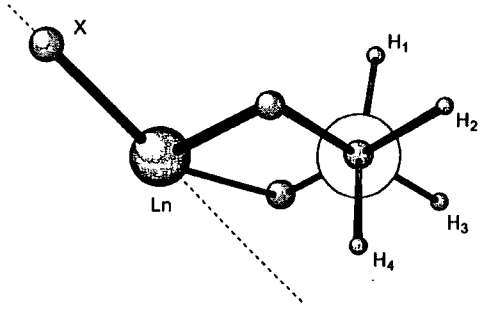

Figure 2.2 :Relative orientations of macrocyclic ring protons on one ethylene diamine chelate, illustrating how the distance between the proton and the lanthanide(III) ion and its principal magnetic axis, affects the shift observed for these protons.

The ^{1}H NMR spectrum of the di–aqua ytterbium(III) complex exhibits one major species in solution, with the high frequency region of the spectrum displaying eight distinct resonances. The four most shifted resonances at +113, +77 +63 and +50 ppm

correspond to one set of axial protons of the macrocyclic ring (H_4, **Figure 2.2**).[14] The other four high frequency shifted resonances correspond to the most shifted equatorial protons (H_3) on the macrocyclic ring (**Figure 2.3**). This pattern of shifted resonances is assigned to the di–aqua species, since the triflate counterion does not bind to the lanthanide(III) centre in aqueous media.

The corresponding thulium complex was subject to greater spectral linewidths (~5 ppm), on account of the longer electronic relaxation time relative to ytterbium. However, given the greater spectral widths also observed (+300 → −280 ppm), interpretation of the spectra was not affected. As in the case of the ytterbium(III) complexes, the four most shifted resonances at +293, +230 +178 and +137 ppm correspond to the axial protons of the macrocyclic ring (H_4), with the other four high frequency shifted resonances at +110, +72, +63 and +35 ppm corresponding to the most shifted equatorial protons on the macrocyclic ring (H_3). The difference in linewidths between axial and equatorial macrocyclic ring protons is clearly more evident in the case of thulium, when compared to the corresponding ytterbium complex. In systems exhibiting less significant line broadening (ie. europium and ytterbium complexes), this difference has been attributed to the larger coupling constants exhibited by the axial protons.[14] However, for the thulium complexes the difference in linewidth between the axial and equatorial macrocyclic ring protons are not accounted for by this, since the linewidths observed are much greater than the coupling constants between the ring protons. Furthermore, the difference in lidewidths observed increases with magnetic field strength. This difference in linewidths observed can therefore be postulated to arise due to the distance ($1 / r^6$) and magnetic field strength dependence of relaxation enhancement of nuclei close to the lanthanide(III) ion (Curie spin relaxation).[15]

In a typical anion binding experiment, the anionic species was added in up to a fivefold excess to a solution of the complex (4 mM), maintaining the pH at 7.4. Subsequent measurement of the ^{1}H NMR spectra was recorded at 500 MHz and 295 K, with each spectrum referenced to the methyl proton resonance of *tert*–butanol, which was set as 0 ppm. The ^{1}H NMR spectra obtained are representative of the limiting proton shifts, in which the anion is fully bound to the complex. Increasing the concentration of anion in the samples beyond this point yielded no

observable changes in the proton NMR spectra obtained. The axial protons on the macrocyclic ring are shifted to highest frequency in each ternary adduct (**Figures 2.3** and **2.4**). The variations in the shifts of the macrocyclic ring protons in these spectra demonstrate the exquisite sensitivity of the axial proton resonances to the coordination environment.

Confirmation of the presence of the phosphate group coordinated directly to the lanthanide(III) centre in phosphorylated anion adducts was provided by ^{31}P NMR. For example, to a solution of $[Yb7(H_2O)_2]^{3+}$ (4 mM) was added the glucose–6–phosphate (8 mM) in D_2O at pH 7.4, 295 K. The resulting proton–decoupled ^{31}P NMR spectrum was subsequently recorded at 162 MHz. The spectrum consists of two resonances, one at 4 ppm corresponding to the unbound glucose–6–phosphate in solution, and a second broad resonance at −43 ppm ($\omega_{1/2} = 159$ Hz), corresponding to the paramagnetically shifted phosphorus atom bonded to the oxygen atom binding to the ytterbium(III) centre.

Independent titrations were also performed under the same conditions as above, in order to determine the stoichiometry of the observed ternary adducts with the various anions studied. In each titration, addition of 0.5 equivalents of anion was sufficient to produce one set of resonances for the di–aqua complex and a corresponding set of resonances for the ternary adduct, both of equal intensity. The simultaneous observation of two sets of resonances provides evidence that the ternary adducts are in slow exchange on the NMR timescale with the di–aqua precursor complex. Subsequent addition of a further 0.5 equivalents, to give a total of one equivalent of anion, led to the disappearance of the resonances due to the di–aqua complex, leaving only one set of resonances. The remaining set of resonances are identical to those attributed to the fully bound ternary adduct, thus, confirming a 1:1 stoichiometry is observed in solution.

Only two exceptions to the observation of 1:1 stoichiometry were observed. The first case involved the di–phosphate ester cAMP, which produced no significant evidence of binding to the lanthanide(III) centre, even when present in more than tenfold excess. The second possible exception to 1:1 stoichiometry was observed in the ternary adducts of inorganic phosphate. Addition of one third of an equivalent of

hydrogen phosphate to the lanthanide(III) complex led to the observation of a small amount of precipitate formation.

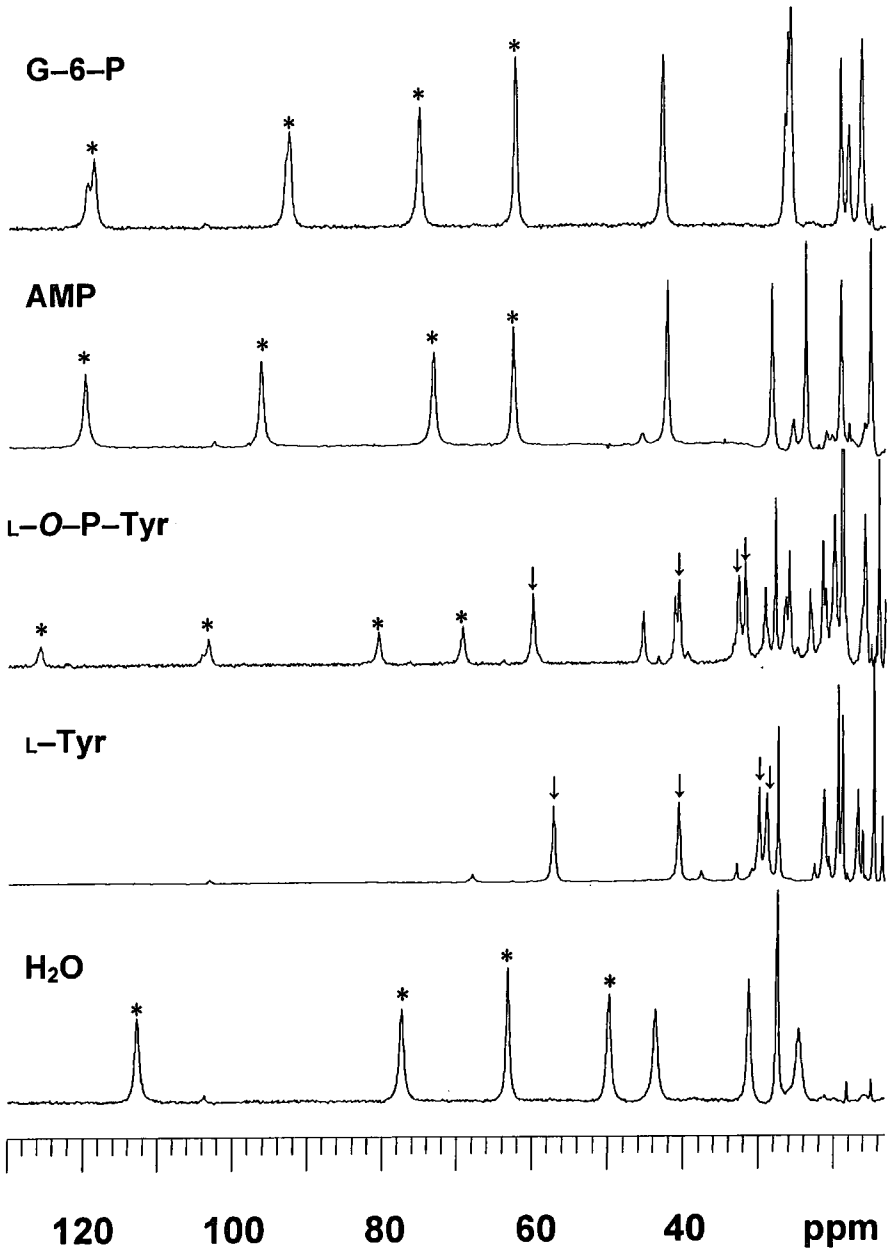

Figure 2.3 : ^{1}H NMR spectra of $[Yb7(H_2O)_2]^{3+}$ (4 mM) in the presence of selected anions (20 mM) at 500 MHz, pH 7.4, 295 K. Asterisks (*) and arrows (↓) indicate the most shifted axial protons of the macrocyclic ring for complexes possessing an axial bound water molecule and a chelated binding mode with an axial amino group, respectively.

The proton NMR spectrum of this solution displays two sets of axial proton resonances of approximately equal intensity, corresponding to the di–aqua complex and the phosphate bound ternary adduct. This observation may suggest that the formation of an insoluble bis–lanthanide(III) phosphate bridging complex is possible,

which is not observed in the presence of excess hydrogen phosphate. Increasing the phosphate concentration such that 0.5 equivalents of hydrogen phosphate were present, produces a proton NMR spectrum consisting of only one set of resonances, corresponding to the phosphate bound ternary complex.

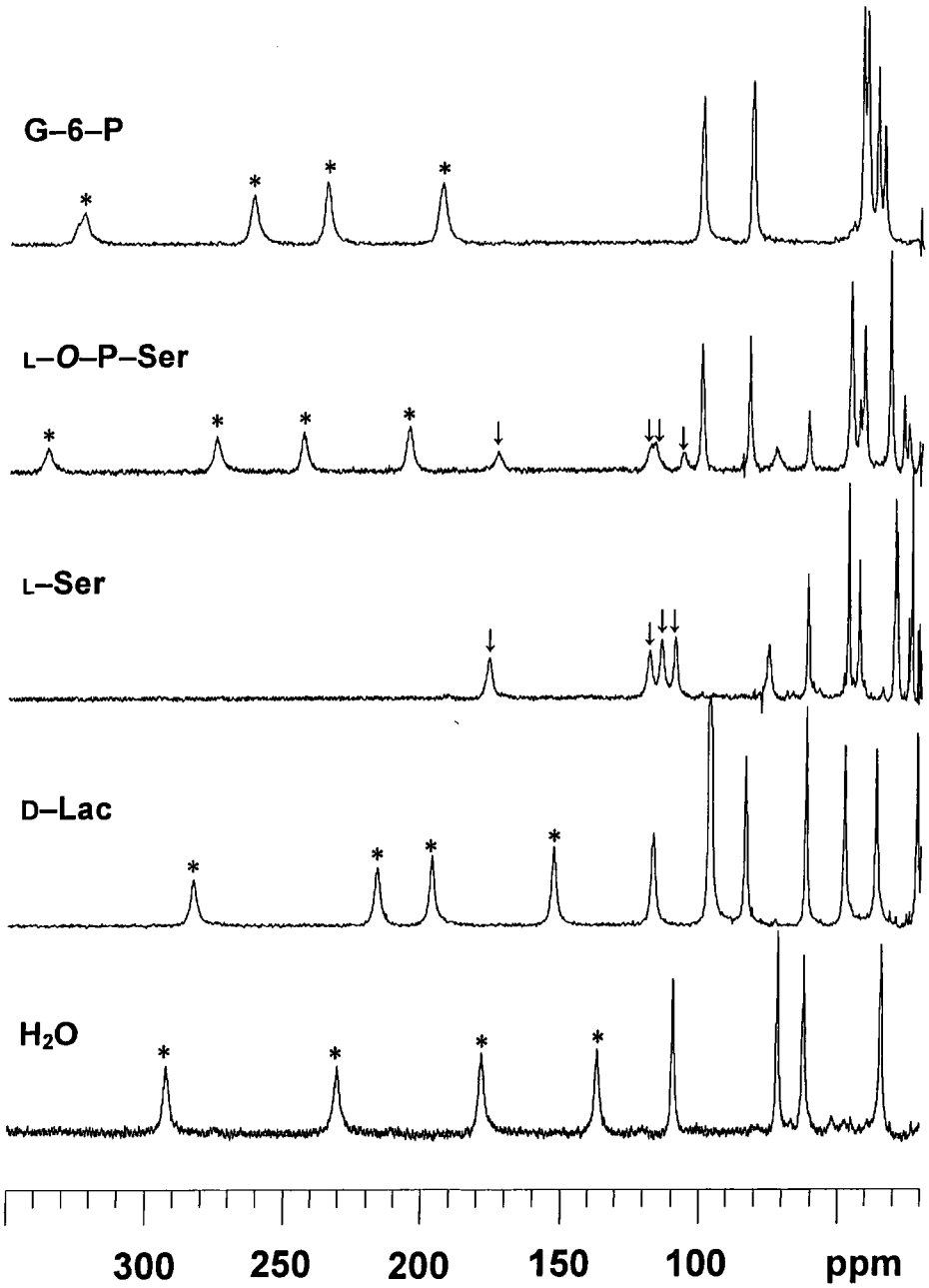

Figure 2.4 : ^{1}H NMR spectra of $[Tm7(H_2O)_2]^{3+}$ (4 mM) in the presence of selected anions (20 mM) at 500 MHz, pH 7.4, 295 K. Asterisks (*) and arrows (↓) indicate the most shifted axial protons of the macrocyclic ring for complexes possessing an axial bound water molecule and a chelated binding mode with an axial amino group, respectively.

This differential behaviour observed in the binding of hydrogen phosphate may be attributed to the presence of an additional hydroxyl group, which is absent in all the

other mono–phosphate esters studied. The presence of this hydroxyl group may facilitate the additional formation of a hydrogen bonding network between the axial water molecules bound to the lanthanide(III) centre, increasing the stability of the bis–lanthanide(III) phosphate adduct (see **Figure 2.5**).

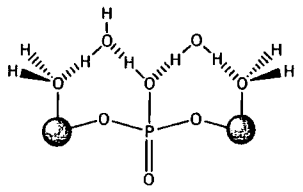

Figure 2.5 : Illustration of a possible hydrogen bonding network between a bridging hydrogen phosphate anion and the axial bound water molecules of the lanthanide(III) complexes.

The mean shift of the most shifted macrocyclic ring protons was calculated for each of the ternary adducts, and the values obtained are tabulated in **Table 2.1**. The mean shift of the four axial ring proton resonances has previously been shown to be characteristic of the polarisability of the axial donor (see **Section 1.4.2**),[6] and for each of the ternary adducts studied here, there appears to be no exception to this observation.

Anion[a]	$[Tm7(H_2O)_2]^{3+}$ [b]	$[Yb7(H_2O)_2]^{3+}$ [b]
$CF_3SO_3^-$	210	76
HPO_4^{2-}	247	100
O–P–Serine^{2-}	265 (125)	91 (45)
O–P–Threonine^{2-}	268 (135)	92 (43)
O–P–Tyrosine^{2-}	281 (120)	95 (40)
N–Ac–*O*–P–Tyrosine^{2-}	274	92
G–6–P^{2-} [c]	255	87
AMP^{2-}	258	88
F^-	299	99
Lactate$^-$	212	71
AcO^-	207	69
Serine	130	44
Threonine	137	44
Tyrosine	122	39
CO_3^{2-}	78	27

Table 2.1 : Calculated mean chemical shifts of the most shifted macrocyclic ring protons for all of the ternary adducts of ligand 7. [a] The triflate anion does not coordinate to the lanthanide(III) centre and data quoted are representative of the di–aqua complex. [b] Values in brackets indicate the observed mean shift of the minor species. [c] G–6–P is the abbreviation used in all references to glucose–6–phosphate.

For the related ytterbium and thulium macrocyclic complexes, the shifted resonances

of H_4 are known to be determined purely by the pseudo–contact contribution.[16] Analysis of the average shifts obtained for the axial macrocyclic ring protons in the ytterbium and thulium ternary adducts, reveals a clear correlation between the relative shifts. The linear relationship obtained, see **Figure 2.6**, is consistent with the theory that the axial macrocyclic proton resonances are dominated by a common pseudo–contact contribution to the paramagnetic shift. Furthermore, the varying spectral range of shifts exhibited by the thulium adducts is consistent with previous observations in the corresponding ytterbium adducts, wherein the polarisability of the axial donor determines the overall proton spectral width.[17]

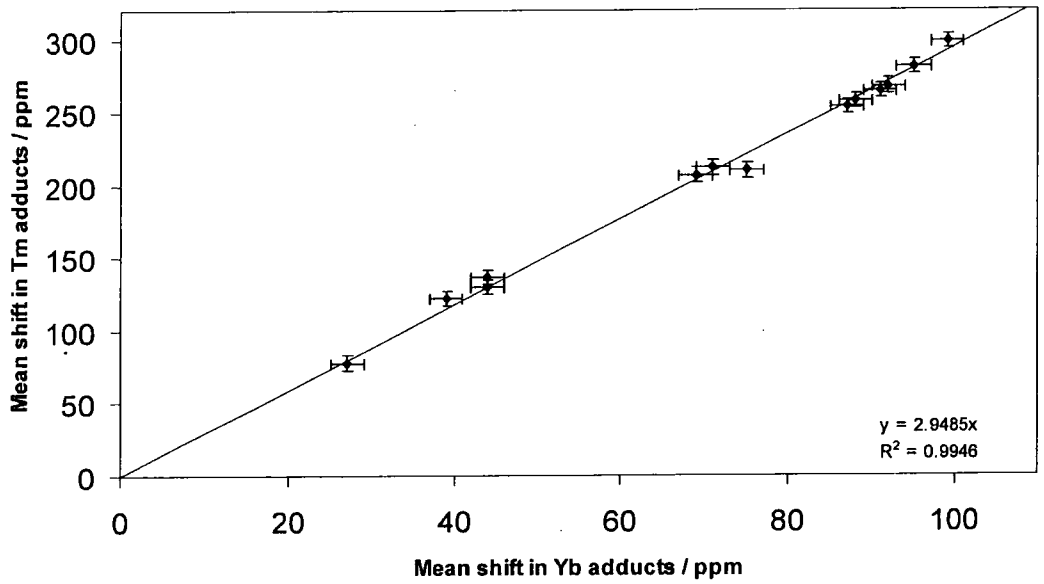

Figure 2.6 : Correlation between the mean chemical shifts observed for the four inequivalent axial ring protons on the macrocyclic ring for the ternary adducts of $[Tm7(H_2O)_2]^{3+}$ and $[Yb7(H_2O)_2]^{3+}$, respectively.

In each of the ternary adducts, with the exception of the *O*–phosphorylated amino acids, the presence of one species in solution is clearly evident. However, in the case of the *O*–phosphorylated amino acids, there is obviously another minor species in solution. The axial ring protons in this minor species resonated to lower frequency in comparison to the phosphate bound adduct. Upon closer analysis, it is apparent that these resonances are very similar to those found in the presence of the corresponding non–phosphorylated amino acids (see **Figures 2.3** and **2.4**). The binding of amino acids to $[Yb7(H_2O)_2]^{3+}$ has already been established through the analysis of several X–ray crystal structures, proving that binding occurs via a chelated binding mode. This binding mode is such that the nitrogen atom resides on the apical site of the

square antiprismatic structure, with the amino acid carbonyl group oxygen occupying a coordination site similar to the ligand carbonyl oxygen atoms (see **Figure 2.7**).

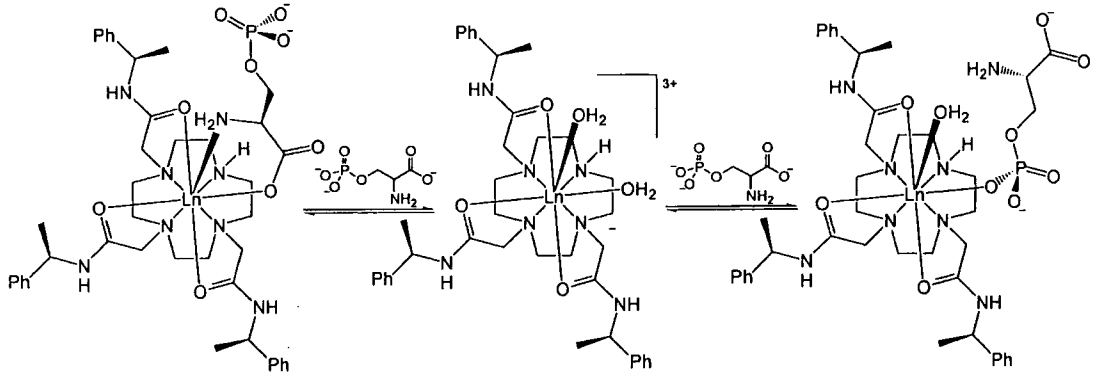

Figure 2.7 : Illustration of the expected phosphate binding mode of the *O*–phosphorylated amino acid adducts, along with the competitive binding mode involving chelation of the amino acid group to the lanthanide(III) ion.

A subsequent ^{1}H NMR experiment involving $[Yb7(H_2O)_2]^{3+}$ in the presence of equal quantities of inorganic phosphate and L–tyrosine, produced a very similar spectrum.

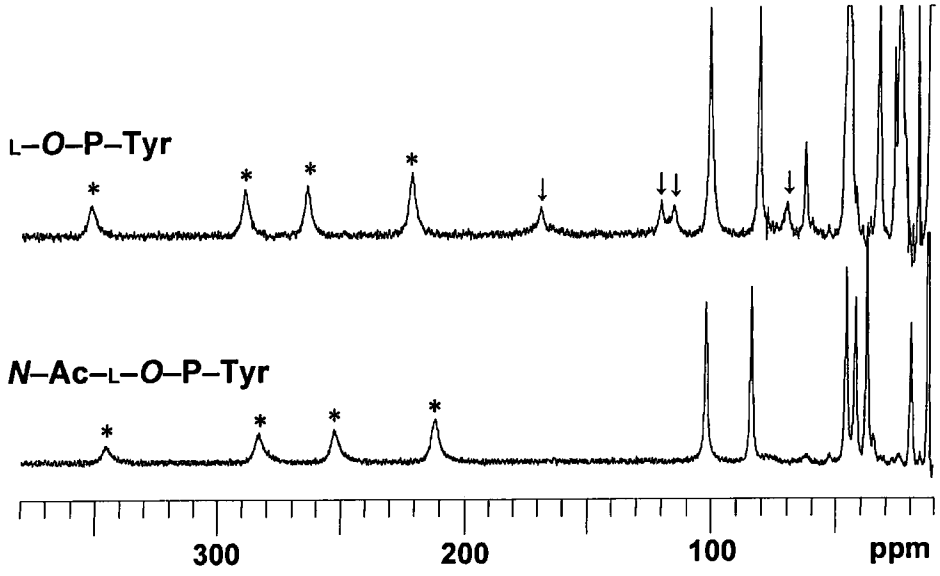

Figure 2.8 : ^{1}H NMR spectra of $[Tm7(H_2O)_2]^{3+}$ (4 mM) in the presence of *O*–Phosphotyrosine (top) and *N*–acetyl–*O*–phosphotyrosine (bottom) at 500 MHz, pH 7.4, 295 K. Asterisks (*) denote the phosphate bound adduct and arrows (↓) indicate the minor amino–carboxylic acid chelate.

Thus, it is evident that amino acid chelation at the lanthanide(III) centre competes with phosphate binding for the thulium and ytterbium complexes of **7**. Further confirmation of the competition between these two binding modes was provided by the analysis of the ^{1}H NMR spectrum obtained for the complexes in the presence of *N*–acetyl–*O*–phosphotyrosine. For the ternary adducts of *N*–acetyl–*O*–

phosphotyrosine, only one set of resonances is observed, consistent with a phosphate bound adduct (**Figure 2.8**).

Acetylation of the nitrogen atom evidently removes the possibility of chelation via amine and carboxylate groups, although a new chelation mode can be envisaged between the newly formed amide carbonyl group and carboxylate (**Figure 2.9**). This seven membered chelation mode has been observed for *N*–acetylglycine, which again displays a characteristic shift pattern for the four axial resonances.[7] With the phosphate group present, however, this seven membered chelation mode is obviously not competitive, since no evidence of this chelation mode was observed in the ^{1}H NMR spectra.

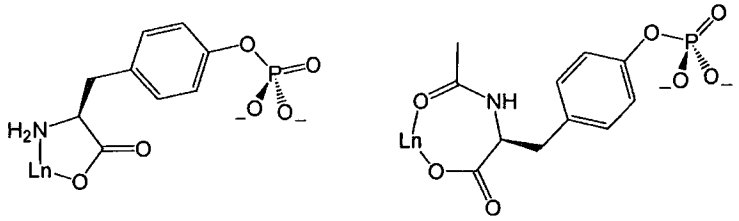

Figure 2.9 : Illustration of the five membered amino–carboxylate chelate which is competitive with phosphate binding, but not possible for *N*–acetyl amino acids (left) and the seven membered amide–carboxylic acid chelate possible upon acetylation, which is does not compete with phosphate binding.

2.2.2 Effects of N–Alkylation on O–Phosphate Binding Selectivity

Parallel ^{1}H NMR studies were performed with the corresponding *N*–methylated complexes, $[Tm\mathbf{8}(H_2O)_2]^{3+}$ and $[Yb\mathbf{8}(H_2O)_2]^{3+}$. The proton NMR spectrum of the ytterbium(III) complex was not very well resolved and all resonances were very broad in appearance. The high frequency region of the spectrum exhibits three broad resonances at +110, +99 +96 ppm, in the relative ratio 1:2:1, corresponding to the four axial protons of the macrocyclic ring. These values were very similar to the dipolar shift observed for the axially symmetric $[Yb\mathbf{DOTAMPh}]^{3+}$ complex, in which the four equivalent macrocyclic ring protons resonate at +101 ppm.[17] The similarity between the shifts in these two complexes suggests that in the *N*–methylated complex there is a more symmetrical arrangement of the axial protons relative to the ytterbium centre, when compared with the corresponding *N*–H complex. The broad appearance of the resonances in the proton NMR spectrum of $[Yb\mathbf{8}(H_2O)_2]^{3+}$ may be a consequence of relatively slow water exchange on the NMR

timescale between a mono– and di–aqua species. Evidence to support this theory has also been obtained for the corresponding europium complex of ligand **8**.[6] Measurement of the luminescence lifetime of the europium complex revealed a bi–exponential decay, which can be attributed to the presence of a mono– and di–aqua species, with the latter exhibiting the shorter luminescent lifetime as a consequence of the greater quenching by two bound water molecules (see **Section 1.3.3**).

In contrast to the differences observed between the ytterbium complexes of **8** and **7**, the thulium complex, $[Tm\mathbf{8}(H_2O)_2]^{3+}$, did not appear to be broadened significantly when compared to the corresponding complex of ligand **7**. However, this may be a result of the greater line broadening inherent in the thulium complex, resulting in the masking of any broadening due to a chemical exchange phenomenon. The larger magnetic anisotropy, which leads to the larger dipolar shifts observed for $[Tm\mathbf{7}(H_2O)_2]^{3+}$, also produces a more well resolved spectrum than in the case of $[Yb\mathbf{8}(H_2O)_2]^{3+}$. This improved resolution leads to the observation of four separate high frequency shifted resonances for the axial macrocyclic ring protons at +325, +320, +311 and +296 ppm.

Addition of anions to the thulium and ytterbium complexes of ligand **8** led to the formation of distinctive proton NMR spectra, representative of the limiting proton shifts, in which the anion is fully bound to the complex (**Figure 2.10**). The presence of the fully bound ternary bound complexes was again confirmed by observing no further changes in the proton NMR resonances, upon addition of larger concentrations of anions. In contrast to the parent di–aqua complexes of ligand **8**, the proton NMR spectra of the ternary adducts consist of sharp, well resolved resonances, suggesting that any dynamic exchange phenomenon involving the ligand is not relevant on the NMR timescale. The axial protons on the macrocyclic ring are shifted to highest frequency in each ternary adduct, and again demonstrate the sensitivity of these dipolar shifts to the coordination environment. The mean shift of the axial protons of the macrocyclic ring in these *N*–methylated adducts was also calculated and are tabulated in **Table 2.2**.

These mean values corroborate well with the values obtained for the corresponding ternary adducts of ligand **7**, suggesting that also with the methyl group present, the

ternary adducts of ligand **8** adopt very similar coordination modes.

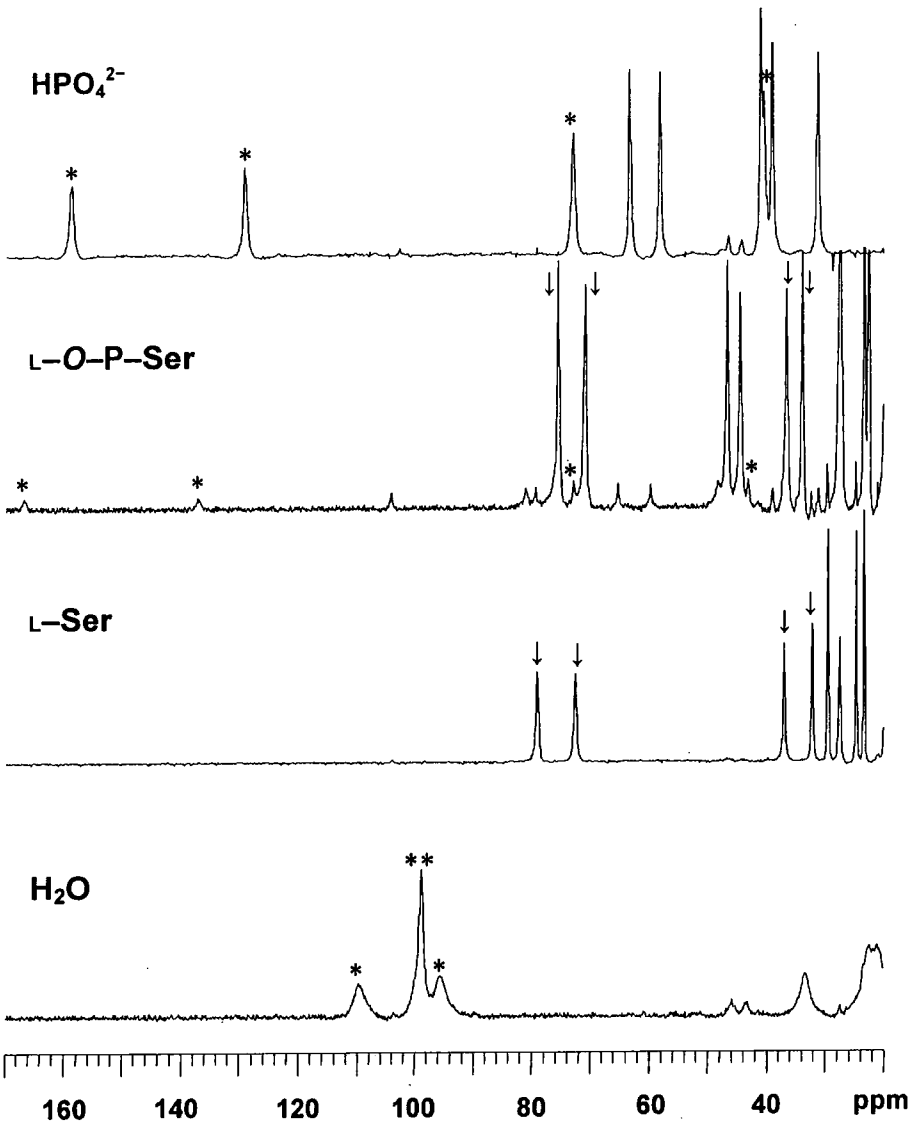

Figure 2.10 : ^{1}H NMR spectra of $[Yb\mathbf{8}(H_2O)_2]^{3+}$ (4 mM) in the presence of selected anions (20 mM) at 500 MHz, pH 7.4, 295 K. Asterisks (*) and arrows (↓) indicate the most shifted axial protons of the macrocyclic ring for complexes possessing an axial bound water molecule and a chelated binding mode with an axial amino group, respectively.

However, the difference between the most shifted axial proton resonance and the least shifted resonance for the ternary adducts of ligand **8** is much larger than those observed in the corresponding ternary adducts of ligand **7**. For example, the difference between the most shifted and least shifted axial proton resonances in the AMP adducts of $[Yb\mathbf{7}(H_2O)_2]^{3+}$ and $[Yb\mathbf{8}(H_2O)_2]^{3+}$ are 57 and 136 ppm, respectively. For the former complex, this chemical shift difference is virtually identical to the difference observed in the di–aqua complex of 62 ppm, as expected

since the axial water molecule is retained in both cases. However, in the *N*–methylated analogue, the difference in chemical shift between the most and least shifted axial protons is only 14 ppm. The large change in the shift range of the axial protons in the ternary adducts of $[Yb\mathbf{8}(H_2O)_2]^{3+}$ may suggest there is a large distortion of the macrocyclic ring upon coordination of an anion to the lanthanide(III) centre, causing some axial protons to approach closer to the principal magnetic axis. This is emphasised in the ternary adducts of ligand **8**, where the chemical shifts observed in the di–aqua complex appear to be very similar to the axially symmetric **DOTAMPh** complexes. Unfortunately, none of the single crystals obtained for any complexes of ligand **8** were suitable for X–ray structural analysis, and therefore there is no geometrical data available to support the hypothesis of ring distortion.

Anion[a]	$[Tm\mathbf{8}(H_2O)_2]^{3+}$ [b]	$[Yb\mathbf{8}(H_2O)_2]^{3+}$ [b]
$CF_3SO_3^-$	313	101
HPO_4^{2-}	349	100
O–P–Serine^{2-}	161 (360)	54 (107)
O–P–Threonine^{2-}	171 (365)	57 (109)
O–P–Tyrosine^{2-}	158 (373)	53 (110)
N–Ac–*O*–P–Tyrosine^{2-}	360	124
G–6–P^{2-}	356	105
AMP^{2-}	362	108
F^-	430	114
Lactate$^-$	265	89
AcO^-	231	76
Serine	165	55
Threonine	171	58
Tyrosine	152	51
CO_3^{2-}	94	32

Table 2.2 : Calculated mean chemical shifts of the most shifted macrocyclic ring protons for all of the ternary adducts of ligand **8**. [a] The triflate anion does not coordinate to the lanthanide(III) centre and data quoted are representative of the aqua complex. [b] Values in brackets indicate the observed mean shift of the minor species, which in this case corresponds to a phosphate binding mode.

Another interesting point worthy of noting, is the partial resolution of the resonance observed for the highest frequency shifted axial proton, and the two most shifted equatorial protons (see **Figure 2.11**) in the glucose–6–phosphate (G–6–P) adduct of $[Yb\mathbf{8}(H_2O)_2]^{3+}$. This partial resolution was also observed for the highest shifted axial ring proton resonance of the corresponding G–6–P adducts involving ligand **7**,

although the effect is not as pronounced, with the second resonance appearing as a shoulder on the peak observed (see **Figure 2.3** and **2.4**).

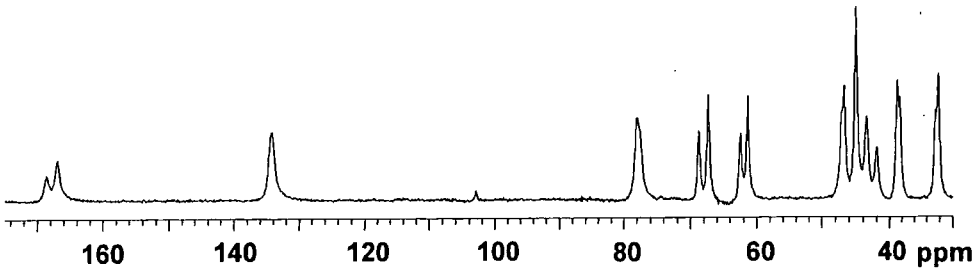

Figure 2.11 : ^{1}H NMR spectra of $[Yb8(H_2O)_2]^{3+}$ (4 mM) in the presence of glucose–6–phosphate (20 mM) at 500 MHz, pH 7.4, 295 K, illustrating the partial resolution observed for the most shifted axial and equatorial ring proton resonances.

The intensities of the signals were not identical, with the most high frequency shifted of each pair of signals the lowest in intensity (approximately 1:2). Since the separation between these signals is only 1–2 ppm, it is too low to be attributed to the two possible SAP geometries, as observed for some amino acids.[7] Consideration of the solution phase chemistry of glucose can be drawn upon to allow a rationalisation of the observed chemical shift non–equivalence (see **Figure 2.12**).

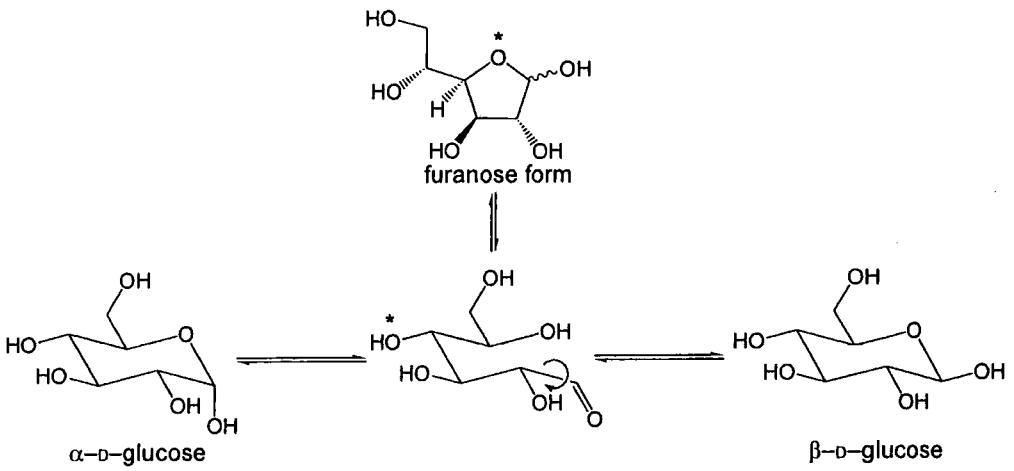

Figure 2.12 : Illustration of the solution phase interconversion of glucopyranoses between α– and *β*–anomeric forms via the acyclic form, and the structure of the furanose form of glucose. The asterisk (*) indicates the oxygen atom used to form the furanose ring.

For example, many boronic acid based glucose sensors preferentially bind to glucose in the less abundant furanose form.[18] However, in the case of the G–6–P ternary adducts, since no direct interaction with the hydroxyl groups on the glucose molecule is thought to occur, it is unlikely that chemical shift non–equivalence is due to distinction of furanose and pyranose forms. Another possible interpretation arises

from the fact that carbohydrates, such as glucose, exist in solution as an equilibrium mixture of anomers (**Figure 2.12**). In the case of glucose, the *β*– anomer is favoured over the α– anomer (36:64), with negligible amounts of the straight chain form present (~0.02%). Since the phosphorylated form of glucose is expected to exhibit similar solution equilibrium behaviour, the two distinct resonances observed could be tentatively assigned to the presence of α–glucose and *β*–glucose ternary adducts. However, given that the adduct is present as a phosphate bound species, it is surprising that such a remote chiral centre can impart such discrimination, unless other interactions are present, especially when the proximate chiral centre in lactate bound adducts leads to very little resolution of the most shifted axial proton resonances.[19]

One major difference in the complexes of ligand **8**, when compared to those of ligand **7**, was the reversal in selectivity between the amino acid chelate binding mode and the phosphate binding mode. For these *N*–methylated complexes the amino acid chelate was the dominant species present in the ternary adducts of the *O*–phosphorylated amino acids, typically in a ratio of 4:1 compared to the phosphate binding mode. This preference for an amino acid chelate binding mode was also observed in competitive situations in solution, where an amino acid and phosphate anion were present in solution. In these situations typical ratios of amino acid chelate to phosphate binding modes were greater than 10:1. This increased preference for the chelated binding mode in the ternary adducts of ligand **8**, when compared to those of ligand **7**, is likely to be associated with the reduced free energy of hydration for the former complexes, favouring the more hydrophobic chelated structure. The reduced hydration exhibited by the complexes of ligand **8** relative to ligand **7**, arises due to the absence of the ring N–H group, which can act as a hydrogen bond donor to one or two 'second sphere' solvent water molecules.[20]

2.2.3 Introduction to Europium and Terbium Ternary Adducts

The lanthanide(III) ions europium and terbium have larger ionic radii than thulium and ytterbium, and hence possess a lower charge density. The lower charge density at the metal centre ultimately leads to a lower affinity for anionic compounds. Despite this lower anion affinity, the complexes europium(III) with ligands **7** and **8** and

terbium(III) with ligand **8** were investigated as possible phosphate selective probes. The main reason for examining these europium and terbium complexes, was the observation that amino acid chelation does not occur in the complexes of these lanthanides with ligand **7**.[14] The only evidence of amino acid binding was due to weak association of the carboxylate group and a hydrogen bonding network between the protonated amino group and the lanthanide bound axial water molecule (**Figure 2.13**). This structure has been postulated using information obtained from the analysis of variable temperature ^{17}O NMR studies and NMRD profiles of the corresponding gadolinium complex, which indicates the presence of only one bound water molecule with an exchange rate approximately four times slower than that found for the parent complex.[14,20]

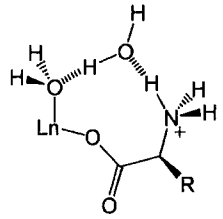

Figure 2.13 : Illustration of the postulated binding mode which accounts for the weak binding of an amino acid to the lanthanide(III) complexes of ligand **7**, when the lanthanide is europium, gadolinium or terbium.

Typically, the association constants obtained from luminescence titrations for the binding of anions to terbium(III) complexes are approximately one order of magnitude greater than the corresponding europium(III) complex.[6] Similarly, *N*–methylation of the macrocyclic ring nitrogen also leads to an increase in the observed association constant by approximately one order of magnitude, and is attributed to the lower free energy of hydration in this series of complexes.[6,20]

The investigation of terbium(III) ternary anion complexes has most often been obtained from luminescence studies, due to the strong lanthanide based luminescence exhibited in such complexes.[6,21] However, in contrast to europium based emission, the emission bands observed from terbium(III) complexes are not particularly sensitive to the coordination environment. Given the lack of information that can be obtained about the structure of the ternary adducts of terbium(III) from luminescence measurements, a proton NMR investigation was necessary. Despite the large line widths generally observed in the proton NMR spectra of terbium systems, the large

magnetic anisotropy and hence large spectral widths, were expected to assist in the resolution of the axial proton resonances, therefore providing information on the binding modes exhibited.

2.2.4 O–Phosphate Binding Selectivity of Europium and Terbium Complexes

The proton NMR spectra of the terbium complex, and adducts of $[Tb\mathbf{8}(H_2O)_2]^{3+}$, were recorded at 65 MHz due to the large sweep widths required (> 700 ppm) and to minimise the line broadening observed at high magnetic field strengths. Typically, because of the lower charge density of terbium in comparison to thulium and ytterbium, ten equivalents of the anion was added to ensure that the observed spectra are representative of the fully bound ternary adduct. In each case, the presence of the fully bound ternary adduct in solution was confirmed by observing no changes in the proton NMR shifts upon increasing the concentration of the given anion.

The di–aqua complex, $[Tb\mathbf{8}(H_2O)_2]^{3+}$, exhibits four broadened resonances at −339, −294, −278 and −272 ppm, corresponding to the axial macrocyclic ring protons. In the case of the terbium(III) adducts, the resonances are shifted to lower frequency since terbium(III) has a negative value for the Bleaney constant, see **Table 1.2**. In the presence of *O*–phosphoserine, the resulting proton NMR spectrum consists of a mixture of three sets of resonances. Correlation of these resonances with those obtained for the corresponding hydrogen phosphate, serine and acetate adducts of $[Tb\mathbf{8}(H_2O)_2]^{3+}$, suggests that the binding of the amino acid is still competitive with the phosphate binding mode in the *N*–methylated terbium(III) complex. This behaviour may be contrasted with the corresponding ytterbium ternary adducts of ligand **8**, for which the selectivity observed for phosphorylated amino acids was completely biased towards the amino acid binding mode.

Further investigations into the ternary anion adducts of $[Eu\mathbf{7}(H_2O)_2]^{3+}$ and $[Eu\mathbf{8}(H_2O)_2]^{3+}$ were pursued with the aim of observing further increases in the selectivity of the phosphate binding mode. The small sweep widths and minimal line broadening observed in europium (III) complexes allowed spectra to be recorded and interpreted successfully at 500 MHz.

The proton NMR spectrum of $[Eu\mathbf{8}(H_2O)_2]^{3+}$ displayed three differentiable

resonances at +24.0, +18.4 and +17.7 ppm, corresponding to the axial protons of the macrocyclic ring. The entire spectrum appeared to be exchange broadened, coinciding with the observations made for the corresponding ytterbium complex (see **Section 2.2.1**, page 46). Addition of a fivefold excess of anions to a solution of $[Eu\mathbf{8}(H_2O)_2]^{3+}$ was sufficient to produce a proton NMR spectrum consisting of sharp, well resolved resonances, representative of the fully bound ternary adduct, in which no further spectral changes were observed upon increasing the concentration of anion present. The anions chosen in this study provided a comparison of the selectivity preference between the *O*–phosphate binding mode and amino acid or peptide *N*–terminus chelation (**Figure 2.14**).

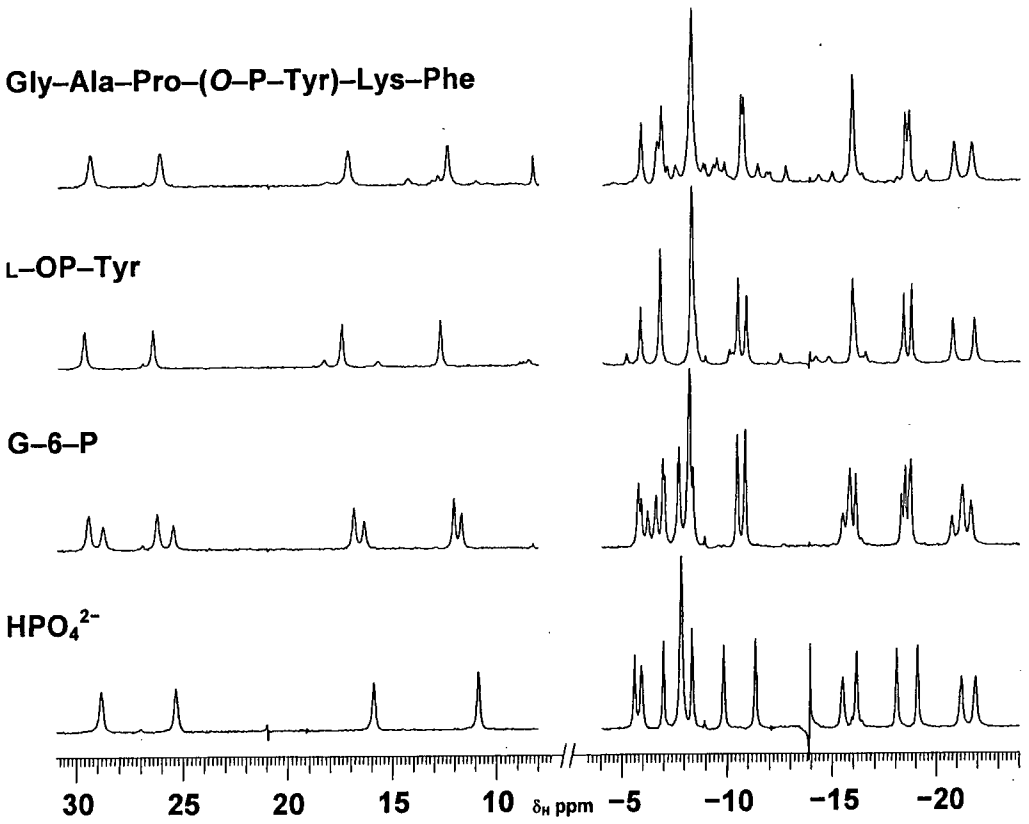

Figure 2.14 : ^{1}H NMR spectra of $[Eu\mathbf{8}(H_2O)_2]^{3+}$ (4 mM) in the presence of selected anions (20 mM) at 500 MHz, pH 7.4, 295 K. The spectra illustrate the major binding mode in all cases is through the phosphate anion.

The increased resolution obtainable in the proton NMR spectra of the europium complexes, when compared to the other lanthanides in this study, is illustrated by the complete resolution of every axial proton resonance in the G–6–P ternary adduct. Comparison of this spectrum for $[Eu\mathbf{8}(H_2O)_2]^{3+}$ with the corresponding G–6–P adduct of $[Eu\mathbf{7}(H_2O)_2]^{3+}$, in **Figure 2.15**, exemplifies the greater sensitivity of the

shift of the axial proton resonances towards the coordination environment in the *N*–methylated complexes.

The spectra shown in **Figure 2.14** clearly demonstrate the dominance of the phosphate anion binding mode, even when the possibility of amino acid chelation is available, as in the ternary adduct with *O*–phosphotyrosine. Therefore, the complex $[Eu\mathbf{8}(H_2O)_2]^{3+}$ illustrates the power of the lanthanide(III) ion in tuning the selectivity towards anion binding, providing a complete reversal of the preference for amino acid chelation exhibited by $[Yb\mathbf{8}(H_2O)_2]^{3+}$.

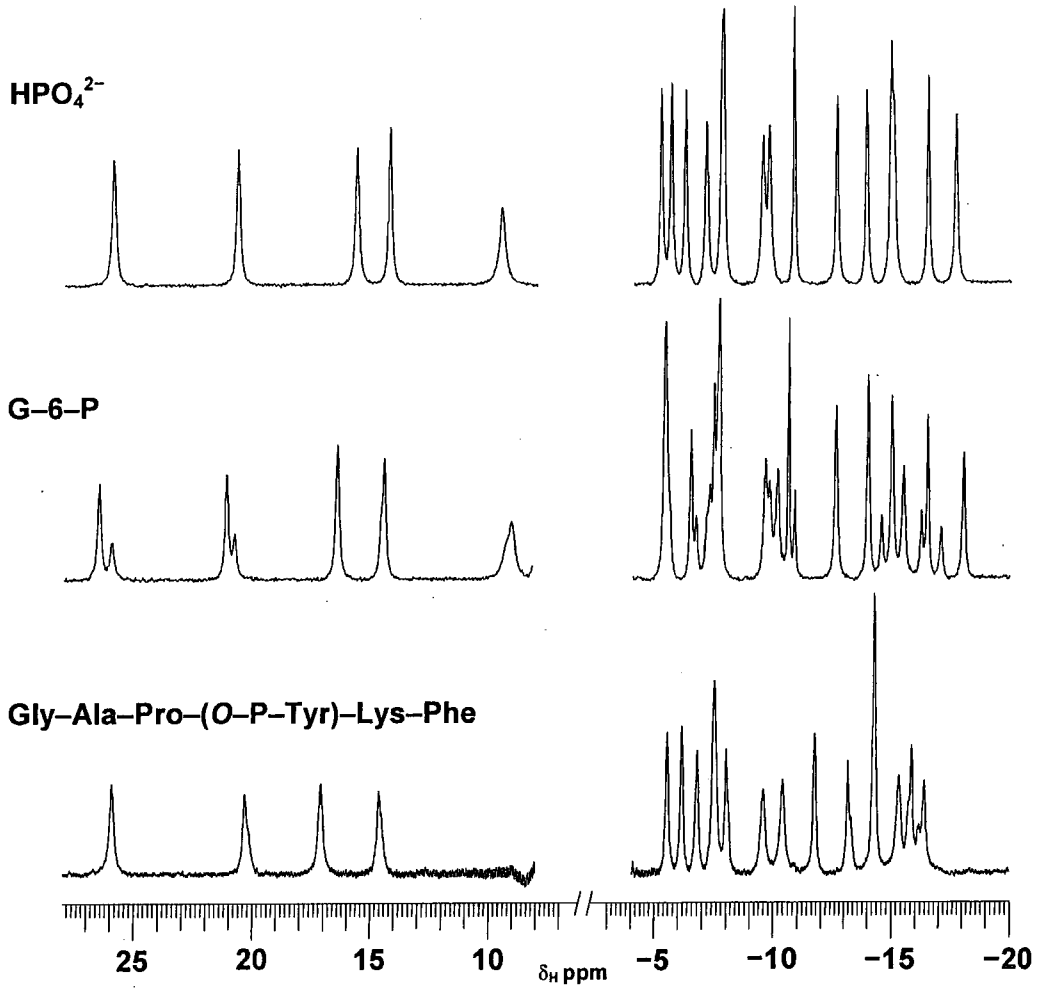

Figure 2.15 : ^{1}H NMR spectra of $[Eu\mathbf{7}(H_2O)_2]^{3+}$ (4 mM) in the presence of selected anions (20 mM) at 500 MHz, pH 7.4, 295 K. The spectra illustrate the major binding mode in all cases is through the phosphate anion.

Despite the domination of the phosphate binding mode, there is still evidence of a further binding mode, albeit at very low concentration (~10%), in the ternary adduct of $[Eu\mathbf{8}(H_2O)_2]^{3+}$ with *O*–phospho–tyrosine and to a greater extent in the

phosphorylated hexapeptide adduct. Therefore, given that ternary adducts of ligand 7 show a greater preference for the phosphate binding mode than the corresponding ternary adducts of ligand **8**, the complex $[Eu7(H_2O)_2]^{3+}$, despite sacrificing anion affinity, was expected to provide exceptional selectivity towards the phosphate binding mode.

Addition of a fivefold excess of phosphorylated anions to the complex $[Eu7(H_2O)_2]^{3+}$, produced a proton NMR spectrum consistent with the fully bound anion adduct. All the ternary adducts of this complex with phosphorylated anions gave rise to a proton NMR spectrum consisting of one dominant set of resonances. In each case, the resonances of the most shifted axial protons correlated well with every phosphorylated anion adduct studied, consistent with the chemoselective binding to the phosphate oxygen atom (**Figure 2.15**). Even in the presence of competitive binding modes such as amino acid chelation, no evidence of any other binding mode was suggested by the proton NMR analysis, as illustrated for the ternary adduct with the selected phosphorylated hexapeptide.

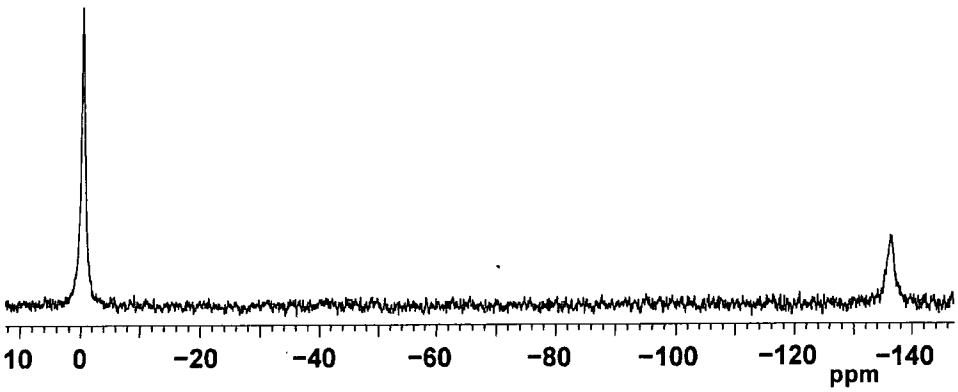

Figure 2.16 : ^{1}H–decoupled ^{31}P NMR spectra of $[Eu7(H_2O)_2]^{3+}$ (4 mM) in the presence of *O*–phoshotyrosine (8 mM) at 162 MHz, pH 7.4, 295 K, illustrating the presence of unbound and bound *O*–phoshotyrosine in slow exchange on the NMR timescale.

Further confirmation of the presence of the phosphate group coordinated directly to the europium(III) centre was provided by ^{31}P NMR. To a solution of $[Eu7(H_2O)_2]^{3+}$ (4 mM) was added the phosphorylated anion or peptide (8 mM) in D_2O at pH 7.4, 295 K. The resulting proton–decoupled ^{31}P NMR spectrum was subsequently recorded at 162 MHz (**Figure 2.16**). The spectrum consists of two resonances, one at 0 ppm corresponding to the unbound phosphate species in solution, and a second broad resonance at −136 ppm ($\omega_{1/2}$ = 223 Hz), corresponding to the

paramagnetically shifted phosphorus atom bonded to the oxygen atom binding to the europium(III) centre.

2.2.5 Selectivity and Stability Observations

During the proton NMR spectroscopic investigations into the ternary adducts of the macrocyclic lanthanide(III) complexes with phosphorylated anions, a number of general observations were made with regards to the selectivity and stability of these adducts.

The *O*–phosphate ternary adducts displayed no observable changes in the characteristic proton NMR spectrum even in the presence of human serum albumin (0.35 mM). No changes were observed even after a period of over one month. Similarly, the proton NMR spectrum of the lanthanide(III) complexes in the presence of human serum albumin (0.35 mM), consists of one set of severely broadened resonances corresponding to the di–aqua complex. Subsequent addition of 0.5 equivalents of *O*–phosphorylated anion is sufficient to produce a new set of resonances corresponding to the *O*–phosphate bound ternary adduct, which are clearly distinguished from the original broadened resonances. As expected, further addition of *O*–phosphorylated anion leads to only one set of resonances in the proton spectrum.

Interestingly, a distinct preference in the selectivity between the *O*–phosphorylated amino acids was observed. Addition of ten equivalents of *O*–phosphoserine to a solution of $[Yb7(H_2O)_2]^{3+}$ containing five equivalents of *O*–phosphotyrosine gave rise to a proton NMR spectrum in which more than 80% of the lanthanide(III) complex was present as the *O*–phosphotyrosine anion adduct. This proton NMR spectrum remained unchanged at room temperature for at least one week, indicating a significant preference for *O*–phosphotyrosine over *O*–phosphoserine. The only plausible explanation for such a preference for binding may be ascribed to the lower free energy of hydration associated with the tyrosine residue when compared to the serine residue.

2.3 Luminescence Studies of Phospho–Anion Binding

As discussed in **Section 1.3.4**, the sensitivity of selected emission bands in the

luminescence emission spectra of europium(III) complexes is particularly valuable in the analysis of the coordination environment around the lanthanide(III) centre. Typically useful spectral characteristics are the $^7F_1 \leftarrow {}^5D_0$ transition ($\Delta J = 1$), which displays up to three components representative of the symmetry around the lanthanide(III) centre,[22] and the hypersensitive $^7F_2 \leftarrow {}^5D_0$ transition ($\Delta J = 2$).[23]

Addition of a tenfold excess of *O*–phosphorylated anions to the complexes $[Eu\mathbf{7}(H_2O)_2]^{3+}$ and $[Eu\mathbf{8}(H_2O)_2]^{3+}$, gave luminescence spectra representative of the fully bound ternary anion complex, with addition of further anions leading to no observable perturbations in the spectra (**Figure 2.17**).

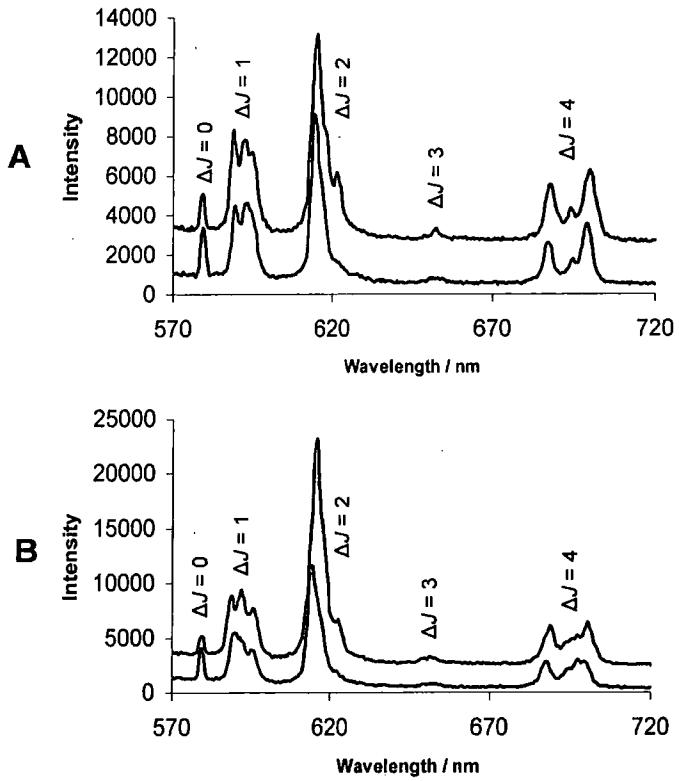

Figure 2.17 : Representative luminescence emission spectra of $[Eu\mathbf{7}(H_2O)_2]^{3+}$ (1 mM) (A) and $[Eu\mathbf{8}(H_2O)_2]^{3+}$ (1–mM) (B) (295 K, pH 7.4, 0.1 M MOPS), as the di–aqua complex (lower spectra) and in the presence of G–6–P (10 mM).

Each ternary adduct produced distinctive modifications to the splitting pattern of the $\Delta J = 1$ band, accompanied by an increase in the intensity of the $\Delta J = 2$ to $\Delta J = 1$ ratio. These changes are particularly evident in the case of $[Eu\mathbf{8}(H_2O)_2]^{3+}$, perhaps providing further confirmation of the increased distortion of the macrocyclic ring upon anion binding, which was previously hypothesised from the corresponding paramagnetically shifted proton NMR spectra (**Section 2.2.2**). The other noticeable

feature upon anion binding, is the new component present in the $\Delta J = 2$ band at approximately 620 nm, and is most significant in the $[Eu\mathbf{7}(H_2O)_2]^{3+}$ complex.

The structural rigidity of the lanthanide(III) complexes $[Eu\mathbf{7}(H_2O)_2]^{3+}$ and $[Eu\mathbf{8}(H_2O)_2]^{3+}$, along with the inherent chirality present, allows the use of circularly polarised luminescence (CPL) to further probe the coordination environment in the corresponding ternary anion adducts.[24] Again the emission spectra were recorded in the presence of a tenfold excess of the given anions, thus ensuring the spectra are representative of the fully bound ternary anion adducts. The *O*–phosphorylated anions were chosen such that the maximum information was obtained regarding the binding modes present in the corresponding ternary anion adducts. In each of the CPL spectra, which concentrate on the splitting observed for the $^7F_1 \leftarrow {}^5D_0$ transition, the europium(III) ion was excited directly using the $^7F_0 \rightarrow {}^5D_0$ transition at 579.4 nm (**Figures 2.18** and **2.19**). For the ternary adducts of $[Eu\mathbf{7}(H_2O)_2]^{3+}$, the CPL spectra exhibit only subtle changes, as expected given that the corresponding emission spectra also displayed only subtle variations. However, the CPL spectra of the ternary adducts of $[Eu\mathbf{7}(H_2O)_2]^{3+}$ with G–6–P and hydrogen phosphate are almost identical and are certainly distinctive from the spectra of the other adducts investigated (**Figure 2.18**).

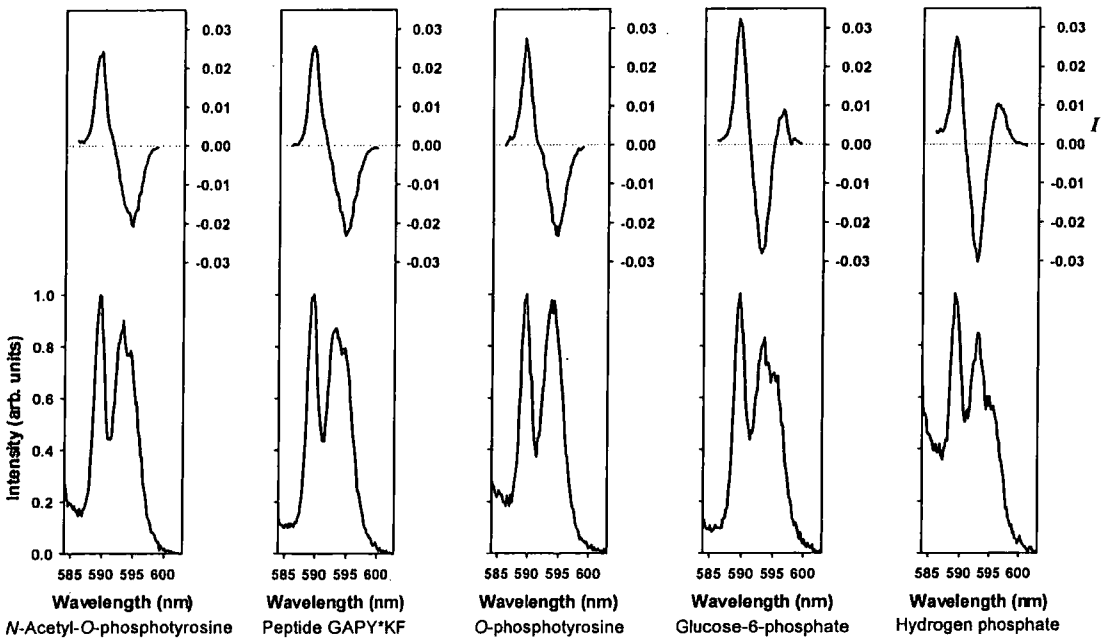

Figure 2.18 : CPL emission spectra of $[Eu\mathbf{7}(H_2O)_2]^{3+}$ (1 mM) (293 K, pH 7.4, 0.1 M MOPS), in the presence of phosphorylated anions (10 mM), focussing on the splitting observed in the $^7F_1 \leftarrow {}^5D_0$ transition.

Furthermore, given that the ternary adduct of $[Eu\mathbf{7}(H_2O)_2]^{3+}$ with *N*–acetyl–*O*–phosphotyrosine is known to be bound via a phosphate binding mode (confirmed from the proton NMR study), the identical CPL spectra obtained for ternary adducts of the selected phosphorylated peptide and *O*–phosphotyrosine, also confirms that these adducts bind through the phosphate oxygen atom.

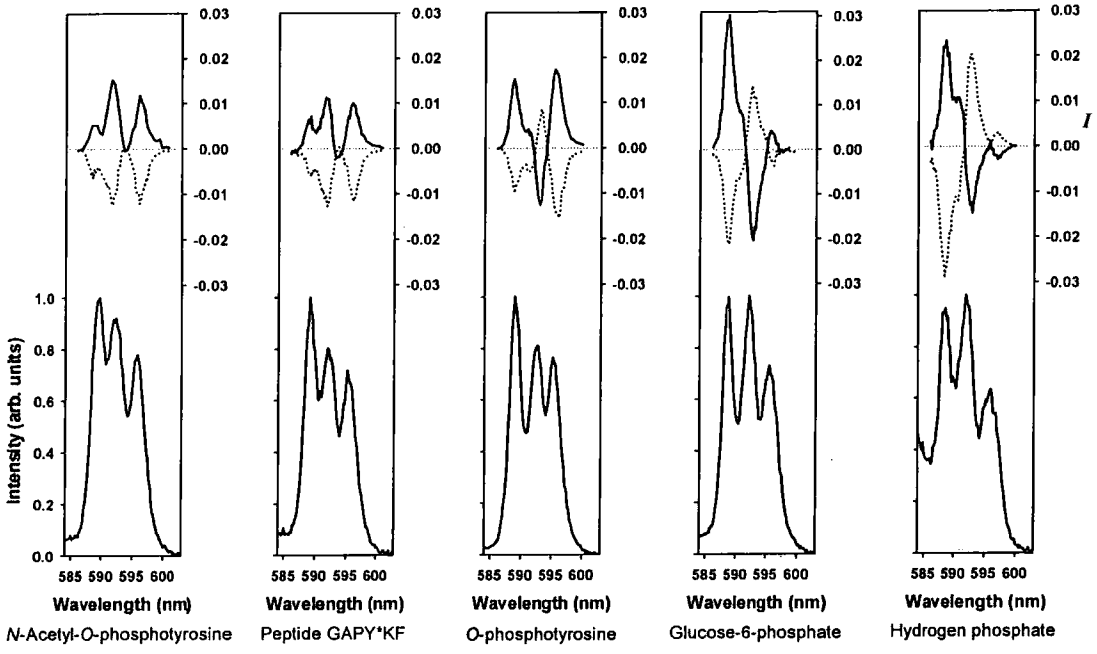

Figure 2.19 : CPL emission spectra of $[Eu\mathbf{8}(H_2O)_2]^{3+}$ (1 mM) (293 K, pH 7.4, 0.1 M MOPS), in the presence of phosphorylated anions (10 mM), focussing on the splitting observed in the $^7F_1 \leftarrow {}^5D_0$ transition.

The CPL spectra in the corresponding anion adducts of $[Eu\mathbf{8}(H_2O)_2]^{3+}$ display more marked differences for each of the adducts. In each of the ternary adducts, an almost identical mirror image CPL spectrum was obtained when measurements were made using the same complex with the opposite chirality on the pendant arms, consistent with the reversal in the helicity around the lanthanide(III) centre.[25] As observed in the ternary adducts of $[Eu\mathbf{7}(H_2O)_2]^{3+}$, the difference between the spectra involving G–6–P and hydrogen phosphate are distinctly different from the other adducts. These CPL spectra again confirm that a similar phosphate binding mode occurs in the ternary adducts of $[Eu\mathbf{8}(H_2O)_2]^{3+}$ with *N*–acetyl–*O*–phosphotyrosine and the selected phosphorylated peptide. However, in this case, the CPL spectrum of the *O*–phosphotyrosine adduct is slightly different and may indicate the presence of a small contribution from a coordination mode other than via the phosphate oxygen, consistent with the results obtained from the proton NMR study.

2.4 Conclusions

Proton NMR and luminescence spectroscopies provide a convenient means of monitoring the solution state structure of the ternary adducts of macrocyclic lanthanide(III) complexes with various phosphorylated anions. In each ternary anion adduct the most high frequency shifted resonances correspond to the four inequivalent axial macrocyclic ring protons. In each case, the distinctive pattern of these shifts can be used to identify the anion adducts present in solution and the binding mode exhibited towards the lanthanide(III) centre. Similarly, the differentiation of anion binding modes is also available from luminescence spectroscopy, particularly via observation of the splitting pattern for the $^7F_1 \leftarrow {}^5D_0$ transition, especially when coupled with the additional information available from CPL spectra.

Using these techniques, it has been established that although the thulium and ytterbium complexes display the greatest affinity towards anions, amino acid or *N*–terminal chelation is a competitive binding mode. In contrast, the corresponding europium complexes display a significant preference towards the phosphate binding mode. For all the lanthanides, complexes involving the *N*–methylated ligand show an increase in the competition from the chelating binding modes, and this becomes most significant for the smaller lanthanide(III) ions. This change in preferential binding modes is exemplified for the ytterbium complexes of the *N*–methylated ligand, which display an almost complete reversal in binding mode preference, with the amino acid chelation mode being the dominant ternary adduct.

This investigation into the binding of phosphorylated anions with well–defined lanthanide(III) complexes has revealed that such complexes have the potential to function as receptors for phosphorylated peptides or proteins. Such receptors could assist in the structural analysis of proteins, utilising the phosphorylated sites to introduce a paramagnetic species into the protein, rather than relying upon direct replacement of endogenous metal ions from binding proteins.[26] Furthermore, when suitably functionalised with an efficient sensitiser, such complexes may provide a means of monitoring the occurrence of intracellular phosphorylation processes, using microscopy techniques, thus presenting an insight into the pathways of such complex biological processes.

2.5 Selectivity Between Phosphorylated Sites Within Peptides

In the studies discussed above, it has been established that in the presence of phosphorylated peptides, the europium receptor $[Eu7(H_2O)_2]^{3+}$, exhibits a large preference towards the formation of a ternary phospho–anion adduct, via binding to the phosphate oxygen atom. In these binding modes, a distinct preference for the *O*–phosphotyrosine residue over the corresponding *O*–phosphoserine residue was observed, and attributed to the possible differences in free energy of hydration between them. To further investigate any selectivity based on the environment in close proximity to the bound phosphate group, the binding of $[Eu7(H_2O)_2]^{3+}$ to a tri–phosphorylated peptide was examined. The chosen peptide was the insulin receptor fragment 1154–1165, which contains three tyrosine residues (**Figure 2.20**). This peptide sequence was chosen as it was possible to obtain the insulin receptor fragment in various phosphorylated forms from a commercial source. In addition, similar insulin receptor fragments have been found to exhibit well–resolved sharp proton resonances in their proton NMR spectra.[27] This is particularly true for the aromatic region, where the assignment of each tyrosine residue was known for a very similar peptide fragment.[28]

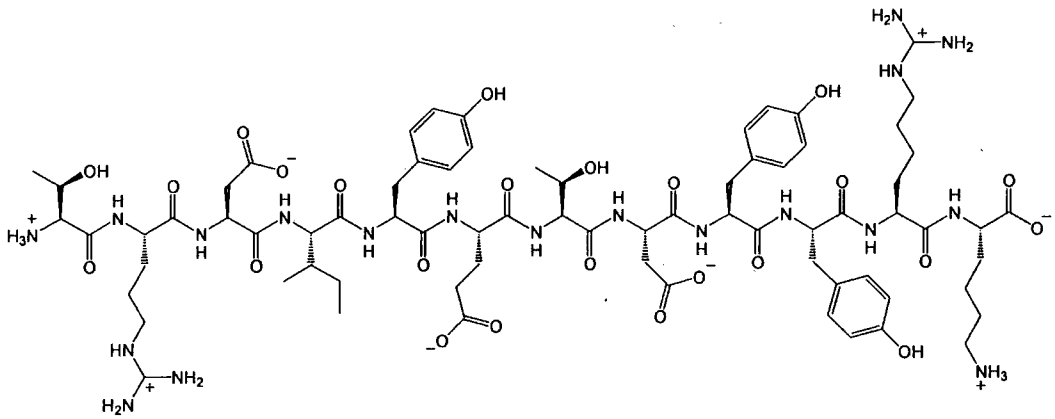

9Y* : Thr–Arg–Asp–Ile–Tyr–Glu–Thr–Asp–Tyr*–Tyr–Arg–Lys

10Y* : Thr–Arg–Asp–Ile–Tyr–Glu–Thr–Asp–Tyr–Tyr*–Arg–Lys

5,9,10Y* : Thr–Arg–Asp–Ile–Tyr*–Glu–Thr–Asp–Tyr*–Tyr*–Arg–Lys

Figure 2.20 : Illustration of the insulin receptor fragment and the two mono– and one tri–phosphorylated peptides used in the study, along with the abbreviations used. Asterisks (*) denote a phosphorylated residue.

Furthermore, 2D proton NMR TOCSY spectra of this peptide fragment revealed one observable set of resonances for each amino acid residue, consistent with the population of one major conformation in solution. This result is in contrast to the outcome of preliminary work with the neurotensin peptide. In this case, more than two major species, in slow exchange at 600 MHz, were evident from the analysis of NMR TOCSY spectra, hindering the confident assignment of each amino acid residue.

Earlier studies of the interaction of lanthanide complexes with proteins utilised gadolinium(III) complexes, with either an overall positive or negative charge, to monitor any preferential binding sites upon the protein surface.[29] The relaxation effect of the gadolinium(III) ion was used to determine the distance between the complex and the residues within the protein structure. Analysis of the results suggested that these charged complexes exhibit a small preference towards localised areas of opposite charge on a peptide surface.[29] However, for the europium receptor complex, $[Eu\mathbf{7}(H_2O)_2]^{3+}$, there is a definitive chemoselectivity towards the *O*–phosphotyrosine residues. Therefore, and in contrast to the earlier work, the nature of the peptide surface can only determine regioselectivity and has no influence upon the chemoselectivity. Thus, in the case of $[Eu\mathbf{7}(H_2O)_2]^{3+}$, the selectivity towards the different phosphate binding sites in the peptide was anticipated to be primarily determined by electrostatic contributions. Therefore, the tyrosine residue with the greatest number of proximate negatively charged residues was expected to constitute the more preferential binding site. In the peptide **5,9,10Y***, this was anticipated to be tyrosine–9, since this residue is directly adjacent to negatively charged aspartate and phosphate groups. The least preferred phosphorylated residue was thought to be tyrosine–10, despite its closeness to the phosphate group of tyrosine–9, as it is next to positively charged arginine and lysine residues.

The binding of $[Eu\mathbf{7}(H_2O)_2]^{3+}$ to a phosphate group on the peptide was anticipated to induce shifts in the resonances of nearby NMR active nuclei, without inducing significant line broadening,[29] and hence allow the identification of residues close to the binding site. Therefore, this peptide fragment was obtained from commercial sources (Peptide Protein Research Ltd) in two mono–phosphorylated forms and one tri–phosphorylated form (**Figure 2.20**). Using these three peptides it was postulated

that any preferential binding site in the tri–phosphorylated system could be easily distinguished through the comparison of proton NMR chemical shift information obtained for the corresponding mono–phosphorylated systems. However, given the complexity of the proton NMR spectra of the peptides, due to the many overlapping resonances observed, it was decided that significant information could only be obtained from 2D data.

2.5.1 2D Proton NMR of Phosphorylated Peptides

The use of 2D NMR techniques to assign the huge number of overlapping resonances observed in peptides and proteins is a long standing area of study.[30,31] Such experiments provide a map of the *J*–connectivities present in the peptide or protein backbone, and can also provide information on the secondary structure exhibited.[32] In the employment of proton NMR techniques, the use of H_2O, or H_2O/D_2O mixtures, rather than pure D_2O, as the solvent is necessary in order to visualise the amide proton resonances, which would otherwise undergo deuterium exchange in D_2O. Exchanging the protons from the amide nitrogen atoms removes essential structural information from the resulting NMR spectra.[31] These amide resonances are useful since the resulting NMR TOCSY signals produced from the amide proton through the amino acid side chain, provide a distinctive pattern which can be used to identify the resonances of each amino acid residue (**Figure 2.21**). Furthermore, the through space nuclear Overhauser effect, which is measurable between an amide proton and the α–proton of the adjacent amino acid,[30,31] can be used to distinguish between identical amino acid residues within the peptide, thus providing the amino acid sequence of the peptide or protein.

The need for H_2O as a solvent produces one obvious problem, namely the very intense proton resonance. Thus, effective water suppression sequences are essential in order to minimise the solvent resonance, thus allowing the resolution of the peptide resonances.[33] In the studies reported here, the pulse sequence 'Watergate' was used for this purpose.

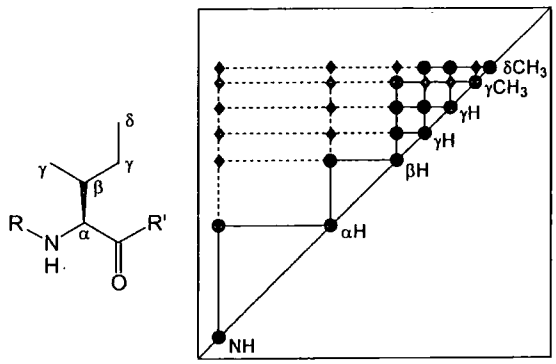

Figure 2.21 : Illustration the expected ^{1}H NMR TOCSY pattern for an isoleucine residue, highlighting the additional cross peaks observed in a TOCSY experiment (♦) along with those observed in the corresponding COSY experiment (●).

Figures 2.22 and **2.23** show the ^{1}H NMR TOCSY spectra (95% H_2O:D_2O, 298 K, pH 7.4) obtained for the peptides **10Y*** and **5,9,10Y*** respectively. The presence of only one observable set of resonances in each spectrum indicates that one major conformation of the peptide exists in solution. This is an important factor in these selectivity experiments, since any shifted resonances in the presence of the europium receptor may be masked by the signals arising due to the different peptide conformations present.

The ^{1}H TOCSY spectra obtained for peptide **10Y*** was used to assign successfully the resonances corresponding to each of the amino acid residues (see **Figure 2.22**), via the unique TOCSY pattern of resonances observed in the amide proton region for each different amino acid residue (**Figure 2.21**). Although there is more than one arginine, aspartate and threonine residue within the peptide chain, distinguishable resonances were observed for each of these residues in each case. Tyrosine–5 was clearly distinguishable in all the peptide sequences, although tyrosines–9 and 10 were only present as distinguishable resonances for the sequence **9Y***.

The information obtained from the NMR TOCSY spectra, however, does not allow the assignment of each TOCSY pattern to individual residues, since only through bond correlations are obtained. Assigning the resonances of each identical residue in the peptide chain sequence requires through space correlations between adjacent amino acid residues, which are provided using a proton NMR NOESY spectrum.[30,31] However, attempts to obtain proton NOESY or ROESY spectra of these peptides under a variety of spin mixing times resulted in rather weak correlation peaks.

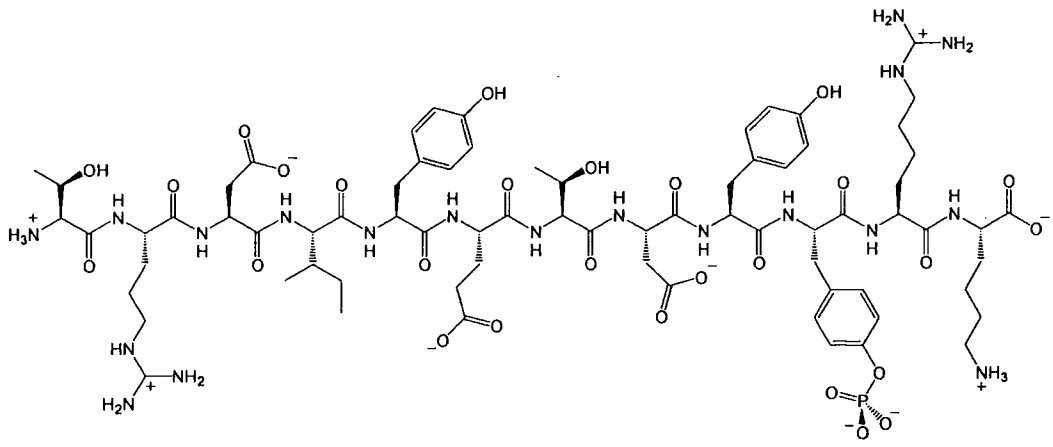

10Y*: Thr–Arg–Asp–Ile–Tyr–Glu–Thr–Asp–Tyr–Tyr*–Arg–Lys

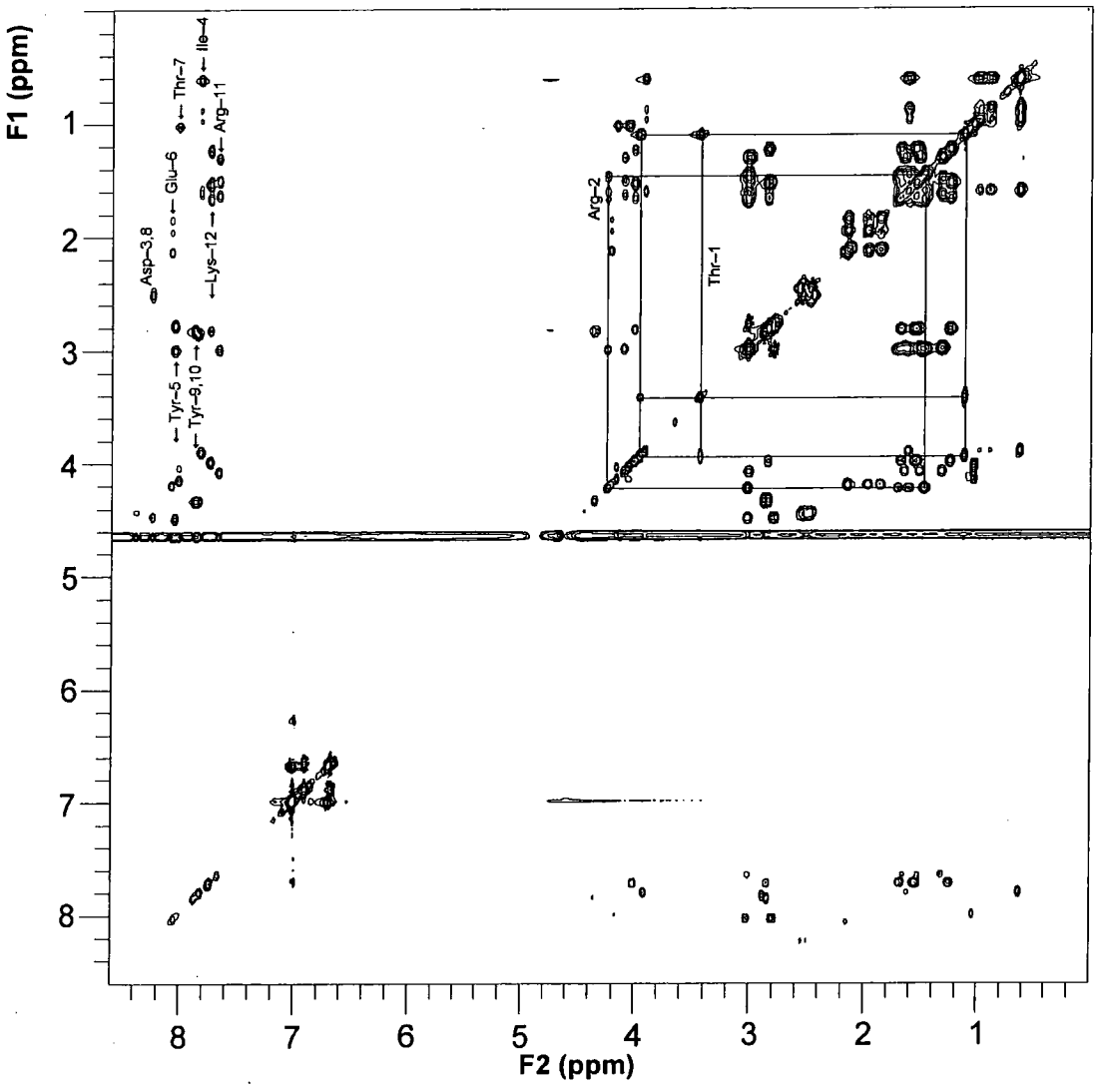

Figure 2.22 : ^{1}H NMR TOCSY spectrum of the peptide **10Y***, illustrating the presence of one set of resonances corresponding to the presence of one major conformation in solution. Assigned resonances are highlighted for each of the amino acid residues.

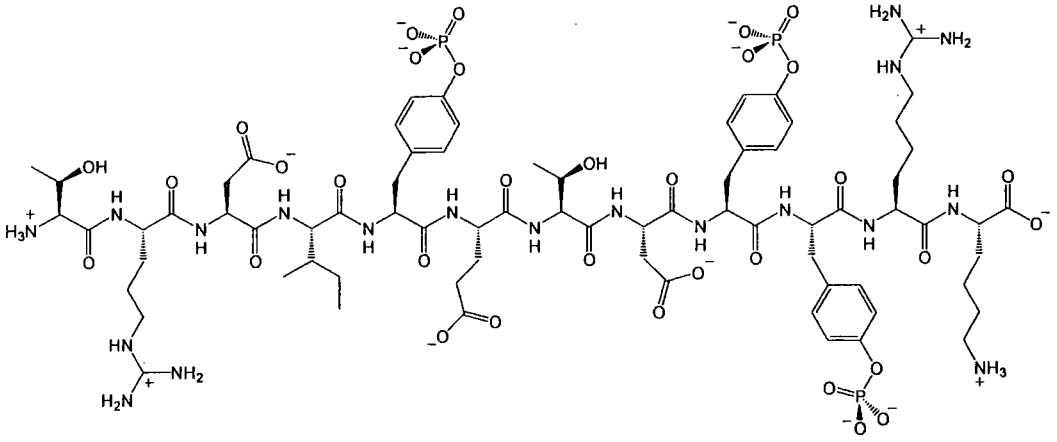

5,9,10Y*: Thr–Arg–Asp–Ile–Tyr*–Glu–Thr–Asp–Tyr*–Tyr*–Arg–Lys

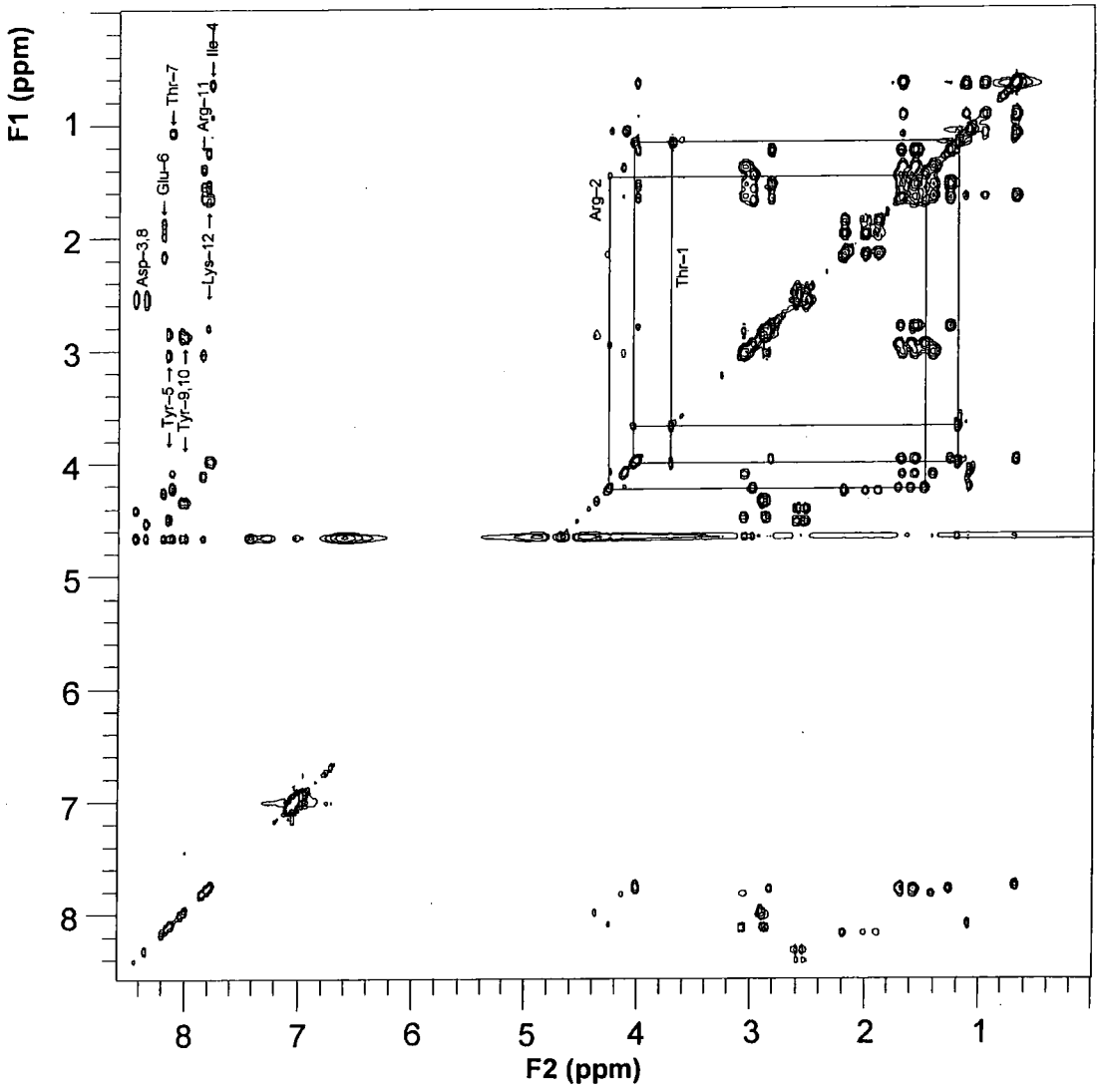

Figure 2.23 : ^{1}H NMR TOCSY spectrum of the peptide **5,9,10Y***, illustrating the presence of one set of resonances corresponding to the presence of one major conformation in solution. Assigned resonances are highlighted for each of the amino acid residues.

The presence of only weak NOESY and ROESY correlation peaks has also been observed for a shorter fragment of the insulin receptor peptide (1154–1161).[27] As a consequence, the resonances for the arginine, aspartate and tyrosine residues could not be distinguished at this stage. However, the distinction of these residues was anticipated to be highlighted when analysing the spectra of these peptides in the presence of the europium receptor complex, due to the paramagnetically induced shifts of nearby nuclei.

In contrast, the two threonine residues were easily distinguished, since an amide proton is absent in the *N*–terminal threonine residue. Thus, the threonine resonances which correlated with an amide proton could be assigned to threonine–7. Close inspection of the unassigned resonances remaining in the spectra then allowed the assignment of the *N*–terminal threonine residue.

For each of the three peptides studied, the general position of the resonances corresponding to each amino acid residue remained virtually identical, despite their differing degree of phosphorylation. The most significant changes in the positions of resonances occur in the amide region for the residues adjacent to tyrosine sites. For example, comparison of the amide proton shift for isoleucine–4 in **10Y*** and **5,9,10Y*** indicates that there is a low frequency shift upon phosphorylation of tyrosine–5. Careful analysis of these subtle shift differences for the residues adjacent to tyrosine sites in the differentially phosphorylated peptides allowed the tentative assignment of arginine–11, and hence arginine–2, and also tyrosine–5.

2.5.2 2D Proton NMR of Phosphorylated Peptides in the Presence of the Europium Complex

Addition of the europium receptor complex ($[Eu7(H_2O)_2]^{3+}$) to the mono–phosphorylated peptides **9Y*** and **10Y*** led to the formation of a phosphate bound ternary adduct. This was confirmed by observing the paramagnetically shifted proton NMR spectra, over the region +40 to −30 ppm. This gave the distinct pattern and mean chemical shift expected for the four resonances of the axial macrocyclic ring protons in a phosphate bound ternary adduct, as revealed in **Section 2.2.4**. Further indication of the presence of this binding mode was obtained from the corresponding ^{31}P NMR spectrum, which displayed a broad shifted resonance at −136 ppm, in

addition to the resonance at 0 ppm observed for the peptide in the absence of the europium receptor. This shifted resonance is characteristic of the phosphate bound ternary adduct, and an identical resonance was observed for the *O*–phosphotyrosine ternary adduct with $[Eu\mathbf{7}(H_2O)_2]^{3+}$.

The proton NMR TOCSY spectra of the mono–phosphorylated peptides were repeated in the presence of 0.25 and 0.5 equivalents of $[Eu\mathbf{7}(H_2O)_2]^{3+}$. Given that the ternary anion adducts of $[Eu\mathbf{7}(H_2O)_2]^{3+}$ were observed to be in slow exchange on the NMR timescale, it was anticipated that a new set of resonances would be observed in addition to those of the unbound peptide. Thus, increasing the concentration of $[Eu\mathbf{7}(H_2O)_2]^{3+}$ in solution should increase the intensity of any shifted resonances relative to the original resonance. More than 0.5 equivalents of $[Eu\mathbf{7}(H_2O)_2]^{3+}$ generally led to significant broadening of the residual water resonance and poor water suppression, resulting in rather poor quality spectra and therefore little useful additional information was obtained.

As anticipated, the presence of the phosphate bound europium receptor led to the shifting of some, but not all, amino acid residues in the peptide chain as a result of the low magnetic anisotropy exhibited by the europium(III) ion.[34,35] The spectrum obtained for the peptide **10Y*** (**Figure 2.24**) in the presence of 0.5 equivalents of $[Eu\mathbf{7}(H_2O)_2]^{3+}$, exhibited the smallest number of shifted resonances relative to the original spectrum (**Figure 2.22**).

Through inspection of **Figure 2.24**, it is evident that there is a new set of shifted resonances for the lysine residue and one of the arginine residues. The second set of arginine resonances display no evidence of any additional shifted resonances. Given the proximity of arginine–10 to the phosphate binding site and the great distance between arginine–2 and the phosphate binding site, this allows the tentative assignment of arginine–10 to the resonances experiencing the paramagnetic shift. This assignment corroborates the earlier assignment of this residue based on the shift of its resonance upon phosphorylation of the adjacent tyrosine–10 residue. The only other distinctive shifts occur for two of the tyrosine residues. Again, in this case the distance of tyrosine–5 from the binding site at tyrosine–10, strongly suggests that the two sets of shifted resonances can be assigned to tyrosine–9 and 10, although no

conclusive distinction can be made between them. Despite the greater shift observed in one set of resonances compared to the other, the resonances experiencing the greatest shift cannot be assumed to belong to the closest tyrosine residue, since the angle dependence of the induced paramagnetic shift can be highly significant. No noticeable shifting of resonances was observed for any of the other residues within the peptide chain.

Figure 2.25 illustrates the spectrum obtained for the peptide **9Y*** in the presence of 0.5 equivalents of $[Eu7(H_2O)_2]^{3+}$. As for the peptide **10Y***, a number of shifted resonances was observed relative to the original spectrum. As expected, the residues possessing paramagnetically induced shifts in the peptide **10Y*** are also shifted in the **9Y*** peptide, since the phosphate binding sites in both cases are adjacent. Thus, shifted resonances belonging to the lysine–12 and arginine–11 residues were accompanied by the shifting of resonances for the same two tyrosine residues observed in the spectrum of the **10Y*** peptide. In addition to the shifts observed for the **10Y*** peptide, in the presence of the europium receptor, peptide **9Y*** also displayed additional shifted resonances corresponding to the threonine–7 residue. There is also significant evidence for a shift in the resonances of aspartate–8. However, the poor resolution and broadening in this region of the spectrum means that the suspected shifts cannot be assigned conclusively. The observation of paramagnetically shifted resonances for residues closer to the *N*–terminus is consistent with the smaller distance between these residues and the phosphate binding site in the **9Y*** peptide. Therefore, the fact that the effective distance over which the paramagnetic shift of the europium(III) ion is measurable (<10 Å)[29] is significantly less than the dimensions of the peptide (of the order of 40 Å), provides a means of identifying the difference between binding at the phosphorylated site of tyrosine–9 and 10.

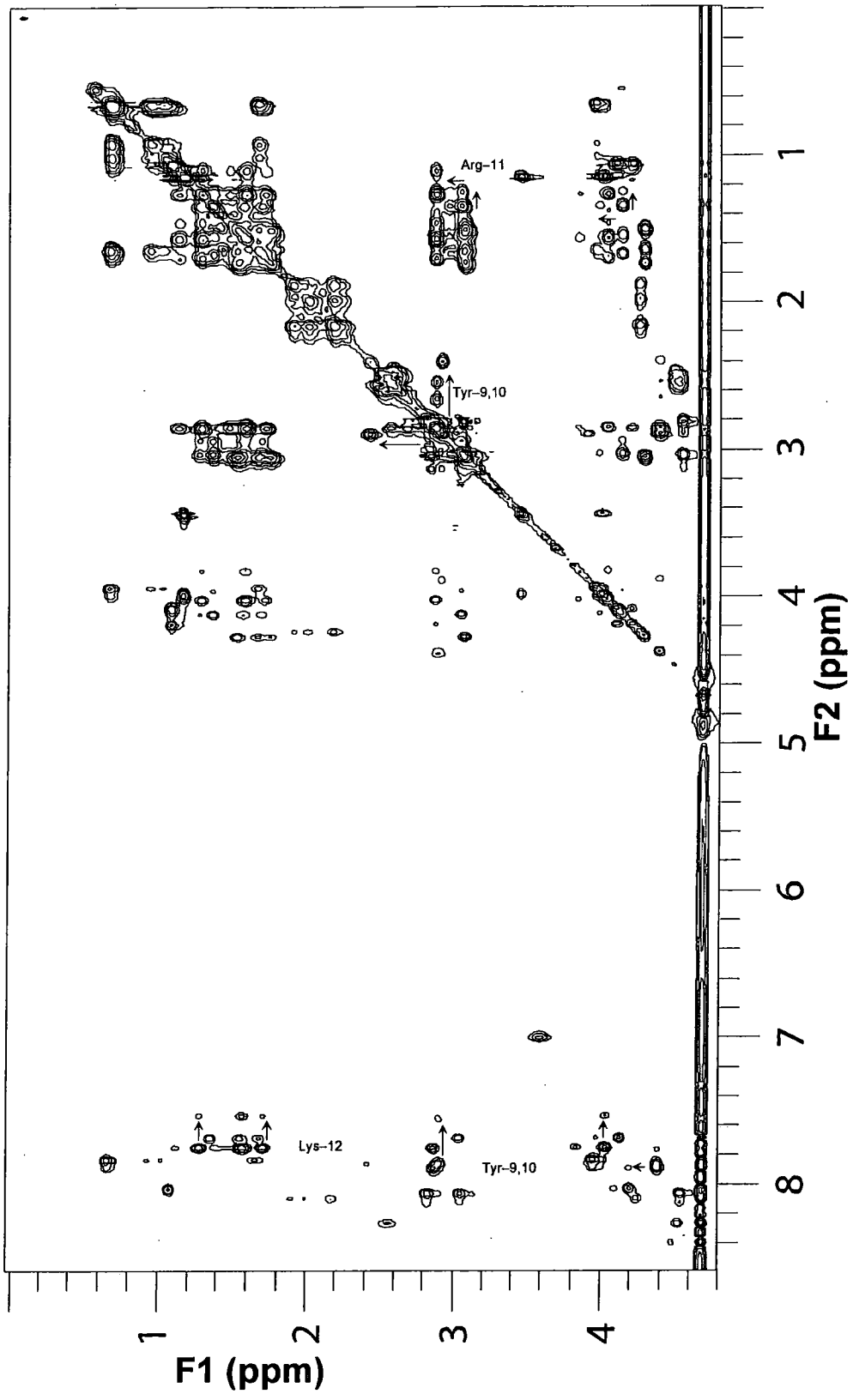

Figure 2.24 : ^{1}H NMR TOCSY spectrum of the peptide **10Y*** in the presence of 0.5 equivalents of $[Eu7(H_2O)_2]^{3+}$, illustrating some of the shifted resonances for amino acid residues in close proximity to the europium(III) centre.

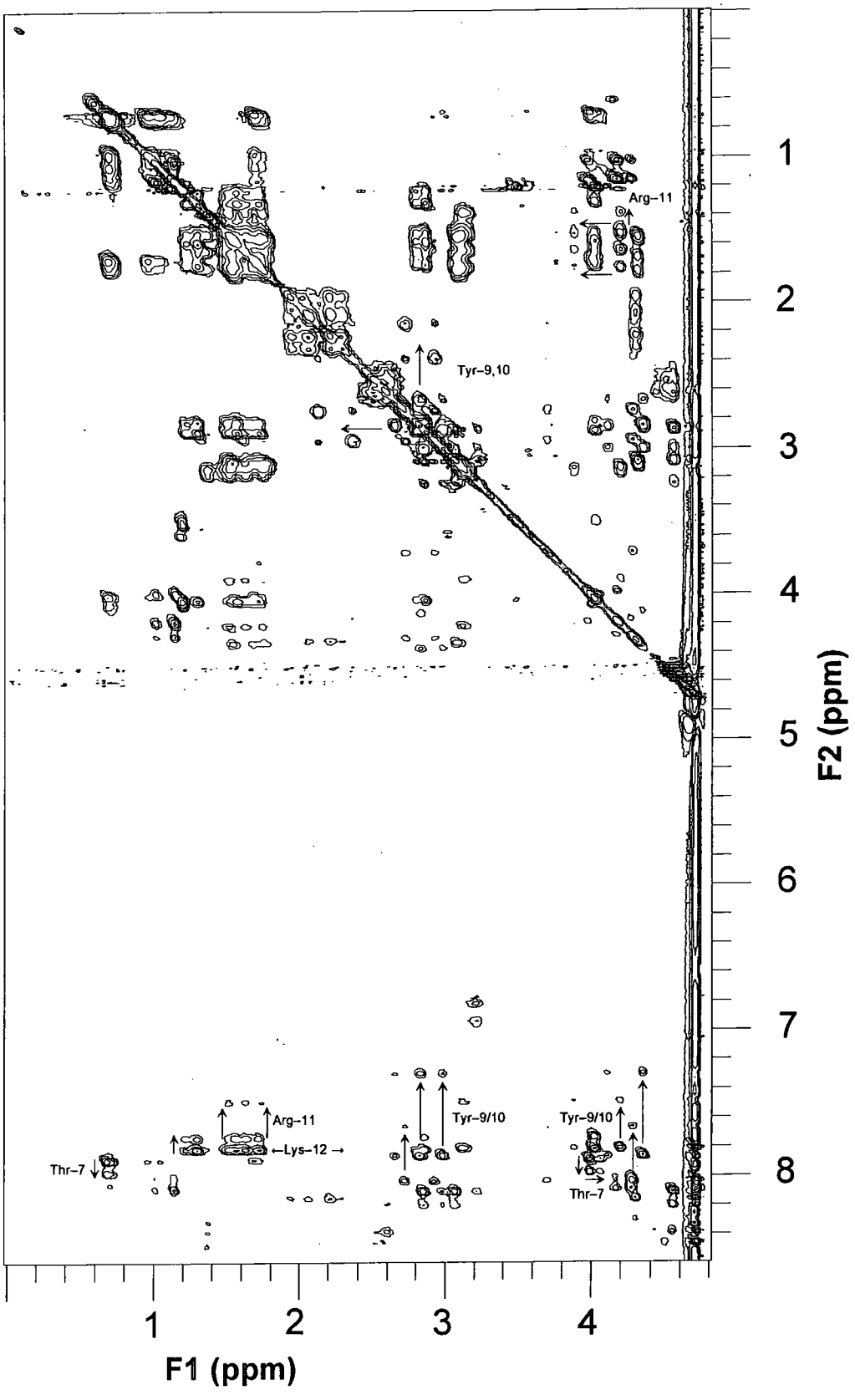

Figure 2.25 : ^{1}H NMR TOCSY spectrum of the peptide **9Y*** in the presence of 0.5 equivalents of $[Eu7(H_2O)_2]^{3+}$, illustrating some of the shifted resonances which indicate the presence of the proximate europium(III) centre.

No sample of the peptide **5Y*** was obtained, and hence no spectral data for this compound was available. However, given the short distance over which the europium receptor had been observed to influence the shifts of nuclei within the peptide, it was anticipated that any binding to the *O*–phosphotyrosine–5 residue in **5,9,10Y*** could be easily distinguished, due to the shifting of the resonances of *N*–terminal residues. Therefore, using the information obtained from the ^{1}H TOCSY spectra of the mono–phosphorylated peptides, the binding of the europium complex to the tri–phosphorylated peptide, **5,9,10Y*** was investigated in the same manner.

Addition of only 0.25 equivalents of $[Eu\mathbf{7}(H_2O)_2]^{3+}$ (relative to the peptide, not the phosphate binding sites) to the **5,9,10Y*** peptide was sufficient to observe shifted resonances in the measured ^{1}H TOCSY spectrum. Indeed, addition of up to 0.75 equivalents of $[Eu\mathbf{7}(H_2O)_2]^{3+}$ was possible without causing severe line–broadening and deterioration in spectral quality. This spectrum is illustrated in **Figure 2.26**, and clearly indicates that more than one binding site is occupied, since there are many more shifted resonances present than in the previous two cases.

Upon closer inspection it is evident that even at low concentrations of $[Eu\mathbf{7}(H_2O)_2]^{3+}$, there are shifted resonances present which were not observed in the two mono–phosphorylated peptides. This observation is good evidence that the europium complex is binding to *O*–phosphotyrosine–5. Analysis of the spectrum in the presence of 0.75 equivalents of europium complex reveals intense shifted resonances for the *N*–terminal threonine residue and the isoleucine–4 residue. This spectrum confirms that significant binding also occurs to tyrosine–9 or 10, as intense and significantly shifted resonances for the C–terminal lysine residue are also observed in these cases. Comparison of the appearance of the shifted resonances for the C–terminal lysine with the corresponding shifts observed in each of the mono–phosphorylated peptides, suggests that these shifts are primarily caused by the binding to the *O*–phosphotyrosine–9 residue.

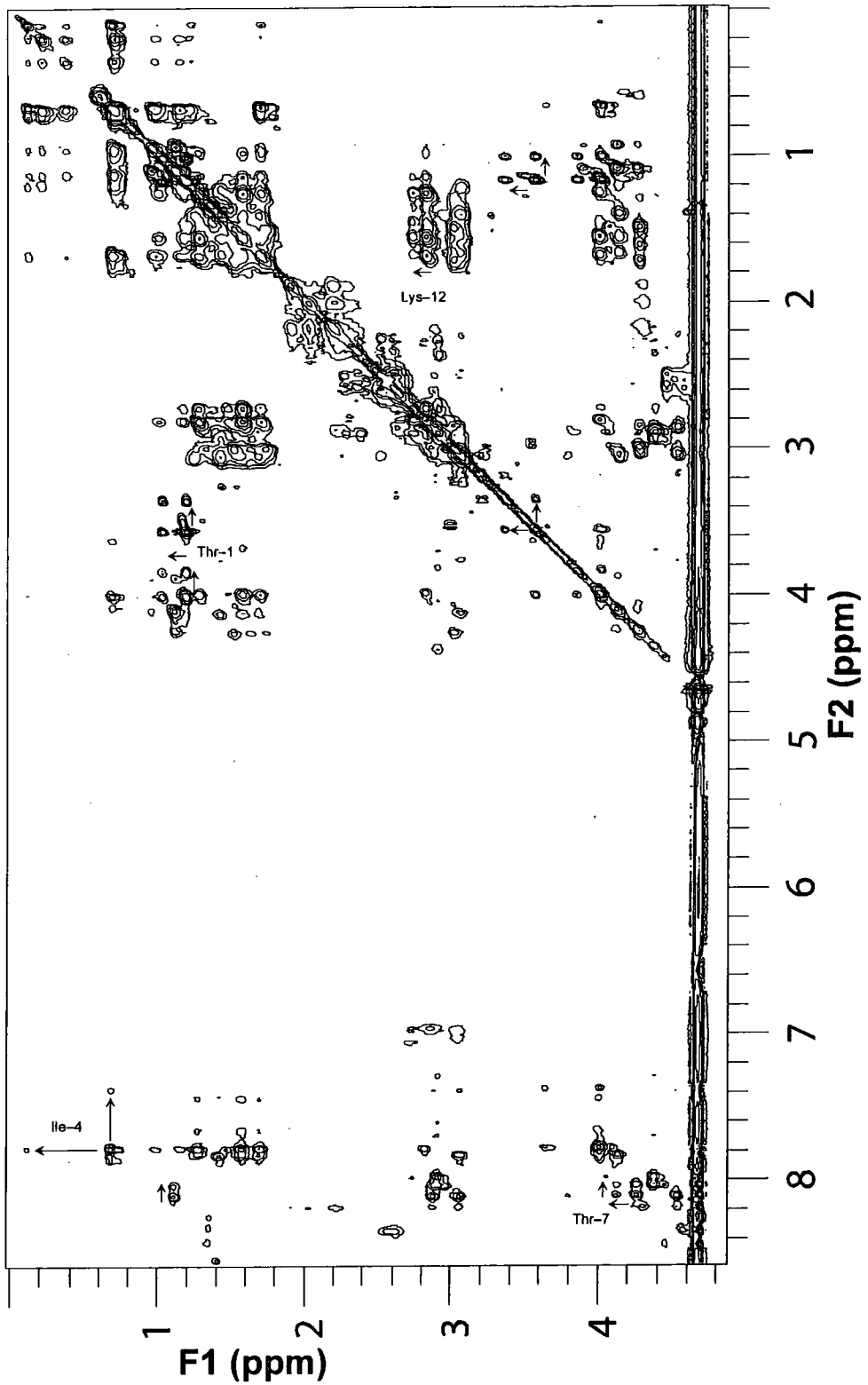

Figure 2.26 : ^{1}H NMR TOCSY spectrum of the peptide **5,9,10Y*** in the presence of 0.75 equivalents of $[Eu7(H_2O)_2]^{3+}$, illustrating the presence of multiply shifted resonances indicating that binding of the europium complex occurs to more than one phosphorylated tyrosine residue.

2.6 Conclusions

The analysis of the proton NMR TOCSY spectra of a differentially phosphorylated peptide has been used to assign the observed proton resonances to each amino acid residue within the peptide sequence. Addition of the europium receptor complex, $[Eu7(H_2O)_2]^{3+}$ results in the formation of a phosphate bound ternary adduct with the peptide. The nuclei present in the amino acid residues that are close in space to the phosphate binding site are influenced by the unpaired electron density on the europium(III) ion. This interaction induces a shifting of the resonances observed for the NMR active nuclei within the amino acid residue, which is proportional to the distance and angle of the nuclei from the europium(III) ion. Since the magnetic anisotropy of the europium(III) ion is very small, the distance from the europium(III) ion within which the paramagnetically induced shifts are observed (<10 Å), is significantly less than the overall dimensions of the peptide chain (of the order of 40 Å). This occurrence is particularly advantageous in the analysis of the proton NMR TOCSY spectra of the phosphorylated peptides in the presence of the europium receptor complex. Instead of observing a gradual diminution of the induced paramagnetic shift along the peptide chain, a distinct cut–off point on the peptide chain exists, after which, the paramagnetically induced shift is too small to be observed. For example, in the mono–phosphorylated peptides **9Y*** and **10Y***, although the europium ternary adduct is only one amino acid residue closer to the *N*–terminus for the peptide **9Y*** in comparison to **10Y***, shifted resonances for the threonine–7 residue are clearly observed in the former case but not in the latter.

An investigation into any phosphate binding site selectivity within the peptide chain was undertaken using the tri–phosphorylated peptide **5,9,10Y***. In the presence of the europium receptor complex, the proton NMR TOCSY spectrum of this peptide exhibited numerous residues possessing paramagnetically shifted resonances. This occurrence suggests that the selectivity exhibited by the europium receptor complex towards *O*–phosphotyrosine residues is not increased significantly by the presence of proximate negative charges. On the other hand, the shifts observed for the C–terminal lysine residue in the tri–phosphorylated peptide does suggest that there is some preference for binding to the *O*–phosphotyrosine–9 residue. This is consistent with the premise that the positively charged residues adjacent to *O*–phosphotyrosine–

10, to some extent, reduce the binding preference towards this site.

Although this simple europium receptor complex exhibits only modest selectivity towards specific *O*–phosphotyrosine residues within this peptide sequence, the unequivocal preference towards an *O*–phosphotyrosine binding mode, even in the presence of carboxylate side chain groups and notwithstanding the possibility of *N*–terminal chelation, must not be ignored. Thus, the complex $[Eu7(H_2O)_2]^{3+}$ can be considered as a useful tool in the assignment of peptide sequences containing phosphorylated residues. Furthermore, there is the possibility of replacing the europium(III) ion with lanthanide(III) ions possessing larger magnetic anisotropies, such as dysprosium or terbium, which should exhibit very similar phosphate chemoselectivity. The use of lanthanide(III) ions which can induce paramagnetically induced shifts over a much greater distance (ie. in excess of 30 Å for dysprosium),[29] would allow the analysis of amino acid residues at far greater distances from the *O*–phosphotyrosine site. Furthermore, the combination of results obtained when using europium and dysprosium complexes of ligand **7**, would yield high resolution shift data for a large number of amino acid residues close to the *O*–phosphotyrosine binding site, as illustrated for a lanthanide exchanged calcium binding protein.[36]

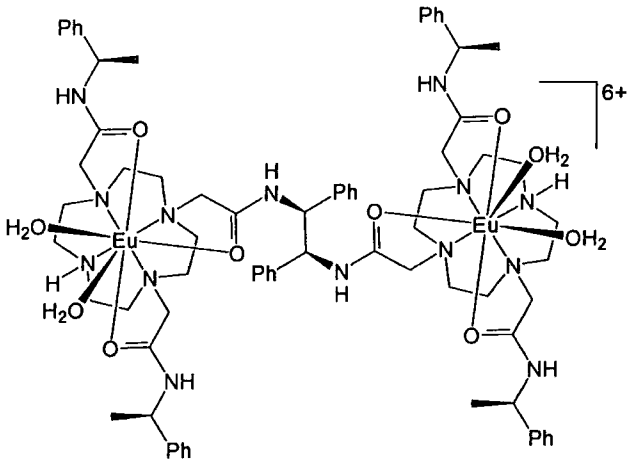

Figure 2.27 : Illustration of a possible dimeric complex generated from the coupling of two integral pendant arms, in order to minimise changes in the geometry around the lanthanide(III) ions.

One possible way of increasing the selectivity of specific *O*–phosphotyrosine sites is through the use of a dimeric europium receptor complex. The simplest dimeric complex envisaged, which is depicted in **Figure 2.27**, utilises the commercially available chiral compounds of 1,2–diamino–1,2–diphenylethane to provide the

diamide spacer group between the cyclen rings. Such a dimeric system could be used to bind regioselectively to two closely spaced *O*–phosphotyrosine sites within the peptide chain, as in the tri–phosphorylated peptide. The combined binding of the dimeric complex with two phosphotyrosine residues would be anticipated to effectively double the affinity constants observed for the simple monomeric europium receptor complex. Hence, with such increases in affinity constant by targeting close lying *O*–phosphotyrosine residues, the selectivity for *O*–phosphotyrosine–9 and *O*–phosphotyrosine–10 would be expected to be significantly higher than for the single *O*–phosphotyrosine–5 residue.

2.7 References

1 M. D. Best and E. V. Anslyn, *Chem. Eur. J.*, 2003, **9**, 51.

2 Y. Bretonnière, M. J. Cann, D. Parker and R. Slater, *Org. Biomol. Chem.*, 2004, **2**, 1624.

3 S.–H. Li, C.–W. Yu, W.–T. Yuan and J.–G. Xu, *Anal. Sci.*, 2004, **7**, 1375.

4 D. Parker and J. Yu, *Chem. Commun.*, 2005, 3141.

5 A. Beeby, I. M. Clarkson, R. S. Dickins, S. Faulkner, D. Parker, L. Royle, A. S. de Sousa, J. A. G. Williams and M. Woods, *J. Chem. Soc., Perkin Trans. 2*, 1996, 493.

6 J. I. Bruce, R. S. Dickins, L. J. Govenlock, T. Gunnlaugsson, S. Lopinski, M. P. Lowe, D. Parker, R. D. Peacock, J. J. B. Perry, S. Aime and Mauro Botta, *J. Am. Chem. Soc.*, 2000, **122**, 9674.

7 R. S. Dickins, A. S. Batsanov, J. A. K. Howard, D. Parker, H. Puschmann and S. Salamano, *Dalton Trans.*, 2004, 70.

8 F. Chuburu, M. Le Baccon and H. Handel, *Tetrahedron*, 2001, **57**, 2835.

9 J.–J. Yaouanc, N. Le Bris, G. Le Gall, J.–C. Clément, H. Handel and H. Des Abbayes, *J. Chem. Soc., Chem. Commun.*, 1991, 206.

10 V. Patinec, J.–J. Yaouanc, J.–C. Clément, H. Handel and H. des Abbayes, *Tet. Lett.*, 1995, **36**, 79.

11 S. Brandès, C. Gros, F. Denat, P. Pullumbi, R. Guilard, *Bull. Soc. Chim. Fr.*, 1996, **133**, 65.

12 V. Boldrini, G. B. Giovenzana, R. Pagliarin, G. Palmisano and M. Sisti, *Tet. Lett.*, 2000, **41**, 6527.

13 W. Yang, C. M. Giandomenico, M. Sartori and D. A. Moore, *Tet. Lett.*, 2003, **44**, 2481.

14 R. S. Dickins, S. Aime, A. S. Batsanov, A. Beeby, M. Botta, J. I. Bruce, J. A. K. Howard, C. S. Love, D. Parker, R. D. Peacock and H. Puschmann, *J. Am. Chem. Soc.*, 2002, **124**, 12697.

15 J. A. Peters, J. Huskens and D. J. Raber, *Prog. Nucl. Magn. Reson. Spectrsc.*, 1996, **28**, 283.

16 J. Ren and A. D. Sherry, *J. Magn. Reson. Ser. B*, 1996, **111**, 178.

17 R. S. Dickins, D. Parker, J. I. Bruce and D. J. Tozer, *Dalton Trans.*, 2003, 1264.

18 H. Eggert, J. Frederiksen, C. Morin and J. C. Norrild, *J. Org. Chem.*, 1999, **64**, 3846.

19 R. S. Dickins, C. S. Love and H. Puschmann, *Chem. Commun.*, 2001, 2308.

20 M. Botta, S. Aime, A. Barge, G. Bobba, R. S. Dickins, D. Parker and E. Terreno, *Chem. Eur. J.*, 2003, **9**, 2102.

21 A. Beeby, S. Faulkner, D. Parker and J. A. G. Williams, *J. Chem. Soc., Perkin Trans. 2*, 2001, 1268.

22 D. R. Foster and F. S. Richardson, *Inorg. Chem.*, 1983, **22**, 3996.

23 A. F. Kirby, D. Foster and F. S. Richardson, *Chem. Phys. Lett.*, 1983, **95**, 507.

24 J. I. Bruce, D. Parker, S. Lopinski and R. D. Peacock, *Chirality*, 2002, **12**, 562.

25 R. S. Dickins, J. A. K. Howard, C. L. Maupin, J. M. Moloney, D. Parker, J. P. Riehl, G. Siligardi and J. A. G. Williams, *Chem. Eur. J.*, 1999, **5**, 1095.

26 I. Baig, I. Bertini, C. Del Bianco, Y. K. Gupta, Y.–M. Lee, C. Luchinat and A. Quattrone, *Biochemistry*, 2004, **43**, 5562; R. Barbieri, I. Bertini, G. Cavallaro, Y.–M. Lee, C. Luchinat and A. Rosato, *J. Am. Chem. Soc.*, 2002, **124**, 5581.

27 N. R. Glover and A. S. Tracey, *J. Am. Chem. Soc.*, 1999, **121**, 3579.

28 B. A. Levine, B. Clack and L. Ellis, *J. Biol. Chem.*, 1991, **266**, 3565.

29 C. F. G. C. Geraldes and C. Luchinat, *Metal Ions in Biological Systems*, **Volume 40**, Eds. H. Sigel and A. Sigel, Marcel Dekker, New York, 2003, Chapter 14.

30 A. Kumar, R. R. Ernst and K. Wüthrich, *Biochem. Biophys. Res. Commun.*, 1980, **95**, 1.

31 A. Kumar, G. Wagner, R. R. Ernst and K. Wüthrich, *Biochem. Biophys. Res. Commun.*, 1980, **96**, 1156.

32 K. Wüthrich, G. Wider, G. Wagner and W. Braun, *J. Mol. Biol.*, 1982, **155**, 311.

33 G. Otting and K. Wüthrich, *J. Magn. Reson.*, 1987, **75**, 546.

34 V. S. Mironov, Y. G. Galyametdinov, A. Ceulemans, C. Görller–Walrand and K. Binnemans, *J. Chem. Phys.*, 2002, **116**, 4673.

35 I. Bertini, M. B. L. Janik, Y.–M. Lee, C. Luchinat and A. Rosato, *J. Am. Chem. Soc.*, 2001, **123**, 4181.

36 M. Allegrozzi, I. Bertini, M. B. L. Janik, Y.–M. Lee, G. Liu and C. Luchinat, *J. Am. Chem. Soc.*, 2000, **122**, 4154.

CHAPTER 3

Azaxanthones as Lanthanide(III) Sensitisers

3.1 Azaxanthones as Lanthanide(III) Sensitisers

3.1.1 Introduction

As discussed in **Chapter 1**, despite the valuable optical properties exhibited by many of the lanthanide(III) ions, such as long lived emission lifetimes, the major drawback in the use of the lanthanide(III) ions as luminescent receptors arises from their low extinction coefficients. Thus, to make practical use of simple lanthanide(III) complexes as emissive probes requires the use of laser excitation or concentrated solutions, the latter being undesirable due to possible increases in self quenching phenomena. Therefore, an alternative approach has been pursued, which avoids the need for high intensity light sources and high concentrations, and involves sensitised emission. Sensitised emission is achieved via the incorporation of a suitable chromophore, with high extinction coefficient, into the structure of the ligand encapsulating the lanthanide(III) ion. The population of the lanthanide(III) excited state now occurs through the excitation of the chromophore into its triplet excited state, followed by energy transfer to the lanthanide(III) excited state. This process effectively increases the extinction coefficient of the lanthanide(III) ion resulting in increased quantum yields of emission. In addition, the use of a chromophore opens the possibility for excitation wavelengths approaching 400 nm and beyond, with the maximum wavelength possible limited by the excited state energy of the lanthanide(III) ion.[1] Increased excitation wavelengths also help to eliminate the need for expensive quartz optics and the absorption of energy by other species in the analytical sample, for example, aromatic amino acids and nucleic acids.

The benefits of using sensitised emission have led to the investigation of numerous chromophores as possible sensitisers for lanthanide(III) complexes. Even simple aromatic compounds offer sensitisation of lanthanide(III) ions. For example, the aromatic amino acids phenylalanine, tryptophan and tyrosine can act as a sensitiser for terbium(III) ions. However, such simple aromatic molecules generally do not allow the use of near–UV excitation. Longer wavelength excitation of lanthanide(III) ions has been successfully demonstrated recently using acridone,[2] benzophenone,[3] acetophenone[4] and phenanthridine[5] derivatives.

In this work it was decided to look at the scope and utility of compounds based on

the 1–azaxanthone structure (**Compound 9**), as chromophores for the europium(III) and terbium(III) ions. Recently published photophysical data[6] on the 1–azaxanthone compound, suggested that these aromatic heterocyclic compounds would be well suited to the role of sensitisers. The basic 1–azaxanthone structure has a triplet energy of 25400 cm^{-1}, which is sufficiently higher in energy than the emissive states of both europium(III) and terbium(III) (17200 cm^{-1} and 20400 cm^{-1} respectively). This compound also displays very little fluorescence in polar solvents (φ_{H_2O}=0.012). The quantum yield of intersystem crossing (φ_{ISC}) of 0.82 is indicative of efficient population of the triplet excited state. The only issue with this compound is that the absorption wavelength is only 333 nm, below the desired threshold of 350 nm determined by the optics present in microscopy based techniques. However, due to the ease with which modifications to the core structure of 1–azaxanthones can be made (**Scheme 3.1**),[7] it was deemed possible to increase this absorption wavelength by incorporating suitable electron donating groups. Following optimisation of the chromophore, its incorporation into macrocyclic ligands will then provide a means of investigating the binding of anions, through comparison with the information obtained using proton NMR spectroscopy.

3.1.2 Synthesis of 1–Azaxanthones

In order to successfully employ the 1–azaxanthone structure as a suitable chromophore, it was necessary to consider how this core structure could be functionalised in order to increase the absorption wavelength, and how the chromophore could be incorporated into a suitable macrocyclic ligand.

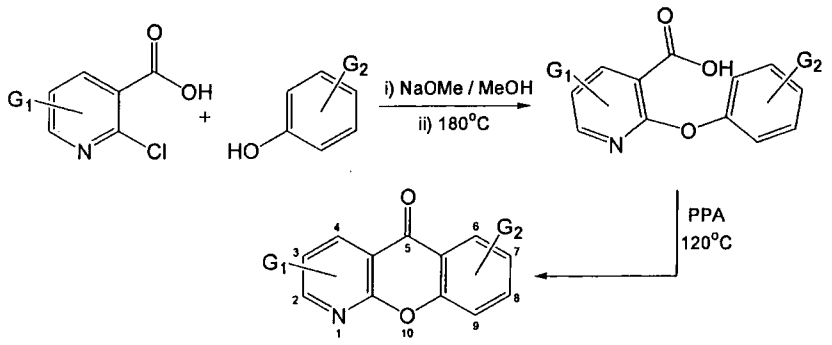

Scheme 3.1 : Outlining the synthetic route employed to synthesise the 1–azaxanthone compound, illustrating how additional functionality can be introduced via the starting materials. The numbering system given is adopted in all future references to the azaxanthone structures.

Furthermore, the chromophore may be required to incorporate a linking group for attachment to a solid phase resin. Only the outer rings of the extended aromatic system are suitable for the introduction of additional functional groups. After considering a possible synthetic route to the 1–azaxanthone compound, it was resolved that the required functionalisation can be introduced easily into the starting materials (**Scheme 3.1**). For example, the use of the α–methyl derivative of 2–chloronicotinic acid, **10**, as a starting material was particularly advantageous, since it is commercially available. The presence of this methyl group allows the possibility of further functionalisation at this position following bromination (**Scheme 3.2**). This site was initially incorporated into all of the structures, in order to provide a point of attachment to the macrocyclic ligand.

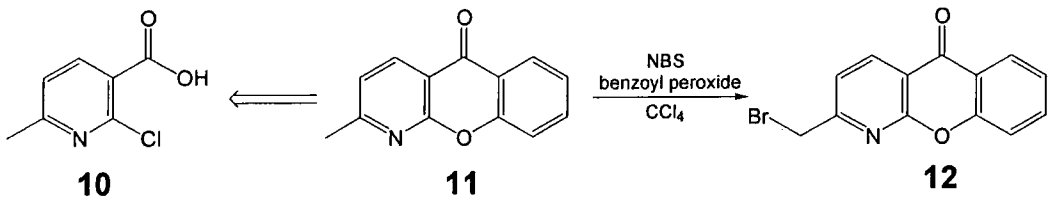

Scheme 3.2 : Synthetic route used to obtain 2–bromomethyl functionalised 1–azaxanthones via bromination of 2–methyl 1–azaxanthone.

3.1.3 Strategies for Ligand Design

Despite the ease with which the 1–azaxanthone can be modified, the overall function of the complex must not be ignored, as this may govern restrictions upon the overall ligand structure.

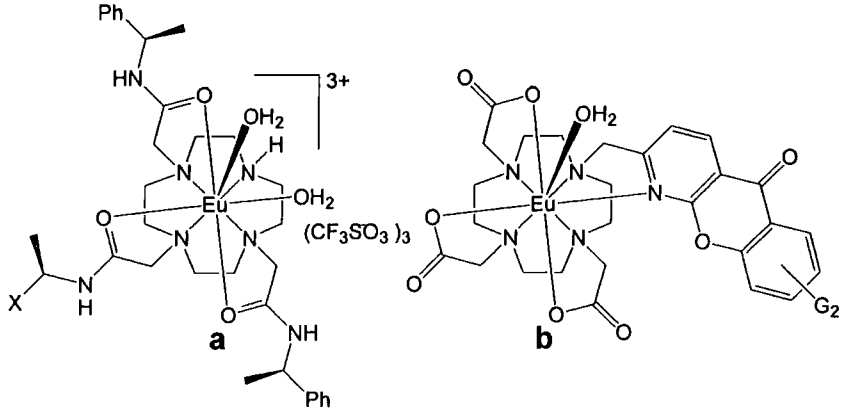

Figure 3.1 : Possible structures of complexes incorporating a 1–azaxanthone chromophore a) at position X, in order to minimise changes in structure which might adversely affect phosphate binding, b) directly attached to the macrocyclic ring allowing coordination of the pyridine nitrogen to the lanthanide(III) ion.

For instance, if the chromophore is to be incorporated into the phosphate selective europium(III) complex, as discussed in **Chapter 2**, it is desirable to retain the geometry around the europium(III) centre, in order to avoid any changes in anion binding selectivity. Thus, the geometrical requirements of the ligand restrict the chromophore to the position indicated in **Figure 3.1a**. Conversely, incorporation of the chromophore into a complex to function purely as a luminescent label, does not necessarily apply the same restrictions on the ligand structure. Therefore a more flexible approach in the ligand design is available, in order to obtain a complex which is kinetically stable and exhibits high quantum yields. To achieve such conditions, coordinatively saturated complexes are desirable – in order to reduce the quenching caused by coordinated solvent molecules. A possible structure of a luminescent label can be envisaged, with the chromophore occupying a coordination site, helping to reduce solvent coordination and ensuring that energy transfer is efficient (**Figure 3.1b**).

3.1.4 Increasing the Absorption Wavelength

Through careful choice of the phenolic starting material, it was possible to introduce electron donating groups, bearing lone pairs of electrons, into the benzenoid ring system of the azaxanthone structure. The introduction of such electron donating groups was expected to extend the conjugation length of the aromatic system and hence increase the absorption wavelength. In particular, substitution into the 8–position (**15**), allowing delocalisation of the nitrogen lone pair into the carbonyl group, was predicted to have the greatest effect upon the absorption wavelength.

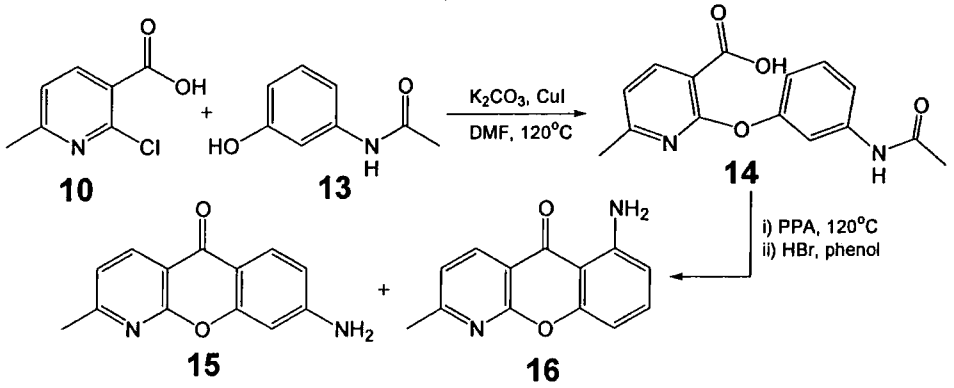

Scheme 3.3 : Outlining the synthetic route towards 8–amino–2–methyl–1–azaxanthone (**15**) showing the expected second product of the cyclisation reaction 6–amino–2–methyl–1–azaxanthone (**16**).

Initially, the introduction of an amino functionality into the 8–position of the 1–azaxanthone was chosen as a means of increasing the absorption wavelength. Although the synthesis of a compound similar to **15** (without the additional methyl group) was reported in the literature,[8] no reports on the photophysical properties of this compound could be found. Such a target molecule requires the use of a 3–aminophenol derivative as the phenolic component in the nucleophilic aromatic substitution reaction with the nicotinic acid component, **10**.[8] Thus, protection of 3–aminophenol was achieved using acetic anhydride in ethyl acetate. The Ullman reaction of the protected aminophenol, **13**, with 2–chloro–6–methylnicotinic acid in DMF at 120°C gave the coupled product, **14**, in 65% yield. Subsequent cyclisation of **14** in PPA at 120°C yielded a mixture of products. Following the removal of the acetyl protecting group from the amine using HBr, purification via column chromatography gave the desired 8–amino–2–methyl–1–azaxanthone (**15**) along with the other possible cyclisation product, 6–amino–2–methyl–1–azaxanthone (**16**), in equal quantities.

The photophysical properties of these two amino substituted 1–azaxanthones were measured and are tabulated in **Table 3.1**, alongside data for the unsubstituted compound for comparison.

Chromophore	λ_{max} / nm[a]	ε / dm^{3}mol^{-1}cm^{-1} [a]	λ_{em} / nm[a,b]	E_T / cm^{-1} [c]
15	356	19000	458 (520)	21600
16	404	8100	545 (1.1)	–[d]
11	330	8800	405 (1)	24800

Table 3.1 : Measured photophysical properties of amino substituted 1–azaxanthones compared to 1–azaxanthone. [a] Measurements recorded in methanol at 295 K. [b] Values in brackets indicate relative emission intensity relative to 1–azaxanthone (1). [c] Measured at 77K in EPA (diethyl ether, isopentane and ethanol, 5:5:2) glass. [d] No low temperature phosphorescence detected.

As anticipated, the photophysical properties of the 2–methyl–1–azaxanthone compound (**11**), do not deviate significantly from those observed for the 1–azaxanthone compound previously reported.[1] The absorption spectrum of compound **11** displays a small red shift in λ_{max} upon increasing the solvent polarity. For example, the longest wavelength absorption maximum was at 329, 330 and 334 in

EPA (diethyl ether, isopentane and ethanol, 5:5:2), methanol and water respectively. This red shift in the absorption wavelength is consistent with the increasing contributions from low lying $\pi\pi^*$ states to the lowest energy $n\pi^*$ state, which is dominant in non–polar solvents.[9] Evidence for the existence of an $n\pi^*$ triplet excited state was sought by examining the phosphorescence emission spectrum of **11** at 77 K in an EPA glass matrix. The lowest energy (zero–zero) transition was observed at 24,800 cm^{-1}, and three lower energy bands were observed with a separation of the order of 1,650 cm^{-1}. The fine structure exhibited in this emission band is characteristic of the carbonyl stretching frequency harmonics of ~1650 cm^{-1} (**Figure 3.2**), and consistent with a triplet with predominantly $n\pi^*$ character.[1]

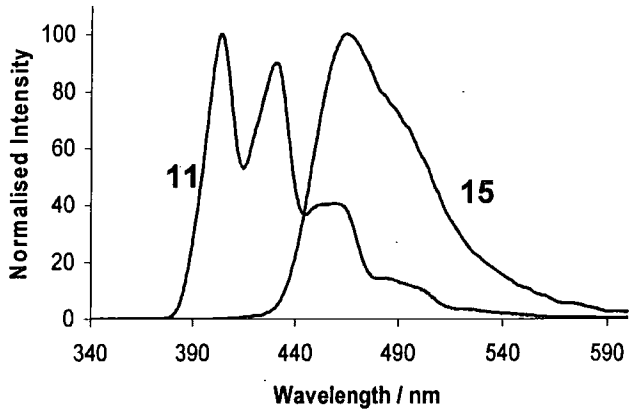

Figure 3.2 : Phosphorescence emission spectrum of compounds **11** and **15**, measured in an EPA glass matrix at 77 K, illustrating the vibrational structure present in the former, compared with the much less structured emission observed in the amino compound, **15**.

Following amino substitution of compound **11**, to give compound **15**, a red shift of 26 nm in the absorption maximum, in methanol, was observed. This shift in absorption wavelength was also accompanied by a dramatic increase in extinction coefficient. Such increases in extinction coefficient values are desirable in potential sensitisers, since if more light is absorbed, the greater the possible transfer of energy to the luminescent lanthanide(III) ion. Along with the increase in absorption wavelength, and hence a decrease in the singlet excited state energy, there was a more significant lowering of the triplet excited state energy to 21,600 cm^{-1}. As expected, the lowering of the triplet energy level in this case is sufficient to make this chromophore unsuitable for use as a sensitiser for terbium(III) ions.[1] This is a consequence of the resulting small energy gap between the triplet excited state of the

chromophore and the terbium emissive state, which may be expected to lead to thermally activated back energy transfer from the emissive state to the chromophore triplet excited state, limiting the overall efficiency.[12]

Although compound **15** looks promising as an improvement to the 1–azaxanthone core structure, the influence of the amino group on the emissive properties of this compound was deleterious. The observed fluorescence emission at room temperature was extremely intense, with a 500 fold increase in intensity observed relative to the unsubstituted 1–azaxanthone. Low temperature phosphorescence emission was also very different from that observed for the parent compound **11**, in that no clear vibrational structure was observed (**Figure 3.2**). This lack of vibrational structure, combined with the very intense fluorescence and absorption observed at room temperature, suggests that the presence of the amino group lowers the energy of the π^* orbital, such that the singlet and triplet states of compound **15** are predominantly $\pi\pi^*$ in character. Similar observations have been made for 4,4′–bis(dimethyl–amino)benzophenone (Michler's ketone) in comparison to benzophenone.[10] Further evidence for the reduced interaction of the $n\pi^*$ level with the lowest excited state was evident in the absorption spectrum of compound **15**. This absorption spectrum clearly displays a shoulder on the short wavelength side of the absorption maximum (**Figure 3.3**).

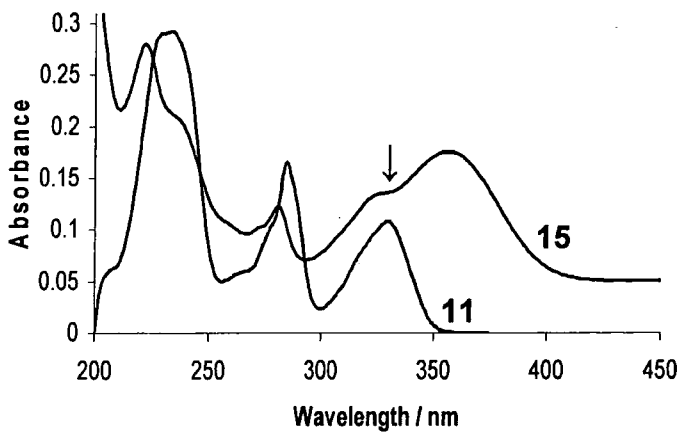

Figure 3.3 : Absorption spectra of compounds **11** and **15**, measured in methanol at 295 K, illustrating how the shoulder observed on the absorption maximum for compound **15** correlates well with the absorption maximum in the parent compound **11**.

This shoulder has also been observed in the absorption spectrum of Michler's ketone derivatives in more polar solvents,[11] and is thought to arise from a transition

involving the $n\pi^*$ state. Support for this theory was evident when comparing the absorption spectrum of compound **15** with that of the parent compound **11**. In this case, the shoulder observed in the former spectrum corresponds well with the absorption maximum observed for the parent compound **11**. This observation supports the fact that considerable mixing of the $n\pi^*$ and $\pi\pi^*$ states contributes to the excited states of the 1–azaxanthone compound.[9] In contrast for compound **15**, the amino substituent stabilises the $\pi\pi^*$ excited state to a much greater extent than the $n\pi^*$ state leading to the observation of separate transitions in the absorption spectrum.

Compound **16**, with the amino group adjacent to the carbonyl group, was the side product formed during the synthesis of compound **15**. It exhibited an extraordinary increase in absorption wavelength. A red shift of 74 nm was observed, compared to compound **11**. This was sufficient to take the tail of the absorption into the visible region of the spectrum, and solutions of compound **16** appeared faintly yellow. Given the large difference in red shift observed between compounds **15** and **16**, in the latter case there must be some additional factor, along with the increase in conjugation with the carbonyl group, responsible for this dramatic shift. The proximity of the amino group to the carbonyl group may not only suggest that conjugation effects are stronger, but also that intramolecular hydrogen bond formation was a possibility, and therefore this may also be associated with the observed red shift. Formation of such an intramolecular hydrogen bond should direct the amino nitrogen atom to adopt a more planar conformation, when compared to the pyramidal conformation observed in aniline.[10] Such a conformation would lead to an increase in the orbital overlap between the nitrogen lone pair and the aromatic π orbitals, hence increasing the degree of lone pair conjugation. Further evidence for intramolecular hydrogen bond formation was the very low intensity of fluorescence emission observed (λ_{em} = 545 nm) with this compound, along with the absence of phosphorescence emission at low temperature. These observations point towards the deactivation of the excited states via coupling with the intramolecular hydrogen bond. Such lowering of emission intensity has also been observed in thioxanthones possessing substituents adjacent to the carbonyl group.[13] In this case, the extent to which the quenching of emission was observed was shown to be dependent upon the substituent adjacent to the carbonyl group. Increasing the strength of the hydrogen

bond donor from a methyl C–H bond to a hydroxyl O–H bond leads to significant lowering of the quantum yields of emission of the compound. Furthermore, the quenching resulting from the weak intramolecular C–H$^{\cdots}$O interaction was shown to only exist in aprotic solvents, whilst the much stronger O–H$^{\cdots}$O interaction led to a complete lack of fluorescence even with methanol as the solvent.

3.1.5 Effect of Eliminating Intramolecular Hydrogen Bonding upon Photophysical Properties

Since the amino substituted compounds were successful in increasing the absorption wavelength, further investigation was warranted into the nature of the dramatic shift observed in compound **16** and also the extent to which the wavelength is increased upon alkylation of the nitrogen atom. Unfortunately, attempts to alkylate compounds **15** and **16** proved unsuccessful, even under forcing conditions with excess methyl iodide and base in DMF, possibly as a result of the conjugation of the nitrogen lone pair. Consequently, it was decided to introduce alkyl groups into the phenolic component before forming the 1–azaxanthone compound. However, reaction of 3–dimethylaminophenol with 2–chloro–6–methylnicotinic acid under similar conditions used to form compound **7** proved unsuccessful, with no products isolated. Therefore, it was deemed necessary to maintain an amide moiety present for the coupling reaction, thus requiring synthesis of a 3–*N*–alkyl–*N*–acetyl aminophenol compound, such as **18** (**Scheme 3.4**). The use of this compound also has an additional advantage. Given that alkylation proved unsuccessful for **15** and **16**, the *N*–acetyl group can be reduced, rather than removed, thus supplying an additional alkyl group, which cannot be achieved via deprotection followed by alkylation.

Reduction of 3–acetylaminophenol (**13**) with borane dimethyl sulfide in THF, followed by an acidic workup to remove the borane complex, yielded 3–ethylaminophenol as the hydrochloride salt (**17**) in quantitative yield.

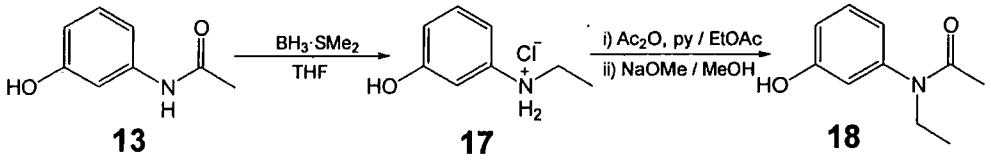

13 17 18

Scheme 3.4 : Synthetic route towards 3–*N*–acetyl–*N*–ethylaminophenol (**18**) via the reduction of 3–acetylaminophenol (**13**) to generate the mono–alkylated amine (**17**).

Subsequent acetylation with excess acetic anhydride in pyridine formed the *O*–, *N*–acetyl compound from which the desired compound **18** was isolated in 86% yield, following treatment with sodium methoxide.

Formation of the coupled product **19** via the nucleophilic aromatic substitution of compound **18** with 2–chloro–6–methylnicotinic acid proceeded in 64% yield following recrystallisation from methanol. Subsequent cyclisation of **19** in PPA at 120°C gave a mixture of three compounds, which were separated by column chromatography and recrystallised. These compounds were the 8–*N*–acetyl–*N*–ethyl compound (**20**) and its deacylated form (**21**) in 26% and 25% yield respectively, along with a small amount of the 6–*N*–ethyl compound (**22**), in 8% yield. No evidence of the 6–*N*–acetyl–*N*–ethyl compound (**23**) was found, suggesting that the rate of formation of this compound was slower than the rate of hydrolysis of the amide protecting group. This behaviour is also consistent with the low yield obtained for compound **22**. The acetylated compound **23** was easily obtained via the acetylation of **22** with acetyl chloride in 98% yield.

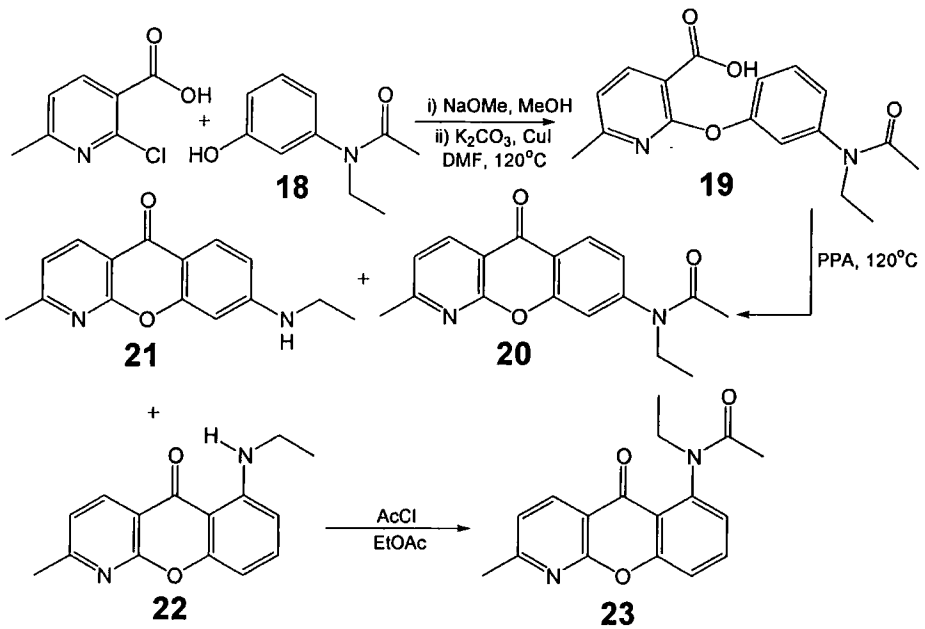

Scheme 3.5 : Synthetic route towards alkylamino substituted 1–azaxanthones, highlighting the lack of compound **16** observed from the cyclisation reaction, which was obtained from compound **22** via acetylation.

The photophysical properties of these four compounds are tabulated in **Table 3.2**. As expected, no significant changes in the absorption and emission properties occur with the addition of one alkyl group to compounds **15** and **16**.

Chromophore	λ_{max} / nm[a]	ε / $dm^3mol^{-1}cm^{-1}$ [a]	λ_{em} / nm[a,b]	E_T / cm^{-1} [c]
20	329	9800	412 (1.4)	24500
21	369	20200	472 (510)	21200
22	421	8900	560 (1.6)	–[d]
23	334	11100	–[e] (0.2)	–[d]

Table 3.2 : Measured photophysical properties of alkylamino and acetylamino substituted 1–azaxanthones. [a] Measurements recorded in methanol at 295 K. [b] Values in brackets indicate relative emission intensity relative to 1–azaxanthone (1). [c] Measured at 77K in EPA glass. [d] No low temperature phosphorescence detected. e Fluorescence emission was too weak to accurately assign the wavelength.

The additional ethyl group in compounds **21** and **22** led only to a further small increase in the absorption wavelength, when compared to the corresponding unsubstituted amino 1–azaxanthones. The accompanying small increase in the extinction coeffiecients may be associated with the small increase in lone pair donor ability of the nitrogen atom.

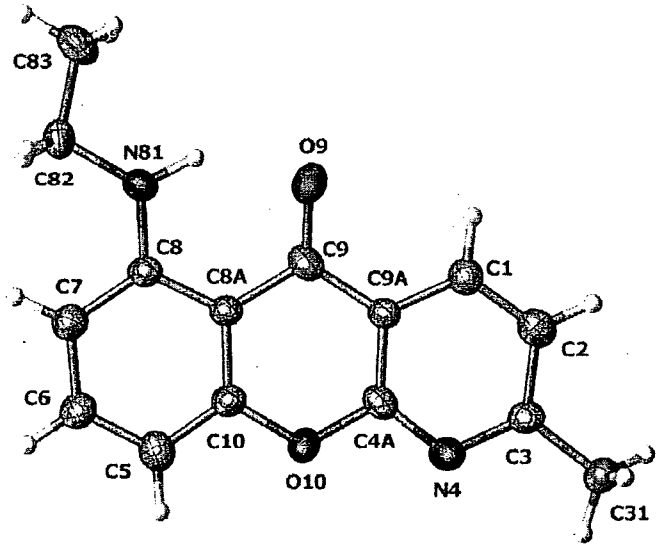

Figure 3.2 : Crystal structure of compound **22**, illustrating the intramolecular hydrogen bonding which exists between the amine N–H and carbonyl group.

The absorption wavelength of compound **22** now falls within the visible region and solutions of this compound exhibit an intense yellow colour. The hydrogen bonding proposed in compound **16** was still expected to be exhibited in compound **22**, due to the remaining hydrogen atom on the amino group. No low temperature phosphorescence could be detected and a low fluorescence emission intensity was

observed at 295 K, in comparison to compound **21**. Further confirmation of the existence of intramolecular hydrogen bonding was obtained following analysis of the crystal structure of compound **22**. This clearly shows the hydrogen bond between the N–H and carbonyl group (**Figure 3.2**). The CNC bond angle (C(82)–N(81)–C(8)) was found to be 124°, and observed torsion angles were consistent with a planar nitrogen atom, in which there is excellent overlap of the nitrogen lone pair with the adjacent π system. No evidence of any other intermolecular interactions or solvent molecules (EtOH) were observed within the crystal structure.

As expected, *N*–acetylation of the amino compounds removes any electron donating contributions to such an extent that the absorption maxima for compounds **20** and **23** are almost identical to the unsubstituted 1–azaxanthone compound. Compound **20** exhibits strong phosphorescence in an EPA glass matrix at 77 K. The form of this emission was very similar to that of the unsubstituted 1–azaxanthone, displaying the same vibrational structure, consistent with the retention of the low lying $n\pi^*$ triplet excited state. Interestingly, although there was no longer the possibility for intramolecular N–H⁗O hydrogen bond formation in compound **23**, the quenching of the excited states in this compound was evident as both low temperature luminescence and room temperature fluorescence was too weak to confidently assign. In this case, a weak intramolecular C–H⁗O interaction can be suggested to account for the quenching of emission observed.

Despite the quenching observed in compound **23**, even in the absence of hydrogen bonding, the reduction of this compound was still attempted to assess the photophysical properties of the diethyl system.

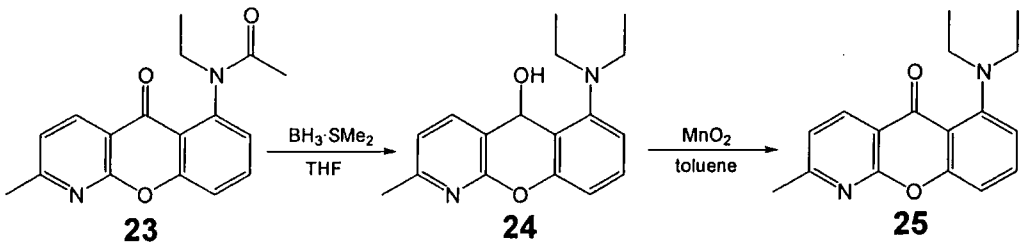

23 **24** **25**

Scheme 3.6 : Proposed synthetic route towards 6–diethylamino–2–methyl–1–azaxanthone (**25**).

Reduction of **23** with borane dimethyl sulfide in THF, was anticipated to yield the 6–diethylamino–1–azaxanthanol compound, **24**, which could be reoxidised to the

corresponding xanthone (**25**) using manganese dioxide (**Scheme 3.6**). However, analysis of the reduced product obtained using proton NMR and electrospray mass spectrometry indicated that complete removal of the carbonyl oxygen had occurred.

3.1.6 Effect of Oxidation at Nitrogen

Given the limited success of achieving more desirable photophysical properties via the introduction of electron donating functional groups into the 1–azaxanthone core structure, another means of increasing the absorption maximum was required. Formation of *N*–oxide compounds via the oxidation of the pyridine nitrogen atoms is well known to increase the electron density present in the pyridine ring, due to the delocalisation of the oxygen lone pair around the ring. Thus, upon forming the *N*–oxide of 1–azaxanthone, the oxygen lone pair was postulated to interact with the π–system, leading to a lowering of the energy of the excited state, and hence lead to an increase in the absorption maximum.

Oxidation of the pyridyl nitrogen atom proved difficult under mild conditions, such as MCPBA in chloroform. More forcing conditions using acetic acid and hydrogen peroxide, maintained at 100°C for 24 hours, also failed to produce any trace of the *N*–oxide compound. However, the use of trifluoroacetic acid and 40% hydrogen peroxide under similar conditions, proved successful in enabling the oxidation to occur at nitrogen in reasonable yields (**Scheme 3.7**).

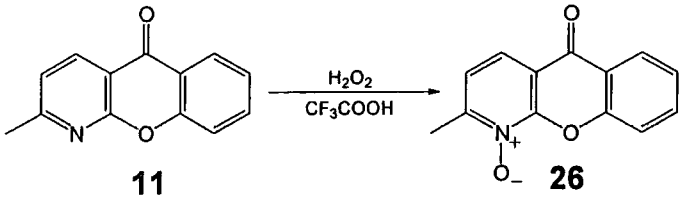

11 **26**

Scheme 3.7 : Synthetic route required for the formation of 2–methyl–1–azaxanthone–*N*–oxide (**26**).

Analysis of the absorption spectrum of the *N*–oxide compound (**26**) revealed the anticipated red shift in the absorption wavelength. This shift in the absorption maximum of 20 nm was not accompanied by a change in the spectral form, as observed for the 8–amino substituted compound (**15**), suggesting the retention of the close lying $\pi\pi^*$ and $n\pi^*$ excited states. However, the increasing $\pi\pi^*$ character of the lowest excited state was evident from the observed increase in the room temperature fluorescence emission intensity, when compared to the parent compound (**11**).

Phosphorescence emission from the *N*–oxide compound at low temperature in an EPA glass matrix is very weak and displays evidence of more than one species in solution. Such an observation is possibly as a result of the decomposition of the *N*–oxide compound. This assumption is plausible, given the fact that this compound could serve as a powerful oxidant, serving as an oxygen transfer reagent to the solvent. Thus, as in the case of the amino substituted 1–azaxanthone compounds, the promising influence of the *N*–oxide upon absorption characteristics appear to be outweighed by the undesirable emission properties and high reactivity of this *N*–oxide compound.

3.2 A Different Approach : 1–Aza–10–thioxanthones

Another approach adopted in the search for the desired photophysical properties required for the sensitisation of lanthanide(III) ions, considered the variation of the endocyclic heteroatom. The large effect of the variation of this heteroatom is clearly evident with the very similar xanthone compound (**27**). In this case, changing the oxygen heteroatom for sulfur, yields the thioxanthone (**28**). The absorption maxima reported for compounds **27** and **28** in acetonitrile are at 337 nm[14] and 380 nm,[15] respectively. Hence, this compound would seem to be a promising choice as a sensitiser. However, thioxanthone itself is not suitable, as it has a high quantum yield of fluorescence, which increases significantly upon increasing the solvent polarity.[16] On the other hand, the intensity of fluorescence emission for xanthone is reduced considerably upon the introduction of a pyridine ring.[6,17] Therefore, it was postulated that the corresponding 2–methyl–1–aza–10–thioxanthone (**29**), would also possess a significantly lower quantum yield of fluorescence, albeit at the expense of a small blue shift in the absorption maximum.

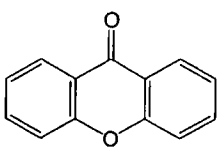

27

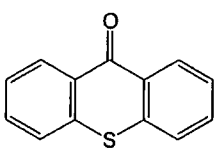

28

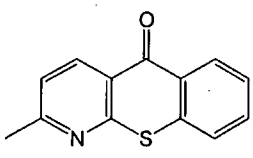

29

The synthetic route towards the 1–aza–10–thiaxanthone compounds follows the same method described previously for the amino substituted 1–azaxanthones, although use of sodium methoxide was not required as the corresponding thiophenol is both more

acidic and more nucleophilic. Therefore, reaction of thiophenol with 6–chloro–2–methylnicotinic acid (**10**), in the presence of potassium carbonate and copper(I) iodide catalyst yields the coupled product **30**. Subsequent cyclisation using PPA provides the heterocyclic 2–methyl–1–aza–10–thioxanthone compound, **29**.

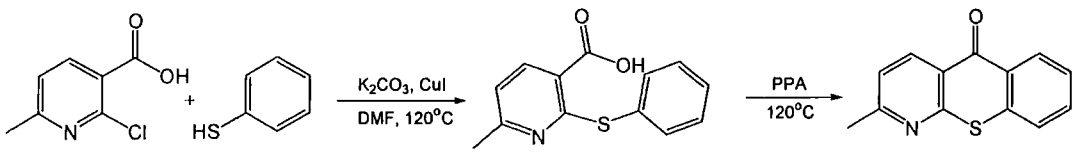

10 **30** **29**

Scheme 3.8 : Synthetic route towards 2–methyl–1–aza–10–thioxanthone (**29**).

As anticipated, the 1–azathioxanthone compound (**29**) displayed very low fluorescence emission at room temperature. The observed emission was around three times more intense than found for the corresponding 1–azaxanthone. The blue shift in absorption wavelength, resulting from the incorporation of the pyridine ring, was only slightly more significant than that observed for 1–azaxanthone, and the resulting absorption maximum of 371 nm, in methanol, was significantly beyond the desired 350 nm excitation threshold. Low temperature phosphorescence emission was also strong, with a triplet energy of 23700 cm^{-1}. This phosphorescence emission also displays some vibrational structure, suggesting there is a significant contribution to the lowest triplet from an $n\pi^*$ excited state.

In contrast to the amino substituted 1–azaxanthones, the lowering in energy of the singlet excited state was not accompanied by a significant lowering of the triplet excited state energy. The concomitant lowering of these excited state energies results in an unexpectedly high energy for the triplet level of compound **29**, and consequently a very small singlet triplet energy gap. This situation is highly desirable in order to promote intersystem crossing from the singlet to triplet excited states. Another significant advantage over the amino substituted 1–azaxanthones, is that the triplet excited state may still be sufficiently above the terbium(III) emissive state, such that thermal repopulation of the triplet level is less likely to occur at room temperature, thereby allowing excitation of terbium(III) ions.

The promising photophysical properties exhibited by the 1–aza–10–thioxanthone core structure means that further functionalisation of this compound, as in the case of

compound (**11**) is unnecessary. However, the presence of the methyl group remains necessary in order to provide a point of attachment to the macrocyclic ligand, ie. via the brominated compound (**Scheme 3.2**). Given that the methyl group is not required to be adjacent to the pyridyl nitrogen, parallel work within the research group focussed on the effect of varying the position of the methyl group within the benzenoid ring.[18]

Synthesis of the methyl substituted 1–aza–10–thioxanthone compounds was achieved via the same reaction conditions used in the synthesis of compound **29**, through the combination of 2–chloronicotinic acid with the appropriately methylated thiophenol compound, to give the four isomers **31–34**.

31 : 6–methyl
32 : 7–methyl

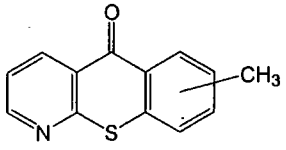

33 : 8–methyl
34 : 9–methyl

The photophysical properties of these structurally related compounds are provided in **Table 3.3**, together with the parent 2–methyl compound for comparison. It is apparent that only very subtle variations in singlet and triplet energy levels occur upon variation of the position of the methyl substituent. In fact, the most significant red shift in the absorption wavelength was only 10 nm, and was observed for compound **32**. Parallel lowering of the triplet energy and red shift in the fluorescence emission wavelength was also observed.

Chromophore	λ_{max} / nm[a]	ε / $dm^3mol^{-1}cm^{-1}$ [a]	λ_{em} / nm[a,b]	E_T / cm^{-1} [c]
29	371	6770	425 (3.2)	23700
31	372	5790	428 (3.7)	23500
32	381	5350	440 (0.7)	22800
33	375	5450	437 (1.0)	23500
34	374	5760	437 (5.1)	23600

Table 3.3 : Photophysical properties of methyl substituted 1–aza–10–thioxanthones. [a] Measurements recorded in methanol at 295 K. [b] Values in brackets indicate relative emission intensity relative to 1–azaxanthone (1). [c] Measured at 77K in EPA glass.

3.3 Conclusions

Despite possessing an absorption maximum less than 350 nm, the 1–azaxanthone core structure is a very suitable sensitiser for both europium(III) and terbium(III) ions. As expected, the ease with which the functionalisation of this core structure can be achieved, allows the introduction of electron donating groups, which results in favourable perturbation of the absorption maximum. Unfortunately, although the introduction of amino groups into the 6– and 8– positions of the 1–azaxanthone ring system led to large increases in the absorption maxima, the emission characteristics were greatly affected. In the case of the 8–amino–1–azaxanthones, the presence of the amino group led to significant lowering of the $\pi\pi^*$ energy level, resulting in very strong fluorescence emission. Amino substituents in the 6–position, led to very large red shifts in the absorption wavelength, but suffered from very weak emission, due to quenching of the excited states via an intramolecular hydrogen bonding interaction. Therefore, although increases in absorption maxima are readily achieved through the introduction of electron donating substituents into the azaxanthone structure, their influence upon the relative excited states and therefore emission properties means this route is not a viable option.

Formation of the *N*–oxide compound of 1–azaxanthone produces a significant red shift in the absorption wavelength of 20 nm, creating a broad absorption band which extends well beyond 350 nm. Most significantly, this shift is not accompanied by a change in the emission characteristics of the parent 1–azaxanthone compound, with relatively low fluorescence emission observed at room temperature. Unfortunately, these properties are accompanied by weak phosphorescence at low temperature. Furthermore, there are questions raised about the stability of this compound as it is a powerful oxidant and readily serves as an oxygen transfer reagent.

The compounds which have perhaps displayed the greatest potential of those studied, as lanthanide(III) sensitisers, are the methyl derivatives of the 1–aza–10–thioxanthone compound. The presence of the methyl group is sufficient for the further elaboration of the sensitiser, allowing its incorporation into the ligand structure of the lanthanide(III) complex. Variation in the position of the methyl substituents was found to induce only subtle changes in the absorption and emission

properties observed. Therefore, the position of the methyl group in the sensitiser compound can be chosen by taking into account the cost and ease of synthesis from the corresponding starting materials.

3.4 References

1 F. J. Steemers, W. Verboom, D. N. Reinhoudt, E. B. van der Tol and J. W. Verhoeven, *J. Am. Chem. Soc.*, 1995, **117**, 9408.

2 A. Dadabhoy, S. Faulkner and P. G. Sammes, *J. Chem. Soc., Perkin Trans. 2*, 2000, 2359.

3 A. Beeby, L. M. Bushby, D. Maffeo and J. A. G. Williams, *J. Chem. Soc., Perkin Trans. 2*, 2000, 1281.

4 J. C. Rodríguez–Ubis, M. T. Alonso, O. Juanes, R. Sedano and E. Brunet, *J. Lumin.*, 1998, **79**, 121; A. Beeby, L. M. Bushby, D. Maffeo and J. A. G. Williams, *J. Chem. Soc., Dalton Trans.*, 2002, 48.

5 D. Parker, P. K. Senanayake and J. A. G. Williams, *J. Chem. Soc., Perkin Trans. 2*, 1998, 2129; I. M. Clarkson, A. Beeby, J. I. Bruce, L. J. Govenlock, M. P. Lowe, C. E. Mathieu, D. Parker and P. K. Senanayake, *New J. Chem.*, 2000, **24**, 377.

6 J. C. Scaiano, D. Weldon, C. N. Pliva and L. J. Martinez, *J. Phys. Chem. A*, 1998, **102**, 6898.

7 F. J. Villani, T. A. Mann, E. A. Wefer, J. Hannon, L. J. Larca, M. J. Landon, W. Spivak, D. Vashi, S. Tozzi, G. Danko, M. Del Prado and R. Lutz, *J. Med. Chem.*, 1975, **18**, 1.

8 H. Fujiwara and K. Kitagawa, *Heterocycles*, 2000, **53**, 409.

9 L. J. Martinez and J. C. Scaiano, *J. Phys. Chem. A*, 1999, **103**, 203.

10 E. J. J. Groenen and W. N. Koelman, *J. Chem. Soc., Faraday Trans. 2*, 1979, **75**, 69.

11 M. El–Sayed, H. Müller, G. Rheinwald, H. Lang and S. Spange, *J. Phys. Org. Chem.*, 2001, **14**, 247.

12 D. Parker and J. A. G. Williams, *J. Chem. Soc., Perkin Trans. 2*, 1996, 1581.

13 M. G. Neumann, M. H. Gehlen, M. V. Encinas, N. S. Allen, T. Corrales, C. Peinado and F. Catalina, *J. Chem. Soc., Faraday Trans.*, 1997, **93**, 1517.

14 K. A. Abdullah and T. J. Kemp, *J. Photochem.*, 1986, **32**, 49.

15 T. Lai and E. C. Lim, *Chem. Phys. Lett.*, 1980, **73**, 244.

16 D. Burget and P. Jacques, *J. Lumin.*, 1992, **54**, 177.

17 M. Barra, C. Bohne and J. C. Scaiano, *J. Am. Chem. Soc.*, 1990, **112**, 8075.

18 P. Atkinson, K. S. Findlay, F. Kielar, R. Pal, D. Parker, S. Richardson, P. A. Stenson and J. Yu, *Org. Biomol. Chem.*, 2006, in press.

CHAPTER 4

Immobilisation of Complexes Exhibiting Phospho–Anion Selectivity

4.1 Immobilisation of Complexes Exhibiting Phospho–Anion Selectivity

4.1.1 Introduction

After achieving the desired level of phosphorylated anion selectivity desired, through the fine–tuning of the lanthanide(III) ion and macrocyclic ligand combination, it was proposed to apply this receptor towards useful practical applications. One application envisaged related to the purification or enrichment of bioactive phosphorylated species, such as peptides or phosphorylated protein fragments.

The careful preparation of phosphorylated peptide or protein samples is an important post–isolation requirement to enable their identification using mass spectrometry.[1,2] Despite the high resolution and sensitivity exhibited by modern mass spectrometers, the need for enrichment or separation procedures arises from the low population of phosphorylated species in isolated samples.[1] If mass spectra are recorded without enrichment or separation, the signals to be observed from phosphorylated species may be obscured by the presence of intense signals due to the corresponding non–phosphorylated species.[3] A common technique used to enrich phosphorylated peptide samples is Immobilised Metal ion Affinity Chromatography (IMAC). This technique is based on the use of a column containing a resin covalently linked to a chelating ligand. This column is then loaded with a charge dense metal ion, such as iron(III)[4] or gallium(III),[5] which is bound by the chelating ligand. Subsequent enrichment of the phosphopeptide occurs through the greater retention of the phosphorylated species through interaction with the highly charged metal ions. However, in these IMAC systems, careful control of the pH of the eluant is required in order to control the retention of phosphorylated species whilst minimising the interference of amino acid residues containing carboxylate groups,[5] ie. aspartate or glutamate.

It was proposed that it may be possible to develop a column based separation system for phosphorylated peptides, in which the column consists of polymeric resin beads, functionalised with a 'phospho–anion selective' europium complex. By passing a solution of the mixture of phosphorylated and non–phosphorylated peptides through the column, elution of the non–phosphorylated peptides should occur first, since very

little interaction between peptides and $[Eu7(H_2O)_2]^{3+}$ has been observed. Subsequent elution of the more strongly bound phosphorylated peptides is anticipated to occur using an eluant such as aqueous triethylammonium carbonate or ammonium carbonate solution. The presence of a high concentration of carbonate anions in the eluant will compete effectively for the binding sites of the europium(III) complex, and hence lead to elution of the phosphorylated peptides. The choice of triethylammonium or ammonium carbonate as eluant is primarily due to its volatility, allowing regeneration of the resin bound complexes under reduced pressure.

4.1.2 Design of Resin Bound Complex

Having investigated the binding of phosphorylated anions to a series of lanthanide(III) macrocyclic complexes, it is clear that the choice of the lanthanide(III) ion and even subtle changes to the macrocyclic ligand can have a dramatic influence over the selectivity for phosphorylated anions. Thus, in the incorporation of $[Eu7(H_2O)_2]^{3+}$ onto the resin beads, it is necessary to avoid changing the geometry around the lanthanide(III) ion in order to circumvent any perturbation from the observed anion binding selectivity. Therefore, the relatively straightforward modification of ligand **7** to incorporate a linker group onto the remaining macrocyclic ring nitrogen atom must be avoided (**Figure 4.1a**). Such a design would be expected to resemble the affinity profile observed for the *N*–methylated complexes, and exhibit reduced selectivity towards phosphate.

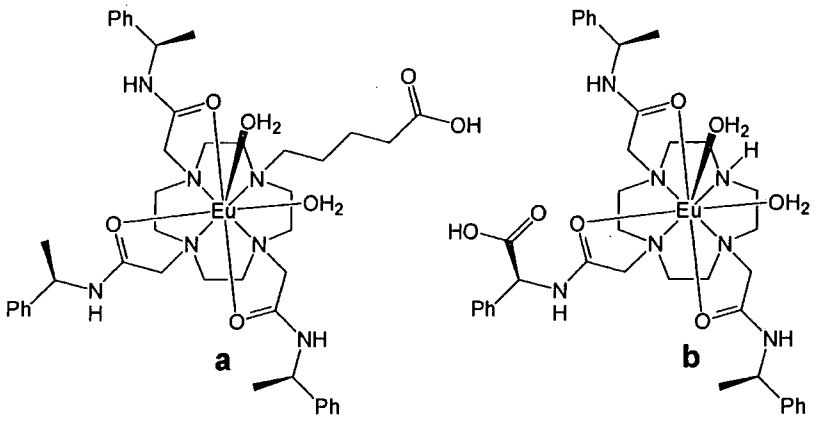

Figure 4.1 : Illustration of the possible sites for linking the macrocycle to the functionalised resin beads; a) via macrocyclic ring nitrogen atom, b) via one of the integral pendant arms.

Undoubtedly, in order to maintain the selectivity for phosphorylated anions observed

for $[Eu7(H_2O)_2]^{3+}$, the linking group must be incorporated into one of the pendant arms of ligand **7**, whilst also retaining the chirality present in the original pendant arm (**Figure 4.1b**).

In order to form the link between resin and macrocycle, it was decided to make use of the relatively stable amide functional group. This group was chosen as it can be formed selectively and under relatively mild conditions, using for example, carbodiimide coupling agents at room temperature. The use of mild reaction conditions is important to minimise the risk of unwanted side reactions, which may lead to decomposition of the europium complex. Furthermore, in synthesising the macrocycle required for a design such as that in **Figure 4.1b**, incorporation of a carboxylic acid group in the pendant arm allows the use of amino acids to maintain the chirality required.

One additional consideration needed when this design was put forward, is the possibility that reaction of the complex onto the resin may not be required to reach the maximum loading capacity. Normally, such an occurrence would not pose any problems. However, under the aqueous conditions around pH 7, in which phosphate selectivity of the europium receptors has been observed, the unreacted amino groups will be protonated. These protonated amino groups could potentially interact with any negatively charged residues in the sample, leading to the increased retention time of non–phosphorylated species. Hence, careful monitoring of the loading capacity achieved or the application of mild conditions to cap the unreacted amino groups (eg. p–nitrophenylacetate in H_2O/dioxane) must not be neglected.

4.1.3 Synthesis of Phenylglycine Conjugate

As discussed in **Section 2.1.2**, the similar reactivity of the macrocyclic ring nitrogen atoms makes selective alkylation reactions difficult without introducing control through the use of protecting groups. In this case, a tri–substituted macrocycle was required in which the 1– and 7– positions contain the same pendant arm, whilst the 4– position contains the modified pendant arm bearing the carboxylate linking group.

Introduction of the 1,7–disubstitution pattern is relatively straightforward.[6] The diprotonated cyclen macrocycle is the major species in the pH range 2 to 8, with the protonated nitrogen atoms adopting a 1,7–relationship in order to minimise–

Coulombic repulsion. Subsequent acylation of this protonated macrocycle with benzyl chloroformate, whilst maintaining the pH at around 2.5, results in the formation of the 1,7–CBz protected cyclen macrocycle, **35**, in 82% yield.[6]

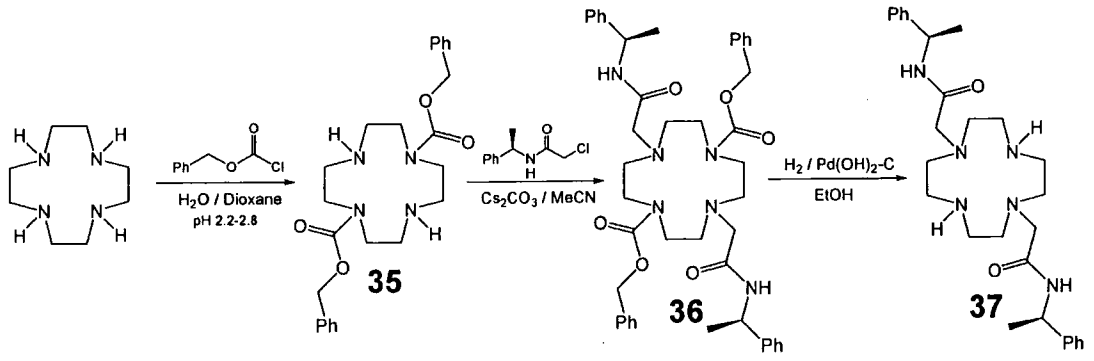

Scheme 4.1 : Synthetic route towards the 1,7–substituted macrocyclic precursor required in the synthesis of the resin linked complex, via the pH controlled acylation of the diprotonated cyclen macrocycle.

With the protecting groups in place, alkylation was performed under forcing conditions with a slight excess of the chiral chloramide, **1**, to give the tetra substituted macrocycle, **36**, in 66% yield. Subsequent removal of the CBz protecting groups via hydrogenation afforded the desired di–alkylated macrocycle in near quantitative yield.

In order to impose minimal disruption to the geometry present in ligand **7**, the chirality of the modified pendant arm, containing the carboxylate linking group, needed to be considered. The carboxylate group, which replaces the methyl group of the chloroamide, **1**, is still significantly smaller than the phenyl ring. The A values for the methyl group and ethoxy carbonyl group in polar media are 7.3 and 8.4 $kJmol^{-1}$, respectively. Therefore, ensuring the orientation of the modified pendant arm is complementary with the arm it replaces, the synthesis was performed using *(S)*–phenylglycine (**Scheme 4.2**).

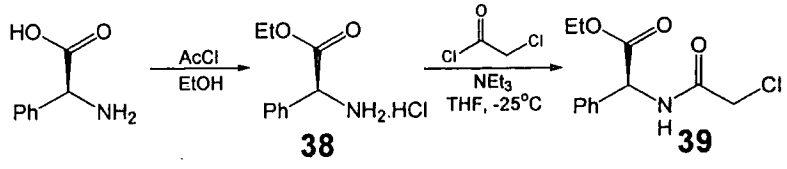

Scheme 4.2 : Synthetic route towards the modified pendant arm, using *(S)*–phenylglycine to introduce the carboxylate group with the appropriate chirality.

Formation of the ethyl ester of *(S)*–phenylglycine occurred in quantitiative yield via–

the acid catalysed esterification in ethanol, with anhydrous HCl generated *in situ* from acetyl chloride. Subsequent acylation of the nitrogen atom with chloroacetyl chloride at low temperature, to minimise dimerisation of **38**, produced the modified pendant arm in 66% yield, following recrystallisation from diethyl ether/petroleum ether.

Despite having obtained the 1,7–disubstituted pattern required, similar complications of selectivity arise in the mono–alkylation of compounds **37**, and **35**, due to the similar reactivity of the remaining ring nitrogen atoms. The attempted mono–alkylation of **37** under mild conditions led to either slow formation of a product mixture, for which good chromatographical separation could not be achieved, or little reaction whatsoever. Such poor selectivity and reaction rates obtained prompted a further investigation into the use of protecting groups to achieve the alkylation pattern required. Given that the trifluoroacetyl protecting group was observed to disfavour the formation of a tetra–substituted cyclen compound (**Section 2.1.2**),[7] it was anticipated that this protecting group may also lead to mono–protection of 1,7–disubstituted macrocycles (**Scheme 4.3**). Unfortunately, reaction of a large excess of ethyl trifluoroacetate with compound **37**, failed to provide any evidence of product formation. In contrast, reaction of compound **35** with excess ethyl trifluoroacetate yielded the differentially trisubstituted compound **40**, as the major product, and in 88% yield following purification by column chromatography.

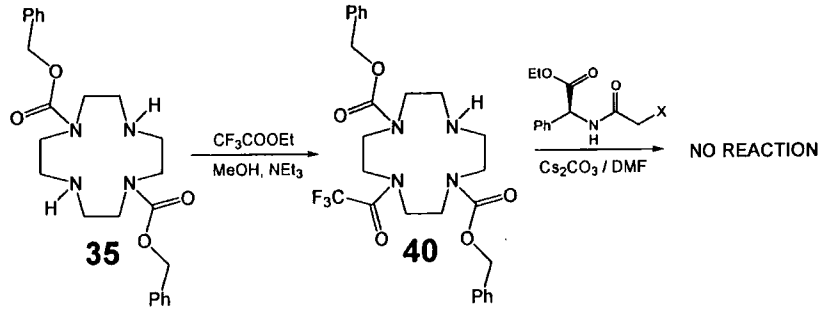

Scheme 4.3 : Illustration of the use of the trifluoroacetyl protecting group to produce differentially protected trisubstituted macrocycles.

In this case the use of the trifluoroacetyl group to differentially protect compound **35** is ideal, since both protecting groups can be removed individually if required. The good yields and ease of formation of compound **40**, makes this compound ideal in

the quest for differentially trisubstituted macrocycles. Unfortunately, the reactivity of the remaining macrocyclic ring nitrogen was found to be very low. Consequently, no alkylation of compound **40** with the chloroamide pendant arm was observed even under very forcing conditions, eq. caesium carbonate/DMF, 120 °C for 48 hours.

Given the low reactivity exhibited by the secondary amine in the trisubstituted cyclen compound, **40**, and the observation of no reaction between ethyl trifluroactetate and the diamide cyclen compound, **37**, the more reactive *tert*–butyldicarbonate anhydride was investigated as a source of introducing a protecting group (**Scheme 4.4**). The use of *tert*–butyldicarbonate anhydride was successful in the formation of the mono–protected 1,7–diamide (**41**), although the greater reactivity of this reagent was evident as significant quantities of tetrasubstituted compound were also isolated. The resulting mono–protected compound (**41**) displayed low reactivity towards alkylating agents. Evidence for the formation of small amounts of the desired product, **42**, was only evident from tlc and mass spectrometry after a reaction period of several days. Evidence obtained from these experiments employing protecting groups on 1,7–substituted cyclen compounds clearly suggests that the protected compounds have a very low reactivity towards α–haloamide alkylating agents. However, it was also observed that the R_f of compound **42** was sufficiently different to the tetrasubstituted side product obtained via the direct alkylation of compound **37** with compound **39**, to allow their chromatographic separation.

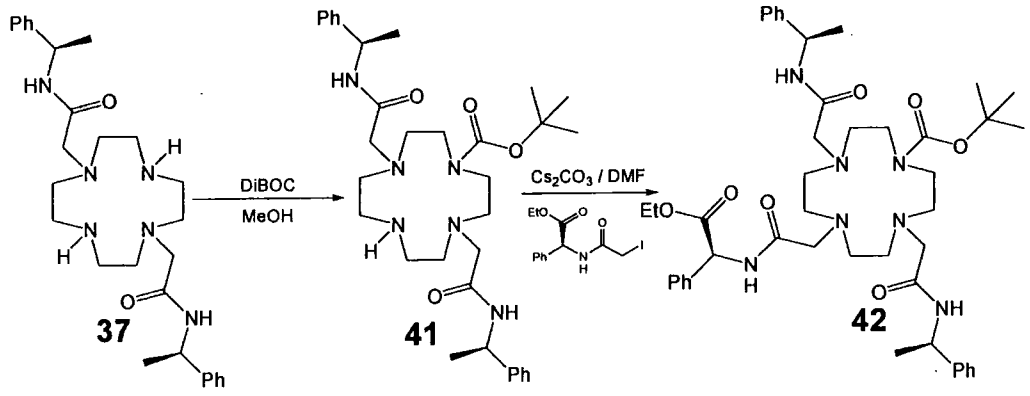

Scheme 4.4 : Illustration of the use of the BOC protecting group to produce differentially protected trisubstituted macrocycles.

Therefore, despite the lack of success in using protecting groups for selective alkylation, a solution to the initial purification problems was realised. Reaction of the

crude reaction mixture from the direct alkylation of compound **37** with compound **39** with *tert*–butyldicarbonate anhydride, produced a mixture of tetrasubstituted compound and compound **42**, which could be more easily purified by column chromatography. Unfortunately, the unreacted compound **37** in the crude reaction mixture also posed problems in the purification. Following its reaction with *tert*–butyldicarbonate anhydride, the resulting tetrasubstituted compound possessed a very similar R_f to the desired compound. Therefore, in obtaining pure compound **42**, it was necessary to pass the crude reaction mixture through an alumina plug to remove any remaining starting material, prior to the reaction with *tert*–butyldicarbonate anhydride. As a direct result of this extra step, although compound **42** could be obtained analytically pure by this route, the yield obtained was only 25%. Subsequent removal of the BOC protecting group was almost quantitative, providing the desired trisubstituted ligand, **43**.

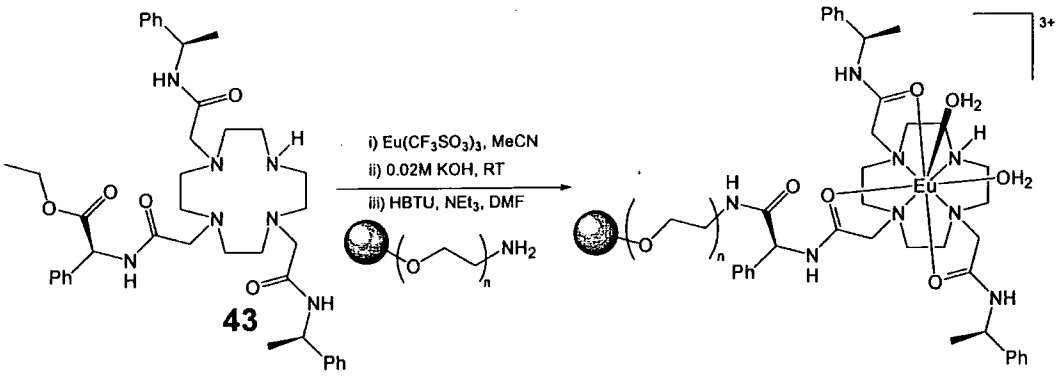

Scheme 4.5 : Synthetic route towards the resin bound europium receptor, via the mild hydrolysis of the ethyl ester following complexation of the ligand.

The corresponding europium(III) complex of ligand **43** was prepared in anhydrous acetonitrile, via reaction with europium(III) trifluoromethanesulfonate salt in anhydrous MeCN at 80°C, followed by precipitation from diethyl ether. The proton NMR spectrum of this complex was very similar to that of the corresponding europium complex, $[Eu7(H_2O)_2]^{3+}$ with the shifts of the axial protons consistent with the same geometry being maintained around the europium(III) centre. Mild hydrolysis of the ethyl ester was achieved using 0.02 M KOH at room temperature over a period of 3 days, followed by ion exchange chromatography, and yielded the carboxylate complex as its dichloride salt. Subsequent reaction of the free carboxylate with an amino functionalised resin, using HBTU at room temperature,

provided the resin bound complex (**Scheme 4.5**). The complex was reacted in order to provide a 5% loading of the resin amino groups.

The resin used (Argogel® NH_2 resin) was chosen due its significant degree of swelling observed in polar solvents, including water, and the high degree of conformational flexibility of the terminal amino groups, due to the presence of polyethylene glycol spacers between the amino group and the polystyrene backbone. These features present in the resin beads were anticipated to increase the amount of information available on the resin bound complexes as proton NMR may be used to analyse such materials.[8] Despite the inherent broadening of the spectrum and the presence of intense resonances from the resin backbone and tethering groups, the proton NMR spectrum of the resin bound complex was anticipated to be unaffected due to the paramagnetic broadening already present, and the fact that the resonances of interest are shifted far beyond the normal proton NMR spectral window in which these problematic resonances occur. Unfortunately, this was not the case, and the paramagnetically shifted resonances were not observed, possibly due to the combined effect of paramagnetic broadening and the spectral line–broadening associated with presence of the solid phase resin.

Attempts to investigate the resin bound complex using luminescence also failed for two main reasons. Firstly, the available instrumentation possessed optics (required to look at the europium luminescence emission) that only operate successfully at wavelengths greater than 350 nm. Thus, the use of the ligand phenyl groups as sensitisers in this case was not possible. Secondly, since only the inefficient, direct excitation of the europium(III) ion was possible using these optics, the resulting luminescence was too weak to be detected. Thus, the need for a suitable long wavelength sensitising chromophore, as discussed in **Chapter 3**, arises from the limitations of the optics required to monitor the behaviour of the resin bound europium(III) receptor in the presence of *O*–phosphorylated anions.

4.2 Incorporation of a Long–Wavelength Sensitiser into the Resin Bound Complex

Given the possible practical applications of immobilised europium receptors, the need to visualise the emission spectrum of the resin bound complex is crucial to the

determination of the ternary adducts present. Since the optics required to perform such measurements need the use of excitation wavelengths greater than 350 nm, the incorporation of a suitable long wavelength sensitiser was required. The 1–aza–10–thioxanthone compounds discussed in **Chapter 3**, were deemed particularly suitable for this purpose. These sulfur heterocycles provide an excitation wavelength more than 40 nm higher than the corresponding 1–azaxanthones. The fact that this increase in wavelength is obtained simply by replacement of oxygen by sulfur, obviates the emission problems associated with the introduction of electron donating substituents as was found to be the case for several substituted 1–azaxanthones. Furthermore, the synthetic route towards the sensitiser is simplified, such that modification of this structure can focus purely on how to efficiently incorporate it into the macrocyclic ligand.

In order to retain the relevant geometry around the lanthanide(III) ion (as in **Section 4.1.2**) two options can now be envisaged. The first design includes two functional groups on the xanthone sensitiser. One functional group will provide a handle for the attachment of the pendant arm, with the second group being a carboxylate group to provide the link to the resin beads. The second option is more straightforward, avoiding the need for orthogonal functional groups on the sensitiser, and utilises the natural source of chirality imparted by amino acids. This design is virtually identical to that in **Figure 4.1b**, except in this case the aromatic sensitiser will replace the phenyl group.

An additional consideration in the design of a ligand which incorporates a sensitiser is the position of the sensitiser. In order to function efficiently, the sensitiser should be as close to the lanthanide(III) centre as possible, maximising the efficiency of the energy transfer process. This is distance dependent and follows a $1/r^6$ dependence, as proposed by Förster.[9] Therefore, the link between sensitiser and pendant arm should be kept as short as possible, limiting the possibility for movement relative to the lanthanide(III) centre.

4.2.1 Synthesis of the 1–Aza–10–thioxanthone Conjugate

The simplest synthetic route towards a pendant arm incorporating the sensitiser and carboxylate group was anticipated to combine the selectivity of benzylic bromination

and the very good nucleophilicity of the sulfur atom in the amino acid cysteine. The synthetic pathway undertaken is illustrated in **Scheme 4.6**.

Bromination of the benzylic methyl group in compound **44** occurred readily in one step to give the mono–bromo compound, **45**, in 51% yield. A higher effective yield of compound **45** was obtained by isolating the di–bromo compound, which can be formed almost quantitatively using excess NBS and AIBN as initiator. Subsequent debromination of this compound using diethyl phosphite and diisopropylethylamine provides the mono–bromo compound in very good yields.[10] However, the difficulty in achieving pure compound **45** via this route is illustrated in the modest isolated yield of 64%, arising from complications associated with contamination from phosphorus(V) compounds.

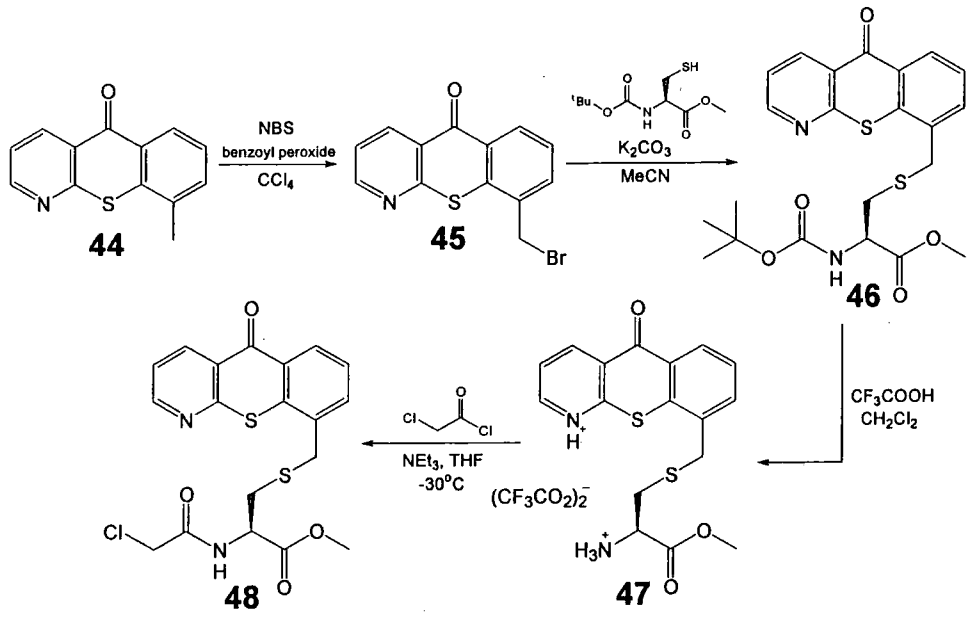

Scheme 4.6 : Synthetic route towards the pendant arm incorporating the 1–aza–10–thioxanthone sensitiser.

Alkylation of *N*–BOC–L–cysteine methyl ester with compound **45** in the presence of potassium carbonate, produced compound **46** as a crystalline solid in 83% yield. Subsequent removal of the *N*–BOC protecting group in the presence of trifluoracetic acid occurred in quantitative yield. Reaction of the very hygroscopic compound, **47**, with chloroacetyl chloride at low temperature gave the sensitiser pendant arm, **48**, as a crystalline solid in 65% yield.

Incorporation of this pendant arm into compound **37**, to produce the trisubstituted

compound as the major product, occurred with high selectivity using mild reaction conditions of EtOH and triethylamine.

The reduced tendency to form the tetra–substituted compound may be due to the increase in steric bulk of the pendant arm, causing steric crowding of the remaining ring NH group. Furthermore, the differences in R_f between the tri– and tetra–substituted compounds was larger in this case allowing direct purification via column chromatography, alleviating the need for acylation of the macrocyclic ring nitrogen to increase the R_f differences, in contrast to the synthesis of compound **43**. Despite these favourable outcomes, the isolated yield of the tri–substituted compound was still only moderate at 53%. Further examination of the products revealed that decomposition of the pendant arm tended to occur when solutions of the compound were exposed to air. This decomposition was noted to occur to an even greater extent in more polar solvents, such as DMF, and in the presence of a carbonate base. Some isolated crude products contained only the xanthone ring system, indicating cleavage of the thioether linkage in the pendant arm. The decomposition of the thioether suggests that the use of serine in the place of cysteine as the amino acid source, may lead to a more stable linkage.

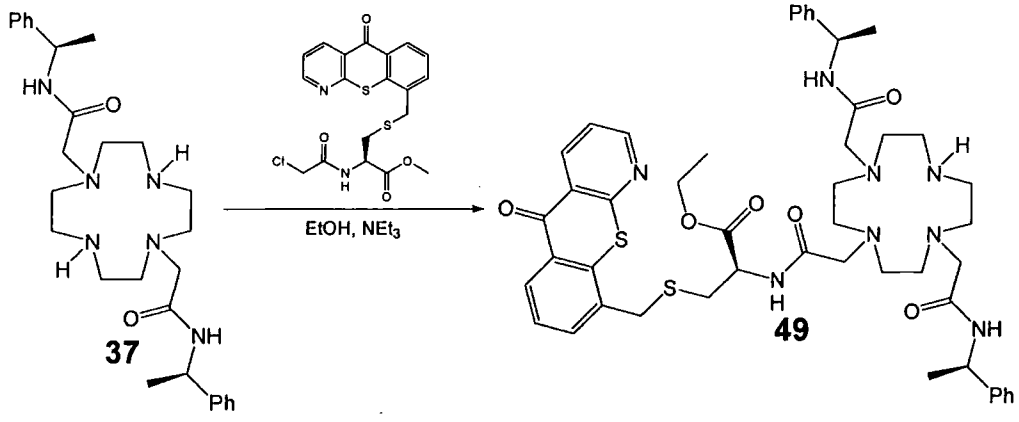

Scheme 4.7 : Synthetic route used to incorporate the pendant arm containing the 1–aza–10–thioxanthone sensitiser.

Sufficient quantities of pure ligand were isolated to allow the synthesis of the corresponding europium(III) complex of compound **49**. This was prepared in anhydrous acetonitrile, via reaction with the appropriate lanthanide(III) trifluoromethanesulfonate salt in anhydrous MeCN at 80°C, followed by precipitation from diethyl ether.

4.2.2 Optical Properties of the Long–Wavelength Sensitiser Containing Complex

The absorption and emission characteristics were measured for the europium complex of compound **49**. As expected, the absorption spectrum of this complex was very similar to that observed solely for the sensitising chromophore, although the absorption wavelength maximum of this complex in aqueous solution was observed at 379 nm (**Figure 4.2**). Such a red shift in the absorption maximum when changing from methanol to aqueous media is consistent with the similar shifts observed for the corresponding 1–azaxanthone compounds.

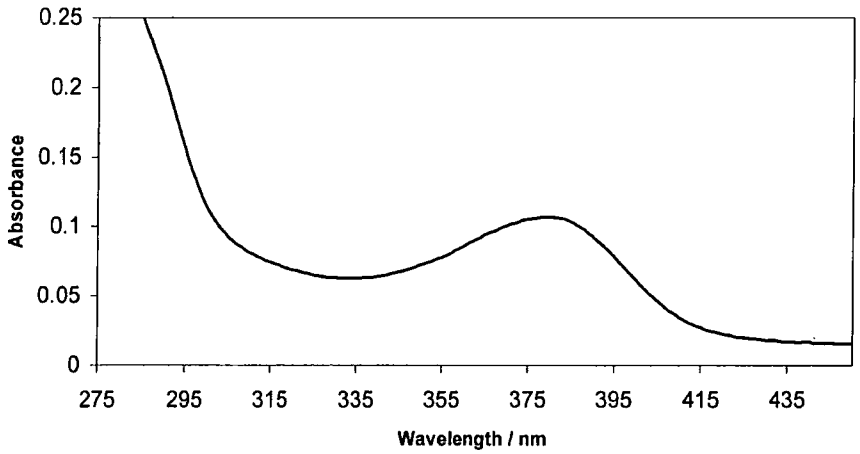

Figure 4.2 : Absorption spectrum of the complex [Eu**49**]$^{3+}$ (50 μM, 295 K, pH 7.4, 0.1 M MOPS).

Indirect excitation of the europium(III) ion, was achieved via irradiation of the absorption maximum of the sensitiser at 379 nm, and led to strong emission from the europium emissive state (**Figure 4.3**). In contrast, direct excitation of the europium(III) ion at 397 nm resulted in no detectable europium emission from the sample. Such an observation further illustrates the necessity for sensitised emission for luminescent lanthanide optical probes, particularly when using very low concentrations of complex.

The effect of added phosphorylated and carbonate anions on the luminescence emission of the complex [Eu**49**]$^{3+}$ was studied. In a typical binding experiment, a concentrated solution of the anionic species was added to a 50 μM solution of the complex in 0.1 M MOPS buffering at pH 7.4 at 295 K. In each case, the total volume of the solution following anion addition had increased by less than 2%, in order to avoid significant changes in the concentration of the complex, which would also

influence the emission intensity.

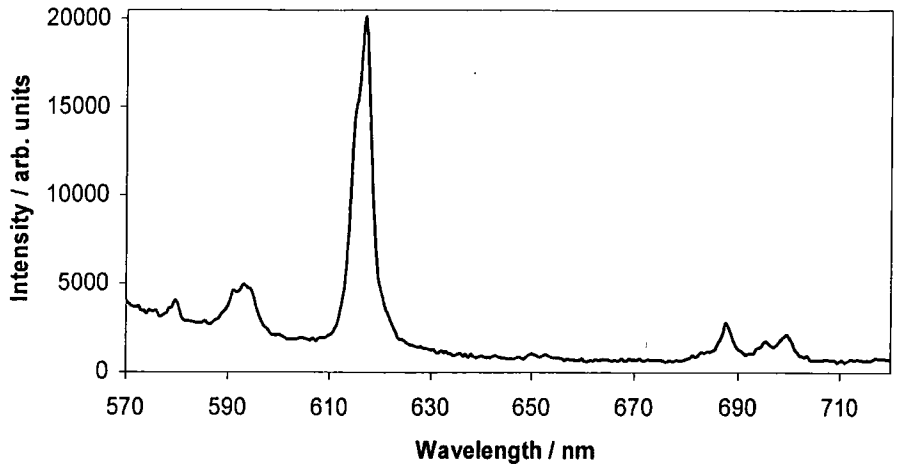

Figure 4.3 : Emission spectrum of the complex $[Eu\mathbf{49}]^{3+}$ (50 μM, 295 K, pH 7.4, 0.1 M MOPS) following indirect excitation via the sensitiser at 379 nm.

Addition of an increasing concentration of glucose–6–phosphate to the complex $[Eu\mathbf{49}]^{3+}$ led to a gradual decrease in the emission intensity observed. This was in contrast to the anticipated behaviour, which was expected to result in an increase in emission intensity upon addition of phosphate anions, as observed for the complex $[Eu\mathbf{7}(H_2O)_2]^{3+}$. The observed increase in the emission intensity for the complex $[Eu\mathbf{7}(H_2O)_2]^{3+}$ upon addition of phosphate anions, is a consequence of the displacement of one of the two bound water molecules from the lanthanide(III) centre, and hence, reduces the quenching effect of nearby O–H oscillators. Given that no observable increase in emission intensity was observed for $[Eu\mathbf{49}]^{3+}$ in the presence of phosphate or carbonate anions, this led to the conclusion that no displacement of bound water molecules by anionic species is occurring.

To further investigate why the anion binding properties of $[Eu\mathbf{7}(H_2O)_2]^{3+}$ were drastically affected after formation of the sensitiser conjugate, the emission of $[Eu\mathbf{49}]^{3+}$ in H_2O and D_2O was used to estimate the hydration level of the europium(III) ion (**Section 1.3.3**). The rate constants for depopulation of the emissive state of europium were 2.90 ms^{-1} and 2.07 ms^{-1} in H_2O and D_2O respectively. Following the application of a correction factor to account for the quenching due to outer sphere water molecules (−0.25 ms^{-1}) and the three amide N–H bonds present in the pendant arms of the ligand (−0.08 ms^{-1} each), an estimated hydration state of 0.4 was obtained. This result clearly shows that there is a

significant deviation in the hydration state of the europium ion in the complex $[Eu\mathbf{49}]^{3+}$ from the di–aqua complex which was expected, given that this is the case for $[Eu\mathbf{DO3Ph}(H_2O)_2]^{3+}$. The hydration state value of 0.4 obtained, may suggest there is an equilibration between a mono–aqua and unhydrated complex in solution, or that a coordinated water molecule exists which possesses a slightly longer Eu–O bond than is usually observed.

The only plausible explanation to account for the lower than expected hydration state must involve the aromatic sensitiser. Given the hydrophobicity of the aromatic sensitiser, rather than extending from the pendant arm into solution, it must adopt a closed structure, folding back over the europium ion, in order to minimise unfavourable solvent interactions. The presence of the sensitiser in close proximity to the europium ion, would have a significant steric influence, excluding water molecules from the europium ion. Similarly, the ability for anionic species to access the europium centre in $[Eu\mathbf{49}]^{3+}$ must also be limited by the presence of the large hydrophobic sensitiser, thus accounting for the lack of anion binding observed.

4.3 Conclusions and Future Work

The preliminary investigation into the incorporation of a sensitising chromophore into a europium complex which has been observed to display chemoselective phospho–anion selectivity has been performed.

The complex $[Eu\mathbf{49}]^{3+}$ demonstrates the suitability of the 1–aza–10–thioxanthone as a long–wavelength sensitiser for the europium(III) ion. Careful planning of the ligand structure was made, in order to avoid any deviation from the geometry exhibited around the europium centre for the complex $[Eu\mathbf{7}(H_2O)_2]^{3+}$, upon inclusion of the sensitiser. However, the hydrophobicity of the sensitiser appears to result in a closed structure, which hinders the binding of anions to the europium centre, thus limiting the suitability of this complex design.

The idea of creating a dimeric europium complex to achieve large binding affinities for multiply phosphorylated peptide sequences was proposed in **Section 2.6**. Through the further expansion of this concept, a solution to the problem associated with the hydrophobic nature of the sensitiser may be envisaged (**Figure 4.4**).

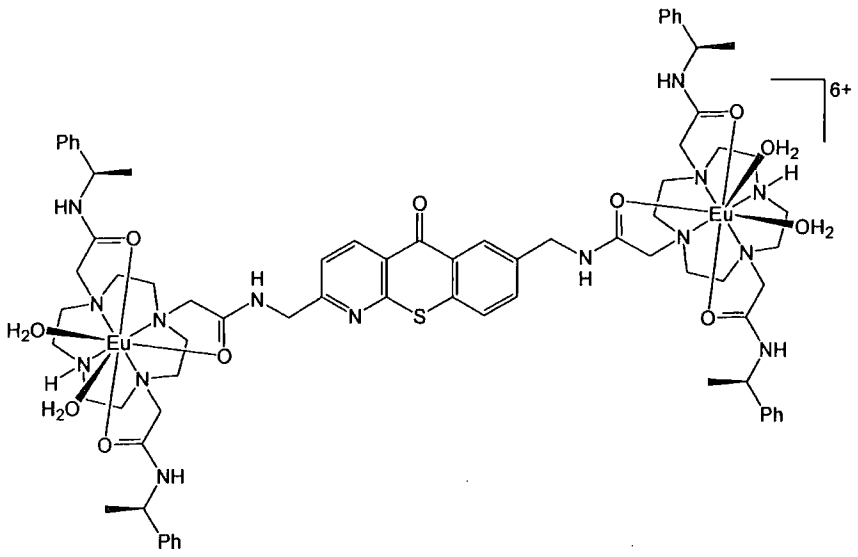

Figure 4.4 : Proposed design of a dimeric europium complex, incorporating the 1–aza–10–thioxanthone moiety as a sensitiser and spacing unit.

This concept provides a route towards a dimeric system incorporating a 1–aza–10–thioxanthone compound, which acts as both the sensitiser and the rigid spacer between the two complexes. Furthermore, the lower flexibility of the sensitiser molecule in the dimeric system should inhibit the possibility for this group to fold back towards the europium centre, thus restoring the anion binding properties.

4.4 References

1 M. Mann, R. C. Hendrickson and A. Pandey, *Annu. Rev. Biochem.*, 2001, **70**, 437.

2 G. Neubauer and M. Mann, *Anal. Chem.*, 1999, **71**, 235.

3 S. Kjellström and N. Jensen, *Anal. Chem.*, 2004, **76**, 5109.

4 L. M. Nuwaysir and J. T. Stults, *J. Am. Soc. Mass. Spectrom.*, 1993, **4**, 662.

5 M. C. Posewitz and P. Tempst, *Anal. Chem.*, 1999, **71**, 2883.

6 Z. Kovacs and A. D. Sherry, *Synthesis*, 1997, 759.

7 W. Yang, C. M. Giandomenico, M. Sartori and D. A. Moore, *Tet. Lett.*, 2003, **44**, 2481.

8 P. A. Keifer, *J. Org. Chem.*, 1996, **61**, 1558.

9 T. Förster, *Discuss. Faraday Soc.*, 1959, **27**.

10 P. Liu, Y. Chen, J. Deng and Y. Tu, *Synthesis*, 2001, 2078.

CHAPTER 5

Experimental Details

5.1 Experimental Details

All reagents were used as supplied by commercial sources unless otherwise stated. Solvents were dried over the appropriate drying agents when required. Water and H_2O refer to high purity water with conductivity ≤ 0.04 μScm^{-1}, obtained from the "Purite$_{STILL}$ Plus" purification system.

Thin layer chromatography was carried out using silica plates (Merck Art 5554) or neutral aluminium oxide plates (Merck Art 5550), both of which are fluorescent under UV irradiation (254 nm). Preparative column chromatography was performed using neutral aluminium oxide (Merck Aluminium Oxide 90, activity II–III, 70–230 mesh), washed in ethyl acetate, or silica (Merck Silica Gel 60, 230–400 mesh).

^1H NMR spectra were recorded at 199.99 MHz on a Varian Mercury–200, 299.91 MHz on a Varian Unity–300, 400.13 MHz on a Bruker Avance spectrometer, 499.78 MHz on a Varian Inova–500 or at 65.6 MHz on a 1.53 T magnet connected to a Varian VXR400 console. All spectra were referenced to solvent residual proton signals, except for complexes in D_2O, where *tert*–butanol was added as an internal reference ($\delta = 0$ ppm).

Electrospray mass spectra were recorded on a VG Platform II instrument (Fisons) with methanol as the carrier solvent. Accurate masses were measured on a Thermo Finnigan LTQ or by the ESPRC Mass Spectroscopy Service at the University of Wales in Swansea.

Melting points were measured using a Reichart–Köfler block and are uncorrected.

All pH measurements were performed using a Jenway 3320 pH meter attached to an Aldrich Chemical Company micro–pH combination electrode, calibrated using pH 4, 7 and 10 buffer solutions.

UV/vis absorption spectra were recorded using a Perkin Elmer Lamda 900 UV/vis/IR spectrometer. Emission spectra were recorded at 295 K using an Instruments SA Fluorolog 3–11 spectrometer and DataMax v2.1 for Windows.

Luminescence spectra of the europium(III) complexes were recorded using a 420 nm cut–off filter, following indirect excitation of the europium(III) ion, either via the phenyl groups in the ligand at 264 nm or at 374 nm for the 1–aza–10–thioxanthone sensitiser. An integration time of 0.5 seconds, increment of 0.5 nm and excitation and emission slit widths of 10 and 1 nm, respectively, were employed throughout.

Lifetime measurements of the complex [Eu**49**]$(CF_3SO_3)_3$ were recorded on a Perkin Elmer LS55 luminescence spectrometer using FL Winlab software. The europium(III) ion was excited indirectly via the 1–aza–10–thioxanthone sensitiser at 374 nm, with an excitation slit width of 10 nm. The total integrated light intensity observed at 618 nm (emission slit width of 2.5 nm) over a period of 0.1 ms was recorded for 20 different delay times, spanning at least three lifetimes. The data points obtained were then fitted to an exponential curve using Microsoft Excel and the lifetime determined as the inverse of the rate constant for the decay in emission.

Phosphorescence emission spectra of the 1–azaxanthone compounds were recorded at 77 K using an Oxford Instruments optical cryostat and LS 55B spectrometer, with EPA (diethyl ether, isopentane and ethanol, 5:5:2) as solvent.

NMR spectral assignments were made using the following numbering systems and notations:

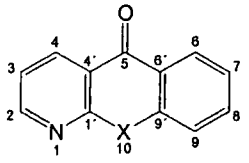

In the NMR spectral assignments of macrocyclic ligands, numbers in brackets after the proton assignments for nuclei on the pendant arms identify the ring nitrogen to which that pendant arm is attached.

In the proton NMR spectral assignments of lanthanide(III) complexes, the subscripts H_{ax}, H_{eq}, $H_{eq'}$ and $H_{ax'}$ refer to the macrocyclic ring protons as illustrated below, where X denotes the axial ligand.

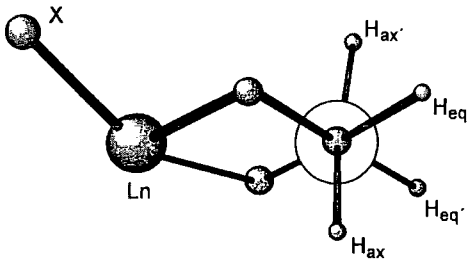

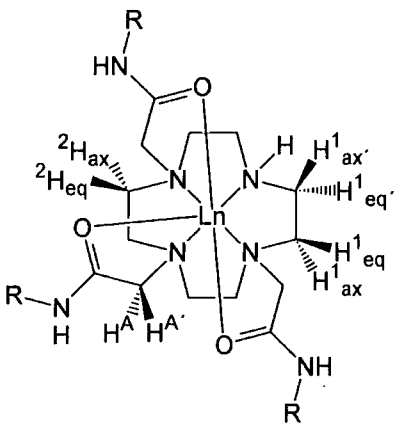

The superscripts, H^1, H^2, H^3 and H^4 indicate that these protons are on the same ethylene diamine unit of the macrocyclic ring, but do not signify the positions of these relative to one another. Similarly, the superscripts H^A, $H^{A'}$, H^B, $H^{B'}$, H^C, $H^{C'}$ denote the diastereotopic α–carbonyl protons on the same pendant arm without indicating the relative positions within the complex.

5.1.1 Synthetic Details

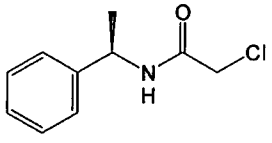

2–Chloro–*N*–[(*R*)–1–phenylethyl]ethanamide (1).[1] A solution of chloroacetyl chloride (4.8 cm^3, 60 mmol) in diethyl ether (100 cm^3) was added dropwise to a stirred solution of (*R*)–α–methylbenzylamine (6.4 cm^3, 50 mmol) and triethylamine (8.4 cm^3, 60 mmol) in diethyl ether (200 cm^3) maintained at 0 °C under an argon atmosphere. After the addition was complete the reaction was allowed to return to room temperature and stirred for 1 hour. The resulting white suspension was washed with hydrochloric acid (1 N, 2 × 250 cm^3), water (300 cm^3), dried (Na_2SO_4) and filtered. The yellow solution was left to stand at room temperature, forming pale yellow crystals, which were purified via recrystallisation from diethyl ether to give the title compound (6.4 g, 32 mmol, 65%) as white needles.

^{1}H NMR (300 MHz, $CDCl_3$) δ 7.40–7.20 (m, 5H, Ph), 6.78 (br, 1H, CONH), 5.14 (m, 1H, CH), 4.10 (d, 1H, *J* 16.5 Hz, CH_2Cl), 4.04 (d, 1H, *J* 16.5 Hz, CH_2Cl), 1.54 (d, 3H, *J* 7.0 Hz, CH_3).

^{13}C NMR (75.4 MHz, $CDCl_3$) δ 165.1 (C=O), 142.4 ($Ph_{(q)}$), 128.7 ($Ph_{(m)}$), 127.6

($Ph_{(p)}$), 126.1 ($Ph_{(o)}$), 49.2 (CH), 42.6 (CH_2Cl), 21.6 (CH_3).

$ESMS^+$ (*m/z*) 198 ($[M+H]^+$, 10%), 220 ($[M+Na]^+$, 100%).

mpt 94–96 °C (lit.[1] 95–96 °C).

2–Chloro–*N*–[(*S*)–1–phenylethyl]ethanamide.[1] This compound was prepared following the above procedure using (*S*)–α–methylbenzylamine. The resulting compound had identical spectroscopic properties to the *R*–enantiomer.

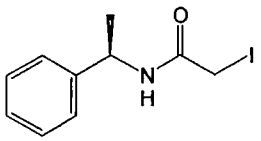

2–Iodo–*N*–[(*R*)–1–phenylethyl]ethanamide. Sodium iodide (508 mg, 3.4 mmol) was added to a stirred solution of 2–chloro–*N*–[(*R*)–1–phenylethyl]ethanamide (670mg, 3.4 mmol) in MeCN (8 cm^3) and the resulting suspension boiled under reflux for 3 hours. The reaction mixture was filtered and the solvent removed under reduced pressure to give a yellow solid. Subsequent recrystallisation from diethyl ether afforded the title compound (786 mg, 2.7 mmol, 80%) as white needles.

^1H NMR (400 MHz, $CDCl_3$) δ 7.40–7.25 (m, 5H, Ph), 6.21 (br, 1H, CONH), 5.09 (m, 1H, CH), 3.72 (d, 1H, *J* 11.6 Hz, CH_2I), 3.69 (d, 1H, *J* 11.6 Hz, CH_2I), 1.52 (d, 3H, *J* 7.0 Hz, CH_3).

^{13}C NMR (100.6 MHz, $CDCl_3$) δ 166.7 (C=O), 142.7 ($Ph_{(q)}$), 128.7 ($Ph_{(m)}$), 127.5 ($Ph_{(p)}$), 126.2 ($Ph_{(o)}$), 49.7 (CH), 21.6 (CH_3), 0.0 (CH_2I).

$ESMS^+$ (*m/z*) 289 ($[M+H]^+$, 15%), 311 ($[M+Na]^+$, 100%).

mpt 107–108 °C.

Found : C, 42.17; H, 4.24; N, 4.83% ($C_{10}H_{12}NOI$ requires C, 41.54; H, 4.18; N, 4.84%).

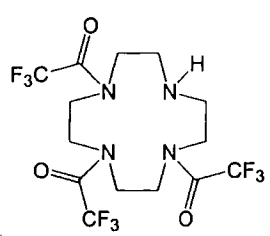

1,4,7–Tris(trifluromethylcarbonyl)–1,4,7,10–tetraazacyclododecane (3).[2] Ethyl

tri–fluoroacetate (5.52 cm^3, 46.4 mmol) was added dropwise over 20 minutes to a stirred solution of 1,4,7,10–tetraazacyclododecane (2.0 g, 11.6 mmol) and triethylamine (1.60 cm^3, 11.6 mmol) in anhydrous MeOH (40 cm^3) maintained at 0°C under an argon atmosphere. After the addition was complete the reaction was allowed to return to room temperature and stirred for 18 hours. The solvents were removed under reduced pressure and the residue purified through a silica plug (eluant ethyl acetate) yielding the title compound (4.92 g, 10.7 mmol, 92%) as a white foam.

^{1}H NMR (400 MHz, $CDCl_3$) δ 3.90 (br m, 4H, $NCH_{2(ring)}$), 3.80–3.40 (br m, 8H, $NCH_{2(ring)}$), 3.10–2.80 (br m, 4H, $NCH_{2(ring)}$).

^{13}C NMR (100.6 MHz, $CDCl_3$) δ 158.3–156.9 (10 resonances, C=O, due to conformers and long range C–F coupling), 116.1 (q, J_{C-F} 288 Hz, CF_3, multiple resonances due to conformers), 53.6–43.1 (multiple resonances, $NCH_{2(ring)}$).

$ESMS^+$ (*m/z*) 483 ($[M+Na]^+$, 100%).

R_f 0.47 (silica, 2% MeOH:CH_2Cl_2).

mpt 77–80 °C.

Found : C, 36.50; H, 3.71; N, 11.90% ($C_{14}H_{17}N_4O_3F_9$ requires C, 36.53; H, 3.72; N, 12.17%).

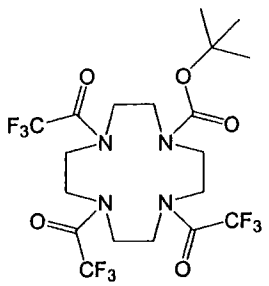

1–*tert*–Butoxycarbonyl–4,7,10–tris(trifluromethylcarbonyl)–1,4,7,10–tetraaza–cyclododecane (4). DiBOC (427 mg, 2.0 mmol) and triethylamine (270 µL, 2.0 mmol) were added to a solution of 1,4,7–tris(trifluromethylcarbonyl)–1,4,7,10–tetraazacyclododecane (750 mg, 1.6 mmol) in anhydrous MeOH (20 cm^3) and the reaction stirred at room temperature under an argon atmosphere for 5 hours. The solvents were removed under reduced pressure and the residue purified via column chromatography (silica, 10% ethyl acetate:CH_2Cl_2) yielding the title compound (700 mg, 1.2 mmol, 77%) as a white foam.

^{1}H NMR (500 MHz, $CDCl_3$) δ 3.90–3.30 (br m, 16H, $NCH_{2(ring)}$), 1.45 (s, 9H,

$C(CH_3)_3$).

^{13}C NMR (125.6 MHz, $CDCl_3$) δ 159.0–157.0 (7 resonances due to conformers, $C{=}O_{(amides)}$+$C{=}O_{(carbamate)}$), 116.2 (multiple q, J_{C-F} 288 Hz, CF_3, multiple resonances due to conformers), 82.5–81.8 (3 resonances, $\mathbf{C}(CH_3)_3$), 53.3–46.9 (multiple resonances, $NCH_{2(ring)}$), 28.3 (CH_3).

ESMS$^+$ (*m/z*) 583 ($[M+Na]^+$, 100%).

HRMS (ES^+) 583.1570 ($C_{19}H_{25}N_4O_5F_9Na$ requires 583.1573, $[M+Na]^+$).

R_f 0.56 (silica, ethyl acetate:CH_2Cl_2 10:90).

mpt 119–122 °C.

Found : C, 40.78; H, 4.56; N, 9.93% ($C_{19}H_{25}N_4O_5F_9$ requires C, 40.72; H, 4.50; N, 10.00%).

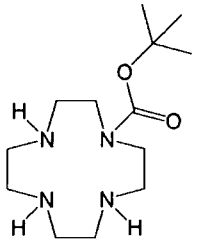

1–*tert*–Butoxycarbonyl–1,4,7,10–tetraazacyclododecane (5). Aqueous potassium hydroxide solution (1 cm^3, 2M) was added to a solution of 1–*tert*–butoxycarbonyl–4,7,10–tris(trifluromethyl–carbonyl)–1,4,7,10–tetraazacyclododecane (375 mg, 670 μmol) in MeOH/water (25 cm^3, 4:1) and stirred at room temperature for 3 hours. The solvents were removed under reduced pressure and the residue taken up in CH_2Cl_2, washed with aqueous $NaHCO_3$ solution (10 cm^3), aqueous NaCl solution (10 cm^3), dried (K_2CO_3) and filtered. Evaporation of the solvents under reduced pressure yielded the title compound (150 mg, 550 μmol, 82%) as a colourless oil.

^1H NMR (300 MHz, $CDCl_3$) δ 3.45 (br m, 4H, $NCH_{2(ring)}$), 2.84 (br m, 8H, $NCH_{2(ring)}$), 2.70 (br m, 4H, $NCH_{2(ring)}$), 1.47 (s, 9H, CH_3).

^{13}C NMR (100.6 MHz, $CDCl_3$) δ 156.6, 156.5 (C=O), 79.9, 77.5 ($\mathbf{C}(CH_3)_3$), 49.0 ($NCH_{2(ring)}$), 48.1 ($NCH_{2(ring)}$), 46.6 ($NCH_{2(ring)}$), 28.4 (CH_3).

ESMS$^+$ (*m/z*) 173 ($[M-COOC(CH_3)_3]^+$, 100%), 273 ($[M+H]^+$, 100%).

HRMS (ES^+) 273.2283 ($C_{13}H_{29}N_4O_2$ requires 273.2285, $[M+H]^+$).

R_f 0.56 (silica, ethyl acetate:CH_2Cl_2 10:90).

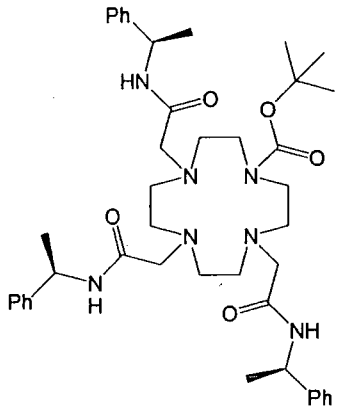

1–*tert*–Butoxycarbonyl–4,7,10–(*RRR*)–tris[(1–phenylethylcarbamoyl)methyl]–1,4,7,10–tetraazacyclododecane (6). To a solution of 1–*tert*–butoxycarbonyl–1,4,7,10–tetraazacyclododecane (50 mg, 180 μmol) in anhydrous MeCN (5 cm^3) was added 2–chloro–*N*–[(*R*)–1–phenylethyl]ethanamide (116 mg, 590 μmol, 3.2 eq.) and Cs_2CO_3 (191 mg, 590 μmol, 3.2 eq.) and the resulting suspension heated at 80°C for 48 hours. The solvents were removed under reduced pressure and the residue taken up in CH_2Cl_2, washed with water (10 cm^3), saturated NaCl solution (10 cm^3), dried (K_2CO_3) and filtered. Evaporated of the solvents under reduced pressure and subsequent purification via column chromatography (alumina, CH_2Cl_2 → 0.3% EtOH) yielded the title compound (118 mg, 160 μmol, 85%) as a white foam.

^{1}H NMR (300 MHz, $CDCl_3$) δ 7.40 (br s, 1H, $NH_{(amide)}$), 7.38–7.17 (br m, 15H, Ph), 7.08–6.92 (br m, 2H, 2 × $NH_{(amide)}$), 5.11 (br m, 3H, CH), 3.40–2.28 (br m, 22H, $NCH_{2(ring)}$ + NCH_2), 1.48 (d, 6H, *J* 7.0 Hz, $CH_{3(4,10)}$), 1.47 (d, 3H, *J* 7.0 Hz, $CH_{3(7)}$), 1.42 (s, 9H, $C(CH_3)_3$).

^{13}C NMR (125.7 MHz, $CDCl_3$) δ 170.2 ($C{=}O_{(7)}$), 169.7 ($C{=}O_{(4,10)}$), 155.8 ($C{=}O_{(carbamate)}$), 143.7 ($Ph_{(q,7)}$), 143.1 ($Ph_{(q,4,10)}$), 128.8 ($Ph_{(m,4,7,10)}$), 127.6 ($Ph_{(p,4,10)}$), 127.3 ($Ph_{(p,7)}$), 126.5 ($Ph_{(o,4,10)}$), 126.4 ($Ph_{(o,7)}$), 79.9 ($\mathbf{C}(CH_3)_3$), 59.4, 58.4 ($NCH_{2(4,10)}$), 57.8 ($NCH_{2(7)}$), 54.3, 53.7, 53.5, 52.9 ($NCH_{2(ring)}$), 48.4 ($CH_{(4,10)}$), 47.8 ($CH_{(7)}$), 28.5 ($C(\mathbf{C}H_3)_3$), 21.9 ($CH_{3(7)}$), 21.3 ($CH_{3(4,10)}$).

ESMS$^+$ (*m/z*) 382 ($[M+Ca]^{2+}$, 100%), 756 ($[M+H]^+$, 100%).

HRMS (ES^+) 756.4809 ($C_{43}H_{62}N_7O_5$ requires 756.4807, $[M+H]^+$).

R_f 0.63 (silica, 2% EtOH:CH_2Cl_2).

mpt 79–81 °C.

1–*tert*–Butoxycarbonyl–4,7,10–(*SSS*)–tris[(1–phenylethylcarbamoyl)methyl]–1,4,7,10–tetraazacyclododecane. This compound was prepared using the above procedure using 2–chloro–*N*–[(*S*)–1–phenylethyl]ethanamide. The title compound displayed identical spectroscopic properties to the *RRR*–enantiomer.

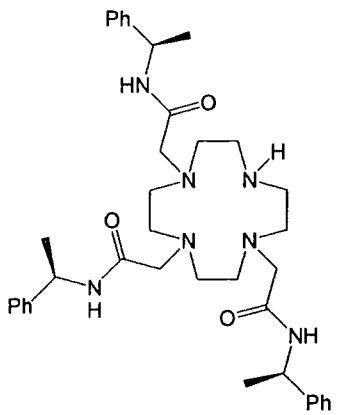

1,4,7–(*RRR*)–Tris[(1–phenylethylcarbamoyl)methyl]–1,4,7,10–tetraazacyclododecane (7). 1–*tert*–Butoxycarbonyl–4,7,10–(*RRR*)–tris[(1–phenylethylcarbamoyl)methyl]–1,4,7,10–tetraazacyclododecane (110 mg, 150 μmol) was dissolved in TFA:CH_2Cl_2 (1 cm^3, 95:5) and stirred under an argon atmosphere for 5 hours. The solvents were removed under reduced pressure and the residue taken up in CH_2Cl_2, washed with aqueous $NaHCO_3$ solution (10 cm^3), dried (K_2CO_3) and filtered. Removal of the solvents under reduced pressure yielded the title compound (94 mg, 140 μmol, 98%) as a white foam.

^{1}H NMR (300 MHz, $CDCl_3$) δ 7.57 (br s, 1H, $NH_{(amide)}$), 7.33–7.20 (m, 17H, Ph + 2 × $NH_{(amide)}$), 5.09 (m, 3H, CH), 2.98 (s, 4H, $NCH_{2(1,7)}$), 2.95 (s, 2H, $NCH_{2(4)}$), 2.60 (br s, 16H, $NCH_{2(ring)}$), 1.48 (d, 6H, *J* 7.0 Hz, $CH_{3(1,7)}$), 1.45 (d, 3H, *J* 7.0 Hz, $CH_{3(4)}$).

^{13}C NMR (50.3 MHz, $CDCl_3$) δ 170.8 ($C{=}O_{(4)}$), 170.5 ($C{=}O_{(1,7)}$), 143.7 ($Ph_{(q)}$), 128.6 ($Ph_{(m)}$), 127.4 ($Ph_{(p)}$), 126.9 ($Ph_{(o)}$), 59.8 ($NCH_{2(1,7)}$), 58.0 ($NCH_{2(4)}$), 54.5, 53.6 ($NCH_{2(ring)}$), 48.9 ($CH_{(1,7)}$), 48.6 ($CH_{(4)}$), 22.1 ($CH_{3(4)}$), 21.9 ($CH_{3(1,7)}$).

$ESMS^+$ (*m/z*) 348 ($[M+Ca]^{2+}$, 100%), 656 ($[M+H]^+$, 30%).

R_f 0.55 (alumina, 5% EtOH:CH_2Cl_2).

mpt 64–66 °C (lit.[3] 63–65°C).

1,4,7–(*SSS*)–Tris[(1–phenylethylcarbamoyl)methyl]–1,4,7,10–tetraazacyclododecane. This compound was prepared using the above procedure using the *SSS*–

enantiomer as starting material. The title compound displayed identical spectroscopic properties to the *RRR*–enantiomer.

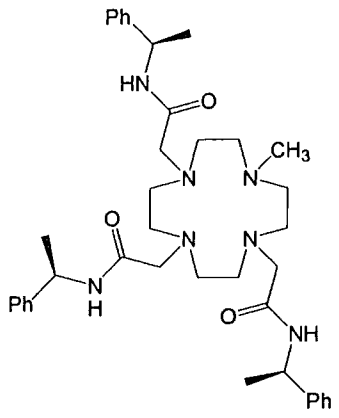

1–Methyl–4,7,10–(*RRR*)–Tris[(1–phenylethylcarbamoyl)methyl]–1,4,7,10–tetra–azacyclododecane (8).[3] 1,4,7–(*RRR*)–Tris[(1–phenylethylcarbamoyl)methyl]–1,4,7,10–tetraazacyclododecane (200 mg, 300 μmol) was added to a mixture of formic acid (2.5 cm^3) and aqueous formaldehyde (37%, 4 cm^3) and boiled under reflux for 24 hours. The solvents were removed under reduced pressure and the residue dissolved in aqueous potassium hydroxide (2 M, 10 cm^3) and extracted with chloroform (3 × 15 cm^3). The combined organic extracts were dried (K_2CO_3), filtered and the solvents removed under reduced pressure, yielding the title compound (180 mg, 270 μmol, 89%) as a white foam.

^{1}H NMR (300 MHz, $CDCl_3$) δ 7.78 (br d, 2H, *J* 8.1 Hz, $NH_{(amide,4,10)}$), 7.38–7.17 (m, 15H, Ph), 6.53 (br d, 1H, *J* 8.4 Hz, $NH_{(amide,7)}$), 5.20–5.00 (m, 3H, CH), 2.97 (s, 4H, $NCH_{2(4,10)}$), 2.79 (s, 2H, $NCH_{2(7)}$), 2.59 (br m, 4H, $NCH_{2(ring)}$), 2.46 (br m, 8H, $NCH_{2(ring)}$), 2.35 (br m, 4H, $NCH_{2(ring)}$), 2.00 (s, 3H, NCH_3), 1.49 (d, 6H, *J* 6.9 Hz, CH_3), 1.45 (d, 3H, *J* 6.9 Hz, CH_3).

^{13}C NMR (75.4 MHz, $CDCl_3$) δ 170.3 ($C{=}O_{(4,10)}$), 169.7 ($C{=}O_{(7)}$), 143.2 ($Ph_{(q)}$), 128.9 ($Ph_{(m,7)}$), 128.8 ($Ph_{(m,4,10)}$), 127.62 ($Ph_{(p,7)}$), 127.57 ($Ph_{(p,4,10)}$), 126.6 ($Ph_{(o,4,10)}$), 126.4 ($Ph_{(o,7)}$), 59.9 ($NCH_{2(4,10)}$), 58.4 ($NCH_{2(7)}$), 56.3, 54.3, 54.2, 53.0 ($NCH_{2(ring)}$), 48.4 ($CH_{(7)}$), 48.2 ($CH_{(4,10)}$), 44.2 (NCH_3), 21.5 ($CH_{3(7)}$), 21.3 ($CH_{3(4,10)}$).

ESMS+ (*m/z*) 355 ($[M+Ca]^{2+}$), 670 ($[M+H]^+$)

mpt 55–56 °C (lit.[3] 54–56°C).

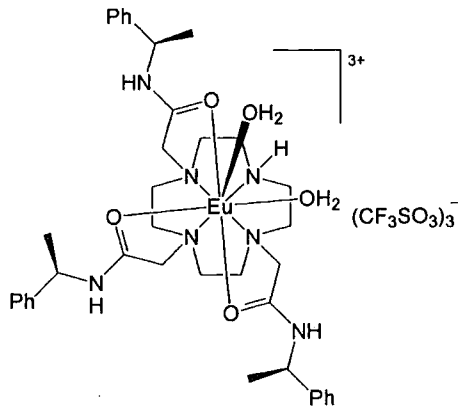

[Eu7(H$_2$O)$_2$](CF$_3$SO$_3$)$_3$.[3] Europium(III) triflate (189 mg, 300 μmol) and 1,4,7–(*RRR*)–tris[(1–phenylethylcarbamoyl)methyl]–1,4,7,10–tetraazacyclododecane (200 mg, 300 μmol) were dissolved in anhydrous MeCN (5 cm^3) and heated at 75°C for 48 hours. The reaction was cooled to room temperature and the solution was added dropwise to stirring, anhydrous diethyl ether (50 cm^3). The white precipitate was isolated by centrifugation, redissolved in the minimum volume of MeCN and precipitated via the same method. A total of three precipitations yielded the title compound (220 mg, 170 μmol, 57%) as a white powdery solid.

^{1}H NMR (200 MHz, D_2O, pD 7.8, partial data and assignment) δ 27.2 (NH), 18.1 (1H, H_{ax}), 15.4 (1H, H_{ax}), 11.5 (1H, H_{ax}), 9.9 (1H, H_{ax}), −3.5 (1H), −4.5 (1H), −4.8 (1H), −5.1 (1H), −7.4 (1H), −9.2 (1H), −9.9 (1H), −10.2 (1H), −11.3 (1H), −3.5 (1H), −14.0 (1H), −14.7 (1H), −15.7 (1H), −15.9 (1H), −19.0 (1H).

ESMS$^+$ (*m/z*) 404 ([M−H]$^{2+}$, 100%), 956 ([M−H+CF$_3$SO$_3$]$^+$, 20%).

mpt 178–179 °C (lit.[3] 178–179 °C).

[Tm7(H$_2$O)$_2$](CF$_3$SO$_3$)$_3$. The thulium complex was prepared via the same general procedure using thulium(III) triflate (160 mg, 260 μmol) and 1,4,7–(*RRR*)–tris[(1–phenylethylcarbamoyl)methyl]–1,4,7,10–tetraazacyclododecane (170 mg, 260 μmol) in anhydrous acetonitrile (5 cm^3), yielding the product (194 mg, 150 μmol, 59%) as a white powdery solid.

^{1}H NMR (500 MHz, D_2O, pD 7.8, partial data and assignment) δ 293 (br, 1H, H_{ax}), 230 (br, 1H, H_{ax}), 178 (br, 1H, H_{ax}), 137 (br, 1H, H_{ax}), 110 (1H, $H_{eq'}$), 72 (1H, $H_{eq'}$), 63 (1H, $H_{eq'}$), 35 (1H, $H_{eq'}$), −37, −43, −53 (br, 1H), −85, −88, −100 (br, 1H), −119 (br, 1H), −142 (br, 2H), −174 (br, 1H), −261 (br, 1H, ring NH).

ESMS$^+$ (*m/z*) 412 ([M−H]$^{2+}$, 100%).

mpt 160–161 °C.

[Yb7(H_2O)$_2$](CF_3SO_3)$_3$.[4] The ytterbium complex was prepared via the same general procedure using ytterbium(III) triflate (189 mg, 300 μmol) and 1,4,7–(*RRR*)–tris[(1–phenylethylcarbamoyl)methyl]–1,4,7,10–tetraazacyclododecane (200 mg, 300 μmol) in anhydrous acetonitrile (5 cm^3), yielding the product (220 mg, 170 μmol, 57%) as a white powdery solid.

^{1}H NMR (500 MHz, D_2O, pD 7.8, partial data and assignment) δ 112.7 (1H, H_{ax}), 77.4 (1H, H_{ax}), 63.2 (1H, H_{ax}), 49.9 (1H, H_{ax}), 43.7 (1H, $H_{eq'}$), 31.3 (1H, $H_{eq'}$), 27.5 (1H, $H_{eq'}$), 24.7 (1H, $H_{eq'}$), −9.8 (9H, CH_3), −16.4, −18.9, −27.5, −28.0, −34.3, −37.3, −38.7, −48.5, −49.4, −75.3 (10H, $H_{ax'}$, CH_2CO), −86.2 (1H, ring NH).

ESMS$^+$ (*m/z*) 413 ([M−H]$^{2+}$, 100%), 975 ([M−H+CF_3SO_3]$^+$, 30%).

mpt 159–160 °C (lit.[4] 160 °C).

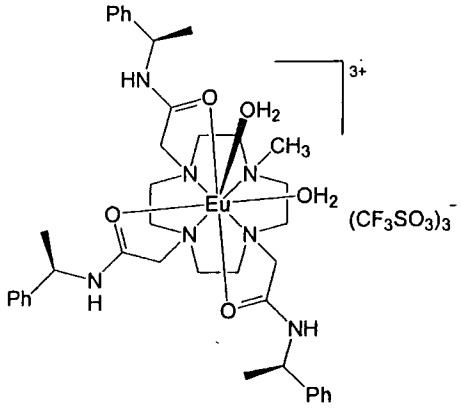

[Eu8(H_2O)$_2$](CF_3SO_3)$_3$.[3] Europium(III) triflate (27 mg, 45 μmol) and 1–methyl–4,7,10–(*RRR*)–tris[(1–phenylethylcarbamoyl)methyl]–1,4,7,10–tetraazacyclo–dodecane (30 mg, 45 μmol) were dissolved in anhydrous MeCN (3 cm^3) and heated at 75°C for 36 hours. The reaction was cooled to room temperature and the solution was added dropwise to stirring, anhydrous diethyl ether (40 cm^3). The white precipitate was isolated by centrifugation, redissolved in the minimum volume of MeCN and precipitated via the same method. A total of three precipitations yielded the title compound (32 mg, 25 μmol, 56%) as a white powdery solid.

^{1}H NMR (500 MHz, D_2O, pD 7.8, partial data and assignment) δ 24.0 (br,1H, H_{ax}), 18.4 (br, 2H, H_{ax}), 17.7 (br, 1H, H_{ax}), −5.7 (br, 4H), −7.5 to −10.2 (br m, 6H), −13.7

to −15.4 (br m, 4H), −19.6 (br, 2H).

ESMS$^+$ (*m/z*) 411 ([M−H]$^{2+}$, 100%), 970 ([M−H+CF_3SO_3]$^+$, 20%).

mpt 179–180°C.

^{1}H NMR (500 MHz, D_2O, pD 7.8, ternary adduct with AMP, partial data and assignment from COSY) δ 29.1 (1H, H^1_{ax}), 25.4 (1H, H^2_{ax}), 16.4 (1H, H^3_{ax}), 11.4 (1H, H^4_{ax}), 2.4 (1H, $H^1_{eq'}$), 0.3 (1H, $H^3_{ax'}$), −0.6 (1H, $H^2_{ax'}$), −1.4 (1H, $H^1_{ax'}$), −2.6 (1H, $H^2_{eq'}$), −5.6 (1H, H^3_{eq}), −6.3 (1H, CH^ACO), −7.1 (1H, $H^3_{eq'}$), −7.5 (3H, NCH_3), −8.6 (1H, H^2_{eq}), −10.5 (1H, CH^BCO), −11.2 (1H, $H^4_{eq'}$), −15.6 (1H, $CH^{B'}CO$), −16.2 (1H, $CH^{A'}CO$), −18.3 (1H, H^4_{eq}), −18.9 (1H, CH^CCO), −21.4 (2H, $H^4_{ax'}$ + $CH^{C'}CO$).

[Tb8(H_2O)$_2$](CF_3SO_3)$_3$. The terbium complex was prepared via the same general procedure using terbium(III) triflate (38 mg, 63 μmol) and 1–methyl–4,7,10–(*RRR*)–tris[(1–phenylethylcarbamoyl)methyl]–1,4,7,10–tetraazacyclododecane (42 mg, 63 μmol) in anhydrous acetonitrile (3 cm^3), yielding the product (50 mg, 39 μmol, 63%) as a white powdery solid.

^{1}H NMR (65.3 MHz, D_2O, pD 5.7, partial data and assignment) δ 358 (br, 1H), 345 (br, 1H), 169–150 (br m, 3H), 103 (br, 2H), 71–68 (br m, 2H), −85 (br, 3H), −120 (br, 2H), −163 (br, 1H), −272 to −278 (br m, 2H, H_{ax}), −294 (br, 1H, H_{ax}), −339 (br, 1H, H_{ax}).

ESMS$^+$ (*m/z*) 414 ([M−H]$^{2+}$, 100%), 976 ([M−H+CF_3SO_3]$^+$, 30%).

mpt 178–180 °C.

[Tm8(H_2O)$_2$](CF_3SO_3)$_3$. The thulium complex was prepared via the same general procedure using thulium(III) triflate (46 mg, 75 μmol) and 1–methyl–4,7,10–(*RRR*)–tris[(1–phenylethylcarbamoyl)methyl]–1,4,7,10–tetraazacyclododecane (50 mg, 75 μmol) in anhydrous acetonitrile (3 cm^3), yielding the product (60 mg, 47 μmol, 63%) as a white powdery solid.

^{1}H NMR (500 MHz, D_2O, pD 7.8, partial data and assignment) δ 325 (br, 1H, H_{ax}), 320 (br, 1H, H_{ax}), 311 (br, 1H, H_{ax}), 296 (br, 1H, H_{ax}), 76 (1H), 61 (1H), 52 (1H), 41 (1H), −51 (1H), −83 (br, 1H), −101 (br, 1H), −118 (1H), −122 (3H, NCH_3), −129 (1H), −139 (1H), −158 (br, 2H), −241 (br, 2H).

ESMS$^+$ (*m/z*) 419 ([M−H]$^{2+}$, 100%), 986 ([M−H+CF_3SO_3]$^+$, 80%).

HRMS (ES^+) 986.3137 ($TmC_{40}H_{54}N_7O_6SF_3$ requires 986.3145, $[M-H+CF_3SO_3]^+$).
mpt 174–175 °C.

$[Yb8(H_2O)_2](CF_3SO_3)_3$. The ytterbium complex was prepared via the same general procedure using 1–methyl–4,7,10–(*RRR*)–tris[(1–phenylethyl–carbamoyl)methyl]–1,4,7,10–tetraazacyclododecane (65 mg, 100 μmol) and ytterbium(III) triflate (60 mg, 100 μmol) in anhydrous acetonitrile (3 cm^3), yielding the product (71 mg, 55 μmol, 57%) as a white powdery solid.
^1H NMR (500 MHz, D_2O, pD 7.8, partial data and assignment) δ 110 (br, 1H, H_{ax}), 99 (br, 2H, H_{ax}), 96 (br, 1H, H_{ax}), 33 (br, 1H), 22 (br m, 2H), −32 (br m, 3H), −48 (3H), −57 (br, 2H), −61 (2H), −65 (br, 2H), −74 (br, 1H).
$ESMS^+$ (*m/z*) 420 ($[M-H]^{2+}$, 100%), 989 ($[M(CF_3SO_3)]^+$, 10%).
HRMS (ES^+) 991.3209 ($YbC_{40}H_{54}N_7O_6SF_3$ requires 991.3192, $[M-H+CF_3SO_3]^+$).
mpt 173–175 °C.

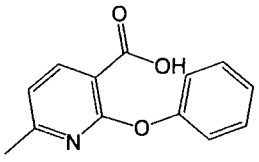

6–Methyl–2–phenoxynicotinic acid.[5] To a stirred solution of NaOMe (660 mg, 12.2 mmol) in anhydrous MeOH (5 cm^3) under an argon atmosphere was added phenol (2.64 g, 28.0 mmol) and 2–chloro–6–methylnicotinic acid (1.0 g, 5.8 mmol). The solvents were removed from the yellow solution via distillation and the residue heated for 1 hour at 180°C. The reaction mixture was cooled to 100°C and poured onto ice (40 g) to give a yellow suspension which was extracted with Et_2O (3 × 50 cm^3). The aqueous solution was acidified with acetic acid yielding a white precipitate upon cooling which was isolated via filtration, washed with water and dried thoroughly under vacuum to yield the title compound (700 mg, 3.1 mmol, 53%) as a white crystalline solid.
^1H NMR (500 MHz, $CDCl_3$) δ 11.2–10.2 (br, 1H, OH), 8.34 (d, 1H, *J* 7.7 Hz, H^4), 7.40 (t, 2H, $H^{3',5'}$), 7.23 (t, 1H, *J* 7.4 Hz, $H^{4'}$), 7.16 (d, 2H, *J* 8.3 Hz, $H^{2',6'}$), 6.99 (d, 1H, *J* 7.7 Hz, H^5), 2.40 (s, 3H, CH_3).
^{13}C NMR (125.7 MHz, $CDCl_3$) δ 167.5 (C=O), 163.1 (C^6), 161.0 (C^2), 153.1 ($C^{1'}$),

143.3 (C^4), 129.5 ($C^{3',5'}$), 125.2 ($C^{4'}$), 121.6 ($C^{2',6'}$), 118.9 (C^5) , 110.6 (C^3) , 24.5 (CH_3).

ESMS$^-$ (*m/z*) 184 ([M−COOH]$^-$, 100%), 228 ([M−H]$^-$, 20%).

HRMS (ES$^+$) 230.0805 ($C_{13}H_{12}NO_3$ requires 230.0812, [M+H]$^+$).

mpt 134–136 °C (lit.[6] 155–156 °C).

Found : C, 67.67; H, 4.79; N, 6.16% ($C_{13}H_{12}NO_3$ requires C, 68.11; H, 4.84; N, 6.11%).

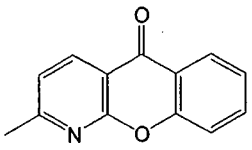

2–Methyl–1–azaxanthone (11).[5] 6–Methyl–2–phenoxynicotinic acid (400 mg, 1.7 mmol) was added to PPA (20 g) and the reaction mixture stirred at 120 °C for 18 hours under an argon atmosphere. The resulting viscous brown liquid was poured onto ice (50 g) and stirred until a homogeneous solution formed. The solution was then basified to pH 12 using aqueous KOH solution (50%) and the yellow precipitate that formed upon cooling was isolated via filtration. Subsequent recrystallisation from toluene/petroleum ether (40–60) yielded the title compound (250 mg, 1.2 mmol, 70%) as a white crystalline solid.

^{1}H NMR (500 MHz, $CDCl_3$) δ 8.60 (d, 1H, *J* 7.8 Hz, H^4), 8.32 (dd, 1H, *J* 8.0, 1.5 Hz, H^6), 7.78 (ddd, 1H, *J* 8.4, 7.2, 1.5 Hz, H^8), 7.61 (dd, 1H, *J* 8.4, 0.9 Hz, H^9), 7.43 (ddd, 1H, *J* 8.0, 7.2, 0.9 Hz, H^7), 7.31 (d, 1H, *J* 7.8 Hz, H^3), 2.72 (s, 3H, CH_3).

^{13}C NMR (125.7 MHz, $CDCl_3$) δ 177.5 (C^5), 165.2 (C^2), 160.0 ($C^{1'}$), 155.7 ($C^{9'}$), 137.4 (C^4), 135.5 (C^8), 126.7 (C^6), 124.7 (C^7), 121.8 ($C^{6'}$), 121.2 (C^3), 118.6 (C^9), 114.3 ($C^{4'}$), 25.2 (CH_3).

ESMS$^+$ (*m/z*) 212 ([M+H]$^+$, 10%), 234 ([M+Na]$^+$, 100%), 445 ([2M+Na]$^+$, 60%).

HRMS (ES$^+$) 212.0707 ($C_{13}H_{10}NO_2$ requires 212.0706, [M+H]$^+$).

R_f 0.30 (Silica, CH_2Cl_2).

mpt 130–131 °C (lit.[7] 136–138 °C).

Found : C, 73.84; H, 4.25; N, 6.55% ($C_{13}H_9NO_2$ requires C, 73.92; H, 4.29; N, 6.63%).

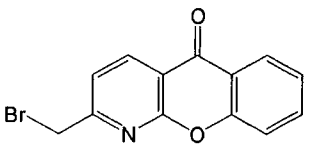

2–Bromomethyl–1–azaxanthone (12). 2–Methyl–1–azaxanthone (150 mg, 710 μmol) was dissolved in CCl_4 (5 cm^3) and the reaction heated to 80 °C under an argon atmosphere. NBS (63 mg, 355 μmol, 0.5 eq) was added along with benzoyl peroxide (2 mg) and the reaction boiled under reflux whilst monitoring the progress using TLC (SiO_2, toluene:CH_2Cl_2:MeOH, 48.5:48.5:3) and ^1H NMR. Two further additions of 0.5 eq NBS were made at 90 minute intervals. After a total reaction time of 4½ hours the suspension was cooled to room temperature and filtered. The solvents were removed under reduced pressure and the residue purified by column chromatography (Silica, toluene → toluene:CH_2Cl_2 80:20) yielding the title compound (71 mg, 245 μmol, 34%) as a white crystalline solid.

^1H NMR (500 MHz, $CDCl_3$) δ 8.73 (d, 1H, *J* 7.9 Hz, H^4), 8.32 (dd, 1H, *J* 8.0, 1.6 Hz, H^6), 7.80 (ddd, 1H, *J* 8.4, 7.2, 1.6 Hz, H^8), 7.63 (d, 1H, *J* 8.4 Hz, H^9), 7.58 (d, 1H, *J* 7.9 Hz, H^3), 7.46 (ddd, 1H, *J* 8.0, 7.2, 1.0 Hz, H^7), 4.62 (s, 2H, CH_2Br).

^{13}C NMR (125.7 MHz, $CDCl_3$) δ 177.2 (C^5), 162.1 (C^2), 159.8 ($C^{1'}$), 155.8 ($C^{9'}$), 138.8 (C^4), 135.9 (C^8), 126.8 (C^6), 125.0 (C^7), 121.7 ($C^{6'}$), 120.9 (C^3), 118.6 (C^9), 116.1 ($C^{4'}$), 32.3 (CH_2Br).

$ESMS^+$ (*m/z*) 290 ($[M+H]^+$, 5%), 312 ($[M+Na]^+$,100%), 601 ($[2M+Na]^+$, 10%).

HRMS (ES^+) 289.9809 ($C_{13}H_8NO_2Br$ requires 289.9811, $[M+H]^+$).

R_f 0.63 (Silica, toluene:CH_2Cl_2:MeOH 48.5:48.5:3).

mpt 169–171 °C.

Found : C, 53.85; H, 2.74; N, 4.85 ; ($C_{13}H_8NO_2Br$ requires C, 53.82; H, 2.78; N, 4.83%).

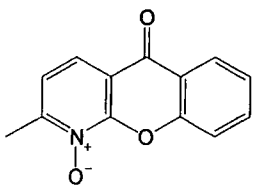

2–Methyl–1–azaxanthone–*N*–oxide (26). 2–Methyl–1–azaxanthone (45 mg, 213 μmol) was dissolved in TFA (400 μL) and H_2O_2 (100 μL, 37%) and the resulting solution boiled under reflux for 4 hours. A further two additions of TFA (400 μL)

and H_2O_2 (100 μL, 37%) were made at 4 hour intervals and then the reaction was evaporated to dryness under reduced pressure. The residue was taken up in aqueous $NaHCO_3$ (10 cm^3) and extracted with CH_2Cl_2 (2 × 10 cm^3). The combined organics were washed with aqueous NaCl (10 cm^3), dried (Na_2SO_4), filtered and evaporated under reduced pressure to give the crude compound as a yellow solid.

Subsequent purification via column chromatography (silica, CH_2Cl_2 → 2% EtOH) yielded the title compound (24 mg, 106 μmol, 50%) as a pale yellow solid.

^{1}H NMR (500 MHz, $CDCl_3$) δ 8.32 (d, 1H, *J* 7.9 Hz, H^6), 8.09 (d, 1H, *J* 8.2 Hz, H^4), 7.88–7.80 (m, 2H, $H^{8,9}$), 7.51 (t, 1H, H^7), 7.34 (d, 1H, *J* 8.2 Hz, H^3), 2.74 (s, 3H, CH_3).

^{13}C NMR (125.7 MHz, $CDCl_3$) δ 176.2 (C^5), 155.2 (C^2), 155.1 ($C^{1'}$), 154.9 ($C^{9'}$), 136.3 (C^8), 126.9 (C^6), 126.0 (C^7), 122.7 (C^4), 121.3 ($C^{6'}$), 120.7 (C^3), 119.1 (C^9), 117.5 ($C^{4'}$), 18.9 (CH_3).

ESMS$^+$ (*m/z*) 228 ($[M+H]^+$, 5%), 250 ($[M+Na]^+$, 100%), 477 ($[2M+Na]^+$, 20%).

HRMS (ES$^+$) 250.0472 ($C_{13}H_9NO_3Na$ requires 250.0475, $[M+Na]^+$).

R_f 0.33 (Silica, 3% EtOH:CH_2Cl_2).

mpt 190–192 °C (lit.[7] 205–205.5 °C).

Found : C, 66.20; H, 4.15; N, 5.83% ($C_{13}H_9NO_3 \cdot ½H_2O$ requires C, 66.10; H, 4.27; N, 5.93%).

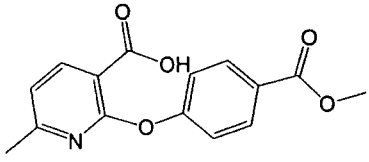

2–(4–Methoxycarbonylphenoxy)–6–methylnicotinic acid. To a stirred solution of NaOMe (660 mg, 12.2 mmol) in anhydrous MeOH (5 cm^3) under an argon atmosphere was added methyl 4–hydroxybenzoate (4.62 g, 28.0 mmol) and 2–chloro–6–methylnicotinic acid (1.0 g, 5.8 mmol). The solvents were removed from the solution via distillation and the residue heated for 24 hours at 180°C. The reaction mixture was cooled to 100°C and poured onto ice (60 g) affording a pale yellow suspension which was extracted with Et_2O (3 × 50 cm^3). The aqueous solution was acidified with acetic acid yielding a white precipitate upon cooling which was isolated via filtration, washed with water and dried thoroughly under vacuum.

Recrystallisation from ethyl acetate/hexane yielded the title compound (1.02 g, 3.6 mmol, 61%) as a white crystalline solid.

^{1}H NMR (500 MHz, $CDCl_3$) δ 8.32 (d, 1H, *J* 8.0 Hz, H^4), 8.07 (d, 2H, *J* 9.0 Hz, $H^{3',5'}$), 7.18 (d, 2H, *J* 9.0 Hz, $H^{2',6'}$), 7.02 (d, 1H, *J* 8.0 Hz, H^5), 3.91 (s, 3H, OCH_3), 2.41 (s, 3H, CH_3).

^{13}C NMR (125.7 MHz, $CDCl_3$) δ 168.2 (COOH), 166.7 ($COCH_3$), 163.2 (C^6), 160.6 (C^2), 157.6 ($C^{1'}$), 143.4 (C^4), 131.4 ($C^{3',5'}$), 126.6 ($C^{4'}$), 121.0 ($C^{2',3'}$), 119.3 (C^5), 111.3 (C^3), 52.3 (OCH_3), 24.4 (CH_3).

ESMS$^-$ (*m/z*) 242 ([M–COOH]$^-$, 75%), 286 ([M–H]$^-$, 100%).

HRMS (ES$^+$) 288.0869 ($C_{15}H_{14}NO_5$ requires 288.0866, $[M+H]^+$).

mpt 139–141 °C.

Found : C, 59.22; H, 4.52; N, 4.49% ($C_{15}H_{13}NO_5 \cdot H_2O$ requires C, 59.01; H, 4.95; N, 4.59%).

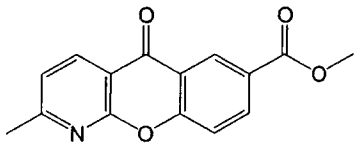

7–Methoxycarbonyl–2–methyl–1–azaxanthone. 2–(4–Methoxycarbonyl phenoxy)–6–methylnicotinic acid (900 mg, 3.1 mmol) was added to PPA (45 g) and the reaction mixture heated at 120 °C for 18 hours under an argon atmosphere with stirring. The resulting viscous brown liquid was poured into cold MeOH (200 cm^3) and stirred until a homogeneous solution formed. The solution was then neutralised to approximately pH 7 using aqueous KOH solution (50%) and the yellow precipitate that formed was extracted thoroughly with $CHCl_3$ (4 × 100 cm^3). The combined organic solvents were dried (K_2CO_3), filtered and evaporated under reduced pressure to give the title compound (430 mg, 1.6 mmol, 51%) as a white powdery solid.

^{1}H NMR (500 MHz, $CDCl_3$) δ 9.00 (d, 1H, *J* 2.1 Hz, H^6), 8.61 (d, 1H, *J* 8.0 Hz, H^4), 8.41 (dd, 1H, *J* 8.8, 2.1 Hz, H^8), 7.65 (d, 1H, *J* 8.8 Hz, H^9), 7.34 (d, 1H, *J* 8.0 Hz, H^3), 3.98 (s, 3H, OCH_3), 2.73 (s, 3H, CH_3).

^{13}C NMR (125.7 MHz, $CDCl_3$) δ 176.9 (C^5), 165.75 (C^2), 165.72 ($COCH_3$), 159.9 ($C^{1'}$), 158.3 ($C^{9'}$), 137.6 (C^4), 136.0 (C^8), 129.2 (C^6), 126.8 (C^7), 121.8 (C^3), 121.4 ($C^{6'}$), 119.0 (C^9), 114.4 ($C^{4'}$), 52.6 (OCH_3), 25.2 (CH_3).

ESMS$^+$ (*m/z*) 270 ([M+H]$^+$, 25%), 292 ([M+Na]$^+$, 95%), 562 ([2M+Na]$^+$, 100%).

HRMS (ES$^+$) 270.0760 ($C_{15}H_{12}NO_4$ requires 270.0761, [M+H]$^+$).

R_f 0.30 (Silica, toluene:CH_2Cl_2:MeOH 48.5:48.5:3).

mpt 194–196 °C.

Found : C, 66.48; H, 4.14; N, 5.13% ($C_{15}H_{11}NO_4$ requires C, 66.91; H, 4.12; N, 5.20%).

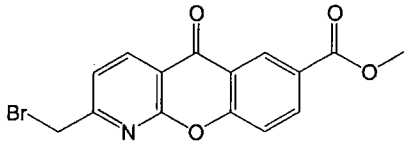

2–Bromomethyl–7–methoxycarbonyl–1–azaxanthone. 7–Methoxycarbonyl–2–methyl–1–azaxanthone (87 mg, 320 μmol) was suspended in CCl_4:MeCN (2:1, 5 cm^3) and the reaction heated to 80 °C under an argon atmosphere. NBS (28.8 mg, 160 μmol, 0.5 eq) was added along with AIBN (2 mg) and the reaction boiled under reflux whilst monitoring the progress using TLC (SiO_2, ethyl acetate:hexane, 50:50) and ^{1}H NMR. Four further additions of 0.5 eq NBS were made at 90 minute intervals. After a total reaction time of 7½ hours the suspension was cooled to room temperature and evaporated under reduced pressure. Purification via column chromatography (Silica, ethyl acetate:hexane, 20:80 → 30:70) yielding the title compound (71 mg, 245 μmol, 34%) as a white crystalline solid.

^{1}H NMR (500 MHz, $CDCl_3$) δ 9.00 (d, 1H, *J* 2.1 Hz, H^6), 8.74 (d, 1H, *J* 8.0 Hz, H^4), 8.44 (dd, 1H, *J* 8.7, 2.1 Hz, H^8), 7.67 (d, 1H, *J* 8.7 Hz, H^9), 7.62 (d, 1H, *J* 8.0 Hz, H^3), 4.62 (s, 2H, CH_2Br), 3.99 (s, 3H, OCH_3).

^{13}C NMR (75.4 MHz, $CDCl_3$) δ 176.7 (C^5), 165.8 (*C*OCH_3), 162.7 (C^2), 159.8 (C$^{1'}$), 158.4 (C$^{9'}$), 139.0 (C^4), 136.6 (C^8), 129.4 (C^6), 127.3 (C^7), 121.6 (C^3), 121.5 (C$^{6'}$), 119.2 (C^9), 116.2 (C$^{4'}$), 52.8 (OCH_3), 32.3 (CH_2Br).

ESMS$^+$ (*m/z*) 348 ([M+H]$^+$, 100%), 370 ([M+Na]$^+$, 30%).

R_f 0.65 (Silica, ethyl acetate:hexane 50:50).

Found : C, 51.64; H, 2.96; N, 3.96; ($C_{15}H_{10}NO_4Br$ requires C, 51.75; H, 2.90; N, 4.02%).

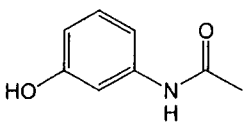

3–Acetylaminophenol (13). Acetic anhydride (16 cm^3, 170 mmol, 2.25 eq) was added dropwise to a stirred solution of 3–aminophenol (8.20 g, 75.1 mmol) in ethyl acetate (80 cm^3) maintained at 0°C over a period of 15 minutes. The resulting solution was stirred for a further 3 hours at room temperature. The solvents were removed under reduced pressure and the residue recrystallised from ethyl acetate/hexane to yield the title compound (10.26 g, 68.7 mmol, 90%).

^{1}H NMR (300 MHz, $(CD_3)_2CO$) δ 9.04 (br s, 1H, NH), 8.27 (s, 1H, OH), 7.35 (t, 1H, H^2), 7.07 (t, 1H, H^5), 6.98 (d, 1H, J 7.5 Hz, H^4), 6.51 (ddd, 1H, J 8.0, 2.4, 1.0 Hz, H^6), 2.82 (s, 3H, CH_3).

^{13}C NMR (75.4 MHz, $(CD_3)_2CO$) δ 169.5 (C=O), 158.7 (C^1), 141.3 (C^3), 130.2 (C^5), 111.2 (C^4), 111.0 (C^6), 107.4 (C^2), 24.3 (CH_3).

ESMS$^-$ (*m/z*) 150 ($[M-H]^-$, 100%).

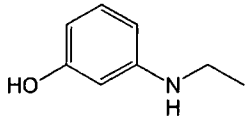

3–Ethylaminophenol (17). Borane–dimethylsulfide solution (8 cm^3, 80 mmol) was carefully added dropwise to a rapidly stirred solution of 3–acetylaminophenol (6.0 g, 40 mmol) in anhydrous THF (100 cm^3) under an argon atmosphere. After the addition was complete the reaction was stirred for 15 minutes at room temperature followed by boiling under reflux for 24 hours.

The reaction was cooled to room temperature and quenched by the careful addition of water (50 cm^3) followed by aqueous HCl (100 cm^3, 6 N) and then evaporated to dryness. The residue was taken up in MeOH and evaporated thoroughly under reduced pressure three times to remove $B(OMe)_3$ and yielding the title compound (6.9 g 40 mmol, 100%) as the hydrochloride salt, which was used without any further purification.

^{1}H NMR (300 MHz, $(CD_3)_2CO$) δ 6.96 (t, 1H, H^5), 6.35 (t, 1H, H^2), 6.31 (ddd, 1H, J 8.1, 2.1, 0.9 Hz, H^6), 6.26 (ddd, 1H, J 8.1, 2.4, 0.9 Hz, H^4), 3.14 (q, 2H, J 7.2 Hz, CH_2), 1.23 (t, 3H, J 7.2 Hz, CH_3).

^{13}C NMR (75.4 MHz, $(CD_3)_2CO$) δ 159.3 (C^1), 148.6 (C^3), 130.6 (C^5), 107.1, 107.0, 102.4 (C^2), 40.6 (CH_2), 14.1 (CH_3).

ESMS$^+$ (*m/z*) 138 ($[M+H]^+$, 100%).

HRMS (ES^+) 138.0912 ($C_8H_{12}NO$ requires 138.0913, $[M+H]^+$).

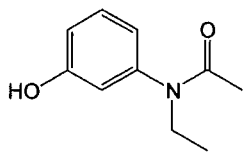

3–(*N*–Acetyl–*N*–ethylamino)phenol (18). Acetic anhydride (7.7 cm^3, 82 mmol, 2.25 eq) was added dropwise to a stirred solution of 3–ethylaminophenol hydrochloride (6.3 g, 36 mmol) and pyridine (6.6 cm^3, 82 mmol, 2.25 eq) in ethyl acetate (50 cm^3) maintained at 0°C under an argon atmosphere over a 15 minute period. After the addition the solution was allowed to warm to room temperature and stirred for a further 3 hours. The reaction mixture was washed with aqueous HCl (0.1 N, 2 × 50 cm^3) and the organic solvents removed under reduced pressure. The residue was dissolved in anhydrous MeOH (15 cm^3) and NaOMe solution (2 M, 2 cm^3) added and the solution stirred at room temperature for 1 hour under an argon atmosphere. A further addition of NaOMe solution (0.5 cm^3) and stirring for 30 minutes was required to force the reaction to completion. The solvents were removed under reduced pressure and the residue taken up in ethyl acetate (50 cm^3), washed with aqueous HCl (1 N, 20 cm^3), water (20 cm^3) and dried ($MgSO_4$). Removal of the solvents under reduced pressure yielded the title compound (5.6 g, 31 mmol, 86%).

^{1}H NMR (500 MHz, $(CD_3)_2CO$) δ 8.68 (s, 1H, OH), 7.27 (t, 1H, H^5), 6.85 (d, 1H, *J* 7.3 Hz, H^6), 6.74 (d, 1H, *J* 7.0 Hz, H^4), 6.74 (d, 1H, *J* 2.1 Hz, H^2), 3.66 (q, 2H, *J* 7.1 Hz, CH_2), 1.75 (s, 3H, CH_3CO), 1.04 (t, 3H, *J* 7.1 Hz, CH_3).

^{13}C NMR (125.7 MHz, $(CD_3)_2CO$) δ 169.9 (C=O), 159.4 (C^1), 145.0 (C^3), 131.1 (C^5), 119.9 (C^2), 116.0 (C^4), 115.7 (C^6), 44.1 (CH_2), 22.6 (CH_3CO), 13.4 (CH_3)..

ESMS$^-$ (*m/z*) 178 ($[M-H]^-$, 100%).

mpt 113–115 °C.

Found : C, 66.75; H, 7.29; N, 7.80% ($C_{10}H_{13}NO_2$ requires C, 67.02; H, 7.31; N, 7.82%).

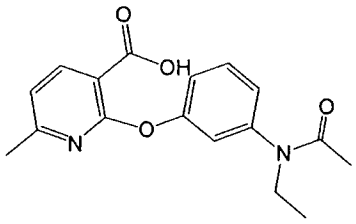

2–[(3–(*N*–Acetyl–*N*–ethylamino)phenoxy]–6–methylnicotinic acid (19). 2–Chloro–6–methyl–nicotinic acid (2.88 g, 16.7 mmol) was added to a stirred solution of 3–(*N*–acetyl–*N*–ethylamino)phenol (3.0 g, 16.7 mmol) in NaOMe solution (2 M, 16.8 cm^3) and stirred for 5 minutes at room temperature under an argon atmosphere. The solvents were removed under reduced pressure and the residue dissolved in DMF (15 cm^3). K_2CO_3 (1.16 g, 8.4 mmol) and CuI (0.1 g, 0.5 mmol) were added to the reaction and the resulting suspension heated at 140°C for 12 hours monitoring the reaction using tlc.

Upon completion the reaction was cooled to room temperature and the solvents removed under reduced pressure. The residue was taken up in water (150 cm^3) and filtered. The aqueous solution was acidified with aqueous HCl (1 N) and the resulting precipitate collected via filtration and dried thoroughly. Recrystallisation from MeOH yielded the title compound (3.5 g, 11.1 mmol, 64%).

^{1}H NMR (500 MHz, $CDCl_3$) δ 8.32 (d, 1H, *J* 7.8 Hz, H^4), 7.43 (t, 1H, $H^{5'}$), 7.16 (d, 1H, *J* 7.9 Hz, $H^{6'}$), 7.01 (d, 1H, *J* 8.1 Hz, $H^{4'}$), 7.00 (s, 1H, $H^{2'}$), 6.99 (d, 1H, *J* 7.8 Hz, H^5), 3.76 (q, 2H, *J* 7.1 Hz, CH_2), 2.37 (s, 3H, CH_3), 1.92 (s, 3H, $COCH_3$), 1.12 (t, 3H, *J* 7.1 Hz, CH_2CH_3).

^{13}C NMR (125.7 MHz, $CDCl_3$) δ 170.7 ($C{=}O_{(acid)}$), 167.4 ($C{=}O_{(amide)}$), 162.5 (C^6), 160.7 (C^2), 154.2 ($C^{1'}$), 143.3 (C^4), 130.5 ($C^{5'}$), 124.4 ($C^{4'}$), 122.3 ($C^{2'}$), 121.0 ($C^{6'}$), 118.9 (C^5), 111.4 (C^3), 44.0 (CH_2), 24.4 (CH_3), 22.8 ($COCH_3$), 13.1 (CH_2CH_3).

$ESMS^-$ (*m/z*) 313 ($[M–H]^-$, 100%).

HRMS (ES^+) 337.1151 ($C_{17}H_{18}N_2O_4Na$ requires 337.1159, $[M+Na]^+$).

mpt 179–180 °C (from MeOH).

Found : C, 64.82; H, 5.76; N, 8.78% ($C_{17}H_{18}N_2O_4$ requires C, 64.96; H, 5.77; N, 8.91%).

***N*–Substituted–1–azaxanthones.** 2–[(3–(*N*–Acetyl–*N*–ethylamino)phenoxy]–6–methylnicotinic acid (2.0 g, 6.4 mmol) was added to PPA (100 g) and heated at

120°C under an argon atmosphere with stirring for 16 hours. The resulting viscous solution was poured onto ice (300 g) and stirred until a homogeneous solution formed. The solution was then basified to pH 12 using aqueous KOH (50%) and the yellow precipitate that formed upon cooling was isolated via filtration. The resulting brown solid consisted of a mixture of three products which were purified via column chromatography (silica, $CHCl_3$ → 5% MeOH) and recrystallisation from the stated solvent.

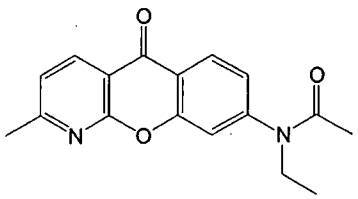

8–(*N*–Acetyl–*N*–ethylamino)–2–methyl–1–azaxanthone (20) (490 mg, 1.7 mmol, 26%) recrystallised from EtOH.

^{1}H NMR (500 MHz, $CDCl_3$) δ 8.60 (d, 1H, J 7.9 Hz, H^4), 8.36 (d, 1H, J 8.4 Hz, H^6), 7.41 (d, 1H, J 2.0 Hz, H^9), 7.34 (d, 1H, J 7.9 Hz, H^3), 6.25 (dd, 1H, J 8.4, 2.0 Hz, H^7), 3.85 (q, 2H, J 7.1 Hz, CH_2), 2.73 (s, 3H, CH_3), 1.98 (s, 3H, $COCH_3$), 1.17 (t, 3H, J 7.1 Hz, $CH_2C\mathbf{H}_3$).

^{13}C NMR (125.7 MHz, $CDCl_3$) δ 176.6 (C^5), 169.4 ($C{=}O_{(amide)}$), 165.5 (C^2), 160.0 ($C^{1'}$), 156.1 ($C^{9'}$), 149.2 (C^8), 137.4 (C^4), 128.3 (C^6), 124.5 (C^7), 121.7 (C^3), 120.8 ($C^{6'}$), 117.6 (C^9), 114.3 ($C^{4'}$), 44.4 (CH_2), 25.2 (CH_3), 23.0 ($COCH_3$), 13.4 ($CH_2\mathbf{C}H_3$).

ESMS$^+$ (*m/z*) 297 ([M+H]$^+$, 30%), 319 ([M+Na]$^+$, 100%), 615 ([2M+Na]$^+$, 70%).

HRMS (ES$^+$) 319.1052 ($C_{17}H_{16}N_2O_3Na$ requires 319.1053, [M+Na]$^+$).

mpt 180–182 °C (from EtOH).

Found : C, 68.35; H, 5.38; N, 9.41% ($C_{17}H_{16}N_2O_3$ requires C, 68.91; H, 5.44; N, 9.45%).

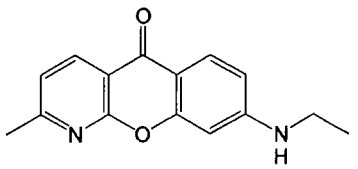

8–Ethylamino–2–methyl–1–azaxanthone (21) (410 mg, 1.6 mmol, 25%)

recrystallised from toluene.

^{1}H NMR (500 MHz, $CDCl_3$) δ 8.54 (d, 1H, *J* 7.9 Hz, H^4), 8.06 (d, 1H, *J* 8.8 Hz, H^6), 7.23 (d, 1H, *J* 7.9 Hz, H^3), 6.59 (dd, 1H, *J* 8.8, 2.1 Hz, H^7), 6.54 (d, 1H, *J* 2.1 Hz, H^9), 3.28 (q, 2H, *J* 7.2 Hz, CH_2), 2.67 (s, 3H, CH_3), 1.33 (t, 3H, *J* 7.2 Hz, $CH_2\mathbf{C}H_3$).

^{13}C NMR (125.7 MHz, $CDCl_3$) δ 176.0 (C^5), 163.5 (C^2), 160.1 ($C^{1'}$), 158.4 ($C^{9'}$), 154.4 (C^8), 137.1 (C^4), 128.1 (C^6), 120.7 (C^3), 114.7 ($C^{4'}$), 112.2 ($C^{6'}$), 112.0 (C^7), 96.9 (C^9), 38.1 (CH_2), 25.0 (CH_3), 14.5 ($CH_2\mathbf{C}H_3$).

ESMS$^+$ (*m/z*) 255 ($[M+H]^+$, 15%), 277 ($[M+Na]^+$, 40%), 532 ($[2M+Na]^+$, 100%).

HRMS (ES$^+$) 277.0946 ($C_{15}H_{14}N_2O_2Na$ requires 277.0945, $[M+Na]^+$).

mpt 177–178 °C (from toluene).

Found : C, 69.88; H, 5.80; N, 10.76% ($C_{15}H_{14}N_2O_2 \cdot \frac{1}{4}H_2O$ requires C, 69.62; H, 5.65; N, 10.82%).

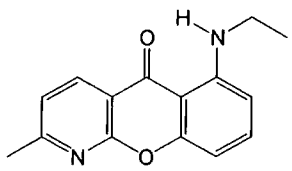

6–Ethylamino–2–methyl–1–azaxanthone (22) (130 mg, 0.5 mmol, 8%) recrystallised from MeOH.

^{1}H NMR (500 MHz, $CDCl_3$) δ 9.31 (br s, 1H, NH), 8.46 (d, 1H, *J* 7.9 Hz, H^4), 7.47 (t, 1H, H^8), 7.22 (d, 1H, *J* 7.9 Hz, H^3), 6.68 (d, 1H, *J* 8.8 Hz, H^7), 6.47 (d, 1H, *J* 8.5 Hz, H^9), 3.31 (q, 2H, *J* 7.2 Hz, CH_2), 2.67 (s, 3H, CH_3), 1.38 (t, 3H, *J* 7.2 Hz, $CH_2\mathbf{C}H_3$).

^{13}C NMR (125.7 MHz, $CDCl_3$) δ 180.1 (C^5), 164.2 (C^2), 159.5 ($C^{1'}$), 157.5 ($C^{9'}$), 151.9 (C^6), 136.61 (C^4), 136.57 (C^8), 120.7 (C^3), 114.6 ($C^{4'}$), 106.4 ($C^{6'}$), 104.5 (C^7), 102.7 (C^9), 37.8 (CH_2), 25.0 (CH_3), 14.4 ($CH_2\mathbf{C}H_3$).

ESMS$^+$ (*m/z*) 255 ($[M+H]^+$, 50%), 277 ($[M+Na]^+$, 100%), 531 ($[2M+Na]^+$, 70%).

HRMS (ES$^+$) 277.0946 ($C_{15}H_{14}N_2O_2Na$ requires 277.0945, $[M+Na]^+$).

mpt 142–144 °C (from MeOH).

Found : C, 66.11; H, 5.77; N, 9.96 % ($C_{15}H_{14}N_2O_2 \cdot H_2O$ requires C, 66.16; H, 5.92; N, 10.29%).

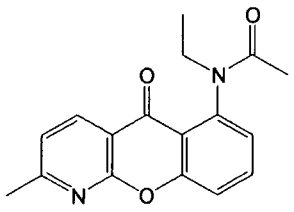

6–(*N*–Acetyl–*N*–ethylamino)–2–methyl–1–azaxanthone (23). Acetyl chloride (13.5 μL, 190 μmol) was added dropwise to a stirred solution of 6–ethylamino–2–methyl–1–azaxanthone (48 mg, 190 μmol) in ethyl acetate (10 cm^3) under an argon atmosphere. Following the addition, the reaction was stirred at room temperature for a further 4 hours during which time a yellow precipitate formed. The solvents were removed under reduced pressure to give a pale yellow solid. The solid residue was suspended in $CHCl_3$ (15 cm^3) and quickly washed with saturated $NaHCO_3$ solution (5 cm^3). The organic solvents were dried (K_2CO_3), filtered and evaporated under reduced pressure to give the title compound (55 mg, 185 μmol, 98%) as a pale yellow solid.

^1H NMR (400 MHz, $CDCl_3$) Major diastereoisomer (~80%) δ 8.53 (d, 1H, J 7.9 Hz, H^4), 7.80 (t, 1H, H^8), 7.67 (d, 1H, J 8.5 Hz, H^9), 7.31 (d, 1H, J 7.9 Hz, H^3), 7.20 (d, 1H, J 7.6 Hz, H^7), 4.31 (dq, 1H, J 13.9, 7.3 Hz, CH_2), 3.22 (dq, 1H, J 13.9, 7.3 Hz, CH_2), 2.71 (s, 3H, CH_3), 1.76 (s, 3H, $COCH_3$), 1.10 (t, 3H, J 7.3 Hz, $CH_2\mathbf{C}H_3$)

^{13}C NMR (100.6 MHz, $CDCl_3$) Major diastereoisomer only δ 176.2 (C^5), 169.5 ($C{=}O_{(amide)}$), 165.4 (C^2), 159.0 ($C^{1'}$), 157.3 ($C^{9'}$), 142.3 (C^6), 137.6 (C^4), 135.0 (C^8), 127.0 (C^7), 121.6 (C^3), 119.4 (C^9), 118.2 ($C^{6'}$), 114.8 ($C^{4'}$), 43.8 (CH_2), 25.1 (CH_3), 22.7 ($COCH_3$), 12.9 ($CH_2\mathbf{C}H_3$).

$ESMS^+$ (*m/z*) 297 ($[M+H]^+$, 30%), 319 ($[M+Na]^+$, 100%), 615 ($[2M+Na]^+$, 70%).

HRMS (ES^+) 319.1052 ($C_{17}H_{16}N_2O_3Na$ requires 319.1053, $[M+Na]^+$).

mpt 171–173 °C (from EtOH).

Found : C, 68.65; H, 5.47; N, 9.44% ($C_{17}H_{16}N_2O_3$ requires C, 68.91; H, 5.44; N, 9.45%).

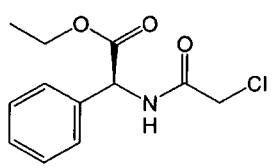

(*S*)–(2–Chloroacetylamino)phenylacetic acid ethyl ester (39). A solution of

chloroacetyl chloride (0.88 cm^3, 11.2 mmol) in THF (20 cm^3) was added dropwise to a stirred solution of (*S*)–2–phenylglycine ethyl ester hydrochloride (2.0 g, 9.3 mmol) and triethylamine (2.85 cm^3, 20.5 mmol) in THF (50 cm^3) maintained at –25 °C under an argon atmosphere. The reaction was allowed to return to room temperature and stirred for 90 minutes. The resulting blue suspension was filtered and washed with THF (2 × 25 cm^3) to give a dark blue solution, which was decolourised with activated carbon to give a yellow/green solution. Upon reduction of the solvent volume, pale yellow crystals were produced. Subsequent recrystallisation from Et_2O/petroleum ether yielded the title compound (1.52 g, 6.0 mmol, 64%) as white needles.

^1H NMR (300 MHz, $CDCl_3$) δ 7.58 (br, 1H, NH), 7.40–7.30 (m, 5H, Ph), 5.55 (d, 1H, *J* 7.5 Hz, CH), 4.26 (dq, 1H, *J* 10.8, 7.2 Hz, OCH_2), 4.17 (dq, 1H, *J* 10.8, 7.2 Hz, OCH_2), 4.10 (d, 1H, *J* 16.5 Hz, CH_2Cl), 4.04 (d, 1H, *J* 16.5 Hz, CH_2Cl), 1.23 (t, 3H, *J* 7.2 Hz, CH_3).

^{13}C NMR (75.4 MHz, $CDCl_3$) δ 170.3 ($C{=}O_{(ester)}$), 165.5 ($C{=}O_{(amide)}$), 136.1 ($Ph_{(q)}$), 129.2 ($Ph_{(m)}$), 128.9 ($Ph_{(p)}$), 127.3 ($Ph_{(o)}$), 62.3 (OCH_2) 56.8 (CH), 42.5 (CH_2Cl), 14.1 (CH_3).

$ESMS^+$ (*m/z*) 278 ($[M+Na]^+$, 100%), 533 ($[2M+Na]^+$, 10%).

mpt 90–92 °C.

Found : C, 56.43; H, 5.58; N, 5.37% ($C_{12}H_{14}NO_3Cl$ requires C, 56.38; H, 5.52; N, 5.48%).

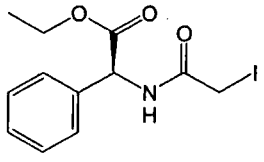

(*S*)–(2–Iodoacetylamino)phenylacetic acid ethyl ester. Sodium iodide (220 mg, 1.5 mmol) was added to a stirred solution of (*S*)–(2–chloroacetylamino)phenyl acetic acid (375mg, 1.5 mmol) in MeCN (4 cm^3) and the resulting suspension boiled under reflux for 3 hours. The reaction mixture was filtered and the solvent removed under reduced pressure to give a pale orange solid. The solid was taken up in CH_2Cl_2 (10 cm^3) and washed with sodium thiosulfate solution (10 cm^3). The organics were separated and evaporated under reduced pressure yielding a pale yellow solid.

Subsequent recrystallisation from diethyl ether afforded the title compound (250 mg, 0.7 mmol, 49%) as pale yellow needles.

^{1}H NMR (300 MHz, $CDCl_3$) δ 7.40–7.30 (m, 5H, Ph), 6.99 (br, 1H, NHCO), 5.51 (d, 1H, *J* 7.2 Hz, CH), 4.25 (dq, 1H, *J* 10.8, 7.2 Hz, OCH_2), 4.16 (dq, 1H, *J* 10.8, 7.2 Hz, OCH_2), 3.76 (d, 1H, *J* 11.7 Hz, CH_2I), 3.71 (d, 1H, *J* 11.7 Hz, CH_2I), 1.23 (t, 3H, *J* 7.2 Hz, CH_3).

^{13}C NMR (75.4 MHz, $CDCl_3$) δ 170.6 ($C{=}O_{(ester)}$), 166.5 ($C{=}O_{(amide)}$), 136.1 ($Ph_{(q)}$), 129.1 ($Ph_{(m)}$), 128.8 ($Ph_{(p)}$), 127.3 ($Ph_{(o)}$), 62.3 (OCH_2) 57.2 (CH), 14.1 (CH_3), –1.2 (CH_2I).

ESMS$^+$ (*m/z*) 278 ($[M+Na]^+$, 100%), 533 ($[2M+Na]^+$, 10%).

mpt 79–80 °C.

Found : C, 41.66; H, 4.08; N, 3.93% ($C_{12}H_{14}NO_3I$ requires C, 41.52; H, 4.06; N, 4.03%).

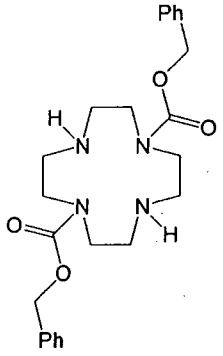

1,7–Bis(benzyloxycarbonyl)–1,4,7,10–tetraazacyclododecane (35).[8] A solution of benzyl chloroformate (2.70 cm^3, 18.9 mmol) in dioxane (8 cm^3) was added dropwise to a stirred solution of 1,4,7,10–tetraazacyclododecane (1.25 g, 7.26 mmol) in H_2O (10 cm^3) and dioxane (9 cm^3) at pH 2.5 (acidified with 6N HCl) over a 3 hour period. During the addition the pH was maintained between 2.2 and 2.8 via the addition of aqueous NaOH solution (2 M). After the addition was complete, adjustments to the pH were continued until no further decreases in pH were observed. The solvents were removed under reduced pressure to give a yellow solid which was extracted with Et_2O (4 × 30 cm^3).

The remaining solid residue was taken up in aqueous NaOH solution (20%, 20 cm^3) and extracted thoroughly with Et_2O (4 × 30 cm^3). The combined extracts were washed with NaOH solution (5%, 2 × 20 cm^3), dried (Na_2SO_4) and the solvents

removed under reduced pressure yielding the title compound (2.62 g, 5.95 mmol, 82%) as a colourless viscous oil.

^{1}H NMR (500 MHz, $CDCl_3$) δ 7.40–7.30 (m, 10H, Ph), 5.14 (s, 4H, OCH_2), 3.41 (br m, 8H, NCH_2), 2.95–2.70 (br m, 10H, NCH_2+2×NH).

^{13}C NMR (125.7 MHz, $CDCl_3$) δ 156.9, 156.8 (C=O), 136.8, 136.7 ($Ph_{(q)}$), 128.6, 128.5, 128.1, 128.0, 127.9, 127.8 (Ph), 67.2, 67.1 (OCH_2), 51.2–48.3 (8 resonances, NCH_2).

ESMS$^+$ (*m/z*) 442 ([M+H]$^+$, 100%), 881 ([2M+H]$^+$, 5%).

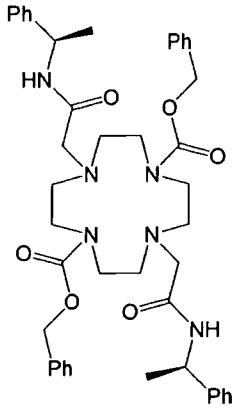

1,7–Bis(benzyloxycarbonyl)–4,10–(*RR*)–bis[(1–phenylethylcarbamoyl)methyl]–1,4,7,10–tetraazacyclododecane (36). Caesium carbonate (2.47 g, 7.6 mmol) and 2–chloro–*N*–[(*R*)–1–phenylethyl]ethanamide (1.50 g, 7.6 mmol) were added to a solution of 1,7–bis(benzloxycarbonyl)–1,4,7,10–tetraazacyclododecane (1.52 g, 3.5 mmol) in MeCN (5 cm^3) under an argon atmosphere. The resulting suspension was boiled under reflux for 48 hours and the solvents removed under reduced pressure. The residue was taken up in CH_2Cl_2, filtered and the solvents removed under reduced pressure yielding the crude compound. Subsequent purification via column chromatography (silica, gradient CH_2Cl_2 → 3% MeOH) yielded the title compound (1.75 g, 2.3 mmol, 66%) as a white solid.

^{1}H NMR (300 MHz, $CDCl_3$) δ 7.50–7.20 (m, 22H, Ph + NH), 5.11 (m, 2H, CH), 3.41 (br s, 8H, $NCH_{2(ring)}$), 3.14 (s, 4H, NCH_2), 2.73br s, 8H, $NCH_{2(ring)}$), 1.43 (d, 6H, *J* 5.7 Hz, CH_3).

^{13}C NMR (75.4 MHz, $CDCl_3$) δ 170.0 ($C{=}O_{(amide)}$), 156.8 ($C{=}O_{(carbamate)}$), 143.7, 136.3, 128.6, 128.3, 128.2, 127.2, 126.3 (Ph), 67.3 (OCH_2), 59.0 (NCH_2), 56.1, 55.2, 54.7, 48.8, 47.6, 46.8 ($NCH_{2(ring)}$), 48.5 (CH), 21.8 (CH_3).

$ESMS^+$ (*m/z*) 763 ($[M+H]^+$, 25%), 785 ($[M+Na]^+$, 100%).

HRMS (ES^+) 763.4177 ($C_{44}H_{55}N_6O_6$ requires 763.4178, $[M+H]^+$).

R_f 0.30 (silica, 4% MeOH:CH_2Cl_2).

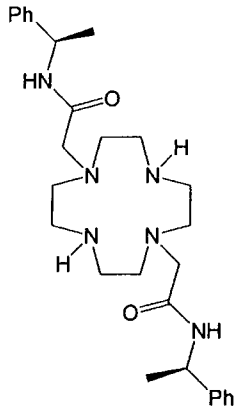

1,7–(*RR*)–Bis[(1–phenylethylcarbamoyl)methyl]–1,4,7,10–tetraazacyclododecane (37). 1,7–Bis(benzyloxycarbonyl)–4,10–(*RR*)–bis[(1–phenyl)ethylcarbamoyl methyl]–1,4,7,10–tetraazacyclododecane (1.85 g, 2.42 mmol) was dissolved in EtOH (20 cm^3) and $Pd(OH)_2$ on carbon (100 mg) was added. The reaction mixture was hydrogenated using a Parr hydrogenator (25°C, 25psi) for 3 days. The reaction mixture was filtered through a bed of celite to remove the catalyst and the solvents evaporated under reduced pressure. Subsequent purification via column chromatography (silica, CH_2Cl_2 → 3% $^iPr_2NH$) yielded the title compound (1.19 g, 2.40 mmol, 99%) as a white foam.

^1H NMR (500 MHz, $CDCl_3$) δ 7.94 (d, 2H, *J* 8.5 Hz, $NH_{(amide)}$), 7.34 (d, 4H, *J* 7.5 Hz, $Ph_{(o)}$), 7.28(t, 4H, *J* 7.5 Hz, $Ph_{(m)}$), 7.20 (t, 2H, *J* 7.5 Hz, $Ph_{(p)}$), 5.04 (m, 2H, CH), 3.27 (s, 4H, NCH_2), 2.73 (s, 8H, $CH_{2(ring)}$), 2.64 (s, 8H, $CH_{2(ring)}$), 1.44 (d, 6H, *J* 7.0 Hz, CH_3).

^{13}C NMR (75.4 MHz, $CDCl_3$) δ 170.4 (C=O), 143.8 ($Ph_{(q)}$), 128.5 ($Ph_{(m)}$), 127.1 ($Ph_{(p)}$), 126.5 ($Ph_{(o)}$), 60.1 (NCH_2), 52.7 ($NCH_{2(ring)}$), 48.7 (CH), 46.8 ($NCH_{2(ring)}$), 21.7 (CH_3).

$ESMS^+$ (*m/z*) 495 ($[M+H]^+$, 100%).

HRMS (ES^+) 495.3448 ($C_{28}H_{42}N_6O_2$ requires 495.3447, $[M+H]^+$).

R_f 0.39 (silica, 8% $^iPr_2NH$:CH_2Cl_2).

mpt 53–55 °C.

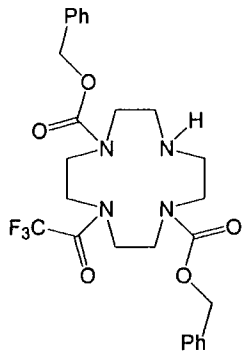

4–trifluoromethylcarbonyl–1,7–(*RR*)–bis[(1–phenylethylcarbamoyl)methyl]–1,4,7,10–tetraazacyclododecane (40). A solution of ethyl trifluoroacetate (126 μL, 1.1 mmol) in MeOH (5 cm^3) was added dropwise to a solution of 1,7–(*RR*)–bis[(1–phenyl) ethylcarbamoylmethyl]–1,4,7,10–tetraazacyclododecane (310 mg, 700 μmol) and triethylamine (147 μL, 1.1 mmol) in MeOH (15 cm^3) at room temperature under an argon atmosphere. After the addition was complete the reaction was stirred at room temperature for a further 16 hours. The solvents were removed under reduced pressure and the residue purified by column chromatography (silica, ethyl acetate) yielding the title compound (330 mg, 620 μmol, 88%) as a pale yellow oil.

^{1}H NMR (500 MHz, $CDCl_3$) δ 7.42–7.30 (m, 10H, Ph), 5.20–5.10 (m, 4H, CH_2Ph), 4.10–2.60 (br m, 17H, $CH_{2(ring)}$ + NH).

^{13}C NMR (125.7 MHz, $CDCl_3$) δ 157.6–156.5 (multiple resonances, $C{=}O_{(amide)}$ + $C{=}O_{(carbamate)}$), 136.5–135.8 (multiple resonances, $Ph_{(q)}$), 128.8–127.6 (multiple resonances, $Ph_{(m)}$ + $Ph_{(p)}$ + $Ph_{(o)}$), 116.2 (multiple q, J_{C-F} 288 Hz, CF_3), 67.6–66.9 (multiple resonances, CH_2Ph), 52.0–43.9 (multiple resonances, $NCH_{2(ring)}$).

ESMS$^+$ (*m/z*) 537 ($[M+H]^+$, 20%), 559 ($[M+Na]^+$, 100%).

R_f 0.69 (silica, ethyl acetate).

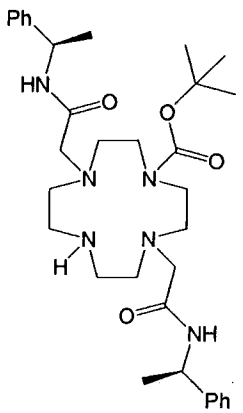

4–*tert*–Butoxycarbonyl–1,7–(*RR*)–bis[(1–phenylethylcarbamoyl)methyl]–1,4,7,10–tetraazacyclododecane (41). A solution of diBOC (75 mg, 340 μmol) in MeOH (2 cm^3) was added dropwise to a solution of 1,7–(*RR*)–bis[(1–phenyl) ethylcarbamoylmethyl]–1,4,7,10–tetraazacyclododecane (150 mg, 300 μmol) in MeOH (8 cm^3) at room temperature under an argon atmosphere. After the addition was complete the reaction was stirred at room temperature for a further 8 hours. The solvents were removed under reduced pressure and the residue purified by column chromatography (silica, CH_2Cl_2 → 2% $^iPrNH_2$) yielding the title compound (130 mg, 220 μmol, 72%) as a white foam.

^1H NMR (300 MHz, $CDCl_3$) δ 7.75 (br, 2H, $NH_{(amide)}$), 7.35–7.15 (m, 10H, Ph), 5.13 (m, 2H, CH), 3.21 (br s, 4H, $CH_{2(ring)}$), 3.10 (s, 4H, NCH_2), 2.90–2.60 (br m, 8H, $CH_{2(ring)}$), 2.54 (br s, 4H, $CH_{2(ring)}$), 1.49 (d, 6H, *J* 7.0 Hz, CH_3), 1.40 (s, 9H, $C(CH_3)_3$).

^{13}C NMR (75.4 MHz, $CDCl_3$) δ 170.4 ($C{=}O_{(amide)}$), 156.4 ($C{=}O_{(carbamate)}$), 143.5 ($Ph_{(q)}$), 128.6 ($Ph_{(m)}$), 127.2 ($Ph_{(p)}$), 126.5 ($Ph_{(o)}$), 80.2, 80.0 ($\mathbf{C}(CH_3)_3$), 59.5 (NCH_2), 54.5 ($NCH_{2(ring)}$), 48.9 ($NCH_{2(ring)}$), 48.5 ($NCH_{2(ring)}$), 48.3 (CH), 28.5 ($C(\mathbf{C}H_3)_3$), 21.7 (CH_3).

$ESMS^+$ (*m/z*) 595 ($[M+H]^+$, 100%), 617 ($[M+Na]^+$, 50%).

HRMS (ES^+) 595.3962 ($C_{33}H_{51}N_6O_4$ requires 595.3966, $[M+H]^+$).

R_f 0.35 (alumina, 2% EtOH:CH_2Cl_2).

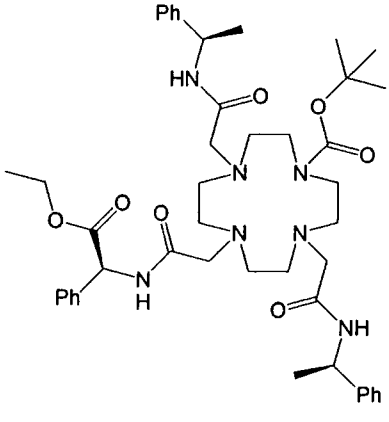

1–*tert*–Butoxycarbonyl–7–(*S*)–[{(ethoxycarbonylphenylmethyl)carbamoyl} methyl]–4,10–(*RR*)–[(1–phenylethylcarbamoyl)methyl]–1,4,7,10–tetraazacyclo dodecane (42). A solution of 1,7–(*RR*)–[(1–phenylethylcarbamoyl)methyl]–1,4,7,10–tetraazacyclododecane (150 mg, 300 μmol) and (*S*)–(2–iodoacetylamino)

phenylacetic acid ethyl ester (105 mg, 300 μmol) in anhydrous MeCN (4 cm^3) was heated at 75°C for 6 hours under an argon atmosphere. After this time $NaHCO_3$ (34 mg, 400 μmol) was added and the resulting suspension heated at 75 °C for a further 12 hours and the solvents removed under reduced pressure. The residue was dissolved in CH_2Cl_2, filtered and the solvents removed under reduced pressure. Removal of starting material was achieved by passing the crude material through a plug of alumina (eluant CH_2Cl_2 → 0.5% EtOH).

DiBOC (65 mg, 300 μmol) was added to a solution of the crude product in MeOH (5 cm^3) and stirred at room temperature under an argon atmosphere for 8 hours. The solvents were removed under reduced pressure and the residue purified via column chromatography (alumina, CH_2Cl_2 → 0.2% EtOH) yielding the title compound (60 mg, 74 μmol, 25%) as a white foam.

^1H NMR (500 MHz, $CDCl_3$) δ 7.59 (d, 1H, *J* 7.5 Hz, $NH_{(7)}$), 7.48 (br d, J 7.0 Hz, 1H, NH), 7.38–7.20 (m, 15H, Ph), 7.15 (br, 1H, *J* 7.0 Hz, NH), 5.54 (d, 1H, *J* 7.5 Hz, $CH_{(7)}$), 5.14 (br m, 2H, $CH_{(4,10)}$), 4.25–4.10 (m, 2H, OCH_2), 3.40–3.00 (br m, 6H, NCH_2), 3.00–2.20 (br m, 16H, $NCH_{2(ring)}$), 1.49 (d, 6H, *J* 7.0 Hz, CH_3), 1.43 (s, 9H, $C(CH_3)_3$), 1.22 (t, 3H, *J* 7.0 Hz, $CH_2\mathbf{C}H_3$).

^{13}C NMR (125.7 MHz, $CDCl_3$) δ 171.4 ($C{=}O_{(ester)}$), 170.5 ($C{=}O_{(amide,7)}$), 170.2, 169.8 ($C{=}O_{(amides,4,10)}$), 155.8 ($C{=}O_{(carbamate)}$), 143.7, 143.3 ($Ph_{(q,4,10)}$), 136.2 ($Ph_{(q,7)}$), 129.2 ($Ph_{(m,7)}$), 128.9 ($Ph_{(p,7)}$), 128.8, 128.6 ($Ph_{(m,4,10)}$), 127.4 ($Ph_{(o,7)}$), 127.5, 127.2 ($Ph_{(p,4,10)}$), 126.4, 126.3 ($Ph_{(o,4,10)}$), 79.8 ($\mathbf{C}(CH_3)_3$), 62.1 (OCH_2), 59.5, 57.5 ($NCH_{2(4,10)}$), 57.9 ($NCH_{2(7)}$), 56.2 ($CH_{(7)}$), 54.1, 53.7, 52.7, 52.3, 48.1 ($NCH_{2(ring)}$), 48.4, 47.9 ($CH_{(4,10)}$), 28.5 ($C(\mathbf{C}H_3)_3$), 21.6, 21.3 (CH_3), 14.0 ($CH_2\mathbf{C}H_3$).

$ESMS^+$ (*m/z*) 815 ($[M+H]^+$, 100%), 837 ($[M+Na]^+$, 60%).

HRMS (ES^+) 836.4682 ($C_{45}H_{63}N_7O_7Na$ requires 836.4681,$[M+Na]^+$).

Rf 0.52 (alumina, 2% EtOH:CH_2Cl_2).

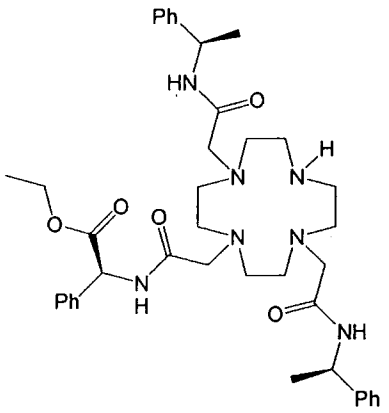

4–(*S*)–[{(Ethoxycarbonylphenylmethyl)carbamoyl}methyl]–1,7–(*RR*)–[(1–phenylethylcarbamoyl)methyl]–1,4,7,10–tetraazacyclododecane (43). 1–*tert*–Butoxy carbonyl–7–(*S*)–[{(ethoxycarbonylphenylmethyl)carbamoyl}methyl]–4,10–(*RR*)–[(1–phenylethylcarbamoyl)methyl]–1,4,7,10–tetraazacyclododecane (60 mg, 74 μmol) was dissolved in TFA:CH_2Cl_2 (1 cm^3, 9:1) and stirred under an argon atmosphere for 5 hours. The solvents were removed under reduced pressure and the residue taken up in CH_2Cl_2, washed with aqueous $NaHCO_3$ solution (10 cm^3), dried (K_2CO_3) and filtered. Removal of the solvents under reduced pressure yielded the title compound (50 mg, 70 μmol, 95%) as a white foam.

^{1}H NMR (500 MHz, $CDCl_3$) δ 7.65 (br s, 1H, $NH_{(4)}$), 7.55 (br, 1H, NH), 7.40–7.20 (m, 15H, Ph), 7.20 (br, 1H, NH), 5.52 (d, 1H, *J* 7.6 Hz, $CH_{(4)}$), 5.10 (m, 2H, $CH_{(1,7)}$), 4.19 (dq, 1H, *J* 10.7, 7.1 Hz, OCH_2), 4.13 (dq, 1H, *J* 10.7, 7.1 Hz, OCH_2), 3.40–3.00 (br m, 6H, $NCH_{2(1,4,7)}$), 2.70–2.40 (br m, 17H, $NCH_{2(ring)}$, $NH_{(ring)}$), 1.48 (d, 6H, *J* 7.1 Hz, CH_3), 1.21 (t, 3H, *J* 7.1 Hz, CH_2CH_3).

^{13}C NMR (125.7 MHz, $CDCl_3$) δ 170.9 ($C{=}O_{(ester)}$), 170.8, 170.3 ($C{=}O_{(amide,1,4,7)}$), 143.5 ($Ph_{(q,1,7)}$), 136.3 ($Ph_{(q,4)}$), 129.1 ($Ph_{(m,4)}$), 128.8 ($Ph_{(p,4)}$), 128.7, 128.6 ($Ph_{(m,1,7)}$), 127.4 ($Ph_{(o,4)}$), 127.5, 127.3 ($Ph_{(p,1,7)}$), 126.5, 126.4 ($Ph_{(o,1,7)}$), 62.0 (OCH_2), 59.8 ($NCH_{2(1,4,7)}$), 56.4 ($CH_{(4)}$), 54.4, 53.4, ($NCH_{2(ring)}$), 48.5 (CH), 47.2 (CH), 21.6 (CH_3), 14.1 (CH_2CH_3).

ESMS$^+$ (*m/z*) 715 ($[M+H]^+$, 100%), 737 ($[M+Na]^+$,10%).

HRMS (ES^+) 722.4003 ($C_{39}H_{53}N_7O_5Na$ (methyl ester) requires 722.4000,$[M+Na]^+$).

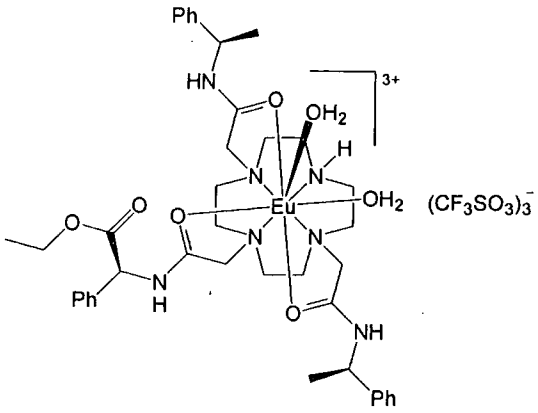

[Eu43(H_2O)$_2$](CF_3SO_3)$_3$. Europium(III) triflate (42 mg, 70 μmol) and 4–(*S*)–[{(Ethoxycarbonyl–phenylmethyl)carbamoyl}methyl]–1,7–(*RR*)–[(1–phenylethyl carbamoyl)methyl]–1,4,7,10–tetraazacyclododecane (50 mg, 70 μmol) were dissolved in anhydrous MeCN (4 cm^3) and heated at 75°C for 48 hours. The reaction was cooled to room temperature and the solution was added dropwise to stirring, anhydrous diethyl ether (50 cm^3). The white precipitate was isolated by centrifugation, redissolved in the minimum volume of MeCN and precipitated via the same method. A total of three precipitations yielded the title compound (76 mg, 57 μmol, 81%) as a white powdery solid.

^{1}H NMR (500 MHz, D_2O, pD 7.8, partial data and assignment) δ 25.0 (1H, NH), 15.8 (1H, H^1_{ax}), 13.3 (1H, H^2_{ax}), 12.7 (br, 1H), 10.2 (1H, H^3_{ax}), 7.4 (1H, H^4_{ax}), −2.6 (1H, $H^3_{ax'}$), −4.4 (1H, CH^ACO), −5.0 (1H, $CH^{A'}CO$), −6.5 (2H, $H^1_{ax'}$ + $H^4_{eq'}$), −6.9 (1H, H^1_{eq}), −8.2 (1H, $H^1_{eq'}$), −9.9 (1H, CH^BCO), −10.5 (1H, CH^CCO), −11.4 (1H, $H^2_{eq'}$), −12.1 (1H, H^3_{eq}), −14.6 (1H, $H^3_{eq'}$), −15.9 (1H, $H^2_{ax'}$), −17.1 (1H, $CH^{C'}CO$), −17.5 (1H, $CH^{B'}CO$), −20.2 (1H, H^2_{eq}).

ESMS$^+$ (*m/z*) 433 ([M−H]$^{2+}$, 100%), 1014 ([M−H+CF_3SO_3]$^+$, 15%).

mpt 198–200 °C.

Found : C, 37.62; H, 4.25; N, 7.07% ($EuC_{43}H_{59}N_7O_{16}S_3F_9 \cdot H_2O$ requires C, 37.78; H, 4.50; N, 7.17%).

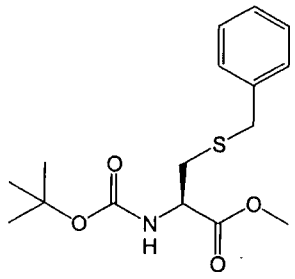

***N*–*tert*–Butoxycarbonyl–*S*–benzyl–L–cysteine methyl ester.** Benzyl bromide (253 μL, 2.1 mmol) and K_2CO_3 (294 mg, 2.1 mmol) were added to a solution of *N*–*tert*–butoxycarbonyl–L–cysteine methyl ester (500 mg, 2.1 mmol) in MeCN (5 cm^3) under an argon atmosphere and stirred at room temperature for 18 hours.

The solvents were removed under reduced pressure and the solid residue taken up in ethyl acetate and filtered. The filtrate was washed with saturated $NaHCO_3$ solution (2 × 30 cm^3), saturated NaCl solution (30 cm^3), dried ($MgSO_4$) and filtered. The solvents were removed under reduced pressure yielding the crude product as a colourless oil. Purification was achieved by passing the crude compound through a silica plug (eluant ethyl acetate:hexane 20:80) to give the title compound (652 mg, 2.0 mmol, 94%) as a white crystalline solid.

^1H NMR (500 MHz, $CDCl_3$) δ 7.33–7.22 (m, 5H, Ph), 5.28 (d, 1H, *J* 7.3 Hz, NH), 4.53 (m, 1H, CH), 3.74 (s, 3H, OCH_3), 3.72 (s, 2H, CH_2Ph), 2.88 (dd, 1H, *J* 13.9, 4.6 Hz, SCH_2), 2.81 (dd, 1H, *J* 13.7, 5.6 Hz, SCH_2), 1.45 (s, 9H, ^tBu).

^{13}C NMR (75.4 MHz, $CDCl_3$) δ 171.7 ($C{=}O_{(ester)}$), 155.2 ($C{=}O_{(carbamate)}$), 137.8 ($Ph_{(q)}$), 129.0, 128.7 ($Ph_{(o,m)}$), 127.3 ($Ph_{(p)}$), 80.2 ($C(CH_3)$), 53.2 (CH), 52.6 (OCH_3), 36.7 (CH_2Ph), 33.7 (SCH_2), 28.4 (CH_3).

$ESMS^+$ (*m/z*) 348 ($[M+Na]^+$, 100%), 673 ($[2M+Na]^+$, 90%).

R_f 0.44 (silica, ethyl acetate:hexane 20:80).

mpt 47–49 °C.

Found : C, 58.98; H, 7.15; N, 4.37 ($C_{16}H_{23}NO_4S$ requires C, 59.05; H, 7.12; N, 4.30%).

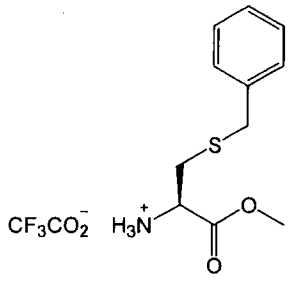

S–Benzyl–L–cysteine methyl ester trifluoroacetate salt. *N–tert*–Butoxycarbonyl–*S*–benzyl–L–cysteine methyl ester (600 mg, 1.8 mmol) was dissolved in TFA/CH_2Cl_2 (2 cm^3, 95:5) and stirred under an argon atmosphere at room temperature for 3 hours. The solvents were removed under reduced to give the title compound (38 mg, 65 μmol, 100%) as a very hygroscopic crystalline solid.

^1H NMR (300 MHz, $CDCl_3$) δ 7.8–6.8 (br, 3H, NH_3), 7.4–7.2 (m, 5H, Ph), 4.08 (dd, 1H, *J* 7.2, 4.9 Hz, CH), 3.78 (s, 3H, OCH_3), 3.74 (s, 2H, CH_2Ph), 3.06 (dd, 1H, *J* 15.0, 4.9 Hz, SCH_2), 2.98 (dd, 1H, *J* 15.0, 7.2 Hz, SCH_2).

^{13}C NMR (75.4 MHz, $CDCl_3$) δ 168.6 (C=O), 136.9 ($Ph_{(q)}$), 129.1, 128.9 ($Ph_{(o,m)}$), 127.8 ($Ph_{(p)}$), 53.7 (CH), 52.3 (OCH_3), 36.3 (CH_2Ph), 31.2 (SCH_2).

$ESMS^+$ (*m/z*) 209 ($[M–NH_3]^+$, 80%), 226 (M^+, 100%).

HRMS (ES^+) 226.0896 ($C_{11}H_{16}NO_2S$ requires 226.0896).

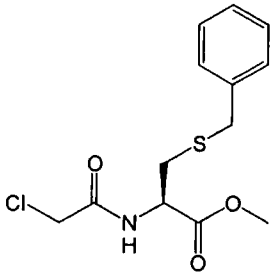

***N*–2–Chloroacetyl–*S*–benzyl–L–cysteine methyl ester.** A solution of chloroacetyl chloride (79 μL, 990 μmol) in anhydrous THF (10 cm^3) was added dropwise over 15 minutes to a solution of *S*–benzyl–L–cysteine methyl ester trifluoroacetate salt (280 mg, 830 μmol) in anhydrous THF (20 cm^3) and NEt_3 (253 μL, 1.82 mmol, 2.2 eq) maintained at –25°C under an argon atmosphere. The reaction mixture was slowly raised to room temperature and stirred for 1 hour.

The reaction mixture was filtered and the blue filtrate decolourised with activated carbon, filtered and evaporated under reduced pressure. The solid residue taken up in

CH_2Cl_2 (30 cm^3), washed with aqueous HCl (1N, 2 × 25 cm^3) and saturated NaCl (20 cm^3). The organic solvents were dried ($MgSO_4$), filtered and evaporated under reduced pressure yielding a pale yellow oil. Purification was achieved by passing the crude compound through a silica plug (eluant ethyl acetate:hexane 30:70) to give the title compound (187 mg, 620 μmol, 75%) as a white solid.

^1H NMR (500 MHz, $CDCl_3$) δ 7.35–7.24 (m, 6H, Ph+NH), 4.79 (dt, 1H, *J* 7.8 Hz, CH), 4.07 (d, 1H, *J* 15.4 Hz, CH_2Cl), 4.04 (d, 1H, *J* 15.4 Hz, CH_2Cl), 3.77 (s, 3H, OCH_3), 3.72 (s, 2H, CH_2Ph), 2.94 (dd, 1H, *J* 14.2, 5.1 Hz, SCH_2), 2.89 (dd, 1H, *J* 14.2, 5.6 Hz, SCH_2).

^{13}C NMR (75.4 MHz, $CDCl_3$) δ 171.7 ($C{=}O_{(ester)}$), 165.9 ($C{=}O_{(amide)}$), 137.5 ($Ph_{(q)}$), 129.0, 128.8 ($Ph_{(o,m)}$), 127.5 ($Ph_{(p)}$), 52.9 (OCH_3), 52.0 (CH), 42.5 (CH_2Cl), 36.7 (CH_2Ph), 33.1 (SCH_2), 28.4 (CH_3).

$ESMS^+$ (*m/z*) 302 ($[M+H]^+$, 10%), 324 ($[M+Na]^+$, 100%), 625 ($[2M+Na]^+$, 40%).

HRMS (ES^+) 324.0432 ($C_{13}H_{16}NO_3SClNa$ requires 324.0432).

R_f 0.19 (silica, ethyl acetate:hexane 20:80).

mpt 57–58 °C.

Found : C, 51.84; H, 5.35; N, 4.52% ($C_{13}H_{16}NO_3SCl$ requires C, 51.74; H, 5.34; N, 4.64%).

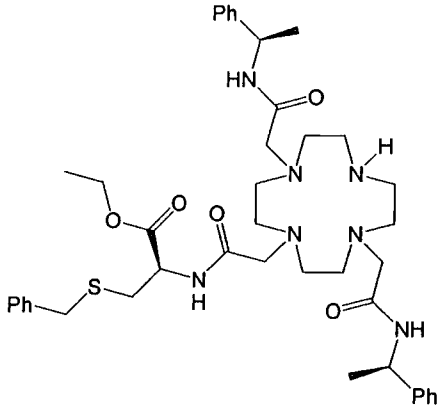

4–(*S*)–[{(2–Benzylsulfanyl–1–ethoxycarbonylethyl)carbamoyl}methyl]–1,7–(*RR*)–[(1–phenyl–ethylcarbamoyl)methyl]–1,4,7,10–tetraazacyclododecane. To a solution of 1,7–(*RR*)–[(1–phenylethylcarbamoyl)methyl]–1,4,7,10–tetraazacyclo dodecane (250 mg, 500 μmol) in anhydrous EtOH (15 cm^3) and triethylamine (60 μL, 410 μmol) was added *N*–2–Chloroacetyl–*S*–benzyl–L–cysteine methyl ester (125 mg, 410 μmol) and the reaction heated at 60°C for 40 hours. The solvents were

removed under reduced pressure and the residue taken up in CH_2Cl_2 and filtered. The organics were washed with water (10 cm^3), aqueous $NaHCO_3$ solution (10 cm^3), aqueous NaCl solution (10cm^3), dried (K_2CO_3) and filtered. Evaporation of the solvents followed by purification via column chromatography (silica, 0.5% $^iPrNH_2$:CH_2Cl_2 → 1% $^iPrNH_2$: 2% EtOH:CH_2Cl_2) yielded the title compound (150 mg, 200 μmol, 50%) as a white foam.

^1H NMR (500 MHz, $CDCl_3$) δ 7.53 (br, 2H, $NH_{(1,7)}$), 7.35–7.24 (m, 16H, Ph+$NH_{(4)}$), 5.12 (m, 2H, $CH_{(1,7)}$), 4.62 (br m, 1H, CH), 4.15 (q, 2H, *J* 7.0 Hz, OCH_2), 3.68 (s, 2H, CH_2Ph), 3.30–3.10 (br m, 4H, $NCH_{2(1,7)}$), 3.10–2.90 (br m, 2H, $NCH_{2(4)}$), 2.88 (dd, 1H, *J* 14.0, 4.5 Hz, SCH_2), 3.85–2.60 (br, 19H, $NCH_{2(ring)}$+$NH_{(ring)}$+SCH_2), 1.49 (d, 6H, *J* 7.0 Hz, CH_3), 1.25 (t, 3H, *J* 7.0 Hz, CH_2CH_3).

^{13}C NMR (75.4 MHz, $CDCl_3$) δ 171.3 ($C{=}O_{(ester)}$), 170.8 ($C{=}O_{(4)}$), 170.3 ($C{=}O_{(1,7)}$), 143.6 ($Ph_{(q,1,7)}$), 137.6 ($Ph_{(q,4)}$), 129.0, 128.7 ($Ph_{(o,m,4)}$), 128.6 ($Ph_{(m,1,7)}$), 127.4 ($Ph_{(p,4)}$), 127.3 ($Ph_{(p,1,7)}$), 126.5 ($Ph_{(o,1,7)}$), 61.9 (OCH_2), 59.9 ($NCH_{2(1,4,7)}$), 56.4, 54.5, 53.4, 52.9 ($NCH_{2(ring)}$), 51.5 ($CH_{(4)}$), 48.7 ($NCH_{2(ring)}$), 46.8 ($CH_{(1,7)}$), 36.7 (CH_2Ph), 33.1 (SCH_2), 21.8 (CH_3), 14.2 (CH_2CH_3).

$ESMS^+$ (*m/z*) 407 ($[M+Ca]^{2+}$, 40%), 775 ($[M+H]^+$, 100%), 797 ($[M+Na]^+$, 20%).

HRMS (ES^+) 774.4374 ($C_{42}H_{60}N_7O_5S$ requires 774.4371).

R_f 0.60 (silica, CH_2Cl_2:EtOH:$^iPrNH_2$ 94:3:3).

mpt 62–65°C.

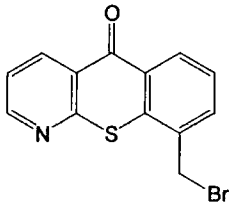

9–Bromomethyl–1–aza–10–thioxanthone (45).

Method A. To a solution of 9–methyl–1–aza–10–thioxanthone (250 mg, 1.1 mmol) in CCl_4 (12 cm^3) maintained at 80°C under argon was added NBS (100 mg, 550 μmol) followed by benzoyl peroxide (3 mg). The reaction mixture was boiled under reflux for 2 hours. A second addition of NBS (100 mg, 550 μmol) followed by benzoyl peroxide (3 mg) was made and the reaction boiled under reflux for a further 2 hours. At this point ^1H NMR analysis indicates ~70% mono–bromination.

The reaction mixture was cooled to room temperature and filtered. The filtrate was washed with saturated $NaHCO_3$ (10 cm^3), saturated NaCl (10 cm^3), dried (Na_2SO_4), filtered and the solvents evaporated under reduced pressure. Purification was achieved via column chromatography (silica, EtOAc:Hexane 10:90 → 30:70; compound loaded in CH_2Cl_2/toluene) yielding the title compound (170 mg, 560 μmol, 51%) as a pale yellow solid.

^1H NMR (500 MHz, $CDCl_3$) δ 8.85–8.80 (m, 2H, $H^{2,4}$), 8.61 (dd, 1h, *J* 8.0, 1.4 Hz, H^6), 7.77 (dd, 1H, *J* 7.4, 1.4 Hz, H^8), 7.52 (t, 1H, H^7), 7.49 (dd, 1H, *J* 8.0, 4.7 Hz, H^3), 4.78 (s, 2H, CH_2Br).

^{13}C NMR (125.7 MHz, $CDCl_3$) δ 180.8 (C^5), 157.8 ($C^{1'}$), 153.8 (C^2), 137.9 (C^4), 137.2 ($C^{9'}$), 135.0 (C^8), 134.3 (C^9), 130.7 (C^6), 130.0 ($C^{6'}$), 126.6 (C^7), 126.0 ($C^{4'}$), 122.2 (C^3), 29.5 (CH_2Br).

EI^+ (*m/z*) 305 ($[M+H]^+$, 100%).

R_f 0.21 (silica, ethyl acetate:hexane 20:80).

mpt 181–184 °C.

Found : C, 51.00; H, 2.76; N, 4.44% ($C_{13}H_8NOSBr$ requires C, 51.00; H, 2.63; N, 4.57%).

Method B. To a solution of 9–methyl–1–aza–10–thioxanthone (250 mg, 1.1 mmol) in CCl_4 (12 cm^3) maintained at 80°C under argon was added NBS (196 mg, 1.1 mmol) followed by AIBN (3 mg). The reaction mixture was boiled under reflux for 2 hours. A second addition of NBS (196 mg, 1.1 mmol) followed by AIBN (3 mg) was made and the reaction boiled under reflux for 2 hours. A further addition was made in the same manner to give a total addition of 3 equivalents of NBS.

The reaction mixture was cooled to room temperature and filtered. The filtrate was washed with saturated $NaHCO_3$ (10 cm^3), saturated NaCl (10 cm^3), dried (Na_2SO_4), filtered and the solvents evaporated under reduced pressure to give crude 9–dibromomethyl–1–aza–10–thioxanthone (410 mg, 1.06 mmol, 97%) as a pale yellow solid which was used without further purification.

^1H NMR (300 MHz, $CDCl_3$) δ 8.84 (dd, 1H, *J* 4.6, 1.8 Hz, H^2), 8.81 (dd, 1H, *J* 8.1, 1.8 Hz, H^4), 8.63 (dd, 1H, *J* 8.1, 1.3 Hz, H^6), 8.36 (br d, 1H, *J* 7.4 Hz, H^8), 7.63 (t, 1H, H^7), 7.50 (dd, 1H, *J* 8.1, 4.6 Hz, H^3).

^{13}C NMR (75.4 MHz, $CDCl_3$) δ 180.3 (C^5), 157.0 ($C^{1'}$), 153.8 (C^2), 137.8 (C^4), 137.7

(C^9), 134.7 (C^8), 133.4 ($C^{9'}$), 131.7 (C^6), 129.2 ($C^{6'}$), 127.0 (C^7), 126.0 ($C^{4'}$), 122.6 (C^3), 35.1 (CH_2Br).

EI^+ (*m/z*) 386 ($[M+H]^+$, 100%).

Found : C, 39.84; H, 1.98; N, 3.91% ($C_{13}H_7NOSBr_2$ requires C, 40.55; H, 1.83; N, 3.64%).

Diethyl phosphite (550 μL, 4.0 mmol) and $^iPr_2NEt$ (700 μL, 4.0 mmol) was added to a solution of 9–dibromomethyl–1–aza–10–thioxanthone (385 mg, 1.0 mmol) in THF (10 cm^3) maintained at 0°C under argon was added. After 5 minutes stirring at 0°C the reaction was slowly allowed to reach room temperature and stirred for a further 24 hours.

The resulting brown suspension was added to ice (40 g) and extracted with CH_2Cl_2 (3 × 40 cm^3). The combined organic extracts were washed with water (50 cm^3), saturated NaCl solution (50 cm^3), dried (Na_2SO_4), filtered and evaporated under reduced pressure yielding a pale yellow solid. Purification was achieved via column chromatography (silica, EtOAc:Hexane 10:90 → 30:70; compound loaded in CH_2Cl_2/toluene) yielding the title compound (195 mg, 640 μmol, 64%) as a pale yellow solid.

This compound had identical spectroscopic properties to that obtained via method A.

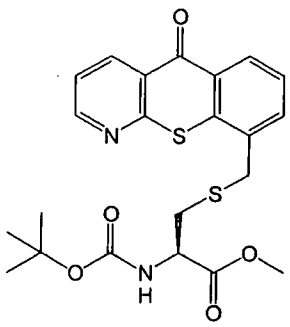

***N*–*tert*–Butoxycarbonyl–*S*–(1–aza–10–thioxanthon–9–ylmethyl)–L–cysteine methyl ester (46).** 9–Bromomethyl–1–aza–10–thioxanthone (80 mg, 260 μmol) and K_2CO_3 (48 mg, 350 μmol) were added to a solution of *N*–*tert*–butoxycarbonyl–L–cysteine methyl ester (61 mg, 260 μmol) in MeCN (5 cm^3) under an argon atmosphere and stirred at room temperature for 18 hours.

The solvents were removed under reduced pressure and the solid residue taken up in CH_2Cl_2 and filtered. The filtrate was washed with saturated $NaHCO_3$ solution (2 × 20

cm^3), saturated NaCl solution (20 cm^3), dried ($MgSO_4$) and filtered. The solvents were removed under reduced pressure yielding the crude product as a white solid. Purification via recrystallisation from acetone yielded the title compound (100 mg, 220 μmol, 83%) as a white crystalline solid.

^{1}H NMR (500 MHz, $CDCl_3$) δ 8.85–8.75 (m, 2H, $H^{2,4}$), 8.56 (d, 1H, *J* 8.1 Hz, H^6), 7.66 (d, 1H, *J* 7.0 Hz, H^8), 7.47 (t, 1H, H^7), 7.46 (dd, 1H, *J* 8.0, 4.7 Hz, H^3), 5.36 (br d, 1H, *J* 7.8 Hz, NH), 4.61 (br m, 1H, CH), 4.05 (s, 2H, CH_2Ar), 3.77 (s, 3H, OCH_3), 3.02 (dd, 1H, *J* 14.0, 5.0 Hz, SCH_2), 2.93 (dd, 1H, *J* 14.0, 5.5 Hz, SCH_2), 1.45 (s, 9H, $C(CH_3)_3$).

^{13}C NMR (75.4 MHz, $CDCl_3$) δ 181.0 (C^5), 171.5 ($C{=}O_{(ester)}$), 158.1 ($C^{1'}$), 155.3 ($C{=}O_{(carbamate)}$), 153.6 (C^2), 137.7 (C^4), 136.8 ($C^{9'}$), 134.4 (C^8), 134.2 (C^9), 130.0 ($C^{6'}$), 129.4 (C^6), 126.2 (C^7), 126.0 ($C^{4'}$), 122.0 (C^3), 80.4 ($\mathbf{C}(CH_3)_3$), 53.4 (CH), 52.9 (OCH_3), 34.7 (SCH_2), 34.4 (CH_2Ar), 28.4 ($C(\mathbf{C}H_3)_3$).

ESMS$^+$ (*m/z*) 483 ($[M+Na]^+$, 100%).

HRMS (ES^+) 483.1019 ($C_{22}H_{24}N_2O_5S_2Na$ requires 483.1019, $[M+Na]^+$).

mpt 174–175 °C.

Found : C, 56.29; H, 5.23; N, 5.74% ($C_{22}H_{24}N_2O_5S_2{\cdot}½H_2O$ requires C, 56.27; H, 5.37; N, 5.97%).

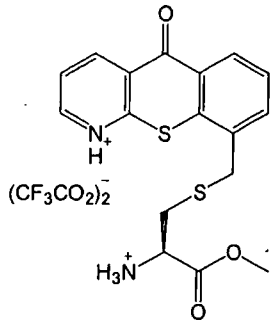

***S*–(1–Aza–10–thioxanthon–9–ylmethyl)–L–cysteine methyl ester trifluoroacetate salt (47).** *N–tert*–Butoxycarbonyl–*S*–(1–aza–10–thioxanthon–9–ylmethyl)–L–cysteine methyl ester (200 mg, 430 μmol) was dissolved in TFA/CH_2Cl_2 (2 cm^3, 95:5) to give a yellow solution which was stirred under an argon atmosphere at room temperature for 3 hours.

The solvents were removed under reduced to give the title compound (256 mg, 430 μmol, 100%) as a very hygroscopic solid, which was used without further

purification.

^{1}H NMR (500 MHz, $CDCl_3$) δ 8.80 (br s, 1H, H^2), 8.77 (d, 1H, J 8.0 Hz, H^4), 8.51 (d, 1H, J 8.0 Hz, H^6), 7.66 (d, 1H, J 7.5Hz, H^8), 7.50 –7.44 (m, 2H, $H^{3,7}$), 4.36 (br s, 1H, CH), 4.09 (s, 2H, CH_2Ar), 3.82 (s, 3H, OCH_3), 3.30–3.20 (m, 2H, SCH_2).

^{13}C NMR (175.4 MHz, $CDCl_3$) δ 180.5 (C^5), 168.6 ($C{=}O_{(ester)}$), 157.1 ($C^{1'}$), 153.0 (C^2), 138.5 ($C^{9'}$), 136.0 ($C^{6'}$), 134.7 (C^4), 133.3 (C^8), 129.7 (C^6), 126.6 (C^7), 126.1 ($C^{4'}$), 122.4 (C^3), 53.9 (CH), 52.7 (OCH_3), 34.0 (CH_2Ar), 32.2 (SCH_2).

ESMS$^+$ (*m/z*) 361 ($[M+H]^+$, 40%), 383 ($[M+Na]^+$, 100%).

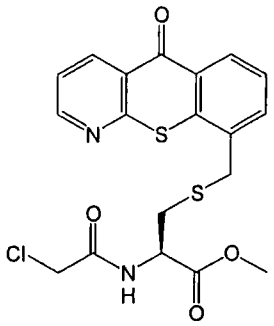

***N*–2–Chloroacetyl–*S*–(1–aza–10–thioxanthon–9–ylmethyl)–L–cysteine methyl ester (48).** A solution of chloroacetyl chloride (34 μL, 430 μmol) in anhydrous THF (15 cm^3) was added dropwise over 10 minutes to a solution of *S*–(1–aza–10–thioxanthon–9–ylmethyl)–L–cysteine methyl ester trifluoroacetate salt (250 mg, 430 μmol) in anhydrous THF (15 cm^3) and NEt_3 (180 μL, 1.3 mmol, 3.0 eq) maintained at –30°C under an argon atmosphere. The reaction mixture was stirred at –30°C for a further 20 minutes and then slowly raised to room temperature and stirred for 1 hour. The solvents were evaporated under reduced pressure and the solid residue taken up in CH_2Cl_2, washed with water (15 cm^3) saturated $NaHCO_3$ (15 cm^3) and saturated NaCl (15 cm^3). The organic solvents were dried (Na_2SO_4), filtered and evaporated under reduced pressure yielding a white solid. Recrystallisation from acetone yielded the title compound (120 mg, 280 μmol, 65%) as a white crystalline solid.

^{1}H NMR (400 MHz, $CDCl_3$) δ 8.85–8.75 (m, 2H, $H^{2,4}$), 8.57 (dd, 1H, J 8.1, 1.5 Hz, H^6), 7.66 (dd, 1H, J 7.3, 1.5 Hz, H^8), 7.50 (t, 1H, H^7), 7.47 (dd, 1H, J 7.8, 4.8 Hz, H^3), 7.33 (br d, 1H, J 7.8 Hz, NH), 4.88 (dt, 1H J 7.8 Hz, CH), 4.09 (s, 2H, CH_2Cl), 4.05 (s, 2H, CH_2Ar), 3.80 (s, 3H, OCH_3), 3.08 (dd, 1H, J 14.1, 5.1 Hz, CH_2S), 3.03 (dd, 1H, J 14.1, 5.6 Hz, CH_2S).

^{13}C NMR (75.4 MHz, $CDCl_3$) δ 180.8 (C^5), 170.5 ($C{=}O_{(ester)}$), 166.1 ($C{=}O_{(amide)}$), 157.9 ($C^{1'}$), 153.6 (C^2), 137.7 (C^4), 136.7 ($C^{9'}$), 134.3 (C^8), 133.8 (C^9), 129.9 ($C^{6'}$), 129.4 (C^6), 126.2 (C^7), 125.9 ($C^{4'}$), 122.0 (C^3), 53.1 (OCH_3), 52.1 (CH), 42.5 (CH_2Cl), 34.4 (CH_2Ar), 34.2 (SCH_2).

$ESMS^+$ (*m/z*) 437 ($[M+H]^+$, 2%), 459 ($[M+Na]^+$, 100%).

HRMS (ES^+) 459.0209 ($C_{19}H_{17}N_2O_4S_2ClNa$ requires 459.0211, $[M+Na]^+$).

mpt 190–192 °C.

Found : C, 51.94; H, 3.81; N, 6.12% ($C_{19}H_{17}N_2O_4S_2Cl$ requires C, 52.23; H, 3.92; N, 6.41%).

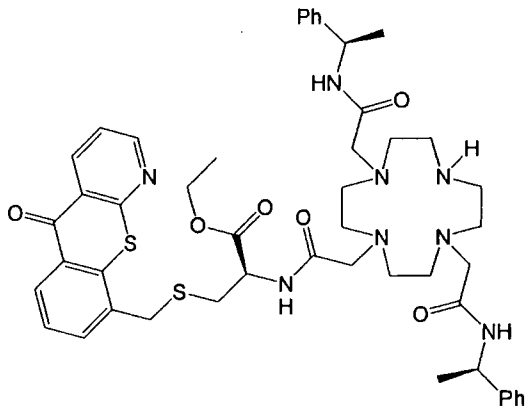

4–(*S*)–[{(2–(1–aza–10–thioxanthon–9–ylmethylsulfanyl)–1–ethoxycarbonylethyl) carbamoyl}methyl]–1,7–(*RR*)–[(1–phenylethylcarbamoyl)methyl]–1,4,7,10–tetraazacyclododecane (49). To a solution of 1,7–(*RR*)–[(1–phenylethyl carbamoyl)methyl]–1,4,7,10–tetraazacyclododecane (44 mg, 90 μmol) in anhydrous EtOH (6 cm^3) and triethylamine (10 μL, 70 μmol) was added *N*–2–Chloroacetyl–*S*–(1–aza–10–thioxanthon–9–ylmethyl)–L–cysteine methyl ester (30 mg, 70 μmol) and the suspension heated at 60°C for 3 days to give a homogeneous solution. The solvents were removed under reduced pressure and the residue taken up in CH_2Cl_2 and filtered. The organics were washed with water (10 cm^3), aqueous $NaHCO_3$ solution (10 cm^3), aqueous NaCl solution (10cm^3), dried (K_2CO_3) and filtered. Evaporation of the solvents followed by purification via column chromatography (silica, CH_2Cl_2 → 1% $^iPrNH_2$:CH_2Cl_2) yielded the title compound (34 mg, 38 μmol, 53%) as a pale yellow foam.

^1H NMR (300 MHz, $CDCl_3$) δ 8.85–8.75 (m, 2H, $H^{2,4}{}_{(4)}$), 8.57 (d, 1H, *J* 8.0 Hz, $H^6{}_{(4)}$), 7.66 (d, 1H, *J* 7.3 Hz, $H^8{}_{(4)}$), 7.50–7.40 (m, 2H, $H^{7,3}{}_{(4)}$), 7.40–7.18 (m, 11H,

Ph+$NH_{(4)}$), 5.18–4.90 (m, 3H, $CH_{(1,4,7)}$), 4.62 (br m, 1H, CH), 4.20–4.00 (m, 4H, OCH_2+CH_2Ar), 3.50–2.60 (br m, 24H, NCH_2+SCH_2), 1.50–1.44 (m, 6H, CH_3), 1.20 (t, 3H, *J* 7.0 Hz, CH_2CH_3).

$ESMS^+$ (*m/z*) 474 ($[M+Ca]^{2+}$, 100%), 486 ($[M+Cu]^{2+}$, 70%), 909 ($[M+H]^+$, 60%).

HRMS (ES^+) 909.4159 ($C_{48}H_{61}N_8O_6S_2$ requires 909.4150).

R_f 0.60 (silica, CH_2Cl_2:EtOH:^{i}PrNH$_2$ 94:3:3).

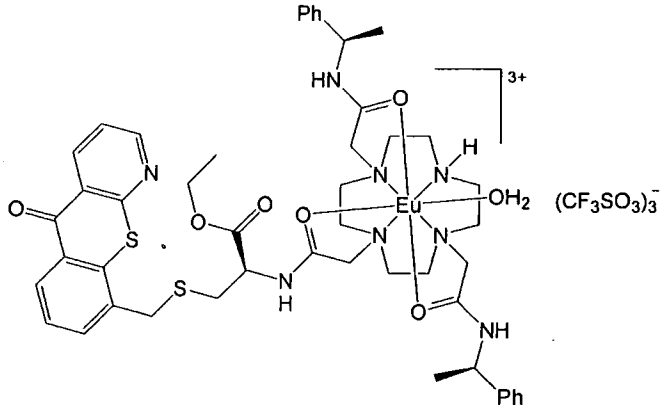

[Eu49](CF$_3$SO$_3$)$_3$. Europium(III) triflate (16 mg, 28 μmol) and 4–(*S*)–[{(2–(1–aza–10–thioxanthon–9–ylmethylsulfanyl)–1–ethoxycarbonylethyl)carbamoyl}methyl]–1,7–(*RR*)–[(1–phenylethylcarbamoyl)methyl]–1,4,7,10–tetraazacyclododecane. (25 mg, 28 μmol) were dissolved in anhydrous MeCN (2 cm^3) and heated at 75°C for 48 hours. The reaction was cooled to room temperature and the solution was added dropwise to stirring, anhydrous diethyl ether (50 cm^3). The white precipitate was isolated by centrifugation, redissolved in the minimum volume of MeCN and precipitated via the same method. A total of three precipitations yielded the title compound (34 mg, 23 μmol, 82%) as a white powdery solid.

$ESMS^+$ (*m/z*) 530 ($[M-H]^{2+}$, 100%), 1209 ($[M-H+CF_3SO_3]^+$, 20%)

HRMS (ES^+) 1209.2731 ($EuC_{49}H_{59}N_8O_9S_3F_3$ requires 1209.2726, $[M-H+CF_3SO_3]^+$).

5.2 References

1 R. S. Dickins, J. A. K. Howard, C. L. Maupin, J. M. Moloney, D. Parker, J. P. Riehl, G. Siligardi and J. A. G. Williams, *Chem. Eur. J.*, 1999, **5**, 1095.

2 W. Yang, C. M. Giandomenico, M. Sartori and D. A. Moore, *Tet. Lett.*, 2003, **44**, 2481.

3 J. I. Bruce, R. S. Dickins, L. J. Govenlock, T. Gunnlaugsson, S. Lopinski, M. P. Lowe, D. Parker, R. D. Peacock, J. J. B. Perry, S. Aime and M. Botta, *J. Am. Chem. Soc.*, 2000, **122**, 9674.

4 R. S. Dickins, S. Aime, A. S. Batsanov, A. Beeby, M. Botta, J. I. Bruce, J. A. K. Howard, C. S. Love, D. Parker, R. D. Peacock and H. Puschmann, *J. Am. Chem. Soc.*, 2002, **124**, 12697.

5 F. J. Villani, T. A. Mann, E. A. Wefer, J. Hannon, L. J. Larca, M. J. Landon, W. Spivak, D. Vashi, S. Tozzi, G. Danko, M. Del Prado and R. Lutz, *J. Med. Chem.*, 1975, **18**, 1.

6 P. Nantkanamirski and J. Piechaczek, *Pol. J. Pharmacol. Pharm.*, 1974, **26**, 545.

7 P. Nantkanamirski and J. Piechaczek, *Pol. J. Pharmacol. Pharm.*, 1976, **28**, 89.

8 Z. Kovacs and A. D. Sherry, *Synthesis*, 1997, 759.

APPENDIX

Colloquia and Conferences

Postgraduate Lecture Courses

NMR in Paramagnetic Systems, Dr. D. H. Powell
Fast Reactions, Dr. M. R. Crampton

Departmental Colloquia

The following Departmental lectures and seminars were attended.

2002

2nd October	Professor Gideon Davies, Department of Chemistry, University of York Structural Enzymology of Glycosyl Transfer: How Enzymes Make and Degrade Polysaccharides
30th October	Professor Tim Bugg, Department of Chemistry, Warwick University Enzymes in Aromatic Degredation
5th November	Dr Cliff Ludman, University of Durham Explosions: A demonstration lecture
13th November	Professor Geoffrey Lawrance, Newcastle University, Australia Designer Ligands: Macrocyclic and alicyclic moleculas for metal complexation and biocatalysis
27th November	Professor Marc Lemaire, University Claude Bernard Lyon 1 Organic Synthesis and Heterogenous Asymmetric Catalysis
4th December	Professor Carsten Bolm, Institut für Organische Chemie der RWTH, Aachen Asymmetric catalysis for enantioselective C–C bond formation (*Degussa lecture*)

2003

15th January	Professor Pat Bailey, Department of Chemistry, UMIST Planned and unplanned routes to bio–active target molecules
22nd January	Dr David Procter, Department of Chemistry, University of Glasgow New Strategies and Methods for Organic Synthesis
12th March	Professor David Lilley, School of Life Sciences, University of Dundee Structure, folding and catalytic activity in RNA molecules
12th November	Dr Jos Brands, MSD process, Hoddesdon Herts The Power of Crystallization–Induced Asymmetric Transformations Efficient Syntheses of NK–1 Receptor Antagonist Aprepitant
3rd December	Dr Malcom Levitt, School of Chemistry, Southampton University Customising selection rules in solid–state NMR and the determination of biomolecular structures

2004

21st January	Professor Mark Bradley, School of Chemistry, University of Southampton Arrays and Combinatorial Chemistry
4th February	Professor P O'Brien, Department of Chemistry, University of Manchester Quantum Dots Realizing the Potential
11th February	Professor D Parker FRS, Department of Chemistry, University of Durham Chiral Lanthanide Complexes: Structure, dynamics and function

17th February Professor A P De Silva, Queens University of Belfast
Designer Molecules for Photonic Signalling

2nd July Professor Sir Harry Kroto, Nobel Laureate in Chemistry (1996)
2010: a NanoSpace Odyssey

17th November Prof. Varinder Aggarwal, School of Chemistry, Bristol.
New methodology for organic synthesis
(*Degussa lecture*)

24th November Prof. Nick Turner, School of Chemistry, Edinburgh.
Directed evolution of enzymes: new biocatalysts for asymmetric synthesis

2005

16th February Prof. Mike North, School of Natural Sciences, Newcastle.
Asymmetric catalysis of C–C bond forming reactions

4th May Prof Jas Pal Badyal, Department of Chemistry, University of Durham.
Molecular Tailoring of Solid Surfaces

25th May Prof. Pavel Kocovsky, Department of Chemistry, University of Glasgow.
Asymmetric Synthesis: From Transition Metals to Organocatalysis

20th September Dr. Christopher Hayes, University of Nottingham.
Fun and games with (+)–lactacystin and modified nucleic acids

Conferences Attended

8th–9th January 2004 RSC UK Macrocyclic and Supramolecular Chemistry Group.*
Sheffield, UK.

20th September 2004 RSC Organic Chemistry Symposium.*
Huddersfield, UK.

23rd–25th September 2004	COST D18 Annual Workshop*
	La Coruna, Spain.
5th–6th January 2005	UK Macrocycles and Supramolecular Chemistry
	Meeting*
	Newcastle, UK.

* Poster presentation.

Publications

"Chemoselective signalling of selected phospho–anions using lanthanide luminescence"

Paul Atkinson, Yann Bretonnière and David Parker, *Chem. Comm.*, 2004, 438.

"NMR and luminescence binding studies of ytterbium, thulium, and europium macrocyclic complexes with phosphorus(V) oxy anions"

Paul Atkinson, Yann Bretonnière and David Parker, *Helv. Chim. Acta*, 2005, **88**, 391.